UNIVERSITAT POLITÈCNICA DE VALÈNCIA

ESCOLA TÈCNICA SUPERIOR D'ENGINYERIA DEL DISSENY

Design of new hybrid nanomaterials with molecular gates as nanodevices for therapeutic applications.

PhD. THESIS

Submitted by

Núria Mas Font

PhD. Supervisors:

Prof. Ramón Martínez Máñez
Dr. José Ramón Murguía Ibáñez

València, December 2014

Instituto Interuniversitario de Reconocimiento Molecular y Desarrollo Tecnológico

Escuela Técnica Superior de Ingeniería del Diseño

RAMÓN MARTÍNEZ MÁÑEZ, PhD in Chemistry and Chair of Chemistry at the Universitat Politècnica de València, and JOSÉ RAMÓN MURGUÍA IBÁÑEZ, PhD in Biological Sciences and Professor of Biomedicine at the Universitat Politècnica de València.

CERTIFY:

That the work *"Design of new hybrid nanomaterials with molecular gates as nanodevices for therapeutic applications."* has been developed by Núria Mas Font under their supervision in the Centro de Reconocimiento Molecular y Desarrollo Tecnológico de la *Universitat Politècnica de València*, as a thesis Project in order to obtain the degree of PhD in Chemistry at the *Universitat Politècnica de València.*

València, October of 2014.

Prof. Ramón Martínez Máñez Dr. José Ramón Murguía Ibáñez

A la meua família (sobretot a la meua parella de perletes, que sou l'alegria de casa) i a les meues xiques.

"Perquè hi haurà un dia que no podrem més i llavors ho podrem tot"
Vicent Andrés i Estellés

"No acceptes la derrota fins que no trobes que en sortiràs guanyant"
Consells, proverbis i insolències, Joan Fuster i Ortells

Agraïments.

Agradecimientos. Acknowledgements.

Arribats a este punt, (per cert abans de dir res: no puc creure'm que estic començant a escriure els agraïments de la tesi!!! I no puc amagar el sentiment de sorpresa, exaltació, nostàlgia, alegria, inseguretat i un cúmul infinit de sensacions a l'hora barrejades que m'invaeixen…). Recapitolant de nou, arribats a este punt toca donar gràcies a tanta, tantíssima gent que ha estat al meu costat aquests darrers anys de tesi, compartint, gaudint i també patint les conqüències que es viuen en el dia a dia en aquesta experiència.

En primer lloc, voldria donar gràcies al meu director, el Prof. Ramón Martínez Máñez, per haver comptat amb mi i donar-me l'oportunitat de desenvolupar la tesi al teu grup. Moltes gràcies per pensar amb mi quan estava fent la tesi del màster i deixar-me seguir amb vosaltres i ensenyar-me tantes coses que he après aquests anys sobre la investigació, la química i tantes altres coses. També donar gràcies al Dr. José Ramón Murguía Ibáñez, també director meu, que encara que ens vam conéixer una miqueta més tard m'has ajudat en molts aspectes de la tesi, ensenyant-me conceptes "bio", prou desconeguts per a mi aleshores (i tants que me'n queden per conéixer ara!). Seguint amb la gent del grup, Fèlix t'he de donar infinites gràcies perquè m'has ajudat tantes vegades en aquests anys, dins el laboratori, amb aquella famosa síntesi dels azoics, quan jo no havia fet cap síntesi orgánica en ma vida. En l'escriptura dels papers i fent eixes figures de "portes" que mai tindré gràcia per a representar com tu i també ara al final ajudant-me en tràmits i correccions de la tesi. Gràcies Loles des d'aquell moment en què ens vas acceptar a Maria i a mi per fer el projecte final de carrera amb tu al IDM i, des d'aleshores (ja fa quasi 7 anys!!) he estat al grup. Gràcies per ensenyar-me tantes coses de materials, tantes visites al SEM i TEM i al STEM fins i tot! Sobretot gràcies per tindre sempre eixe somriure i

dolçor al parlar que et caracteritzen, encara que estigues saturada de feina. Gràcies a Juan, que estaves al despatx amb Fèlix, al que visitava continuament, i aguantar amb ell els debats de les síntesis i càlculs i gràcies pel teu: "Com va xiqueta?". Gràcies Luís, perquè la teua forma de ser i parlar destensionen, fins i tot a una engantxada de l'esquena com jo, i fan riure i pensar a qualsevol, una conversa amb tu mai et deixa indiferent: música, química, materials, història, política, festa i del que siga es pot parlar amb tu. Gràcies als professors i gent de Burjassot que també m'han ajudat en algunes batalles, Pedro, Ana, Boro, Cate i la meua Almu (a tu et reserve per al final…jijiji).

Gràcies a les "mamis del lab", Carmen i Elena, vos vaig conéixer al final de la vostra tesi, saturades de feina, aquests últims anys vos he comprès! I pensava: jo em tornaré loca quan arribe ahí, com poden elles? Gràcies per ajudar-me i ensenyar-me a fer tantes coses al lab i, aguantar-me rient, plorant i fer-me mantenir la calma. Gràcies Elena per ajudar-me en tants marrons ara al final sobretot i a Carmen pel mateix, buscant avaluadors i tribunal (tasca complicadíssima hui dia!) i aguantar-me a la CPI. Gràcies Andrea i Estela. Quines perles! Ais Andrea tia (la meua madrilenya-catalana-valenciana preferida! jijiji), que estoy escribiendo mis agradecimientos! No me lo puedo creer! jajaja. I Estela, la més artista! Quantes coses i moments hem compartit i m'heu ensenyat. Vos admire moltíssim! Teniu una dolçor i un somriure perfecte i sou resabudes! Gràcies amb l'ajuda al lab i fora del lab.

Mare meua, vaig a agafar alé, encara em queda molta gent! Quanta gent som i hem sigut al grup! Gràcies a tota la resta de gent que esteu i/ o heu passat pel 2.6. Alguns coneguts a la tesi, altres al projecte de carrera o màster, ja no ho recorde, se'm barrejen els records (espere no deixar-me a ningú, si és així disculpeu-me! I un beset). Allà va, gràcies a Pilar, que em va acompañar al projecte final

de carrera; Cris Sanfeliu i Inma Candel (primeres companyes de tros de taula); Santi (quina por em feies quan vaig entrar! hahaha); Rosa ("mamá portes"); Hanoi (el cubano-sueco, me acuerdo cuando nos encontramos por la KTH); Maria Sapinya (la meua companyera de batalles! Què guapa i resalà que eres! Quant m'has aguantat!); Julio (vaig fer la primera columna amb tu, ja no se m'oblidarà com s'empaqueta una columna!); Patri, la suecana, el poble del costat, xD; Campos, ma que vals, sabuda i autèntica com tu soles!; Laura, moltes gràcies per ser tan treballadora i perquè molts dels treballs d'esta tesi tenen la teua contribució; Yoli, que et vaja tot genial per Londres; Luís Enrique, reciente doctor Santos, que te vaya todo muy bien en tu nueva etapa; Sameh, gracias por ser como eres, tan trabajador, sencillo y educado, admiro tu trabajo y capacidad de integración en una cultura tan distinta a la tuya, mucha suerte que ya estás también en la recta final! Gràcies Maria Moragues per ser tan organitzada i intentar posar ordre en el 2.6 quan semblava quasi impossible, molta sort a tu també, que ja ho tens ahí! Gracias Ales, el italiano del lab! Gracias por todo, por ser como eres, por haberme ayudado tantísimo en la tesis, con aquella dichosa síntesis entre otras cosas, por los momentos de compartir campana, por las cervezas y momentos de quemar tarjeta, por las fiestas y amigos que compartimos, por las risas y apuestas, fallas y vestirte de saragüell, porque eres mi amigo! Y por esa reciente boda que fue increíble! Os deseo mucha felicidad a ti y a Claudia! Gràcies Romanet, l'electrònic i compi del màster, que abans habitaves a la peixera del 2.6 i, encara que ara estem a les dos puntes del poli, et veig i continuem parlant com si ens veiérem tots els dies. Gràcies als companys que van estar més de pas, Vicente, Krishanu, Ravi (thank you so much for your "sé feliz!"). Michele, grazie mile per il tuo: "Enga enga, la rubia, cómo se moveva…" jaja. Gràcies a Ana, la de Tavernes, eres una gràcia segur que et va genial de profe. Un gràcies especial per a Sílvia, una companya que ens va deixar ara fa un any i que va contribuïr

especialment en un dels treballs d'esta tesi; gràcies perquè mai vas perdre la il·lusió pel treball i la vida.

A la nova gent que habita el 2.6 i/o pertany al grup, alguns vos conec més que altres, que tingueu sort en aquest camí que és la tesi! Toni, Cris M. i Àngela a Amelia, Lorena, Alba, Mónica, Mª Elena, Irene (a tu, especialment moltes gràcies perquè m'has ajudat moltíssim en estos dos últims anys, he après molt de tu, de coses bio i del treball diari i forma de ser, un abraç fort i ànims que arribaràs lluny!).

Gràcies als meus companys de la CPI, on he habitat aquest darrer any. Gràcies per ser com sou, tan organitzats, tan familiars, tan bonicos! Admire moltíssim la vostra forma de ser i treballar i el que s'ho heu currat instal·lant-vos en nous laboratoris i les dificultats que comporta i com heu fet del lab de Nanomedicina, al cub roig, allà on Déu va perdre el gorro, el vostre lloc. Gràcies a Carmen, a Èdgar, ma que eres rebonic! T'estime molt, quant hem viscut junts des d'aquella taula del 2.6 quan encara eres fotoactivable i compartíem a la jefa, jejeje, eres genial! Eres, treballador, humanament grandíssim, generós, un professor boníssim i arribaràs lluny! I no et preocupes per fer-ne vint i tots, tu i jo som arròs bomba carinyet! hahaha. Gràcies Cris T., l'esportista de la casa, admire la capacitat d'aprenentatge teua i perquè has sigut una de les que més difícil ho ha tingut en arribar, aprenent de cèl·lules i coses que no havies fet mai a contrarrellotge pequè Laura se n'anava, dis-li a ta mare que sóc bona xica i que no es preocupe, que encara recorda quan tornares malalta de Cullera en falles, xD. Gràcies Carol, i a Rafa per la seua generositat, pels caramels, dolcets, xicles, papes i cotxinaetes vàries.

Gràcies a tota la gent que ha compartit moments de feina amb mi, per l'ajuda professional i humana. Especialment, a banda de la gent que he nombrat recorde a Raúl i Rafa, del departament, a

Manolo i la gent de microscòpia de la UPV, a Nuria Cabedo del ITQ, a tota la gent del lab de Joserra al IBMCP que em va acollir mentre feia les proves de bactèries, especialment a Rafa i Miguel. Thank you Prof. Timothy O'Brien for accepting me to work in the REMEDI in Ireland. Thank you all the group people. Especialment gràcies a Clara i a Bea, sense vosaltres hauria anat perdudíssima al lab. Gràcies Irene, per aconsellar-me ja des del Facebook, quan encara no em coneixies. Gràcies a la resta de gent que vaig conéixer a l'estada a Galway, perquè sou totes i tots genials i em vau ajudar a oxigenar-me en aquesta recta final de la tesi. Gràcies Hilda, Rubén, Adri, Marta, Lydia, Laura, Estefania, Pablo i Jose. Thank you Mikey, John, Sentil and Claas. Gracias Lidia, la primera persona que conocí al llegar a Galway, en el hostel. Un beso guapa.

Per suposat, gràcies a la meua família i….jajaja que no, que no m'he oblidat de vosaltres! Gràcies a la penya el comboi! Sou grans! Sense vosaltres no hauria superat aquesta tesi. Si no fóra pels infinits combois que hem montat, entenent-nos mútuament perquè estàvem igualment asquejats i compartint idees i formes de viure la vida i perquè no, les ganes de festa! vos assegure que no estaria veient la llum al final del túnel. He pogut reafirmar amistats i fer-ne de noves, sou sens dubte lo millor d'haver fet esta tesi. Cadascú té un paper imprescindible dins aquesta família comboianta: Cris, la perla més dolça de tota la contornà. Amiga i companya coetània de carrera, màster i tesi, companya de pis. Gràcies per tants moments compartits, quantes rises i a l'hora quantes ratllades dient: però què collons fem ací! Jajaja. Ma que vals! Amb eixa risa contagiosa arribaràs a qualsevol lloc, artista! Dani, més del mateix, un altre màrtir d'aquell màster infinit. Et coneixia d'abans, d'alguna festa per Gandia i Cullera, però va ser l'asquejament o millor, les ganes de superar-lo, el que ens va unir! Jajaja. Eres un sol! Ja et queda res també i menys encara per tornar a la terreta. Se't troba a faltar! Un bes fort i ens veiem en res a continuar gaudint i patint moments! Mar,

gràcies rebonica perquè eres súper dolça i, encara que quan se't coneix sembles paradeta, eres igual de pilla que tots nosaltres! Encara recorde quan vas arribar al lab i tots et miràvem com a una invasora més d'allò tan volgut a un laboratori com és l'espai! Jajaja. Però no vas tardar en fer-te el teu espai, i nosaltres a agafar-te confiança, tanta que igual se'ns en va anar un poc de les mans i et vam fer una festa de comiat de soltera de mentida…jajajaja. Ànims que vals molt! I gràcies per haver sigut un dels pilars de la CPI amb Carmen, Èdgar i Cris, que no ho heu tingut fàcil. Lluís, què vaig a dir-te! Eres un crack. També eres una miqueta com Mar, vergonyós al principi, però després no hi ha ningú que et pare, jajaja. Et vaig conéixer al lab, però ha sigut fora d'allí on més t'he conegut, coincidint en molts àmbits: de festa, de mani, de concert, de xerrades i esdeveniments diversos... Gràcies per recolzar-me en molts moments quan ho necessitava. Espere que seguim compartint bones birres i cafés sempre! Ànims i sort, que arribaràs lluny faener! Neus, gràcies per ser tan dolceta i per conéixer tants llocs guais de València que ens han ajudat aquests anys a superar la tesi. Molts ànims que ja no et queda res de res! Açò passarà i de segur que et va genial en el camí que tries, si és cosmètica genial, si no on siga! I la meua Almu, l'ànima de la festa! Ma que eres comboianta! Simpàtica, artista i sempre amb un somriure a la cara! Gràcies per ser tan alegre i positiva i per irradiar tanta energia en cada moment! Eres genial! On tries anar en acabar, triomfaràs! Gràcies Marian, perquè a més de guanyar una bona companya de pis en el seu moment i sobretot, una bona amiga. Gràcies sobretot pels últims combois que hem organitzat per Barcelona, Menorca i Bilbo, que m'han ajudat a agafar moltes forces! Gràcies María Ruíz ja que encara que t'he conegut prou després que a la resta de seguida em vaig donar compte de què eres una tia genial, a punt sempre per a qualsevol comboi, xD! A la resta del comboi, Carles, Santi i Isa, gràcies per formar part d'aquesta penya i ajudar-nos a superar la tesi, escoltant-nos les anècdotes, problemes o parides del lab i de química (bé, d'eixa segona cosa

només tenen potestat de parlar-ne alguns…hahaha) cada vegada que ens veiem. Gràcies a tot el comboi! I que dure per sempre!

A banda de la gent relacionada amb la feina, he de destacar el suport i ajuda rebudes de gent aliena a aquesta tesi, però que estant ahí han fet que puga estar hui acabant aquest procés. Vull agraïr de tot cor l'energia positiva rebuda d'altres persones que vaig conéixer a Irlanda arrel de l'estada a Galway. He conegut a gent que m'estime molt i als qui desitge el millor i que ens veiem prompte! Gràcies a la família de Dun Aengus, a David, va que ja acabe! Continua en peu l'oferta de fer-te soci meu i montar un restaurant a Galway? Jejeje. Un bes per a Juan. Un bes per a Elena, metgesa enamorada de Formentera (com jo!, només lo d'estar enamorada de Formentera xD). Gràcies per escoltar-me! I gràcies al meu "Xavi Gomis, el teclista de The Carminers", eixa descripció em van donar de tu! (gràcies a Miquel i David per parlar-me d'ell i haver-lo conegut!). Gràcies Xavi per les birres compartides, entre elles per descobrir-me la Smithwick's! per apreciar els menjars que preparava i fer d'alumne paeller! Gràcies per ensenyar-me tants llocs genials de Galway i de la "contornà". Gràcies per descobrir-me a Jon Gomm i per presentar-me als teus companys de casa. Gràcies per escoltar-me i fer-me sentir necessària. Gràcies per fer que guanyara un bon amic.

Per suposat, gràcies a les meues amigues, que m'han fet viure molts i bons moments de festa, risa i alegries i m'han ajudat i aguantat les penes. Gràcies germanes! Gràcies sobretot a Marieta i a Ruth perquè si no fóra per eixes birres, eixes converses i eixos bons moments que hem viscut aquests anys, no hauria pogut superar la tesi. Gràcies per créixer amb mi, vos estime! Gràcies també a tu, Marien, perquè sobretot darrerament he fet bones escapades amb tu i ho he passat genial! Ah, i com no, vos he de donar gràcies també per haver anat a aquell Feslloch i presentar-me després a aquest grup de gent que tant m'estime, a tots els "Pollos". Gràcies Rafel, saps el que

t'admire, no he conegut a ningú semblant a tu. Gràcies per ser un punt d'inflexió des que et vaig conéixer. Gràcies per la teua forma de ser, en general i la teua espontaneïtat, en particular. Gràcies per la teua capacitat de reflexió. Gràcies per estimar i confiar tant en la societat, posant-te tu sempre al final de la cua. Gràcies per fer-me créixer (i a la vista està que no en altura… jajaja). I encara que tu no "vulgues" gràcies per fer-te de voler tant. Gerard, gràcies per ser com eres! Per acollir-nos sempre tan bé a ca teua i per tindre la mà més ràpida dels Països Catalans, jajaja. Roger, gràcies per escoltar-me fins i tot quan estàvem de festa i, en general, per les bones converses, fent-me veure les coses des d'una altra perspectiva. Josep, gràcies per ajudar-me a "aguantar" a les dos pelailles, jajajaja. Pep, gràcies per tornar a estimar València, perquè ara pots dir ben fort "València m'agrà!" jajaja. Xavi, home de poca paraula i més acció! Quin crack que eres! Eulàlia, gràcies per compartir uns dies genials de txikiteo per Barna o per Mallorca posant punt i principi, xD. Gràcies a la parella de bascs, Agurne i Oier, per les parides i converses que tenim per whats app diàriament en aquest grup i, sobretot, gràcies per compartir amb mi uns dies genials aquest agost a la vostra terra, fent-me visita turística o ensenyant-me el que era un "güito". Oier, en nada hablas catalán. Gràcies a tota la quadrilla per fer que el dia a dia fóra menys pesat arrancant-me un somriure pel whats app i, sobretot, perquè sou humanament genials i quan ens trobem no fa falta dir res perquè tot isca rodat!

I ara sí, gràcies a tota la meua família, que em dona suport sempre, sou el millor! Un bes fortíssim per a tots vosaltres, especialment a la meua iaia i a ma mare, patidores les dos. Gràcies a tots els meus tios i ties, sempre ajudant-me com pares i mares. Gràcies al meu gerrnà per estar ahí sempre. Gràcies als meus cosins i cosines, especialment a les dos perletes de casa, Arnau i Guillem, heu sigut l'oxigen en aquest llarg camí, sens dubte! I gràcies pare per donar-me força i orgull i seguir fins el final.

I per fi crec que acabe, no volia no volia i al final açò s'ha fet més llarg que un dia sense pa! jajajaja. I és que mai s'acaba d'agraïr prou a les persones que estimes que estiguen al teu costat sempre, passe el que passe, coste el que coste, recolzant-te o posant-li sentit al dia a dia.

Resum

La present tesi doctoral, que porta per títol "Disseny de nous nanomaterials híbrids amb portes moleculars com a nanodispositius per a aplicacions terapèutiques" està centrada en el desenvolupament de nous materials híbrids orgànic-inorgànics funcionals per a aplicacions de lliberació controlada.

Els dos capítols de la present tesi en els que es descriuen els resultats obtesos (el segon i el tercer capítol) estan directament lligats amb l'ús de les nanopartícules mesoporoses de sílice com a soport inorgànic en el desenvolupament de nous materials híbrids orgànic-inorgànics per a aplicacions de lliberació controlada. Així i tot, els resultats s'han dividit en dos capítols depenent de l'estímul aplicat per a la lliberació de la molècula encapsulada. En un dels capítols, els diferents materials desenvolupats es basen en nanodispositius controlats enzimàticament, mentre que a l'altre capítol és un canvi en el pH o en la força electroestàtica (en ambdós casos degut a la presència d'un microorganisme patògen) el que causa la subseqüent lliberació de la càrrega.

En el cas dels nanodispositius controlats enzimàticament, els quals es descriuen al Capítol 2, tres sòlids diferents es van desenvolupar. El primer exemple es va basar en el disseny, síntesi i caracterització de nanopartícules mesoporoses de sílice recobertes amb sals d'azopiridini, que són hidrolitzades per esterases i reductases, les quals es troben presents en la microflora del còlon. Aquestes sals, que contenen un enllaç azoic, es van sel·leccionar per a una possible lliberació selectiva al còlon. Estudis de viabilitat i internalització es van dur a terme amb cèl.lules HeLa, així com els estudis de lliberació de l'agent quimioterapèutic camptotecina. Un segon exemple es va centrar en el disseny, síntesi, caracterització i aplicacions d'un nou nanodispositiu que respon a la presència de proteases per a lliberació controlada, utilitzant nanopartícules de sílice cobertes amb el polímer ε-poli-L-lisina. En aquest cas, es pretenia avaluar

dos mecanismes diferents d'ancoratge del polímer i els dos van donar bons resultats per a aplicacions en lliberació controlada, encara que van mostrar un perfil de lliberació diferent en cada cas. També es van fer estudis de viabilitat i internalització cel·lular amb aquest nou nanodispositiu, així com lliberació de camptotecina en cèl·lules HeLa. Finalment, el darrer nanodispositiu que respon a una acció enzimàtica; inclou el disseny i l'aplicació d'un "scaffold" 3D intel·ligent amb portes moleculars, el qual consisteix amb la combinació de nanopartícules mesoporoses de sílice cobertes i biomaterials porosos clàssics. En aquest cas, les nanopartícules mesoporoses de sílice es van recobrir amb poliamines i ATP. Aquestes nanopartícules es van incorporar a la síntesi d'un "scaffold" de gelatina, el qual es va preparar mitjançant tècniques de prototipat ràpid (RP). En presència de fosfatasa àcida s'induiex la lliberació del colorant encapsulat als pors de les nanopartícules. La fosfatasa àcida es va sel·leccionar com a estímul activador d'aquest material dissenyat ja que és un enzim la concentració del qual és utilitzada per a avaluar l'activitat dels osteoclasts en processos de remodelació òssia i com a marcador en metàstasi d'ossos. Aquestes propietats obrin possibilitats d'ús d'aquesta combinació en el disseny de materials funcionals per a la preparació de nombrosos "scaffolds" avançats amb portes moleculars, que poden ajudar en aplicacions de medicina regenerativa i teràpies de càncer d'ossos.

En relació a l'altre tipus de nanodispositius, que es mostren al Capítol 3, s'ha avaluat el possible ús de les nanopartícules mesoporoses de sílice amb portes moleculars com a possibles vehicles per a la lliberació controlada de fàrmacs quan un microorganisme patogen està present. En aquest cas, el disseny i desenvolupament dels nous materials híbrids orgànic-inorgànics s'han basat en l'ús de nanopartícules mesoporoses de sílice com a matriu inorgànica, recobertes amb entitats moleculars orgàniques que podrien respondre a un canvi en el pH de l'ambient o a un canvi en la força electroestàtica, degut a la presència d'un microorganisme patogen, com ara els fongs o les bactèries. Un d'aquests nanodispositius desenvolupats demostra les aplicacions i propietats antifúngiques

d'un soport carregat amb tebuconazol i recobert amb molècules que actuen de porta molecular dirigida amb un canvi de pH. L'altre material presenta aplicacions antibacterianes contra bactèries gram-positives i gram-negatives, ja que s'utilitza un nanodispositiu carregat amb vancomicina i funcionalitzat amb ε-poli-L-lisina. En els dos casos, s'ha demostrat que l'ús de la nanoformulació pot millorar l'efectivitat del fàrmac encapsulat, millorant-ne i/o ampliant-ne el seu espectre d'àcció, la qual cosa obri un gran ventall de possibilitats en aplicacions d'aquests nanodispositius en el tractament d'infeccions.

En resum, es pot concloure que en aquesta tesi s'han desenvolupat nous sòlids híbrids orgànic-inorgànics, així com s'han descrit les aplicacions d'aquests nanodispositius com a sistemes de lliberació controlada. Els resultats obtesos podrien ser útils en futurs dissenys de materials híbrids avançats en biotecnologia, biomedicina i, concretament, en aplicacions terapèutiques (com ara teràpies contra el càncer, tractament d'infeccions, medicina regenerativa, etc.)

Resumen

La presente tesis doctoral, que lleva por título “Diseño de nuevos nanomateriales híbridos con puertas moleculares como nanodispositivos para aplicaciones terapéuticas” está centrada en el desarrollo de nuevos materiales funcionales híbridos orgánico-inorgánicos para aplicaciones de liberación controlada.

Los dos capítulos de la presente tesis en los que se describen los resultados obtenidos (el segundo y el tercer capítulos) están directamente relacionados con el uso de las nanopartículas mesoporosas de sílice como matriz inorgánica en el desarrollo de nuevos materiales híbridos orgánico-inorgánicos para aplicaciones en liberación controlada. Aún así, los resultados se han dividido en dos capítulos, dependiendo del estímulo aplicado para la liberación de la molécula encapsulada. En uno de los capítulos, los diferentes materiales desarrollados se basan en nanodispositivos controlados enzimáticamente, mientras que en el otro capítulo es un cambio de pH o de fuerza electroestática (en los dos casos debido a la presencia de un microorganismo patógeno) el que causa la consecuente liberación de la carga.

En el caso de los nanodispositivos controlados enzimáticamente, los cuales se describen en el Capítulo 2, se desarrollaron tres sólidos diferentes. El primer ejemplo se basó en el diseño, síntesis y caracterización de nanopartículas mesoporosas de sílice recubiertas con sales de azopiridinio, que se hidrolizan en presencia de esterasas y reductasas, las cuales se encuentran en la microflora del colon. Estas sales, que contienen un enlace azoico, se seleccionaron para una posible liberación selectiva en el colon. Los estudios de viabilidad celular e internalización se llevaron a cabo con células HeLa, así como los estudios de liberación del agente quimioterapéutico camptotecina. Un segundo ejemplo se centró en el diseño, síntesis, caracterización y aplicaciones de un nuevo nanodispositivo que responde a la presencia de proteasas para liberación

controlada, empleando nanopartículas de sílice cubiertas con el polímero ε-poli-L-lisina. En este caso, se pretendía evaluar dos mecanismos diferentes de anclaje del polímero y los dos dieron resultados positivos, aunque presentaron diferentes perfiles de liberación en cada caso. También se realizaron estudios de viabilidad e internalización celular con este nuevo nanodispositivo, así como la liberación de camptotecina en células HeLa. Finalmente, el último nanodispositivo que responde a la acción de un enzima; incluye el diseño y aplicación de un "scaffold" 3D inteligente con puertas moleculares, el cual consiste en la combinación de nanopartículas mesoporosas de sílice con puertas y biomateriales porosos clásicos. En este caso, las nanopartículas mesoporosas de sílice se cubrieron con poliaminas y ATP. Estas nanopartículas se incorporaron durante la síntesis de un "scaffold" de gelatina, el cual se preparó mediante técnicas de prototipado rápido (RP). En presencia de fosfatasa ácida se induce la liberación del colorante encapsulado en los poros de las nanopartículas. La fosfatasa ácida se seleccionó como estímulo activador de este material diseñado, ya que es un enzima cuya concentración se emplea para evaluar la actividad de los osteoclastos en procesos de remodelación ósea y como marcador en metástasis de huesos. Estas propiedades abren posibilidades de uso de esta combinación en el diseño de materiales funcionales para la preparación de numerosos "scaffolds" avanzados con puertas moleculares, que puedan ayudar en aplicaciones de medicina regenerativa y terapias de cáncer de huesos.

Con respecto al otro tipo de nanodispositivos, que se muestra en el Capítulo 3, se ha evaluado el posible uso de las nanopartículas mesoporosas de sílice con puertas moleculares como posibles vehículos para la liberación controlada de fármacos cuando un microorganismo patógeno está presente. En este caso, el diseño y desarrollo de nuevos materiales híbridos orgánico-inorgánicos se ha basado en el uso de nanopartículas mesoporosas de sílice como matriz inorgánica, cubiertas con entidades moleculares orgánicas que podrían responder a un cambio en el pH del ambiente o a un cambio en la fuerza electroestática, debido a la presencia de un microorganismo patógeno, tales

como hongos o bacterias. Uno de estos nanodispositivos desarrollados demuestra las aplicaciones y propiedades antifúngicas de un soporte cargado con tebuconazol y cubierto con moléculas que actúan de puerta molecular dirigida mediante un cambio de pH. El otro material presenta aplicaciones antibacterianas contra bacterias gram-positivas y gram-negativas, ya que se utiliza un nanodispositivo cargado con vancomicina y funcionalizado con ε-poli-L-lisina. En los dos casos, se ha demostrado que el uso de la nanoformulación puede mejorar la efectividad del fármaco encapsulado, mejorando y ampliando el espectro de acción del mismo, lo cual abre un gran abanico de posibilidades en aplicaciones de estos nanodispositivos en el tratamiento de infecciones.

En resumen, se puede concluir que en la presente tesis se han desarrollado nuevos sólidos híbridos orgánico-inorgánicos, así como se han descrito las aplicaciones de estos nanodisposotivos como sistemas de liberación controlada. Los resultados obtenidos podrían ser útiles en futuros diseños de materiales híbridos avanzados en biotecnología, biomedicina y, concretamente, en aplicaciones terapéuticas (como terapias contra el cáncer, tratamiento de infecciones, medicina regenerativa, etc.)

Abstract

The present PhD thesis, which is entitled "Design of new hybrid nanomaterials with molecular gates as nanodevices for therapeutic applications", is focused on the development of new functional hybrid organic-inorganic materials for controlled delivery applications.

Both chapters of the present thesis that report the results obtained (second and third chapters) are directly related with the use of mesoporous silica nanoparticles as inorganic support to develop new hybrid organic-inorganic materials for controlled delivery applications. The results have been divided into two chapters depending on the stimuli applied for the on-comand delivery of the entrapped guest moiety. In one chapter, the different developed materials are enzyme-driven nanodevices, whereas in the other chapter a change in the pH or in the electroestatic force (in both cases due to the presence of a pathogenic microorganism) causes the subsequent release of the cargo.

In the case of the enzymatic-driven nanodevices (see Chapter 2), three different solids have been developed. The first example was based on the design, synthesis and characterization of mesoporous silica nanoparticles capped with azopiridinium salts, which are hydrolized by esterases and reductases, both of which are present in the colon microflora. These salts, containing an azo bond, were selected for a possible selective delivery in the colon. Viability and internalization studies with HeLa cells and controlled delivery studies of the chemoterapeutiuc agent camptothecin have been carried out. A second example was focused on the design, synthesis, characterization and application of a new protease-responsive nanodevice for intracellular-controlled release using silica mesoporous nanoparticles capped in this case with the polymer ε–poly-L-lysine. In this case, it was intended to evaluate two different anchoring protocols of the polymer and both yield fine materials for controlled delivery applications, altough a different release profile was obtained in each case. Cell viability and internalization of this new nanodevice was studied and also the camptothecin

delivery in HeLa cells was tested. Finally, the last enzyme-responsive nanodevice included the design and application of a smart 3D "gated scaffold" which consisted of a combination of capped silica mesoporous nanoparticles and classical porous biomaterials. In this case mesoporous silica nanoparticles were capped with polyamines and ATP. These nanoparticles were incorporated in a gelatin macroporous scaffold during the synthesis, prepared by rapid prototyping (RP) techniques. In presence of acid phosphatase the delivery of the entrapped dye from the nanoparticles' pores was induced. Acid phosphatase was selected as trigger of this designed material bacause it is an enzyme whose concentration is used to assess osteoclast activity in bone remodelling processes, and as a marker for bone metastases. These features open up the possible use of this combination in the design of functional materials for the preparation of a number of advanced gated scaffolds, which could help in regenerative medicine and bone cancer therapy applications.

Regarding the other type of nanodevices (see Chapter 3), it was evaluated the possible use of mesoporous silica nanoparticles with molecular gates as carriers for drug delivery in the presence of a pathogen. Here, the design and development of new organic-inorganic hybrid materials has been based on the use of MCM-41 mesoporous silica nanoparticles as inorganic matrix, capped with organic moieties that could respond to a change in the pH of the environment or a change in the electrostatic force due to the presence of a pathogenic microorganism, such as fungi or bacteria. In one of these developed nanodevices, antifungal applications and properties were demonstrated using a tebuconazole loaded support capped with pH-driven gatekeeping moieties. The other material presented antibacterial properties against gram-positive and gram-negative bacteria and consisted of a vancomycin loaded nanodevice capped with ε-poly-L-lysine. In both cases, it has been demonstrated that the use of a nanoformulation setup can improve the drug effectiveness, enhancement and broadening of the action spectrum of the drug, thus opening a wide range of possible applications of these nanodispositives in the treatment of infections.

In summary, it can be concluded that new hybrid organic-inorganic solids have been developed and their application as controlled delivery systems have been described in this thesis. The obtained results could be useful in future design of advanced hybrid materials for biotechnology, biomedical and, particularly, therapecutic applications (i.e. cancer therapy, treatment of infections, regenerative medicine, etc.)

Results of this thesis have resulted in the following scientific publications:

Núria Mas, Alessandro Agostini, Laura Mondragón, Andrea Bernardos, Félix Sancenón, M. Dolores Marcos, Ramón Martínez-Máñez, Ana M. Costero, Salvador Gil, Matilde Merino-Sanjuán, Pedro Amorós, Mar Orzáez and Enrique Pérez-Payá. **Enzyme-responsive silica mesoporous supports capped with azopyridinium salts for controlled delivery applications.** *Chem. Eur. J.* **2013**, *19,* 1346 – 1356.

Núria Mas, Irene Galiana, Laura Mondragón, Elena Aznar, Estela Climent, Nuria Cabedo, Félix Sancenón, José Ramón Murguía, Ramón Martínez-Máñez, María D. Marcos and Pedro Amorós. **Enhanced efficacy and broadening of antibacterial action of drugs via the use of capped mesoporous nanoparticles.** *Chem. Eur. J.* **2013**, *19*, 11167 – 11171.

Núria Mas, Irene Galiana, Silvia Hurtado, Laura Mondragón, Andrea Bernardos, Félix Sancenón, María D. Marcos, Pedro Amorós, Nuria Abril-Utrillas, Ramón Martínez-Máñez and José Ramón Murguía. **Enhanced antifungal efficacy of Tebuconazole using gated pH-driven mesoporous nanoparticles.** *Int J Nanomedicine,* **2014**, *9, 2597–2606.*

Laura Mondragón, Núria Mas, Vicente Ferragud, Cristina de la Torre, Alessandro Agostini, Ramón Martínez-Máñez, Félix Sancenón, Pedro Amorós, Enrique Pérez-Payá and Mar Orzáez. **Enzyme-responsive intracellular-controlled release using silica mesoporous nanoparticles capped with ε–poly-L-lysine.** *Chem. Eur. J.* **2014***, 20,* 5271 – 5281.

Núria Mas, Daniel Arcos, Lorena Polo, Elena Aznar, Sandra Sánchez-Salcedo, Félix Sancenón, Ana García, M. Dolores Marcos, Alejandro Baeza, María Vallet-Regí, and Ramón Martínez-Máñez. **Towards the development of smart 3D "gated scaffolds" for on-command delivery**. *Small,* **2014**. DOI: 10.1002/smll.201401227.

Other contributions during this PhD thesis have resulted in the following publication:

Andrea Bernardos, Laura Mondragón, Irakli Javakhishvili, Núria Mas, Cristina de la Torre, Ramón Martínez-Máñez, Félix Sancenón, José M. Barat, Søren Hvilsted, Mar Orzaez, Enríque Pérez-Payá and Pedro Amorós. **Azobenzene Polyesters Used as Gate-Like Scaffolds in Nanoscopic Hybrid Systems.** *Chem. Eur. J.* **2012,** *18***,** 13068–13078.

Abbreviations

ADP	Adenosine Diphosphate
Ann V	Annexin V
Apase	Acid Phosphatase
ATP	Adenosine Triphosphate
Azo	Azo pyridin derivative
BET	Brunauer, Emmett and Teller Model
BJH	Barret, Joyner and Halenda Model
BSA	Bovine Serum Albumin
CB[n]	Cucurbit[n]uril Rings
CBPQT^{4+}	Cyclobis(Paraquat-*p*-Phenylene)
CD	Cyclodextrin
CD-GOx	Cyclodextrin modified-glucose oxidase
CFU	Colony Formation Units
CPT	Camptothecin
CTAB	Hexadecyltrimethylammonium Bromide
DLS	Dynamic Light Scattering
D-MEM	Dulbecco's Modified Eagle's Medium
DMF	Dimethylformamide
DIEA	Diisopropylethylamine
DNA	Deoxyribonucleic acid
DNPD	Dioxynaphthalene
DTT	Dithiotheritol
EDX	Energy-dispersive X-ray
EM	Electrophoretic Mobility
ε-PL	ε-poly-L-lysine
ESI-TOF-MS	Electrospray Ionization Time-of-Flight Mass Spectroscopy
FCS	Foetal Calf Serum
FL	Fluorescein

Fmoc	Fluorenylmethoxycarbonyl
GFP	Green Fluorescent Protein
GMP	Guanosine Monophosphate
GOS	Galacto-oligosaccharide
HPLC	High Performance Liquid Chromatography
IR	Infra Red
Ir(ppy)$_3$	Iridium, tris(2-phenylpyidine)
LAMP1	Lysosomal-associated membrane protein 1
LB	Luria Bertani medium
LCST	Lower Critical Solution Temperature
LCT	Liquid Crystal Templating
M9	Minimal Medium
MCM	Mobile Crystalline Material
ME	Mercaptoethanol
MIC	Minimum Inhibitory Concentration
MS	Mass spectrometry
MSN	Mesoporous Silica Nanoparticles
N3	3-[2-(2-Aminoethylamino)Ethylamino]Propyltrimethoxysilane
NMR	Nuclear Magnetic Resonance
OXYMA	Ethyl 2-cyano-2-(hydroxyimino)aceate
PBS	Phosphate-Buffered Saline
PI	Propidium iodide
PMOs	Periodic Mesoporous Organosilicas
PNIPAAm	Poly*(N*-Isopropylacrylamide)
PTI	Photon Technology International
PXRD	Powder X-Ray Diffraction
PyBOP	Benzotriazol-1-yl-oxytripyrrolidinophosphonium Hexafluorophosphate
RP	Rapid Prototyping
Ru(bipy)$_3^{2+}$	Tris(2,2'bipyridyl)Ruthenium(II)
SA-β-gal	Senescence associated β−galactosidase

SBA	Santa Barbara Amorphous Material
SEM	Scanning Electron Microscopy
SMPS	Silica Mesoporous supports
STEM	Scanning transmission electron microscopy
STEM-EDX	Scanning transmission electron microscopy-Energy-dispersive X-ray
SVF	Simulated Vaginal Fluid
tBOC	di-tert-butyl dicarbonate
Teb	Tebuconazole
TFA	Trifluoroacetic acid
TIS	Triisobutylsilane
TEM	Transmission Electron Microscopy
TEOS	Tetraethylorthosilicate
TGA	Termogravimetric Analysis
TTF	Tetrathiafulvalene
UV	Ultraviolet
UVM	Universidad Valencia Material
WST-1	4-[3-(4-iodophenyl)-2-(4-nitro-phenyl)-2H-5-tetrazolio]-1,3-benzene disulfonate (reagent for cell proliferation assays)
XRD	X-ray diffraction

Content

1. General introduction

The content of this PhD thesis is mainly devoted to the design and applications of different nanoscopic organic-inorganic hybrid materials, some of which are based on supramolecular chemistry. This is why in this general introduction the fundament of supramolecular chemistry as well as the concept of hybrid materials and their applications will be discused.

1.1 **Supramolecular Chemistry.**

Chemistry can be defined as the study of the composition, structure, properties and change of matter. It is directly related with atoms and molecules and their interactions and transformations. Chemistry also studies how changes are produced in the matter during reactions and the energetic balance in these processes. Basically, chemistry is the creation of molecular assemblies using a controlled formation or breaking of covalent bonds. Despite the behaviour of each

individual molecule can be known or understood it is not as simple to know how they work once they are building-up more complex units. In this point is when emerges the concept of Supramolecular Chemistry that can be defined as the discipline that studies how simple molecules organize themselves in order to create more complex structures.

Supramolecular Chemistry examines the weak and reversible noncovalent interactions between molecules. These forces include hydrogen bonding, metal coordination, hydrophobic forces, van der Waals forces, $\pi-\pi$ interactions and electrostatic effects, to easily generate unique nanostructured supermolecules that present different properties (often better) than the sum of the properties of each individual component.[1]

Supramolecular Chemistry has been defined as "chemistry beyond the molecule" by one of its founding fathers, Jean-Marie Lehn, who won the Nobel Prize in chemistry with Charles Pedersen and Donald Cram in 1987 for their significant contributions to molecular recognition.[2,3] According to Dr. Lehn, who introduced the term, a supermolecule is an organized complex entity that is created from the association of two or more chemical species held together by intermolecular forces, whereas the term Supramolecular Chemistry may be focused on the organized entities of higher complexity that result from the association of two or more chemical species held together by intermolecular forces.[4]

This is a relatively young discipline, dating back to the late 1960s and early 1970s; however, its roots and many simple supramolecular chemical systems may

[1] K. Ariga, T. Kunitake, *Supramolecular Chemistry-Fundamentals and application*, © Springer-Verlag Berlin Heidelberg edition **2006**.

[2] J. M. Lehn, *Pure Appl. Chem.* **1978**, *50*, 871.

[3] J. M. Lehn, *Angew. Chem. Int. Ed. Engl.* **1988**, *27*, 89.

[4] J. M. Lehn, *Supramolecular Chemistry*, Ed. VCH, **1995**; J.-M. Lehn, Nobel lecture, **1987**.

be traced back almost to the beginnings of modern chemistry.[5,6] Development of Supramolecular Chemistry was inspired primarily by Nature, displaying complex nanostructures trying to mimmic processes that occur in biology, such as substrate binding to a receptor protein, enzymatic reactions, assembling of protein-protein complexes, immunological antigen-antibody association, intermolecular reading, translation and transcription of the genetic code, signal induction by neurotransmitters, etc.

Supramolecular Chemistry has drawn considerable attention in the recent decades as a new emerging and fast-growing domain between chemistry, physics, material science and biochemistry. Its emergence has been mostly due to the deep effect that causes the fact that molecules can be associated by their geometric or electronic affinity yielding supramolecular aggregates that can present new properties and characteristics which are difficult to rise individually. This fact has boosted the development of new concepts in the area of nanoscience and nanotechnology, by the incorporation of molecules onto materials.

Bearing in mind the wide and sophisticated range of concepts and possibilities that can be offered by this noncovalent bond chemistry, supramolecular chemistry can be divided in two main areas:

- *molecular recognition chemistry*, chemistry associated with a molecule recognizing a partner molecule, also defined as Host-Guest chemistry. Molecular recognition is the specific binding of a guest molecule to a complementary host molecule to form a host-guest complex. Often, the definition of which species is the "host" and which is the "guest" is arbitrary. However, in this area, the receptor or host molecule is usually a large molecule or aggregate, such as an enzyme or synthetic cyclic

[5] J. W. Steed, J. L. Atwood, *Supramolecular Chemistry*, Wiley: New York, **2000**.

[6] L. F. Lindoy, I. M. Atkinson, *Self-assembly in Supramolecular Systems,* The Royal Society of Chemistry: Cambridge, **2000**.

compound, possessing a sizeable hole or cavity. The guest molecule may be a monoatomic cation, a simple inorganic anion or a more sophisticated molecule, with a geometric size or shape complementarity to the receptor or host. The basis of molecular recognition is laid on the lock and key principle, i.e the discrimination by a host between different guests (See Figure 1).

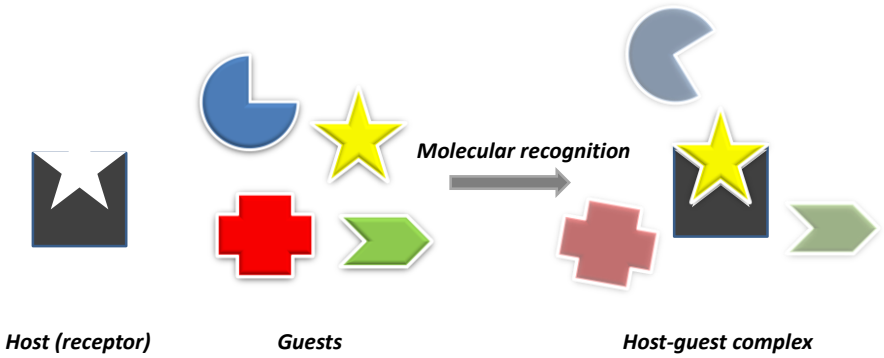

Figure 1. Schematic representation of a molecular recognition event: the host is able to discriminate between different guests.

- *self-assembly chemistry*, chemistry of molecular assembly of many molecules. Molecular self-assembly is the construction of systems without guidance or management from an outside source (other than to provide a suitable environment). The molecules are directed to assemble through noncovalent interactions. Molecular self-assembly also allows the construction of larger structures such as micelles, membranes, vesicles or liquid crystals. Molecular self-assembly is a strategy for nanofabrication that involves designing molecules and supramolecular entities so that shape-complementarity causes them to aggregate into desired structures. Self-assembly has a number of advantages as a strategy: First, it carries out many of the most difficult steps in nanofabrication--those involving atomic-level modification of structure--using the very highly developed techniques of synthetic chemistry. Second, it draws from the enormous wealth of examples in biology for inspiration: self-assembly is one of the most important strategies used in biology for the development of

complex, functional structures. Third, it can incorporate biological structures directly as components in the final systems. Fourth, because it requires that the target structures be thermodynamically the most stable ones to open the system, it tends to produce structures that are relatively defect-free and self-healing.

This PhD thesis is in part related with the second area, the self-assembly chemistry, because it is devoted to the synthesis of the nanoscopic silica based mesoporous materials and their superficial functionalization with organic molecules to obtain triggerable gated systems for drug delivery. However, the molecular recognition chemistry is not out of the range of this thesis, due to the fact that biological processes are closely linked to this concept, in which the application of these nanoscopic materials are based on. A good example, is the relationship between an enzyme and its cleavege site.

1.2 **Organic-inorganic hybrid materials.**

The development of organic-inorganic hybrid materials emerged with the need to develop applications that are often difficult to obtain by using convencional multiple components in classical modular chemistry. An attractive and suitable alternative approach to enhance functionality is the combination of supramolecular concepts with nanoscopic inorganic solids.[7] This could be achieved by using preorganized nanoscopic solid structures and molecular functional units attached to the surface of the inorganic supports in a synergic fashion.[8] Taking this fact into acount, recently reported examples have shown that the anchoring of molecular entities onto 3D nanoscopic scaffoldings offers the opportunity for the development and exploration of new supramolecular

[7] A.B. Descalzo, R. Martínez-Máñez, F. Sancenón, K. Hoffman, K. Rurack, *Angew. Chem.Int.* Ed, **2006**, *45*, 5924.

[8] K. Rurack, R. Martínez-Máñez, *The supramolecular chemistry of organic-inorganic hybrid materials*, **2010**, ed. John Wiley & Sons.

concepts that would hardly be achievable on "flat" surfaces (2D systems).[9,10,11] This is especially true in the field of gated nanochemistry, and it is directly related with the design of nanoscopic supramolecular architectures incorporating chemical entities that can act as a functional gatelike scaffoldings and allow control over the access to (or from) a certain nanometer-scale site at will.[12,13,14,15,16,17,18,19,20,21]

Hybrid organic inorganic materials are not simply physical mixtures. They can be broadly defined as molecular or nano-composites with (bio)organic and inorganic components, intimately mixed where at least one of the component domains has a dimension ranging from a few Å to several nanometers. Therefore, the properties of these hybrid materials are not only the sum of the individual

[9] A. B. Descalzo, K. Rurack, H. Weisshoff, R. Martínez-Máñez, M. D. Marcos, P. Amorós, K. Hoffmann, J. Soto, *J. Am. Chem. Soc.* **2005**, *127*, 184.

[10] M. Comes, M. D. Marcos, R. Martínez-Máñez, F. Sancenón, J. Soto, L. A. Villaescusa, P. Amorós, D. Beltrán, *Adv. Mater.* **2004**, *16*, 1783.

[11] a) M. Comes, G. Rodríguez-López, M. D. Marcos, R. Martínez- Máñez, F. Sancenón, J. Soto, L. A. Villaescusa, P. Amorós, D. Beltrán, *Angew. Chem. Int. Ed*. **2005**, *44*, 2918. b) R. Casasús, E. Aznar, M. D. Marcos, R. Martínez-Máñez, F. Sancenón, J. Soto, P. Amorós, *Angew. Chem. Int. Ed*. **2006**, *45*, 6661. c) C. Coll, R. Martínez- Máñez, M. D. Marcos, F. Sancenón, J. Soto, *Angew. Chem. Int. Ed.* **2007**, *46*, 1675.

[12] A. Nayak, H. Liu, G. Belfort, *Angew. Chem. Int. Ed.* **2006**, *45*, 4094.

[13] I. Vlassiouk, C. D. Park, S. A. Vail, D. Gust, S. Smirnov, *Nano Lett.* **2006**, *6*, 1013.

[14] N. K. Mal, M. Fujiwara, Y. Tanaka, *Nature* **2003**, *421*, 350.

[15] N. K. Mal, M. Fujiwara, Y. Tanaka, T. Taguchi, M. Matsukata, *Chem. Mater.* **2003**, *15*, 3385

[16] R. Casasús, M. D. Marcos, R. Martínez-Máñez, J. V. Ros-Lis, J. Soto, L. A. Villaescusa, P. Amorós, D. Beltrán, C. Guillem, J. Latorre, *J. Am. Chem. Soc.* **2004**, *126*, 8612.

[17] Q. Yang, S. Wang, P. Fan, L. Wang, Y. Di, K. Lin, F.-S. Xiao, *Chem. Mater.* **2005**, *17*, 5999.

[18] C.-Y. Lai, B. G. Trewyn, D. M. Jeftinija, K. Jeftinija, S. Xu, S. Jeftinija, V. S.-Y. Lin, *J. Am. Chem. Soc.* **2003**, *125*, 4451.

[19] J. A. Gruenhagen, C. Y. Lai, D. R. Radu, V. S.-Y. Lin, E. S. Yeung, *Appl. Spectrosc.* **2005**, *59*, 424.

[20] S. Giri, B. G. Trewyn, M. P. Stellmaker, V. S.-Y. Lin, *Angew. Chem. Int. Ed.* **2005**, *44*, 5038.

[21] P. Nednoor, N. Chopra, V. Gavalas, L. G. Bachas, B. J. Hinds, *Chem. Mater.* **2005**, *17*, 3595.

contributions of both phases, but the role of their inner interfaces could be predominant.[22] The advantages of incorporating organic molecules on solid supports by covalent bonding are the following:

- ✓ Pre-organization of the receptor leads to the formation of a dense monolayer (depending on the degree grade of the surface functionalization) of binding/coordination sites arranged in specific positions onto the solid surface. This effect maximizes the interaction with the target analyte.
- ✓ Subsequent anchoring processes can be performed to obtain a solid surface functionalized with different organic molecules. Then, modulation of the hybrid material properties can be controlled with this multifunctionalization by different steps techniques.
- ✓ Leaching processes involving the receptor are avoided.
- ✓ If the receptor used to functionalize the support can offer reversibility, this material could be reusable without lost of its features.

1.3 **Mesoporous materials.**

According to the international Union of Pure and Applied Chemistry (IUPAC), pore sizes are classified into three main categories, namely micropores, meso-pores and macro-pores characterized by pore sizes less than 2 nm, between 2 and 50 nm, and larger than 50 nm respectively.[23] Among them, thanks to their large internal surface area, microporous and mesoporous materials are attracting considerable research attention for applications in catalysis,[24] filtration and separation,[25] gas adsorption and storage,[26] enzyme immobilization,[27] biomedical

[22] C. Sánchez, *J. Mater. Chem.*, **2005**, 15, 3557.

[23] a) G. Zhao, *J. Mater. Chem.*, **2006**, 623. b) D. Schaefer, *MRS Bulletin*, **1994**, *14*, 6.

[24] D.E. De Vos, M. Dams, B.F. Sels, P.A. Jacobs, *Chem. Rev.,* **2002**, *102*, 3615.

[25] X. Liu, Y. Du, Z. Guo, S. Gunasekaran, C. -B. Ching, Y. Chen, S .S .J. Leong, Y. Yang, *Microporous Mesoporous Mater*., **2009**, *122*, 114.

tissue regeneration,[28] drug delivery,[29] and chemical/biochemical sensing.[30] Emblematic microporous materials are crystalline framework solids, such as zeolites,[31] or particular metallophosphates[32] and cacoxenite, which present the largest pore dimensions, respectively, comprised between 10 and 12 Å for zeolites and 14 Å for cacoxenite.[33]

In the present thesis, mesoporous materials have been extensively used, so their characteristics are going to be more deeply explained. Almost twenty years ago, in 1992, patents and journal publications from Mobil company disclosed the synthesis and characterization of a new class of porous materials, a family of uniform pore, silicate based, mesoporous molecular sieves, named the M41S family.[34,35,36,37] These materials present an orderly arrangement of pores, with a very homogeneous pore size, whose average value falls within the range 2-10 nm.[38] Moreover, they have a high pore volume, from the order of 1 cm^3/g and

---

[26] a) M. Kruk, M. Jaroniec, *Chem. Mater*., **2001**, *13*, 3169. b) A. Corma, M. Moliner, M. J. Diaz-Cabanas, P. Serna, B. Femenia, J. Primo, H. Garcia, *New J. Chem.*, **2008**, *32*, 1338. c) C. Ispas, I. Sokolov, S. Andreescu*, Anal. Bioanal. Chem*., **2009**, *393*, 543.

[27] M. Vallet-Regi, M. Colilla, I. J. Izquierdo-Barba, *Biomed. Nanotechnol*., **2008**, *4*, 1.

[28] I. Slowing, B. G. Trewyn, S. Giri, V. S. –Y. Lin, *Adv. Funct. Mater*., **2007**,*17*, 1225.

[29] a) M. Vallet-Regi, F. Balas, D. Arcos, *Angew. Chem., Int. Ed*., **2007**, *46*, 7548. b) K. A. Kilian, T. Bocking, K. Gaus, J. King-Lacroix, M. Gal, J. J. Gooding, *Chem. Commun*., **2007**, 1936.

[30] a) K. A. Kilian, T. Boecking, K. Gaus, M. Gal, J. J. Gooding, *ACS Nano,* **2007**, *1,* 355. b) A.Jane, R. Dronov, A. Hodges, N. H. Voelcker, *Trends Biotechnol*. **2009**,*27*, 230.

[31] M. E. Davis, C. Saldarriaga, C. Montes, J. Garces, C. Crowder, *Nature*, **1988**, *331*, 698.

[32] M. Estermann, L. B. McCusker, C. Baerlocher, A. Merrouche, H. Kessler, *Nature*, **1991**, *352*, 320.

[33] P. B. Moore, J. Shen, *Nature*, **1983**, *306*, 356.

[34] C. T. Kresge, M. E. Leonowicz, W. J. Roth, J. C. Vartuli and J. S. Beck, *Nature*, **1992**, *359*, 710.

[35] C. T. Kresge, M. E. Leonowicz, W. J. Roth and J. C. Vartuli, Synthetic Mesoporous Crystalline Material, US Patent 5,098,684, March 24, **1992**.

[36] C. T. Kresge, M. E. Leonowicz, W. J. Roth and J. C. Vartuli, Synthetic Porous Crystalline Material, Its Synthesis, US Patent 5,102,643, April 7, **1992.**

[37] J. S. Beck, J. C. Vartuli, W. J. Roth, M. E. Leonowicz, K. D. Schmidt, C. T. W. Chu, D. H. Olson, E. W. Sheppard, S. B. McCullen, J. B. Higgins and J. L. Schlenker, *J. Am. Chem. Soc.*, **1992**, *114*, 10834.

[38] Liberación de fármacos en matrices biocerámicas: avances y perspectivas. Monografía XIX. Editors: María Vallet Regí – Antonio Luís Doadrio Villarejo. Real Academia Nacional de Farmacia.

a specific surface area between 500 m^2/g and 1000 m^2/g. Those M41S materials are featured by high chemical inertness and thermal stability. Last but not least, the material synthetic procedure is well described and requires inexpensive and nonhazardous precursors. The peculiarity of presenting all this whole range of properties makes these materials ideal supports for adsorption processes of relatively small molecules and enables them to be suitable platforms for the preparation of hybrid systems for controlled release studies upon exposition to an external stimulus.

Originally, the M41S family grouped under that name three different discrete structures, easily identifiable by X-ray diffraction – MCM-41 (hexagonal phase), MCM-48 (cubic), and MCM-50 (lamellar) (see Figure 2). They were obtained by surfactant-assisted synthesis, called liquid crystal templating, under conditions employed to crystallize microporous solids like zeolites.[39] The interaction of the silicate oligomers with surfactant micelles under different conditions of pH, concentration and temperature is what causes the formation of one or another material. This announcement created an extraordinary amount of interest in the scientific community that still continues today. Since that moment those silica mesoporous supports have been extensively used as inorganic scaffolds in the development of nanoscopic hybrid materials.

[39] C. T. Kresge and W. J. Roth, *Chem. Soc. Rev.,* **2013**, *42*, 3663.

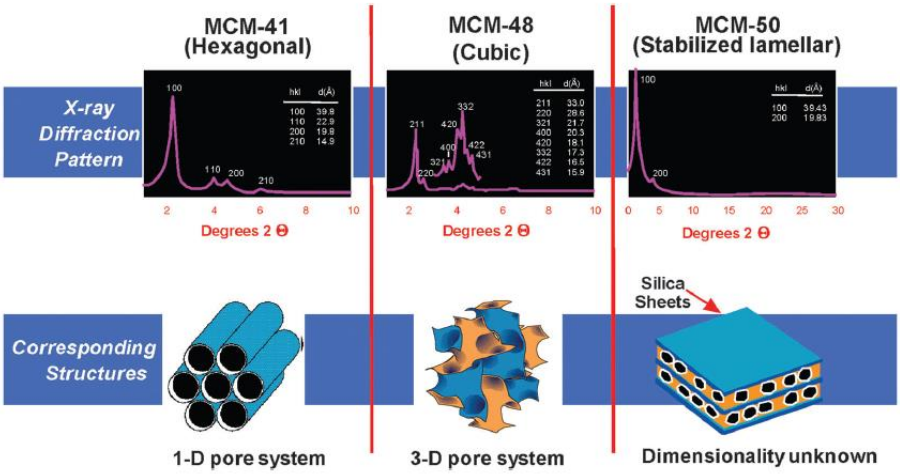

Figure 2. Scheme of the M41S family of mesoporous molecular sieves, including MCM-41, MCM-48 and MCM-50. *(Reprinted with permission from C. T. Kresge and W. J. Roth, Chem. Soc. Rev., 2013, 42, 3663. Copyright © 2013 The Royal Society of Chemistry).*

1.3.1 Synthesis of mesoporous materials.

Mesoporous materials research was initially motivated by the desire for ordered silica/alumina supports with pores of larger dimensions than the ones found in microporous zeolites. As it has been cited above, the first successful studies on surfactant–organised mesoporous materials were carried out on silica, and it still remains as the most studied system.

From the literature it is obvious that the formation of ordered mesoporous materials is closely related with the specific chemistry and chemical interactions involved in the studied system, but also with the physical conditions employed during the synthesis procedure. Some of these parameters are: type of inorganic material and its propensity to crystallise in the walls, their kinetics or their hydrolysis and condensation capacity, type of surface-active molecules, the respective and relative concentrations of surfactant and inorganic species, pH, temperature, synthesis time, type of solvent, etc.

Basically, two main components are needed to build-up a system that presents a high ordered porous structure with homogeneous pore dimensions:

• a template, such as a surfactant, that acts as a structure-directing agent, and is able to form micelles in water solution.

• a polymeric precursor, such as oligomeric silicates, wich are present in the reaction mixture and are able self-organize and to condensate around the template.

Researchers have found that two different mechanisms are involved on the formation process of these composite materials. In retrospect, both initial proposed pathways (1 and 2 in Figure 3) proved to be valid. The predominant pathway appears to be the anionic species initiated one (using cationic surfactants). This concept was explained and expanded upon by many researchers, specifically by the group at the University of Santa Barbara headed by Prof. Galen Stucky[40] and termed cooperative self-assembly. Later, researchers at the University of Southampton demonstrated the other proposed pathway, originally labeled the liquid crystal phase initiated pathway. Prof. George Attard and his co-workers used a preformed liquid crystal phase to synthesize both a silica and a metal (platinum alloy) mesoporous molecular sieve. [41]

[40] a) A. Monnier, F. Scheth, Q. Huo, D. Kumar, D. Margolese, R. S. Maxwell, G. Stucky,M. Krishnamurty, P. Petroff, A. Firouzi, M. Janicke, B. Chmelka, *Science*, **1993**, *261*, 1299. b) S. A. Walker, J. Zasadzinski, A. G. Glinka, J. Nicol, D. Marogloese, G. D. Stucky and B. F. Chmelka, *Science*, **1995**, *267*, 1138.

[41] G. S. Attard, J. C. Glyde, C. G. Göltner, *Nature,* **1995**, *378*, 366.

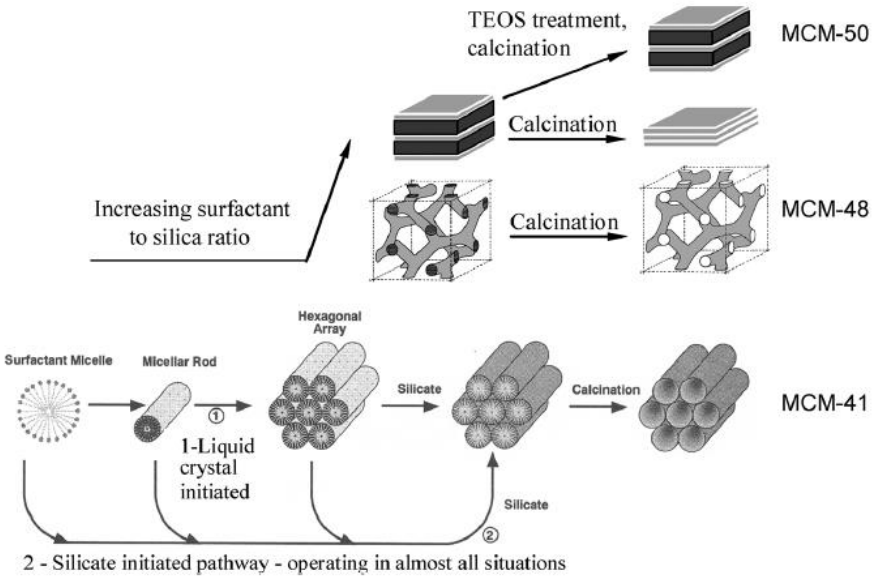

Figure 3. Schematic representation of the initially proposed LCT mechanism of formation pathways (lower half) and its further additions. *(Reprinted with permission from C. T. Kresge and W. J. Roth, Chem. Soc. Rev., 2013, 42, 3663. Copyright © 2013 The Royal Society of Chemistry).*

Using these processes, the original approach has been extended by a number of variations. As an example, the use of triblock copolymer templates under acidic conditions was employed to prepare the so-called SBA (Santa Barbara Amorphous) silica phases,[42] whereas the use of cationic surfactants, such as hexadecyltrimethylammonium bromide (CTAB) was originally used in the synthesis of the first M41S materials, obtaining the hexagonal (MCM-41), the cubic (MCM-48) and lamellar (MCM-50) forms described above.

In M41S materials, a liquid crystal templating (LCT) mechanism was proposed by the Mobil scientists in which supramolecular assemblies of surfactant micelles (e.g., alkyltrimethylammonium surfactants) act as structure directors for the formation of the mesophase (Figure 3). Depending on factors described above, such as concentration and dimensions of the surfactant, temperature, pH

[42] a) D. Zhao, J. Feng, Q. Huo, N. Melosh, G.H. Fredrickson, B.F. Chmelka, G.D. Stucky, *Science*, **1998**, *279*, 548. b) D. Zhao, Q. Huo, J. Feng, B.F. Chmelka, G.D. Stucky, *J. Am. Chem. Soc.*, **1998**, *120*, 6024.

solution, ionic force, etc. different kind of micelles can be obtained. The mechanism proposed behind the composite mesophase formation is best understood for the synthesis under high pH conditions. Under these conditions, anionic silicate species, and cationic or neutral surfactant molecules, cooperatively organize to form hexagonal, lamellar, or cubic structures. In other words, there is an intimate relationship between the symmetry of the mesophases and the final products.[37] The composite hexagonal mesophase is suggested to be formed by condensation of silicate species (formation of a sol-gel) around a preformed hexagonal surfactant array or by adsorption of silicate species onto the external surfaces of randomly ordered rod-like micelles through coulombic or other types of interactions. Next these randomly ordered composite species spontaneously pack into a highly ordered mesoporous phase with an energetically favorable hexagonal arrangement, accompanied by silicate condensation. This process initiates the hexagonal ordering in both the surfactant template molecules and the final product. The elimination of the surfactant from the pores of the materials yield the desired inorganic mesoporous scaffold, which can be carried out by aerobic high temperature calcination or by extraction with adequate solvents.

Among M41S materials, MCM-41 is one of the best known and most widely studied. The MCM-41 synthesis is schematically represented in Figure 3. As it can be seen, the synthesis consists of the polymerization of tetrahethylortosilicate (TEOS), used as inorganic siliceous precursor, around super-micellar-template previously formed in basic water solution. As explained before, the subsequent removal of the surfactant gives the final mesoporous inorganic scaffold, wich presents cylindrical unidirectional empty channels of approximately 2.5 nm of diameter (when CTAB is used as surfactant) arranged in a hexagonal distribution. The final solid presented a delicate structural order that is very difficult to obtain following traditional synthetic routes. One remarkable aspect of using this synthetic method is that the high grade of homogeneity of the initial elements remains in the final material, showing a system of pores not only homogeneously in size but also in form and regularity.

Finally, other important feature of this MCM-41 material is that making small changes in the synthesis route, it is possible to modify final important characteristics in the solid. For instance, when variying the structure directing agent the pore size is easily modulated (from 2 up to 50 nm).[43] In adittion, the particle morphology can also be tuned from micrometric and heterogeneous particles to create thin films, nanoparticles or monoliths.[44]

1.3.2 Functionalization of MCM-41 scaffolds: Obtention of organic-inorganic hybrid materials.

One important feature of the structure of mesoporous materials is their high concentration of structural defects in the form of silanol (Si-OH) groups. If the group H of the silanol is replaced by a chemical species capable of joining R by a covalent bond to the oxygen atom, a family of "hybrid materials" can be generated, in which the chemical composition of the fragment R is different from the inorganic framework. The most common cases are those in which R is an organic functional group or a silane, a chemical species of the type Si-R1, where R1 represents an organic group.[38] This modification of the inorganic matrix by the incorporation of organic components, either on the silica surface, as part of the silicate walls, or trapped within the channels, permits a precise control over the surface properties and pore sizes of the mesoporous sieves for specific applications and usually stabilize the materials towards hydrolysis.[45]

A wide range of properties can also be affected by this mixing of inorganic and organic moieties in the mesostructures. The inorganic components can

[43] S. A. Bagshaw, E. Prouzet, T. J. Pinnavaia, *Science*, **1995**, *269*, 1242.

[44] a) H. B. S. Chan, P. M. Budd, T. D. V. Naylor, *J. Mater. Chem.*, **2001**, *11*, 951. b) Q. Cai, Z.-S. Luo, W.-Q. Pang, Y.-W. Fan, X.-H. Chen and F.-Z. Cui, *Chem. Mater.*, **2001,** *13*, 258. c) S. P. Naik, W. Fan, T. Yokoi, T. Okubo, *Langmuir*, **2006**, *22*, 6391. d) J. Kobler, K. Moller, T. Bein, *ACS Nano*, **2008**, *2*, 791.

[45] K. Moller, T. Bein, *Chem. Mater.*, **1998**, *10*, 2950. b) G. A. Ozin, E. Chomski, D. Khushalani, M. J. MacLachlan, *Curr. Opin. Colloid Interface Sci.*, **1998**, *3*, 181.

provide mechanical, thermal, or structural stability, whereas organic groups can introduce flexibility into the framework, or change, for example, the optical properties of the solid. These additional properties, achieved through the development of hybrid inorganic-organic mesoporous solids, have provided a singnificant progress in the last few years towards their applications in different fields.

The functionalization process involves a treatment of the starting material with a solution of an alkoxide or alkoxysilane containing the functional group in an inert solvent. Then, the organic groups can be attached or anchored in the framework of mesoporous materials. This process can be carried out following two different procedures:

- **Co-condensation procedure:** during the synthesis itself, in one step. The co-condensation method usually leads to a homogeneous distribution of organic units along the material particles and between the surface thereof and the inner surface corresponding to the channels and cavities. The co-condensation procedure allows the incorporation of a relatively large amount of functional groups, which generally falls between 2 and 4 meq/g, in the most favorable cases. Using this mechanism of functionalization, the precursor of the functional group, usually a silane that contains one or more reactive groups such as chlorine, methoxy or ethoxy (terminal trialkoxyorganosilane), is incorporated into the synthesis gel from the start. In aqueous medium, alkoxy groups are hydrolyzed and react with the silica skeleton precursors generally alkoxides of silicon, to form the frame structure, in which the organic groups R are bonded to silicon atoms from the wall and can therefore interact with chemical species eventually present inside the channels and cavities. Some disadvantages that should be taken in account when this method is used are:
    - the degree of mesoscopic order of the products decreases when the trialkoxyorganosilane concentration is increased in the reaction mixture.

- homocondensation reactions between silane groups are increased. As a consequence, the ratio of terminal organic groups that are incorporated into the pore-wall network is, generally, lower than would correspond to the starting concentration in the reaction mixture. Also the homogeneous distribution of different organic functionalities in the framework cannot be guaranteed.
- the incorporated organic groups can lead to a reduction in the pore diameter, pore volume, and specific surface areas.
- finally, only the extraction method is available to carry out the removal of the surfactant, avoiding the calcination that would destroy the structure of the material due to the presence of organic groups in the skeleton.

- **Grafting procedure:** This is a post-synthesis functionalization method, thus allowing a selective modification of the surface of the material. In particular trialkoxysilane derivatives are reacted in the presence of the inorganic scaffold to give the condensation reaction previously reported. Grafting is generally brought preparing a suspension of the required quantity of the solid in an anhydrous solvent in the presence of the reactive silane precursor. The presence of the silanol groups on the silica scaffold surface guarantees the formation of a covalent bond between the trialkoxysilane precursors and the solid surface. It is important to remark that the subsequent covalent modification of the inorganic mesoporous scaffold does not modify the mesoporous structure of the solid, as demonstrated by X-ray diffraction powder evidences because only a superficial modification is usually obtained using this functionalization method.[46]

[46] F. Juan, E. Ruiz-Hitzky, *Adv. Mater.,* **2000**, *12*, 430.

In the present thesis we selected the second reported procedure, the grafting one, in all the synthesized materials. The selection of the grafting procedure, instead of the co-condensation method, is due to certain advantages such as:

- grafting grants the possibility of characterize the organic tiralkoxysilane derivative before the functionalization.
- functionalization by grafting allows a more rapid and efficient surfactant extraction by the calcination method.
- this method allows to firstly load the mesopore with certain molecules of interest and, then functionalizing with another category of organic compound, which is preferentially attached to the outer surface. Using this procedure, suitable hybrid materials for controlled delivery processes (see following section) are obtained.

A schematic representation of the above desribed two possible functionalization procedures for inorganic mesoporous materials is shown in Figure 4.

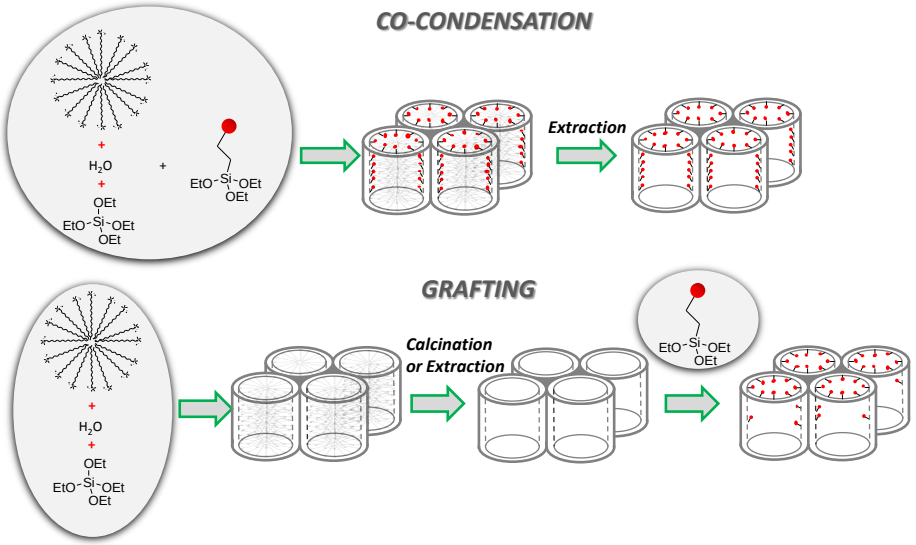

Figure 4. A Schematic representation of the functionalization procedures of MCM-41. Modified from *E. Climent PhD Thesis.*[47]

Finally, it is important to know that another way to incorporate organic compounds onto silicas is the production of *Periodic Mesoporous Organosilicas (PMOs*). This procedure makes possible the incorporation of organic groups as bridging components directly and specifically into the pore walls by the use of bis-silylated single-source organosilica precursors. In contrast to the organically functionalized silica phases described above, which are obtained by postsynthetic or direct synthesis, the organic units in this case are incorporated in the three-dimensional network structure of the silica matrix through two covalent bonds and thus distributed homogeneously in the pore walls. These materials, which are obtained as porous aero- and xerogels, can rise large inner surface areas (up to 1800 m^2 g^{-1}) as well as high thermal stability, whereas usually exhibit completely disordered pore systems. [48]

[47] E. Climent, *Design of new hybrid materials: Study of its application in new detection formats and in controlled release*, **2013**, ISBN: 978-84-9048-015.
[48] B. Hatton, K. Landskron, W. Whitnall, D. Perovic, G. A. Ozin, *Acc. Chem. Res.*, **2005**, *38*, 305.

1.3.3 Characterization of mesoporous materials.

As it has been explained in the above sections, a hybrid organic-inorganic mesoporous material is obtained after different steps that basically involve the synthesis of the inorganic scaffold and the subsequent incorporation of the organic groups by the selected functionalization procedure. Once the hybrid material is obtained, different characterization techniques have to be performed in order to verify different aspects. Among them, it is important to determine the integrity of the mesoporous structure after the functionalization procedure (and loading of the pores), the amount of organic matter that composes the final hybrid material and, in the case of preparation of mesoporous hybrid nanoparticles, it is also interesting to determine the particles average diameter and particles' shape. In the following lines the most useful techniques to characterize these materials will be mentioned.

To verify the achievement and the subsequent preservation, during loading and functionalization processes, of the mesoporous network, powder X-ray diffraction (PXRD), and transmission electronic microscopy (TEM) are very useful characterization techniques. As displayed in Figure 2 (in section 1.3.) one can clearly distinguish between a hexagonal, a cubic or a lamellar mesoporous phase by PXRD technique. Moreover, if the same X-ray diffraction pattern is displayed by the final hybrid material, it means that the mesoporous network remains. Apart from PXRD, TEM microscopy is also a useful technique to demonstrate the formation and preservation of a particular phase as well as the particle size and shape. In relation to the particle size, dynamic light scattering (DLS) can also be employed.

The organic-inorganic ratio of the final hybrid material can be determined by thermogravimetric (TGA) and or elemental analysis (EA). In some cases, it can be also useful the employment of Scanning Electron Microscopy coupled with Energy Dispersive X-ray (SEM/EDX) Spectroscopy. EDX is an X-ray technique used to identify the elemental composition of materials. EDX systems are attachments

to Electron Microscopy instruments (such as SEM) where the imaging capability of the microscope identifies the specimen of interest. The data generated by EDX analysis consist of spectra showing peaks corresponding to the elements making up the true composition of the sample being analysed. Using a combination of several techniques is usually better due to the complex conformation of this type of materials. For instance, problems related to differentiate the amount of two or more different organic molecules in the final material can be solved. For example, when a mesoporous silica based scaffold is firstly loaded with an organic dye and subsequently functionalized on the outer surface with a different trialkoxysilane derivative, the use of only one of these techniques could not be enough. UV-VIS or chromatographic monitorization of the quantity of the loaded compound, also result useful.

In order to demonstrate the effectiveness of both loading and grafting procedures, nitrogen adsorption-desorption isotherms (what is usually called "porosimetry measurements") can be useful. This technique allows the determination of the specific surface area of the material. This value can help us to compare between a calcined MCM-41 (very high surface area) and a loaded and functionalized MCM-41 scaffold (very low surface area). This is an indicative of a correct pore filling and subsequent anchoring of the organic molecules on the outer surface. Porosimetry measurements also give the pore size diameter and volume.

As summary, given the resulting data of all these characterizaion techniques, we should able to state if a hybrid material has conserved its mesoporous network and the degree of functionalization after the whole preparation process.

1.3.4 Applications of Organic-Inorganic Mesoporous Hybrid Materials.

Once described the synthesis procedures and main properties of hybrid organic-inorganic materials it is remarkable to show their extensive applications in several researh fields.

As it has been cited above, mesoporous silica materials have been used as effective scaffoldings for entrapping (bio)molecules because of their features, such as chemical inertness, thermal stability, three dimensional structure, high external surface, uniform pore systems that grants high load capacity, high specific surface area, well-known functionalization procedures and biocompatibility.[49]

Among important applications of this class of substrates, the most remarkable and recently studied are their use in heterogeneous-catalysis,[50] controlled delivery of chemical species,[51] chemical sensors[52] and environmental applications.[53] This PhD project is directly related with the design, synthesis and application of organic-inorganic mesoporous nanoscpic materials for the controlled delivery of chemical species.

---

[49] a) M. Vallet-Regí, A. Rámila, R. P. del Real, J. Pérez-Pariente, *J. Chem. Mater.* **2001**, *13*, 308. b) B. Muñoz, A. Rámila, J. Pérez-Pariente, I. Díaz, M. Vallet-Regi, *Chem. Mater.* **2003**, *15*, 500.

[50] S.-E. Park, and E.-Y. Jeong, 2014, *Heterogeneous Catalysis with Organic–Inorganic Hybrid Materials in Bridging Heterogeneous And Homogeneous Catalysis: Concepts, Strategies, And Applications,* Wiley-VCH Verlag GmbH & Co. KGaA, Weinheim, Germany. doi: 10.1002/9783527675906.ch3

[51] a) J. M. Rosenholm, E. Peuhu, L. T. Bate-Eya, J. E. Eriksson, C. Sahlgren, M. Linden*, Small,* **2010**, *6*, 1234. b) M. Liong, J. Lu, M. Kovochich, T. Xia, S. G. Ruehm, A. E. Nel, F. Tamanoi, J. I. Zink, *ACS Nano*, **2008**, *2*, 889. c) K.K. Cotí, M. E. Belowich, M. Liong, M. W. Ambrogio, Y. A. Lau, H. A. Khatib, J. I. Zink, N. M. Khashab, J. F. Stoddart, *Nanoscale*, **2009**, *1*, 16.

[52] M. K Patra, K. Manzoor, M. Manoth, S. C. Negi, S. R. Vadera, N. Kumar, *Defence Sci J*. **2008**, *58*, 636.

[53] S.S. Thakur, Chauhan G.S*., Ind. Eng. Chem. Res.*, **2014**, *53*, 4838.

In particular, functionalized mesoporous solids, have been extensively used in the development of stimuli-responsive gatekeeping materials that are able to entrap and transport molecules to specific locations,[54] or producing a controlled release of the encapsulated moiety due to the stimuli-responsive feature of the functionalized moieties or because of the presence of target molecules.[55]

In the next chapters of this PhD thesis several organic-inorganic hybrid materials (design, synthesis and applications) are going to be described.

1.3.5 Molecular Gates

Researchers have been inspired by the control of mass transport by channels that are present in nature acting as gates. Thus, the preparation of hybrid materials that mimics these channels, developing nanoscopic gated systems which respond to a stimuli, what is commonly reported as "*molecular gates*",[7] has been an attractive research area. Molecular gates can be defined as architectural nanoscopic supramolecular structures that incorporate various chemicals entities that allow a controlled release. Figure 5 shows a representation of a molecular gate and its working mechanism. The scheme shows an inorganic scaffolding loaded with an entrapped guest and with a suitable molecule anchored in the pore outlets, what is called molecular gatekeeper. The application of an extermal stimulus allows the release of the confined guest due to changes in the molecule than acts as gate.

[54] a) J. M. Rosenholm, E. Peuhu, L. T. Bate-Eya, J. E. Eriksson, C. Sahlgren, M. Linden, *Small*, **2010**, *6*, 1234. b) M. Liong, J. Lu, M. Kovochich, T. Xia, S. G. Ruehm, A. E. Nel, F. Tamanoi, J. I. Zink, *ACS Nano*, **2008**, *2*, 889.

[55] K.K. Cotí, M. E. Belowich, M. Liong, M. W. Ambrogio, Y. A. Lau, H. A. Khatib, J. I. Zink, N. M. Khashab, J. F. Stoddart, *Nanoscale,* **2009**, *1*, 16.

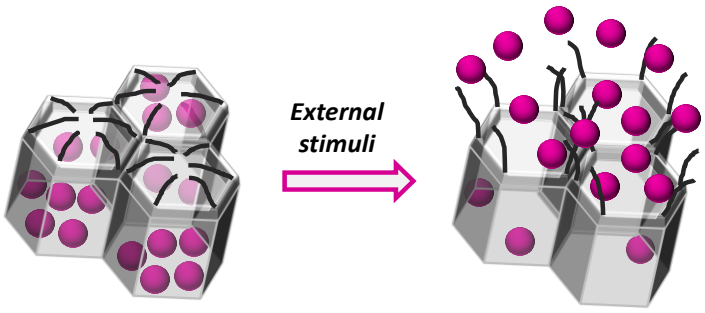

Figure 5. Representation of a nanoscopic molecular gate system working principle.

The first example of a molecular gate was reported by Fujiwara and coworkers in 2003.[14,15] Since then, a number of nanoscopic gated systems using mesoporous hybrid scaffoldings have been described. Inorganic nanoparticles,[18,20,56] polymers,[57] and larger supramolecular assemblies[58] have been used as blocking caps that control the opening/closing mechanism of the pore in mesoporous scaffolds. Moreover, different triggers, such as pH,[16,59] light,[60]

[56] a) E. Aznar, M . D. Marcos, R. Martinez-Manez, F. Sancenon, J. Soto, P. Amoros, P. Guillem, *J. Am. Chem. Soc.*, **2009**, *131*, 6833. b) J. L. Vivero- Escoto, I. I. Slowing, C. Wu, V. S.-Y. Lin, *J. Am. Chem. Soc.* **2009**, *131*, 3462.

[57] a) R. Liu, X. Zhao, T. Wu., P. Y. Feng, *J. Am. Chem. Soc*. **2008**, *130*, 14418. b) C. L. Zhu, X. Y. Song, W. H. Zhou, H. H. Yang, X. R. Wang, *J. Mater. Chem.,* **2009**, **19**, 7765.

[58] a) T. D. Nguyen, Y. Liu, S. Saha, K. C. F. Leung, J. F. Stoddart, J. I. Zink, *J. Am. Chem. Soc.* **2007**, *129*, *626*. b) R. Liu, Y. Zhang, P. Y. Feng, *J. Am. Chem. Soc.* **2009**, *131*, 15128.

[59] a) V. Cauda, C. Argyo, A. Schlossbauer, T. J. Bein, *J. Mater. Chem.*, **2010**, *20*, 4305. b) S. Angelos, Y. –W. Yang, K. Patel, J. F. Stoddart, J. I. Zink, *Angew. Chem. Int. Ed.*, **2008**, *47*, 2222. c) H. Meng, M. Xue, T. Xia, Y. –L. Zhao, F. Tamanoi, J. F. Stoddart, J. I. Zink, E. A. Nel, *J. Am. Chem. Soc.*, **2010**, *132*, 12690. d) J. Liu, X. Du, *J. Mat. Chem.*, **2010**, *20*, 3642. e) W. Guo, J. Wang, S. -J. Lee, F. Dong, S. S. Park, C. –S. Ha, *Chem. Eur. J.*, **2010**, *16*, 8641. f) A. Popat, J. Liu, G. Q. Lu, S. Z. Qiao, *J. Mater. Chem.,* **2012**, *22*, 11173, Y.-Y. Yan, J.-H. g) Y.-L. Sun, Y.-W. Yang, D.-X. Chen, G. Wang, Y. Zhou, C.-Y. Wang, J. F. Stoddart, *Small* , **2013**, *9*, 3224.

[60] a) E. Johansson, E. Choi, S. Angelos, M. Liong, J. I. Zink, *Sol-Gel Sci. Technol.*, **2008**, *46*, 313. b) J. Lai, X. Mu, Y. Xu, X. Wu, C. Wu, C. Li, J. Chen, Y. Zhao, *Chem. Commun.,* **2010**, *46*, 7370. c) Y.-L. Sun, B.-J. Yang, S.X.-A. Zhang, S. X.-A., Y.-W., Yang, *Chem.-Eur. J*., **2012**, *18*, 9212.

redox potential,[57a,61] temperature[62] or target (bio)molecules[63] have been employed as the stimuli that cause the uncapping the pores and the subsequent delivery of the guest molecules.

In these last years, the incorporation of certain biomolecules in the design of these stimuli-responsive nanoscopic gated systems has been deeply explored. In this sense, some biomolecules, specially enzymes,[64] have been used as the stimuli that triggers the uncapping of the gated-scaffolds, whereas other biomolecules, such as sachharides,[65] peptides,[66] or DNA,[67] have been employed as gatekeeping supramolecules.

---

[61] R. Mortera, J. Vivero-Escoto, I. I. Slowing, E. Garrone, B. Onida, V. S.-Y. Lin, *Chem. Commun.,* **2009***,* 3219.

[62] a) C. Liu, J. Guo, W. Yang, J. Hu, C. Wang, S. Fu, *J. Mat. Chem.*, **2009***, 19*, 4764. b) J. Lai, X. Mu, Y. Xu, X. Wu, C. Wu, C. Li, J. Chen, Y. Zhao, *Chem. Commun.,* **2010**, *46*, 7370. c) C. R. Thomas, D. P. Ferris, J. –H. Lee, E. Choi, M. H. Cho, E. S. Kim, J. F. Stoddart, J. –S. Shin, J. Cheon, J. I. Zink, *J. Am. Chem. Soc.,* **2010**, *132*, 10623.

[63] a) C. Coll, R. Casasús, E. Aznar, M. D. Marcos, R. Martínez-Máñez, F. Sancenón, J. Soto, P. Amorós, *Chem. Commun.*, **2007**, 1957. b) E. Aznar, C. Coll, M. D. Marcos, R. Martínez-Máñez, F. Sancenón, J. Soto, P. Amorós, J. Cano, E. Ruiz, *Chem. Eur. J.*, **2009**, *15*, 6877. c) Y. Zhao, B. G. Trewyn, I. I. Slowing, V. S.-Y. Lin, *J. Am. Chem. Soc.,* **2009***, 131*, 8398. d) Y. L. Choi, J. Jaworsky, M. L. Seo, S. J. Lee, J. H. Jung, *J. Mater. Chem.,* **2011**, *21*, 7882. e) A. Schulz, R. Woolley, T. Tabarin, C. McDonagh, *Analyst*, **2011**, *136*, 1722. f) J. Lee, J. Lee, S. Kim, C. –J. Kim, S. Lee, B. Min, Y. Shin, C. Kim, *Bull. Korean Chem. Soc.*, **2011**, 32, 1357. g) I. Candel, A. Bernardos, E. Climent, M. D. Marcos, R. Martínez-Máñez, F. Sancenón, J. Soto, A. Costero, S. Gil, M. Parra, *Chem. Commun*. **2011**, *47*, 8313. h) R. Villalonga, P. Díez, A. Sánchez, E. Aznar, R. Martínez-Máñz, J. M. Pingarrón, *Chem. Eur. J.*, **2013**, *19*, 7889. i) M. Oroval, E. Climent, C. Coll, R. Eritja, A. Aviñó, M.D. Marcos, F. Sancenón, R. Martínez-Máñez, P. Amorós, *Chem. Commun.,* **2013**, *49,* 5480.

[64] a) K. Patel, S. Angelos, W. R. Dichtel, A. Coskun, Y. –W. Yang, J. I. Zink, J. F. Stoddart, *J. Am. Chem. Soc.,* **2008***, 130*, 2382. b) C. Park, H. Kim, S. Kim, C. Kim, *J. Am. Chem. Soc.,* **2009***, 131*, 16614.

[65] A. Bernardos, L. Mondragón, E. Aznar, M. D. Marcos, R. Martínez-Máñez, F. Sancenón, J. Soto, J. M. Barat, E. Pérez-Payá, C. Guillem, P. Amorós, *ACS Nano*, **2010**, *4*, 6353.

[66] F. Porta, G. E. M. Lamers, J. I. Zink, A. Kros, *Phys. Chem. Chem. Phys.,* **2011**, *13*, 9982.

[67] a) A. Schossbauer, S. Warncke, P. M. E. Gramlich, J. Kecht, A. Manetto, T. Carell, T. Bein, *Angew. Chem.Int. Ed.*, **2010**, *49*, 4734. b) Y. Zhang, Q. Yuan, T. Chen, X. Zhang, Y. Chen, W. Tan, *Anal. Chem.*, **2012**, *84*, 1956.

As stated above, a number of examples of molecular gated systems for controlled release have been described in the literature. In the following sections a short review including some of that work, classified depending on the stimulus which drives the gate opening, is presented.

1.3.5.1 *Light-Driven Molecular Gates*

Light was the stimulus employed by Fujiwara and coworkers in the preparation of the first molecular gate system reported.[14,15] They were inspired by the grafting of photoresponsive organic molecules in mesoporous silica supports. The system designed by these authors was based on preparing a release nanodevice by grafting 7-[(3-triethoxysilyl)propoxy]coumarin onto a MCM-41 scaffold. The intermolecular photodimerization of coumarin to the bulky cyclobutane dimer results in the blockage of the pore entrances (upon irradiation with $\lambda > 310$ nm). To test the hybrid material as drug delivery nanodevice, the authors filled the pore voids with cholestane and other steroid hormones. The irradiation at wavelengths > 310 nm induced the photodimerization of the coumarin molecule, closing the pores by formation of the cyclobutane dimer and preventing the leaching of the drugs. However, when this gatekeeping molecule was irradiated with UV light (250-260 nm), the cleavege of the dimmer was induced (by a photo-opening of cyclobutane ring and the coumarin monomer regeneration) allowing the release of the drugs contained inside the pores of the material. Figure 6 shows a schematic representation of this process.

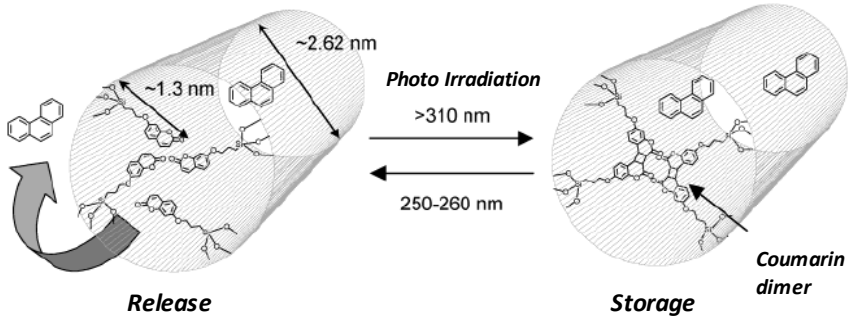

Figure 6. Schematic representation of the first light-driven molecular gate material. *(Reprinted with permission from M. Fujiwara et al., Chem. Mater. 2003, 15, 3385. Copyright © 2003 American Chemical Society).*

In this light-driven molecular gates area, the research groups of Brinker,[68] Zink[69] and Stoddart[70] have designed different nanodevces using azobenzene moieties as photoactivable molecules.

One step forward was given by Martínez-Máñez et al., that described the first example of a two-input (photochemical and chemical) gated hybrid system operative in water.[71] The nanodevice consists of spiropyran photochrome units attached to the external surface of the mesoporous MCM-41 type solid loaded with the dye tris(2,2'-bipyridyl)ruthenium chloride) $[Ru(bipy)^3]^{+2}$. The spiropyran units could be transformed reversibly between two forms, the neutral spirocyclic and the positively charged merocyanine, upon the application of an external UV-

[68] a) N. G. Liu, Z. Chen, D. R. Dunphy, Y. –B. Jiang, R. A. Assink, C. J. Brinker, *Angew. Chem. Int. Ed.*, **2003**, *42*, 1731. b) N. G. Liu, D. R. Dunphy, P. Atanassov, S. D. Bunge, Z. Chen, G. P. Lopez, T. J. Boyle, C. J. Brinker, *Nano Lett.*, **2004**, *4*, 551.

[69] a) S. Angelos, E. Choi, F. Vögtle, L. De Cola, J. I. Zink, *J. Phys. Chem.*, **2007**, *111*, 6589. b) J. Liu, E. Choi, F. Tamanoi, J. I. Zink, *Small*, **2008**, *4*, 421.

[70] D. P. Ferris, Y. –L. Zhao, N. M. Khashab, H. A. Khatib, J. F. Stoddart, J. I. Zink, *J. Am. Chem. Soc.*, **2009**, *131*, 1686.

[71] E. Aznar, R. Casasús, B. García-Acosta, M. D. Marcos, R. Martínez-Máñez, F. Sancenón, J. Soto, P. Amorós, *Adv. Mater.*, **2007**, *19*, 2228.

light source (see Figure 7). The controlled release of this gated material was achieved by the use of negatively charged G1.5 PAMAM dendrimers as molecular caps, due to the coulombic interaction between the negatively charged G1.5 PAMAM dendrimer and the positively charged merocyanine. The cargo of the solid remained on the mesopores in the darkness due to the electrostatic interaction between the negatively charged dendrimers and the positively charged merocyanine form. When the cargo was required to be released, the material was irradiated with visible light, reverting the merocyanine molecule to their neutral spirocyclic form with no affinity for the dendrimers, thus allowing release of the entrapped molecules to the bulk solution.

On the other hand, the second stimulus involved in this system was a change of pH. The solid was switched on/off by simple adjustment of the pH, due to the protonation of the carboxylate moieties present in the dendrimers.

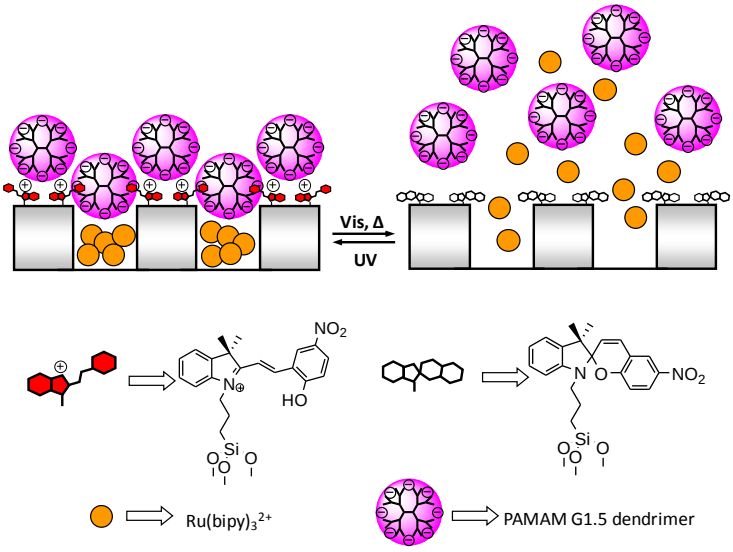

Figure 7. Schematic representation of two-input gated hybrid system, composed by a MCM-41 support functionalized with spirobenzopyran derivatives and capped with PAMAM G1.5 dendrimers. (*Reprinted with the permission from Adv. Mater., 2007, 19, 2228. Copyright © 2007 John Wiley & Sons)*

At acidic pH (pH ca. 2) G1.5 PAMAM dendrimers are protonated, which results in a loss of interaction between them and the charged merocyanine isomer producing the dye delivery. At neutral pH, interaction of G1.5 PAMAM dendrimers with the merocyanine locked the gate in its closed state (see also Figure 7).

More recently, other light-switchable supramolecular nanovalves based on cucurbituril CB[7]-cinnamamides have been reported by Huang et al.,[72,73] and their sustained controlled-release of model compounds in biological media have been tested. Light and pulsed light were used as "remote control" stimuli for the controlled release of cargo from mesoporous silica nanoparticles (MSNs) (Figure 8), showing rapid and directional processes and low invasiveness in biological systems. Cucurbit[7]uril (CB[7]) has a suitable cavity and reasonable water solubility, and can form stable host–guest complexes with *trans*-cinnamamide derivatives, which undergoes a *trans*- to *cis*-conformational change upon UV light irradiation (300 nm), leading to complex dissociation due to steric hindrance effect. The surfaces of MSNs were functionalized with cinnamamide-containing stalks surrounded by CB[7] rings to act as a photoresponsive gating system. In biological relevant media, that is, pure water, phosphate buffer solution (PBS), and fetal bovine serum (FBS), CB[7] can be threaded onto the stalks and bind to trans-cinnamamide units, thus sealing the nanopores to prevent premature release of the preloaded cargos. Upon irradiation with 300 nm of light, the isomerization of *trans*-to-*cis*-cinnamamide units results in the dissociation of CB[7] rings from the stalks, thus opening the gates and releasing the cargos. The hydrophilic nature of the system overcomes the drawback of UV light in real biological systems, and potentially serves the need of accurately controlling drug release dose in targeted disease areas.

[72] Q. Lin, Q. Huang, C. Li, C. Bao, Z. Liu, F. Li, L. Zhu, L. *J. Am. Chem. Soc.*, **2010**, *132*, 10645.
[73] Y.B. Zheng, Q. Hao, Y.-W. Yang, T. J. Huang, *J. Nanophotonics,* **2010**, *4*, 042501.

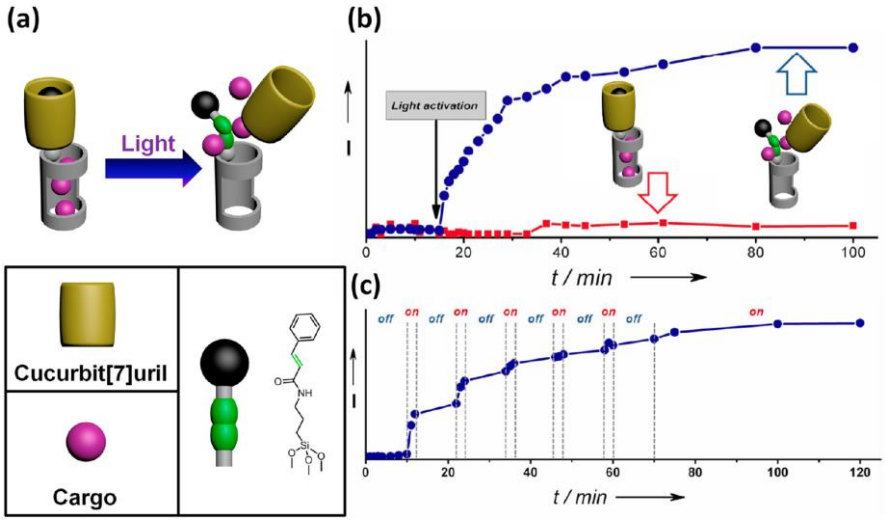

Figure 8. (a) CB[7]-based light-switchable mechanized MSNs and their release profiles upon (b) continuous light and (c) pulsed light irradiation. *(Reprinted with permission from Acc. Chem. Res. 2014, 47, 1950. Copyright © 2014 American Chemical Society).*

Another recent light-responsive hybrid system was reported by R. Martínez-Máñez et al.[74] In this case the authors designed a new nanoscopic mesoporous system capped with a photo-cleavable *o*-methoxybenzylamine fragment for controlled release. *o*-methoxybenzylamine group was selected due to its known photo-cleavage properties. Based on this a bulk compound was designed, which contained the photo-cleavable group and two tert-butyl moieties to achieve an effective pore blockage in the final hybrid material (see Figure 9). This designed molecule resulted to be bulky enough to preclude delivery of the entrapped cargo and, at the same time, it was expected to undergo photolysis upon UV light irradiation. As a result of photolysis, the steric hindrance of the capping molecule decreased considerably, thus allowing the release of the entrapped dye. A schematic representation of the controlled delivery paradigm is shown in Figure 9.

[74] A. Agostini, F. Sancenón, R. Martínez-Máñez, M. D. Marcos, J. Soto, P. Amorós, *Chem. Eur. J.* **2012**, *18*, 12218.

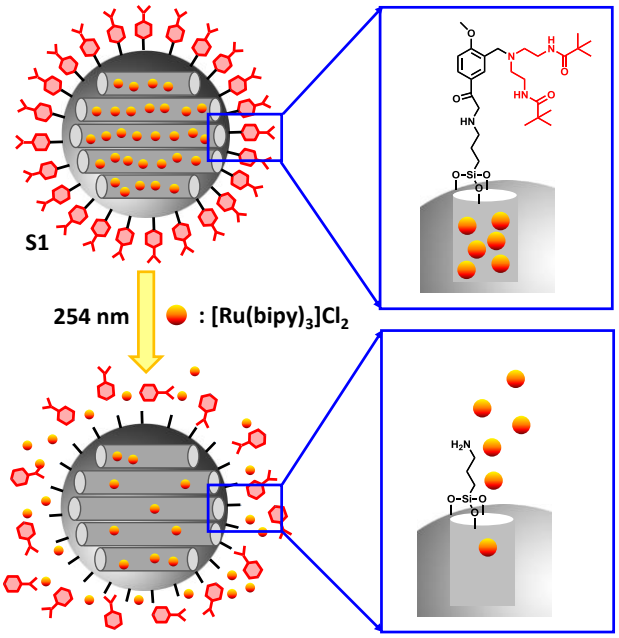

Figure 9. Schematic representation of the photo-driven uncapping mechanism of the designed molecular gate. It is shown the synthesized functionalization molecules structure, that upon irradiation at 254nm result photocleaved and the cargo entrapped in the pores is released. *Reprinted with permission from Chem. Eur. J. 2012, 18, 12218. Copyright © 2012 Wiley-VCH Verlag GmbH&Co. KGaA, Weinheim.*

1.3.5.2 *Redox-Driven Molecular Gates.*

Redox reactions have also been widely used for the development of gated mesoporous hybrid materials. Some of the examples of this type of gated systems display gating response in pure water. Furthermore, the labile redox linkages that connect the capping molecules with the mesoporous surface are easy cleaved by certain reducing agents, what suggests that they could also be opened by certain antioxidants produced by cells.

One approache used in this field is based on the stabilization/destabilization of supramolecular complexes via the

oxidation/reduction of suitable groups. For instance, Stoddart and Zink reported the first example of these redox-driven hybrd materials.[75] The authors developed a mesostructured silica thin film with a luminescent molecule in the inner of the pores, tris(2-phenylpyidine) iridium ($Ir(ppy)_3$), and a [2]pseudorotaxane, formed by 1,5-dioxynaphthalene (DNPD) encircled, through non-covalent interactions, with a cyclobis(paraquat-*p*-phenylene) ($CBPQT^{4+}$) macrocycle, grafted onto surface (see Figure 10). When the reducing agent $NaCNBH_3$ was present, the reduction of the DNPD was produced with the subsequent dethreading $CBPQT^{4+}$ ring and the release of the entrapped complex.

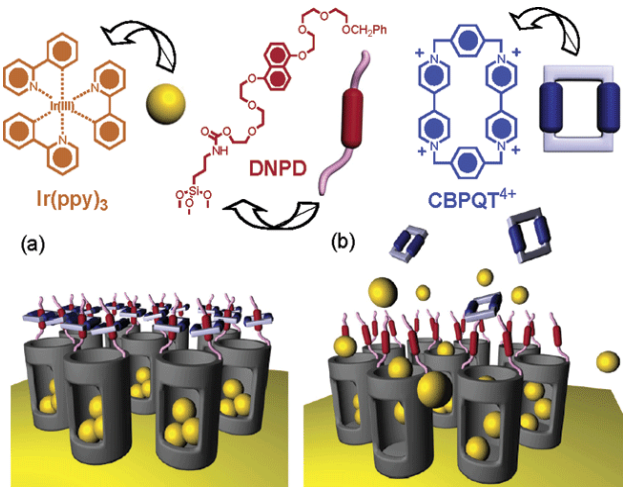

Figure 10. Schematic representation of the performance of redox nanovalves due to the destabilization of the supramolecular complex produced between $CBPQT^{4+}$ and DNPD. *(Reprinted with the permission from J. Am. Chem. Soc., 2004, 126, 3370. Copyright © 2004 American Chemical Society).*

Furthermore, Stoddart's and Zink's groups, have developed similar systems employing pseudorotaxanes and rotaxanes as redox-driven gatting molecules. For example, a reversible molecular valve based on a double redox-

[75] R. Hernandez, H.-R. Tseng, J. W. Wong, J. F. Stoddart, J. I. Zink, *J. Am. Chem. Soc.* **2004**, *126*, 3370.

active bis-stable [2]rotaxane was reported[76] (see Figure 11). In this system, the [2]rotaxane contains DNPD and tetratuiafulvalene (TTF), as redox centers which were connected through a oligoethyleneglycol chain with a rigid terphenylene space, and $CBPQT^{4+}$ as movable molecule. Upon addition of an oxidant or reducing agent, a redox-induced movement was subsequently produced. This fact was due to a change in the oxidation state of TTF and, consequently, the preference of $CBPQT^{4+}$ for TTF or DNPD groups. That redox-induced movement changed the state of the gate from closed to open.

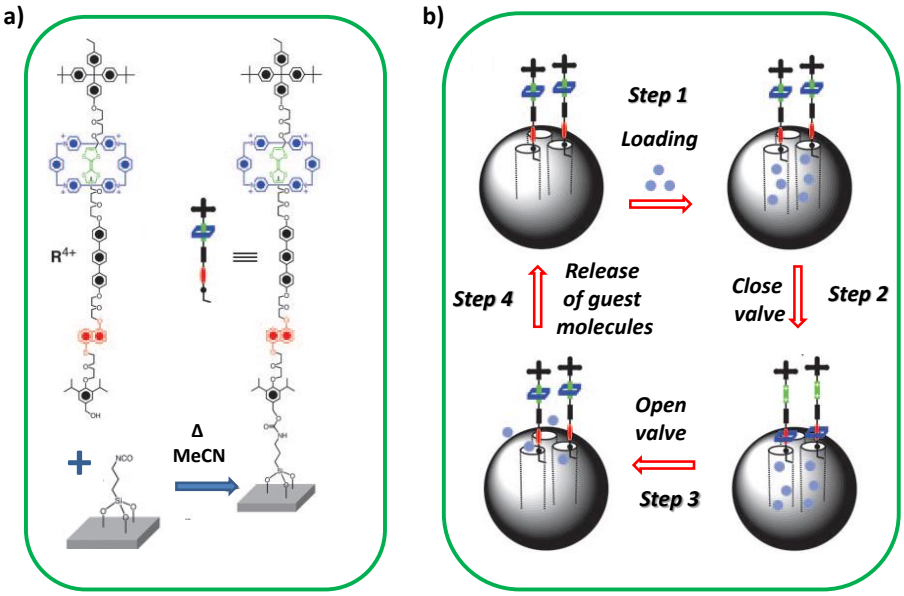

Figure 11. Graphical representations of the surface attachment of bistable rotaxanes to silica particles along with a cycle for loading and release of guest molecules.(a) The structural formula of the bistable [2]rotaxane R4 and the procedure used for tethering R4 to the surface of mesoporous silica particles. (b) The proposed mechanism for the operation of the nanovalve. *(Modified from Proc. Natl. Acad. Sci. U.S.A., 2005, 102, 10029.Copyright ©2005 by The National Academy of Sciences of the USA).*

[76] T. D. Nguyen, H. –R. Tesng, P. C. Celestre, A. H. Flood, Y. Liu, J. F. Stoddart, J. I. Zink, *Proc. Natl. Acad. Sci. U.S.A.*, ***2005***, *102*, 10029.

A different design of redox-driven molecular gates was reported by Lin's group. The authors employed different nanoparticles anchored to the surface of silica mesoporous supports (SMP) through different covalent linkers able to be broken by the addition of certain redox agents, and allowing, as a consequence, the release of the entrapped guests. The first example was presented in 2003.[18] The authors prepared a hybrid material by loading the pores of the MCM-41 scaffold with bioactive molecules (vancomycin or ATP) and functionanalized the external surface of the solid with with 2-(propyldisulfanil)ethylene diamine. The blocking of the pores was induced using 2 nm CdS nanocrystals derivatized with mercaptoacetic acid. The CdS nanoparticles were attached to the modified scaffold through an amidation reaction between the carboxylic acids and the amine group anchored into the solid surface. Then, the presence of reductors, such as dithiotheritol (DTT) or mercaptoethanol (ME), produced the breaking of the disulfide bridges that linked the CdS nanoparticles with the hybrid materials, allowing the cargo release.

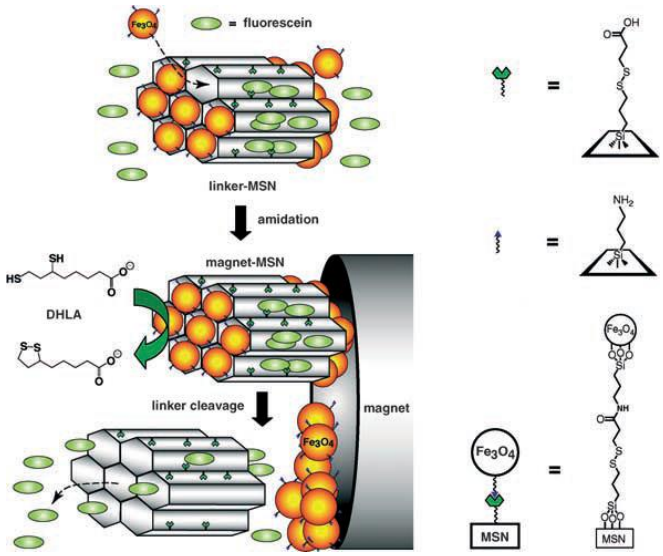

Figure 12. Schematic representation of the stimuli-responsive delivery system based on mesoporous silica nanorods capped with superparamagnetic iron oxide nanoparticles. *(Reprinted with the permission from Angew. Chem. Int. Ed. 2005, 44, 5038. Copyright © 2005 Wiley-VCH Verlag GmbH & Co. KGaA, Weinheim).*

Other similar work presented by the same authors is based on the grafting onto MCM-41 surface of 3-(propyldisulfanyl)propionic acid groups.[20] The pores were loaded with fluorescein dye in this case and then capped with Fe_3O_4 magnetic nanoparticles functionalized with 3-aminopropyltriethoxysilyl groups. An amidation reaction between the carboxylic acids grafted in the inorganic support and the amine of the Fe_3O_4 nanoparticles leads to pore closure. Addition of a reducing agent allowed the rupture of the disulfide linkage and the release of fluorescein. A schematic representation of the system can be observed in Figure 12.

1.3.5.3 *pH-driven Molecular Gates*

pH is other stimulus used to develop open/close protocols in mesoporous gated materials. The inclusion of ionizable organic moieties anchored onto the pore outlets of mesoporous supports, which might change in size or shape upon protonation or deprotonation processes, is a usual procedure followed to prepare materials capable of controlling mass transport by pH modulations. pH-controlled gate-like scaffoldings present certain advantageous features such as reversibility and gate-like behaviour in aqueous solution.

R. Martínez-Máñez and coworkers developed the first pH driven molecular gate in 2004.[16] This new hybrid material consists of a UVM-7 (that belongs to MCM-41 family) solid support functionalized on the external surface with 3-[2-(2-aminoethylamino)ethylamino]propyltrimethoxysilane and in the inner of the pores with thiol groups. The pH dependent open-close paradigm was tested by the addition of a squaraine dye to the reaction mixture. The selection of this dye was due to its particular feature of having an intense light blue color that is lost when reacts with thiols yielding a colorless derivative.[77] When pH is acid, the polyamines are in their protonated form, a rigid-like conformation and blocking the pores access. This inhibited dye access to the pores and the solution

[77] J. V. Ros-Lis, B. García-Acosta, D. Jiménez, R. Martínez-Máñez, F. Sancenón, J. Soto, F. Gonzalvo, M. C. Valldecabres, *J. Am. Chem. Soc.,* **2004,** *126*, 4064.

remained blue. However, when the pH was increased to neutral, the polyamines were partially deprotonated, this allowed the access of squaraine dye to the pores and the reaction between the dye and the thiols was produced, giving a colorless solution. Bearing in mind this system, a similar hybrid material for anion recognition and signaling was reported by the same group. In this case, a MCM-41 solid support was selected, loaded with $Ru(bipy)_3^{2+}$ dye and then the same polyamine reported above was grafted on the outer surface.[78] This developed material was able to diferenciate GMP from ATP and ADP due to the dye delivery inhibition induced by the differential coordination of the polyamines with these nucleotides. The behavior of the same material at different pH and in the presence of several anions (of different sizes, shapes and charge), was studied some years later. In this last case, the hybrid material acted as pH-driven and anion-controlled nano-supramolecular gate-like system.[79] A representative scheme of the developed material is shown in Figure 13.

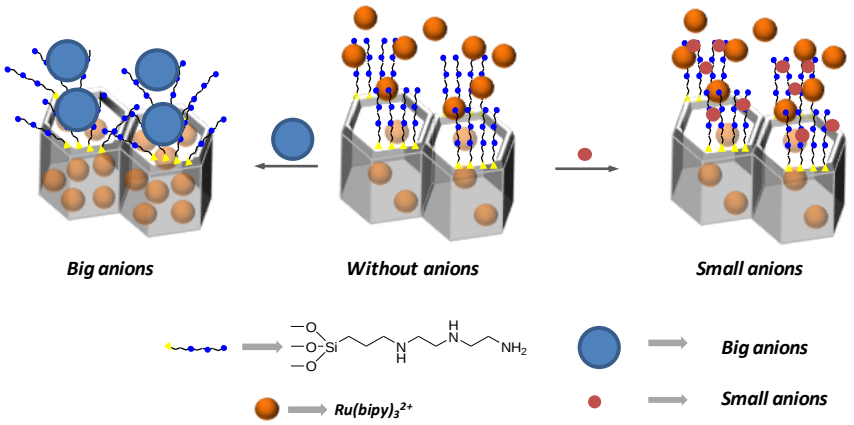

Figure 13. Schematic representation of pH-driven and anion-controlled nano-supramolecular gate-like material. *(Adapted from E. Climent thesis).*[47]

[78] R. Casasús, E. Aznar, M. D. Marcos, R. Martínez-Máñez, F. Sancenón, J. Soto, P. Amorós, *Angew. Chem.Int. Ed.*, **2006,** *45*, 6661.

[79] c) R. Casasús, E. Climent, M. D. Marcos, R. Martínez-Máñez, F. Sancenón, J. Soto, P. Amorós, J. Cano, E. Ruiz, *J. Am. Chem. Soc.,* **2008***, 130*, 1903.

Finally, the same authors reported the use of this pH-controlled gate-like scaffolding as a prototype for the selective delivery of riboflavin at the intestine.[80] The different pH from stomach (acid pH) compared to the intestine (basic pH) was the fact that gave the idea in this nanodevice design. Because of this pH difference, this hybrid material was an applicable delivery system designed to protect the cargo from the acidic conditions of the stomach.

Since that first example of a pH-driven hybrid system with mesoporous materials was described, the interest in exploring this area has increased, and a number of examples have been published. These pH-driven gated materials could find promising applications due to the important role played by pH changes in biological processes. For example, pH variations have been exploited to control the delivery of drugs in specific organs (such as the gastrointestinal tract or the vagina), as it has been cited before with the rivoflavin example, or intracellular compartments (such as endosomes or lysosomes), as well as to trigger the release of the drug when subtle environmental changes are associated with pathological situations, such as cancer or inflammation.[81] Two main strategies exist to develop pH-responsive nanodevices for therapeutic applications: the use of polymers (polyacids or polybases) with ionizable groups, anchored at the material surface, that undergo conformational and/or solubility changes in response to environmental pH variation; and the design of polymeric systems with acid-sensitive bonds whose cleavage enables the release of molecules grafted at the polymer backbone.

Furthermore, anticancer drug-delivery systems that have taken advantage of the slight difference of pH existing between healthy tissues (~7.4) and the extracellular environment of solid tumours (6.5–7.2) have been described. This is mainly a consequence of irregular angiogenesis in fast-growing tumours, which causes a rapid deficit of both nutrients and oxygen and thus a shift towards a

[80] A. Bernardos, E. Aznar, C. Coll, R. Martínez-Máñez, J. M. Barat, M. D. Marcos, F. Sancenón, J. Soto, *J. Control. Rel.*, **2008**, *131*, 181.

[81] S. Mura, J. Nicolas, P. Couvreur, *Nature Mater.*, **2013**, *12*, 991.

glycolytic metabolism, therefore leading to the production of acidic metabolites in the tumour interstitium. Moreover, bacterial infections are generally characterized by very low pH values because of anaerobic fermentation and this effect produces subsequent inflammation. Therefore, pH-driven nanodevices are also suitable for the possible treatment of some pathogen infections. In the next lines, some examples of pH-driven hybrid materials related to drug delivery applications are exposed.

For instance, poly(methacrylic acid)-based copolymers have been used as pH-sensitive coatings at the surface of porous silica nanoparticles,[82] in order to protect drugs against the harsh conditions found in the gastric cavity and to improve their absorption in the intestine. This charge-reversal approach was also applied to MSNs to achieve drug release at neutral pH by taking advantage of electrostatic interactions.[83]

At the cellular level, the acidification of endosomes (pH ~5–6) and their fusion with lysosomes (pH ~4–5) is another pH gradient that can be used for effective intracellular drug accumulation. A MSN delivery system capable of drug delivery based on the function of β–cyclodextrin (β-CD) nanovalves, was designed by Zink and coworkers.[84] The surface of the nanoparticles was functionalized with a series of aromatic amines that acted as the stalk and β-cyclodextrin (β-CD) as the cap (see Figure 14 a). The β-CD ring encircled the stalks as a result of noncovalent bonding interactions under neutral pH conditions and effectively blocked the nanopore openings and traps the included cargo molecules. Lowering of the pH leads to protonation of the aromatic amines, followed by β-CD cap release and cargo diffusion from the nanopores.

[82] W. Qu, Y. Li,L. Hovgaard, S. Li, W. Dai, J. Wang, X. Zhang, Q. Zhang,*Int. J. Nanomed.,* **2012***, 7***,** 4983.
[83] C-H.Lee,L-W. Lo, C-Y. Mou, C-S. Yang, *Adv. Funct. Mater.,* **2008***, 18***,** 3283.

[84] Y. Klichko, N. M. Khashab, Y. –W. Yang, S. Angelos, J. F. Stoddart, J. I. Zink, *Micropor. Mesopor. Mater.*, **2010**, *132*, 435.

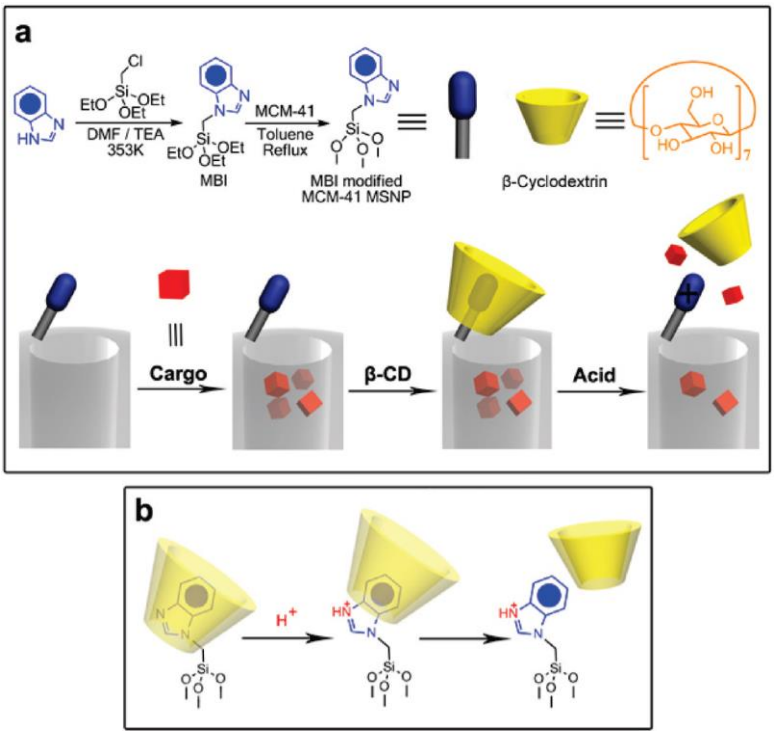

Figure 14. A graphical representation of the pH responsive MSNP nanovalve. a) Synthesis of the stalk, loading of the cargo, capping of the pore, and release of the cap under acidic conditions. b) Details of the protonation of the stalk and release of the *β*-cyclodextrin. *(Reprinted with the permission from J. Am. Chem. Soc., 2010, 132, 12690. Copiright © 2010 American Chemical Society).*

This system was responsive to the endosomal acidification conditions in human differentiated myeloid (THP-1) and squamous carcinoma (KB-31) cell lines. Furthermore, it was demonstrated how to optimize the surface functionalization of the MSNP to provide a platform for rapid doxorubicin release to the nuclei of KB-31 cells. Figure 14 shows a representation of this designed system.

The examples mentioned above demonstrate the potential applicability of pH as external stimuli for controlled release, specially in drug delivery.

1.3.5.4 *Temperature-Driven Molecular Gates*

Temperature has also been used as stimulus in controlled release processes. The first nanoscopic gated hybrid material temperature-driven was prepared using modified silica mesoporous supports (SMP) functionalized with the well-known temperature sensitive polymer, poly(*N*-isopropylacrylamide) (PNIPAAm).[85] This polymer exhibits a hydrophilic–hydrophobic transition at a "lower critical solution temperature" (LCST) of about 32°C in water. Below the LCST, the polymer is in the coil conformation (hydrated), while above the LCST it is in the globule or collapsed state (dehydrated). Temperature triggered control of molecular transport through the porous network of the hybrid particles was demonstrated by measuring release of fluorescein. The fluorescein in the silica/PNIPAAm particles was released slowly at room temperature (below the LCST of PNIPAAm) and faster at 40 °C (above the LCST). This is due to the PNIPAAm chain being hydrated and expanded at room temperature such that the entrapped fluorescein could not easily permeate through the porous network. At 40 °C, the PNIPAAm is dehydrated and collapsed so that the entrapped fluorescein can readily diffuse through the porous network and be released from the microparticles. Using this polymer, several autors designed different approaches for the preparation of thermally responsive hybrid mesoporous materials.[86]

R. Martínez-Máñez and co-workers prepared a new taylor made thermoresponsive hybrid system using paraffines as capping agents.[87] These materials were prepared using MCM-41 nanoparticles functionalized with octadecyltrimethoxysilane and paraffins. These paraffins coated the nanoparticles

[85] Q. Fu, G. V. R. Rao, L. K. Ista, Y. Wu, B. P. Andrzejewski, L. A. Sklar, T. L. Ward, G. P. López, *Adv. Mat.*, **2003***, 15*, 1262.

[86] a) Q. Fu, G. V. R. Rao, T. L. Ward, Y. Lu, G. P. López, *Langmuir*, **2007**, *23*, 170. b) Y. –Z. You, K. K. Kalebaila, S. L. Brock, D. Oupicky, *Chem. Mater.,* **2008***, 20*, 3354.

[87] E. Aznar, L. Mondragón, J.V. Ros-Lis, F. Sancenón, M. D. Marcos, R. Martínez-Máñez, J. Soto, E. Pérez-Payá, P. Amorós*, Angew. Chem. Int. Ed.* **2011**, *50*, 11172.

forming a hydrophobic layer around the pore outlets due to the van der Waals interactions between them and the octadecyl chain covalently linked to the inorganic support. This hydrophobic layer around the pore outlets inhibited the cargo release. When the temperature rises, the paraffin melting point the release of the entrapped guest was produced. With this mechanism a finely tuned tailor-made temperature triggered delivery was achieved. To investigate the biological application of these coated materials as drug nanocarriers for an intracellular temperature-controlled release, a solid loaded with the chemotherapeutic agent doxorubicin was prepared and then it was functionalized with the same procedure than the one explained above. The material was tested in human cervix carcinoma HeLa cells. The sample incubated at 42 °C (melting temperature of the coating paraffin) exhibited features of doxorubicin-induced cell death, whereas that incubated at 37 °C showed healthy cells.

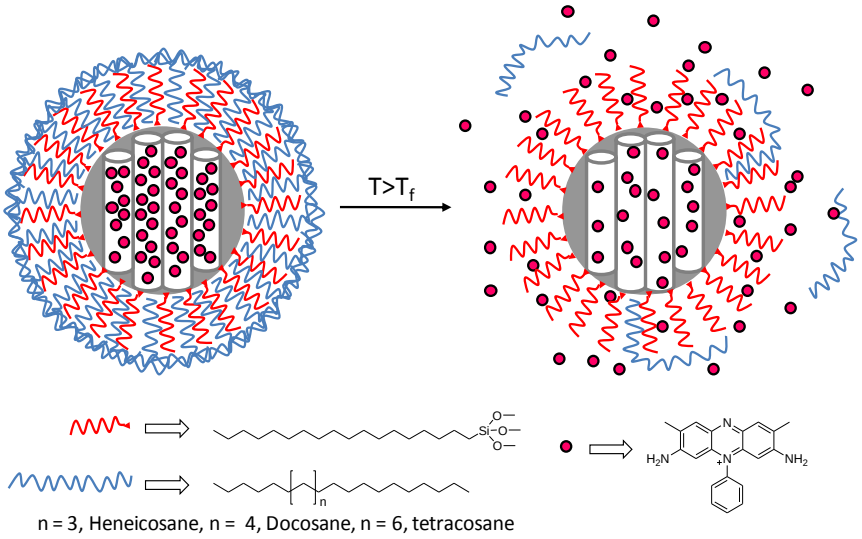

Figure 15. Schematic representation of the gated material functionalized with octadecyltrimethoxysilane and capped with paraffins. The delivery of the entrapped guest (safranine O) is triggered when temperature rises above paraffin melting point. (*Reprinted with the permission from Angew. Chem. Int. Ed., 2011, 50, 11172. Copyright © 2011 WILEY-VCH Verlag GmbH & Co. KGaA, Weinheim).*

With these results and bearing in mind the possibility to select a wide range of paraffins with specific melting points over a wide range of temperatures, this system can be suitable for applications that demand zero release before stimulus implementation and render them important for delivery applications triggered by selected global or local temperature changes, specially in biological applications. A schematic mechanism of the function of this temperature-responsive system can be observed in Figure 15.

Very recently, the same authors developed a novel temperature-controlled delivery system using changes in the conformation of a peptide anchored onto the external surface of mesoporous silica nanoparticles.[88] In this new approach, in which peptides could act as caps, the underlying idea was to use the well-known temperature-controlled α-helix-to-disordered transformation that occurs in certain amino acid sequences. With this concept in mind, a self-aggregating 17-mer peptide, designed to adopt a high level of α-helical conformation, was used as temperature-driven molecular gate. Folding in α-helical bundles inhibited cargo delivery, whereas transformation to a disordered conformation reduced the steric crowding around the pore outlets and the subsequent cargo release was produced. Figure 16 shows the device design and the temperature-responsive uncapping paradigm.

[88] C. de la Torre, A. Agostini, L. Mondragón, M. Orzáez, F. Sancenón, R. Martínez-Máñez, M.D. Marcos, P. Amorós, E. Pérez-Payá, *Chem. Commun.,* **2014**, *50*, 3184.

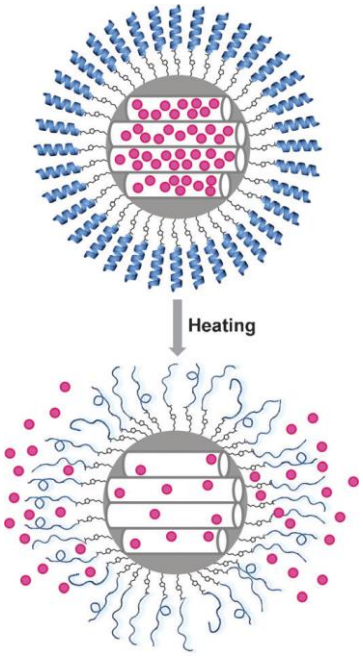

Figure 16. Schematic representation of the temperature-driven peptide-gated material. The release of the loaded safranin dye was achieved by a progressive α-helix-to-disordered transformation when temperature was increased. (*Reprinted with the permission from Chem. Commun., 2014, 50, 3184. Copyright ©The Royal Society of Chemistry 2014).*

1.3.5.5 *Biomolecules-driven molecular gates.*

The presence of certain biomolecules can also be used as trigger that causes the opening of a gated system. In fact, in the last ten years many authors have developed new bio-controlled molecular gates. Several biomolecules can be used as stimuli, although enzymes are the most commonly used in the development of bio-gated hybrid materials. This fact can be explained because of the important role that enzymes have in biological processes. The altered expression profile of specific enzymes (such as proteases, phospoholipases or glycosidases) observed in pathological conditions, such as cancer or inflammation, can be exploited to achieve enzyme-mediated drug release with accumulation of drugs at the desired biological target. Most of the systems devoted to enzyme-mediated drug delivery exploited the presence of these biomolecules in the

cellular environment. This is a promising research field taking into account that the use of tailor-made molecular sequences and specific enzymes is envisioned to have a large potential that may provide exquisite selectivity in the design of advanced gate-opening devices.

Stoddart et al. described the first example of gated mesoporous system that responds to an enzyme. The designed system consisted of a mesoporous support with a [2]rotaxane capped with an ester-linked adamantyl stopper.[64a] Upon addition of porcine liver esterase the bulky adamantyl stopper was released allowing cargo delivery. Bein and co-workers reported another example using protease enzyme.[89] Biotinylated mesoporous silica nanoparticles loaded with fluorescein were prepared in this case. When avidin was added, an avidin-biotin complex was formed, capping the pores of the inorhanic matrix. No delivery of the dye was observed in the absence of the protease trypsin whereas the addition of this enzyme induced the hydrolysis of the attached protein avidin and the release of the entrapped dye.

Martínez-Máñez and co-workers reported a lactose-capped silica mesoporous support that was selectively uncapped using β–D-galactosidase by the rupture of a glycosidic bond.[90] In a further evolution, the same authors prepared nanoscopic MCM-41 loaded with a dye and functionalized, on the pore outlets, with different commercially available hydrolyzed starch derivatives in order to test and improve the efficiency of the previous developed system.[65] Three different commercial available hydrolyzed starch (Glucidex 47, 39, and 29) were used as molecular caps. The pores of the nanoparticle's mesoporous supports were loaded with $[Ru(bipy)_3]^{2+}$ and capped with the trialkoxysilane derivative of the corresponding hydrolyzed starch. All prepared solids showed a close to zero release of the cargo in absence of pancreatin, whereas in presence of this enzyme the dye delivery was iduced due to the hydrolisis of the

[89] A. Schlossbauer, J. Kecht, T. Bein, *Angew. Chem. Int. Ed.*, **2009**, *48*, 3092.

[90] A. Bernardos, E. Aznar, M. D. Marcos, R. Martínez-Máñez, F. Sancenón, J. Soto, J. M. Barat, P. Amorós, *Angew. Chem. Int. Ed.*, **2009**, *48*, 5884.

corresponding capping starch. From the release profile results it was clearly deduced that a simple choice of the hydrolysis degree of starch has a dramatic influence on the delivery profile, that is, the lesser the hydrolysis of starch, the lower the delivery rate. These materials were tested for the controlled release in intracellular media using HeLa and LLC-PK1 cells. Figure 17 represents a scheme of the gated mechanism.

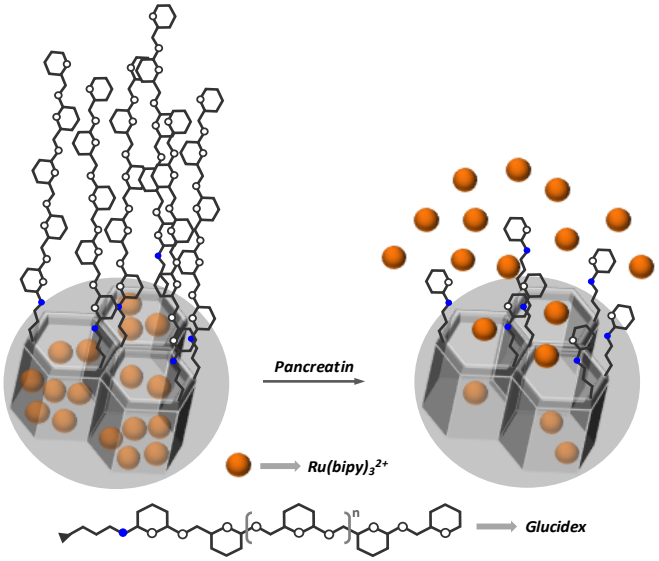

Figure 17. Schematic representation of the gated material capped with hydrolyzed starch derivatives (Glucidex 47, Glucidex 39 and Glucidex 29) and their opening in the presence of pancreatin. *(Reprinted with the permission from Acc. Chem Res. 2013, 46,339. Copyright ©The Royal Society of Chemistry 2013).*

Recently, highly specific delivery system using peptide-coated mesoporous silica nanoparticles have been reported by Heise and co-workers[91] and Martinez-Máñez et al.[92] More in detail, Heise et al. prepared silica nanoparticles loaded with fluorescein-conjugated dextran molecules and

[91] P. D. Thornton, A. Heise, *J. Am. Chem. Soc.*, **2010**, *132*, 2024.

[92] C. Coll, L. Mondragón, R. Martínez-Máñez, F. Sancenón, M. D. Marcos, J. Soto, P. Amorós, E. Pérez-Payá, *Angew. Chem. Int. Ed.*, **2011**, *50*, 2138.

functionalized the outer surface of these nanoparticles with a specific peptide sequence containing terminal bulky fluorenylmethoxycarbonyl (Fmoc) fragments. The final material was able to release their cargo only upon addition of thermolysin to the aqueous suspensions of the hybrid nanoparticles. The cleavage of the peptide sequence was induced, when this enzyme was present, with the subsequent removal of the bulky Fmoc groups and, as a consequence, delivery of the entrapped dye was observed. On the other hand, Martínez-Máñez et al. prepared a MCM-41 loaded with the dye $Ru(bipy)_3^{2+}$ and grafted onto the external surface peptide sequences which were anchored by click chemistry. Aqueous suspensions of this nanoparticles are unable to release the entrapped dye, however addition of targeted proteolytic enzymes induced the enzymatic hydrolisys of the peptide sequences with the subsequent diffusion of the ruthenium complex.

One step forward was achieved by R. Martínez-Máñez's research group, with the preparation of a new nanodevice based on MCM-41 silica nanoparticles able to display selective and controlled cargo delivery in senescent cells.[93] The design strategy involved the use of MSNs loaded with Rhodamine B and capped with a galacto-oligosaccharide (GOS). In the absence of the enzyme β-galactosidase (β-gal), Rhodamine-B cargo remained in the nanoparticles without release. In contrast, in the presence of β-gal, release of the Rhodamine-B was shown. This behavior was assigned to the galactosidase-induced hydrolysis of the glycosidic bonds of the anchored GOS derivative, which results in a reduction of the size of the attached groups and allows delivery of the entrapped cargo. These nanoparticles were able to selectively deliver their cargo in senescence associated β-galactosidase (SA-β-gal) positive β-Gal overexpressing yeast cells, in aged human fibroblasts DC1787, and in X-DC1774 and XDC4646 cells from human Dyskeratosis Congenita patients, whereas no cargo release was observed in

[93] A. Agostini, I. Mondragón, A. Bernardos, R. Martínez-Máñez, M.D. Marcos, F. Sancenón, J. Soto, A. Costero, C. Manguan-García, R. Perona, M. Moreno-Torres, R. Aparicop-Sanchis, J.R. Murguía, *Angew. Chem. Int. Ed.* **2012**, *51*, 10556.

control experiments with H460 non-small-cell lung-cancer cells and wild-type yeast cells.

Enzymes can also be used as capping agents in the design of more sophisticated hybrid materials. For example, R. Martínez-Máñez and co-workers have recently reported a new gated nanodevice able to control cargo delivery using glucose as a trigger and cyclodextrin-modified glucose oxidase as a capping agent.[94] The designed capped system was based on the use of mesoporous silica nanoparticles loaded with a dye and containing propylbenzimidazole moieties anchored on the pore outlets. The mesopores were then capped with an active CD-modified-glucose oxidase (CD-GOx) through the formation of an inclusion complex between the cyclodextrins and the propylbenzimidazole group anchored to the solid support. The presence of the substrate glucose combined with the catalytic action of CD-GOx to produce gluconic acid induced protonation of the benzimidazole group that resulted in dethreading of the inclusion complex and the subsequent cargo release. Figure 18 shows a representation of this system.

[94] E. Aznar, R. Villalonga, C. Giménez, F. Sancenón, M. D. Marcos, R. Martínez-Máñez, P. Díez, J. M. Pingarrón, P. Amorós, *Chem. Commun.,* **2013**, *49*, 6391.

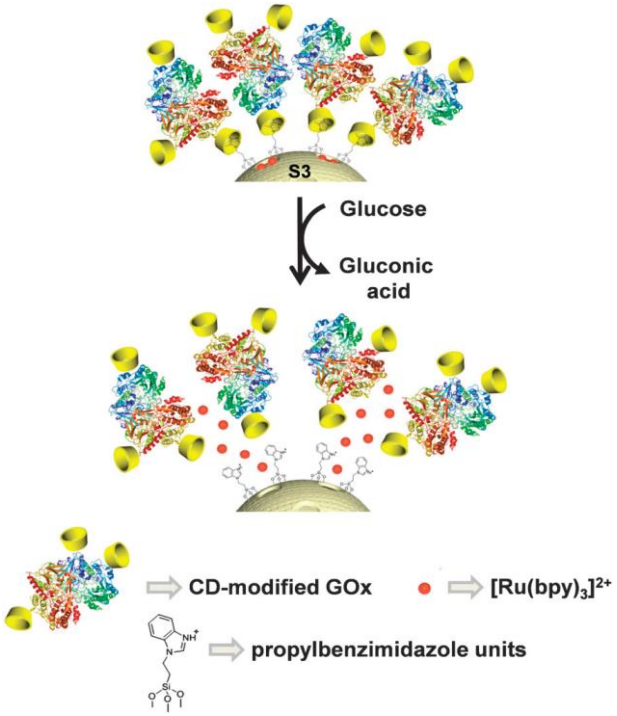

Figure 18. CD-Gox--capped nanoparticles and performance paradigm of the system in presence of glucose. *(Reprinted with the permission from Chem. Commun., 2013, 49, 6391. Copyright ©The Royal Society of Chemistry 2013).*

Other bio-molecules such as oligonucleotides have also been used for the design of hybrid materials for delivery applications. For instance, Martínez-Máñez and co-workers presented a novel nanogated system based on the use of MCM-41 silica nanoparticles capped with oligonucleotides that was selectively opened in the presence of the complementary oligonucleotide.[95] Selectivity studies were carried out to investigate the opening protocol mechanism. For these studies, several oligonucleotides with a similar nature to the complementary strand were used. By a monotorization of dye delivery from the designed nanoparticles, authors demonstrated that uncapping resulted only remarkable in the presence of

[95] E. Climent, R. Martínez-Máñez, F. Sancenón, M. D. Marcos, J. Soto, A. Maquieira P. Amorós. *Angew. Chem. Int. Ed.* **2010**, *49*, 7281.

the complementary strand, due to the full hybridization between the oligonucleotides.

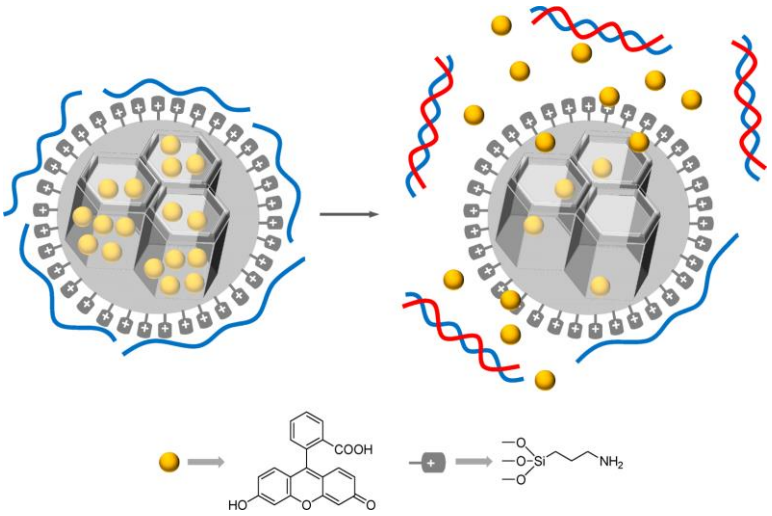

Figure 19. Representation of gated material functionalized with 3-aminopropyltriethoxysilane and capped with a single-stranded oligonucleotide. Delivery of fluorescein is selectively accomplished in the presence of the complementary oligonucleotide. *(Reprinted with the permission from Acc. Chem Res. 2013, 46,339. Copyright ©The Royal Society of Chemistry 2013).*

The possibility of preparing similar systems on different supports and to select and easily synthesize tailor-made oligonucleotides makes this approach of interest in a wide range of timely research fields such as delivery protocols and diagnosis (recognition of certain oligonucleotide chains). In fact, following this design procedure, the same authors presented a sensitive nanodevice for direct and rapid detection of *Mycoplasma*.[96]

From all the triggers described in this section (light, redox potential, temperature or pH changes and presence of biomolecules) for controlled mass transport and delivery, the work carried out in this thesis has been focused on the

[96] E. Climent, L. Mondragón, R. Martínez-Máñez, F. Sancenón, M. D. Marcos, J. R. Murguía, P. Amorós, K. Rurack, E. Pérez-Payá, *Angew. Chem. Int. Ed.* **2013**, *52*, 8938.

the presence of biomolecules, specially enzymes and pathogenic microorganisms (bacteria or fungi). In fact, all the hybrid materials prepared were related with certain biomedical needs and have been developed as proof of concept for therapeutic applications.

2. New nanodevices using enzyme-driven gated silica nanoparticles for therapeutic applications.

2.1 **Objectives**

Bearing in mind the highlight potential of enzyme triggered drug delivery and the wide range of applications of biogated nanomaterials, the aim of this chapter was the design of several nanodevices which responded to certain specific enzymes and their application in controlled release of bioactive molecules into cells. In order to achieve our purpose we selected MCM-41-like silica mesoporpous nanoparticles that were functionalized with different enzyme-responsive caps.

Specifically our objectives were:

- ✓ Design and peparation of a new dual enzyme-driven system based on silica mesoporous supports capped with azopyridinium salts for controlled

delivery actived in presence of esterase and reductase, which are usually found in the colon microflora.

- ✓ Design and synthesis of a new protease-responsive nanodevice for intracellular-controlled release using silica mesoporous nanoparticles capped with ε–poly-L-lysine, anchored to the nanoparticles' surface.
- ✓ Design and development of a smart 3D "gated scaffold" by the incorporation of mesoporous silica nanoparticles in the synthesis of a macroporous gelatin scaffold for on-command delivery induced by acid phosphatase.

The following sections will detail the design and performance of these nanodevices.

2.2 *Enzyme-responsive silica mesoporous supports capped with azopyridinium salts for controlled delivery applications.*

*Núria Mas,[a,b,c] Alessandro Agostini,[a,b,c] Laura Mondragón,[a,b,c] Andrea Bernardos,[a,b,c] Félix Sancenón,[a,b,c] M. Dolores Marcos,[a,b,c] Ramón Martínez-Máñez,[*a,b,c] Ana M. Costero,[a,d] Salvador Gil,[a,d] Matilde Merino-Sanjuán,[a,e] Pedro Amorós,[f] Mar Orzáez[g] and Enrique Pérez-Payá[g]*

[a]*Centro de Reconocimiento Molecular y Desarrollo Tecnológico, Unidad Mixta Universidad Politécnica de Valencia-Universidad de Valencia.*

[b]*Departamento de Química. Universidad Politécnica de Valencia*

Camino de Vera s/n, E-46022 Valencia (Spain) Fax: (+34) 96-387-93-49

E-mail: rmaez@qim.upv.es

[c]*CIBER de Bioingeniería, Biomateriales y Nanomedicina (CIBER-BBN)*

[d]*Departamento de Química Orgánica, Facultad de Químicas, Universitat de Valencia, 46100 Burjassot, Valencia, Spain.*

[e]*Departamento de Farmacia y Tecnología Farmacéutica, Facultad de Farmacia, Universitat de València, Avda. Vicente Andrés Estellés s/n, 46100 Burjassot, Spain*

[f]*Institut de Ciència del Materials (ICMUV). Universitat de València P.O. Box 2085.*

[g]*Laboratorio Péptidos y Proteínas. Centro de Investigación Príncipe Felipe. Avda. Autopista al Saler, 16, E-46012 Valencia, Spain. IBV-CSIC, Jaime Roig, 11, E-46010, Valencia, Spain.*

Received: July 30, 2012. Revised: October 31, 2012

Published online: December 7, 2012

Reprinted with the permission from Chem. Eur. J. 2013, 19, 1346.

Abstract

The preparation of a new capped silica mesoporous material, **Rh-Azo-S**, for on-command delivery applications in the presence of target enzymes is described. The material consists of nanometric mesoporous MCM-41-like supports loaded with Rhodamine B and capped with an azo pyridine derivative. The material was designed to show “zero delivery” and to display a cargo release in the presence of reductases and esterases which are usually present in the colon, mainly due to intestinal microflora. The opening and cargo release of **Rh-Azo-S** in vitro studies were assessed and seen to occur in the presence of these enzymes whereas no delivery was noted in the presence of pepsine. Moreover, **Rh-Azo-S** nanoparticles were used to study controlled Rhodamine B dye delivery in intracellular media. HeLa cells were employed for testing the 'non'-toxicity of nanoparticles. Moreover, delivery of the dye in these cells, via internalisation and enzyme-mediated gate opening, was confirmed by confocal microscopy. Furthermore, the nanoparticles capped with the Azo group and loaded with a cytotoxic camptothecin (**CPT**) were also prepared (solid **CPT-Azo-S**) and used as delivery nanodevices in HeLa cells. When this solid was employed, cell viability decreased significantly due to nanoparticles internalisation and cytotoxic agent delivery.

Introduction

In recent years, in-depth studies into mesoporous silica nanoparticles functionalised with organic molecules acting as “molecular gates” have been undertaken to examine their potential use in a wide variety of delivery applications.[1-9] In these hybrid systems, particular external stimuli can cause the opening of the “gate” allowing the delivery of confined species or permitting the entry of molecules from the solution into mesopores.[8a] Different types of gated systems have been reported depending on the external stimulus used to trigger the cargo delivery. Gated materials responding to light,[10] redox reactions,[11] pH,[12] changes in polarity,[13] temperature[14] and certain bio-molecules[15] as stimuli have

been reported.[16] In this field, the use of enzyme-substrate systems offers opportunities for the design of sensitive and specific mesoporous-based nanodevices for the on-command delivery of entrapped substances. In fact when combined with the unique properties of nanomaterials, the resulting enzyme-responsive system can be designed to perform target functions with high specificity controlled by the triggering enzyme. Moreover, the possibility of using enzymes for selective release applications opens up a wide range of new perspectives in the development of bio-compatible release systems. In particular, and despite some reported systems using enzyme-responsive nanomaterials such as polymer-based nanoparticles, liposomes, gold nanoparticles and quantum dots for programmed drug release, examples of enzyme-induced delivery using capped silica mesoporous nanoparticles are still relatively limited. In this area, the works by Zink,[15] Bein,[17] Kim[18] and co-workers, and some of our works,[19] are worth mentioning.

The specific enzyme-dependent release of molecules from nano-particles will help find interesting applications for different fields ranging from medicine to materials science. It is well-known that oral delivery is the favourite form of therapeutic drug administration. However in some circumstances, the gastrointestinal tract could represent a barrier to certain drugs given different properties.[20] In fact in order to achieve successful colonic delivery, drugs need to be protected from absorption and/or degradation of the upper gastrointestinal tract environment to be then abruptly released into the proximal colon, which is considered the optimum site for the colon-targeted delivery of drugs.[21] Colon targeting is very interesting for the topical treatment of colon-related diseases, such as Crohn's disease, ulcerative colitis, colorectal cancer, amebiasis, etc. Moreover it is also known that intestinal microflora is characterised by a complex and relatively stable community of microorganisms, many with physiological functions. In particular, indigenous microflora are responsible for a wide variety of metabolic processes, including the reduction of a wide range of organic functional groups in environmental and therapeutic compounds.[20,22,23] These metabolic processes are carried out by enzymes; thus, in principle, it is possible to design

drug-entrapped capped material, which are sensitive to specific enzymes, that would favour delivery to previously defined environments. Thus with a pharmaceutical approach, the design of enzyme-responsive gated materials sensitive to colon-resident bacteria could be of interest, especially if these materials could protect the cargo during its transit through the gastrointestinal tract by further allowing cargo delivery triggered by a wide variety of enzymes present in colonic bacteria and in the extracellular media; e.g., azoreductases, glycosidases, esterases, nitroreductases, etc.[24]

Therefore, the aim of our study was, as a proof-of-concept, to design capped mesoporous materials capable of selectively delivering their cargo with the enzymes usually found in the presence of indigenous intestinal microflora. In particular, we paid special attention to reductases and esterases. We believe that these new classes of materials may define prototypes for the future design of therapeutic drug delivery systems for target colon-related diseases in which a "zero release" of the drug before reaching the colon will be a valuable attribute.

Results and discussion

Gated material.

The development of responsive nanoscopic gated materials requires selecting two components; (i) suitable "gate-like ensembles" which will change one or several properties (size, shape, bulkiness, charge, etc.) upon an external stimuli; (ii) the selection of a nano-structured matrix in which the gate-like scaffold is grafted. For the latter, we selected a mesoporous material of the MCM-41 family as a suitable inorganic support given the well-known properties of these solids, such as high homogeneous porosity, inertness and ease of functionalisation on the surface.[25] In relation to the first component, the capping ensemble, we aimed to develop a gate-like platform that can not only operate in aqueous solution, but can be triggered by the presence of reductases and esterases. For this purpose, we selected an azo pyridine derivative (**Azo**) as a suitable capping molecule (that was grafted into the inorganic scaffold through the formation of a

pyridinium salt) by taking into account the already known reported rupture of azo bonds in the presence of reductases[24] and the pyridinium salt hydrolysis by esterases.[26]

The synthesis of the gatekeeper **Azo** derivative is shown in Scheme 1. The **Azo** molecule was designed to contain appended ether groups which were expected to display a dual role; (i) they are bulky enough to inhibit cargo delivery and (ii) allow solubilisation in water after the enzymatic rupture of the attached moiety. The synthetic sequence for **Azo** preparation started with the mesylation of 2-methoxyethanol (**1**), followed by a nucleophilic substitution reaction of the mesylated derivative (**2**) with the disodium salt of *N*,*N*-phenyldiethanolamine (**3**). This resulted in aniline derivative **4,** which was further coupled with 4-aminopyridine (**5**) through the use of sodium nitrite to yield the azo derivative (**Azo**). The synthesis of compound **4** has been described in the literature,[27] and complete details of the **Azo** synthesis are described in the Experimental Section (see also Scheme 1).

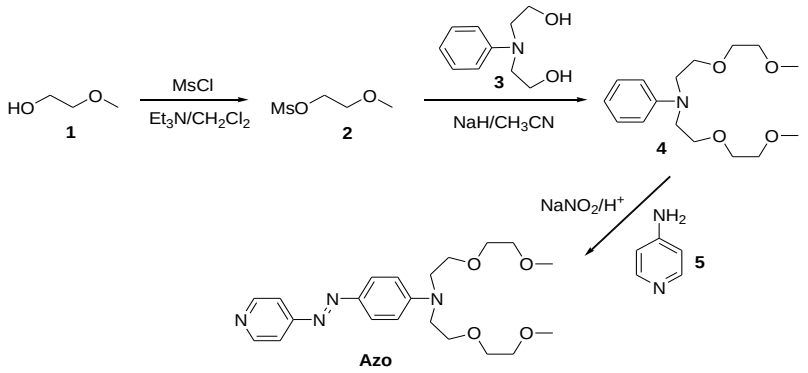

Scheme 1. Synthetic route for the preparation of azo pyridine derivative **Azo**.

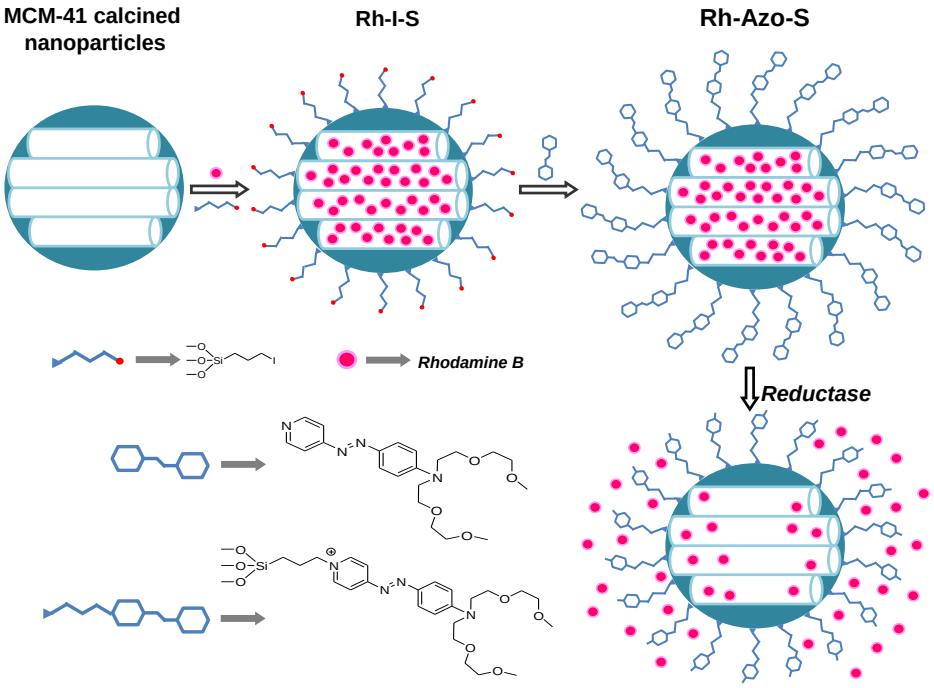

Scheme 2. Schematic representation of the synthesis process of hybrid mesoporous materials **Rh-I-S** and **Rh-Azo-S,** and the uncapping mechanism in the presence of reductases in solution. Reductase was able to hydrolyse the azopyridinium salt anchored onto the mesoporous support by inducing progressive pore opening and the subsequent dye delivery.

The starting nanoparticulated MCM-41 mesoporous solid was synthesised following well-known procedures using *n*-cetyltrimethylammonium bromide (CTAB) and tetraethylorthosilicate (TEOS)[28-30] and the subsequent removal of the surfactant by calcinations. In order to obtain the final gated material, the pores of the support were first loaded with Rhodamine B dye (yielding solid **Rh-S**). Then the material was reacted with 3-iodopropyltrimethoxysilane (resulting in the **Rh-I-S** support). Finally, the selected molecular gatekeeper (the **Azo** product, previously synthesised) was grafted onto the outer surface of the pores of the inorganic scaffold during a 72-hour reflux reaction in acetonitrile, leading to the preparation of the final gated material, **Rh-Azo-S** (Scheme 2). In order to minimise the dye delivery from the mesopores during the synthesis of the capped material, the latter reactions were carried out with excess Rhodamine B dye in the reaction

mixture. The final violet solid (**Rh-Azo-S**) was filtered, washed with acetonitrile and dried at 70°C for 12 h.

Following this grafting procedure, the 3-iodopropyltrimethoxysilane derivative (and, therefore, the azopyridinium dye) was preferentially attached to the pore outlets rather than inside the mesopores, which contain Rhodamine B dye.

Characterisation of materials.

The prepared materials were characterised by standard techniques. Figure 1 shows the X-ray diffraction (XRD) patterns of the nanoparticulated MCM-41 matrix as-synthesised, the MCM-41 calcined and the final **Rh-Azo-S** solid. The MCM-41 as-synthesised (curve a) displayed the four typical low-angle reflections of a hexagonal-ordered matrix indexed at (100), (110), (200) and (210) Bragg peaks. In curve b (MCM-41 calcined), a significant shift of the (100) peak in the XRD and a broadening of the (100) and (200) peaks are observed. These observations are in agreement with the condensation of silanols in the calcination step, which caused an approximate cell contraction of 4 Å. Finally, curve c shows the **Rh-Azo-S** solid XRD pattern. For this material, reflections (110) and (200) were mostly lost due to a reduction in contrast related to the functionalisation process and to the filling of mesopores with Rhodamine B. Nonetheless, the intensity of the (100) peak in this pattern strongly indicates that the loading process with the dye and the additional functionalisation with 3-(iodopropyl)trimethoxysilane and the **Azo** derivative did not modify the mesoporous MCM-41 scaffold.

The TEM analyses of the prepared solids show the typical channels of the MCM-41 matrix visualised as alternate black and white stripes. Figure 2 shows the TEM images for the MCM-41 calcined sample and for the final **Rh-Azo-S** solid. This figure also shows that the prepared MCM-41-based supports were obtained as spherical nanoparticles, with diameters between 80 and 100 nm. The final **Rh-Azo-S** material was also seen to maintain its spherical nature after the loading and functionalisation processes.

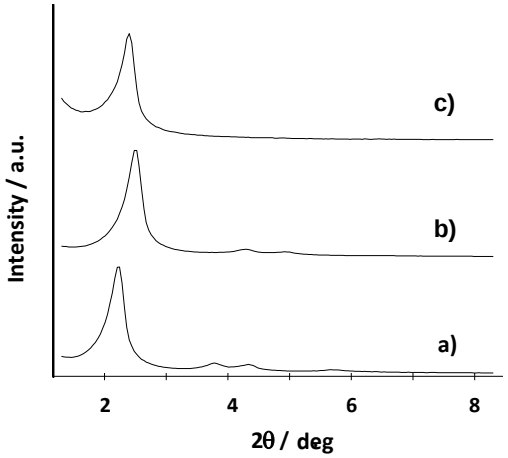

Figure 1. The X-ray pattern of (a) MCM-41 as-synthesised, (b) MCM-41 calcined and (c) **Rh-Azo-S**.

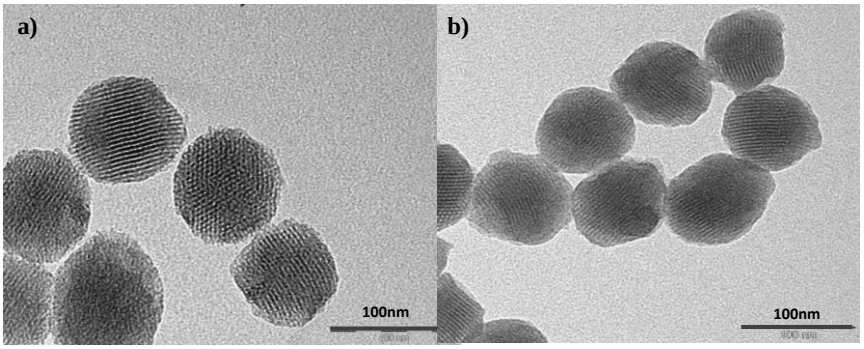

Figure 2. The TEM image of MCM-41 calcined (a), and final solid **Rh-Azo-S** (b) showing the typical porosity of the MCM-41 matrix.

In Figure 3 (curve a), the N_2 adsorption-desorption isotherms of the MCM-41 calcined nanoparticles is represented. This curve contains an adsorption step with a P/P_0 value of between 0.1 and 0.3, corresponding to a type IV isotherm, which is typical of mesoporous materials. This first step is due to nitrogen condensation in the mesopores inlets. With the BJH[31] model on the adsorption curve of the isotherm, the pore diameter and pore volume were calculated to be 2.36 nm and 0.67 cm^3g^{-1}, respectively. The absence of a hysteresis loop in this range and the low BJH pore distribution indicate the cylindrical uniformity of

mesopores. The total specific area was 924.7 m^2g^{-1}, calculated with the BET model.[32] The a_0 cell parameter 41.760 Å (d_{100} = 36.165 Å), the pore diameter (2.36 nm) and the wall thickness value, 18.2 Å, were calculated by the XRD, porosimetry and TEM studies. A second remarkable feature of the curve is the characteristic H1 hysteresis loop that appears in the isotherm at a high relative pressure (P/P_0 > 0.8) and associated with a wide pore size distribution. This corresponds to the filling of the large pores among the nanoparticles (0.53 cm^3g^{-1} calculated by the BJH model) due to textural porosity.

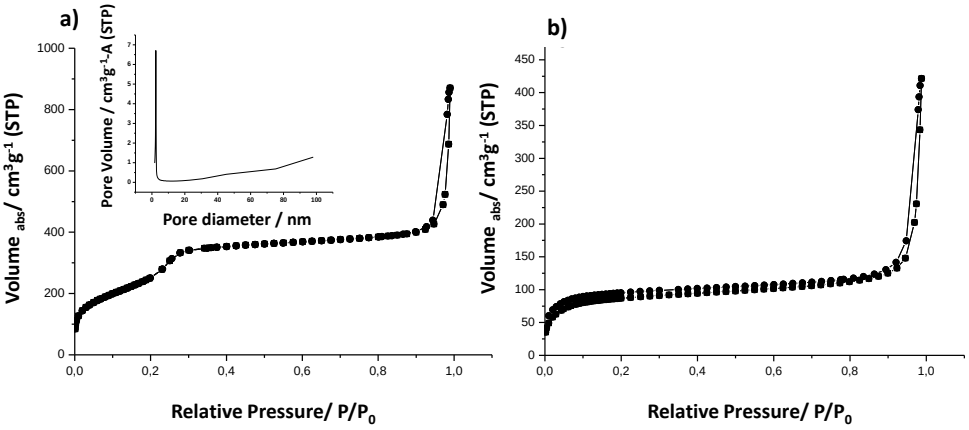

Figure 3. The nitrogen adsorption-desorption isotherms for (a) the MCM-41 calcined mesoporous material and (b) the **Rh-Azo-S** material. Inset: Pore size distribution.

For the **Rh-Azo-S** material, the N_2 adsorption-desorption isotherm is typical of mesoporous systems with filled mesopores (see Figure 3, curve b). In this case, and as expected, a lower N_2 adsorbed volume (BJH mesopore volume = 0.09 cm^3g^{-1}) and surface area (306.9 m^2g^{-1}) were found when compared with the starting MCM-41 material. As observed, this solid presents a curve with no gaps at low relative pressure values if compared to the mother MCM-41 matrix (curve a). Another important feature of this second selected material is that no maximum was observed in the pore size distribution curve, which can be explained by the presence of closed pores. Moreover, Table 1 shows the BET-specific surface values, pore volumes and pore sizes calculated from the N_2 adsorption-desorption isotherms for MCM-41 calcined and **Rh-Azo-S.**

Table 1. BET-specific surface values, pore volumes and pore sizes calculated from the N_2 adsorption-desorption isotherms for selected materials.

Solid	S_{BET} ($m^2\ g^{-1}$)	**Pore Size** [a,b] (nm)	**Total Pore volume** [a] ($cm^3\ g^{-1}$)
MCM-41	924.7	2.36	0.67
Rh-Azo-S	306.9	----	0.09

[a] Pore volumes and pore sizes were associated with only intraparticle mesopores. [b] Pore size estimated by the BJH model applied to the adsorption branch of the isotherm.

Moreover, the contents of grafted molecules and dye in solids **Rh-S**, **Rh-I-S** and **Rh-Azo-S** were determined by thermogravimetric analysis and are shown in Table 2.

Table 2. Content (**α**) in millimol of anchored molecules and dye in millimol per gram of SiO_2, for solids **Rh-S**, **Rh-I-S** and **Rh-Azo-S**.

Solid	$\alpha_{\text{functionalised molecules}}$ (mmol/g SiO_2)	α_{dye} (mmol/g SiO_2)
Rh-S	----	0.666
Rh-I-S	0.149	0.412
Rh-Azo-S	0.250	0.289

Functional enzyme-driven controlled release.

The **Rh-Azo-S** solid is composed of a mesoporous matrix, MCM-41, which contains Rhodamine B in the pores and was capped with the azo derivative molecule, **Azo**. It was expected that the **Azo** moiety would cap the pores and would subsequently avoid cargo delivery. In order to prove not only this fact, but also the action of some enzymes in the hybrid synthesised system, several release experiments were carried out. Firstly, the behaviour of **Rh-Azo-S** in the presence of reductase in water at pH 7.5 (optimal conditions for enzyme activity) was analysed. In a typical experiment the **Rh-Azo-S** solid was suspended in water at pH

7.5 in both the absence and presence of nitrate-reductase, a colon-resident bacterial enzyme[33] (see Figure 4a). The suspension was stirred at room temperature and, at certain time, aliquots were separated and filtered. Dye release was determined by monitoring fluorescence in the aqueous phase of Rhodamine-B dye (λ_{ex} = 554 nm, λ_{em}= 580 nm). A nearly flat baseline was found in the absence of the enzyme, indicating that the Rhodamine-B cargo remains in the nanoparticles without release. In contrast, in the presence of reductase, delivery of Rhodamine-B was observed as an increased dye emission in the solution (see Figure 4a and Scheme 2). Interestingly after 7 h, solid **Rh-Azo-S** released less than 5% of the entrapped dye, whereas a nearly 70% release of the cargo was seen in the presence of the enzyme (release at 24 h corresponds to 0.03 mmol dye/g SiO_2). It is also remarkable to note that the reductase-dependent cargo release from **Rh-Azo-S** was incrementally time-dependent for up to 24 h. This feature could be of interest in controlled release applications where delivery peaks are undesirable.

In addition to the delivery studies carried out with solid **Rh-Azo-S** and reductase, further release experiments were performed out in the presence of esterase, another colon-resident enzyme.[24] In a typical experiment, **Rh-Azo-S** was suspended in water at pH 8 in both the absence and presence of esterase. As in the previous experiment, in the absence of the enzyme, the Rhodamine-B cargo remained inside the nanoparticles, whereas the cargo was delivered to the bulky solution in the presence of the esterase (see Figure 4b). As it is known, esterase is also located in the stomach,[34] and therefore enzyme driven release studies were also taken at gastric pH (between 2 and 4 at the stomach output) in presence of the esterase; satisfactorily no dye release was observed. These results point out the high selectivity performance of the designed hybrid **Rh-Azo-S** material as a suitable carrier for colon drug delivery.

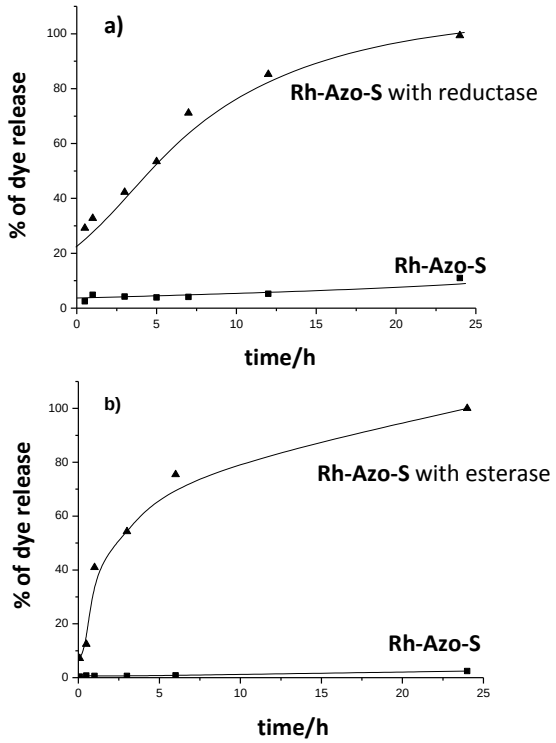

Figure 4. Kinetics of the release of Rhodamine B dye from water suspensions of gated solid **Rh-Azo-S** (a) in the absence and presence of reductase at pH 7.5 and (b) in the absence and presence of esterase at pH 8.

To specifically analyse the enzyme-dependent cleavage of the capping moiety, additional HPLC and electrospray ionization time-of-flight mass spectroscopy (ESI-TOF-MS) studies with solid **Rh-Azo-S** in the presence of redutase and esterase were carried out. In particular, solid **Rh-Azo-S** was suspended in water at pH 7.5 in the presence of reductase for 24 hours. Then, the suspension was filtered and the aqueous phase passed through a size exclusion column in order to eliminate the enzyme. The aqueous phase was then subjected to an HPLC separation and the peaks obtained passed through an ESI-TOF-MS spectrometer in the positive ion mode (the detected ion peaks may reflect proton or sodium addition). The mass spectra of the main product showed a highest peak at *m/z* of 291 (268+23) clearly suggesting an enzyme-catalyzed hydrolysis of the

N=N bond (see Figure 5). A similar experiment with a suspension of solid **Azo-S** in water at pH 8.0 in the presence of esterase was carried out. In this case, the highest peak for the main isolated product was found at *m/z* 425 (402+23) strongly indicating that esterase was able to hydrolyze the pyridinium salt (see also Figure 5).[26] A second product from the HPLC separation showed a peak at *m/z* 178 also suggesting the possible esterase-catalyzed hydrolysis of the N=N bond.

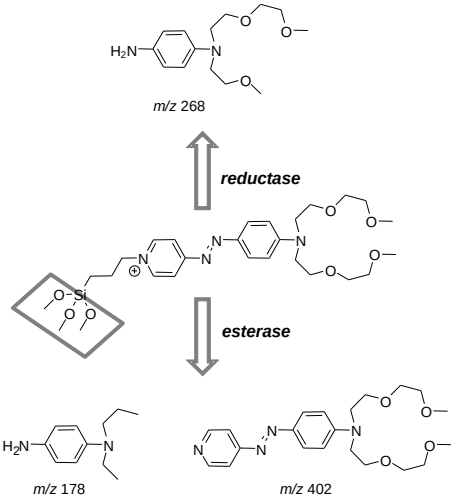

Figure 5. Detected fragments in the enzyme-induced hydrolysis of the azo capping moiety in **Rh-Azo-S** solid.

Moreover, the rupture of molecular gate was studied through ^{13}C NMR. For this purpose a new support **Azo-S** was designed and synthesized. Solid **Azo-S** was prepared from the MCM-41 inorganic support with no loading inside the pores and by grafting the **Azo** compound onto the external surface (through the reaction with the previously anchored 3-iodopropyl groups). The ^{13}C MAS NMR spectrum of solid **Azo-S** showed significant signals grouped into two intervals: 10-75 ppm and 115-165 ppm. The signals in the 10-75 ppm range were ascribed to the propyl chains and to the methylene carbons from the polyether fragments, whereas the group of signals at lower fields were attributed to the aromatic rings of the azopyridinium dye. Then in another experiment, solid **Azo-S** was suspended in water at pH 7.5 that contained esterase. The hydrolysed material, **Azo-S-H**, was

filtered, washed with water and dried. The ^{13}C MAS NMR spectrum of solid **Azo-S-H** displayed broad signals in the 40-10 ppm interval, indicating that the propyl chains linking the pyridinium rings with the solid surface remained unaltered after enzymatic hydrolysis. However, a clearly reduced intensity of aromatic carbons in the 105-160 ppm range was observed due to the specific hydrolysis of the azo moiety induced by the enzyme. Nearly the same results were obtained when solid **Azo-S** was treated with reductase.

In order to test our hypothesis of the potential specific delivery to defined environments, we exposed **Rh-Azo-S** to the presence of the stomach-resident enzyme pepsin. The **Rh-Azo-S** solid was totally resistant to this enzyme activity and the cargo was not delivered. Since we were interested in moving up to cell-based assays, we also demonstrated that **Rh-Azo-S** nanoparticles remained intact with no delivery in the presence of cell culture media, such as D-MEM supplemented with 10% of foetal calf serum (FCS). All these experiments demonstrate that the cargo delivery from **Rh-Azo-S** nanoparticles is only achieved in the presence of reductase or esterase, but not in the presence of other enzymes or when using media with great ionic strength.

Finally, in order to study the importance of the covalent attachment of the azo derivative in the final gated material, and to rule out that a simple adsorption of the **Azo** molecule behaves as a gatekeeper, a control material that did not contain the linker, 3-iodopropyltrimethoxysilane, was prepared. The MCM-41 nanoparticles loaded with Rhodamine B were refluxed for 72 h in acetonitrile in the presence of the molecule, **Azo.** Then, the solid was filtered off and washed with acetonitrile. This solid showed no gated properties and a massive dye delivery was observed in both the presence and the absence of the enzyme.

Delivery of gated materials in intracellular media.

As stated above, this study aimed to design new gated silica mesoporous nanoparticles containing capping systems and to demonstrate their possible use

as drug delivery systems in the presence of reductase or esterase. In addition to the potential use of these systems for selective cargo delivery in the colon, due to the presence of exogenous enzymes produced by indigenous intestinal microflora (such as reductases and esterases), the prepared material would also be suitable for drug delivery applications in cells, especially in the form of nanoparticles.

In a first step, the biocompatibility of **Rh-Azo-S** nanoparticles in different cell lines and their ability to be internalised by cells was analysed. Human cervix adenocarcinoma (HeLa) and breast cancer MCF-7 cell lines were treated with **Rh-Azo-S** at different concentrations over a 24-hour period. Cell viability and cellular internalisation were determined by WST-1 cell viability assays and live confocal microscopy studies (see Figure 6). The confocal images corresponding to HeLa cells demonstrate the intracellular vesicular localisation of **Rh-Azo-S** nanoparticles in red, a typical pattern associated with endocytosis and the subsequent localisation of nanoparticles in lysosomes (Figure 6A). Besides z axis stacks, shown at the bottom and right-hand side of the figure, proved the intracellular localisation of nanoparticles. Similar results were obtained for the MCF-7 cell line (data not shown). Moreover, WST-1 cell viability assays[35] in HeLa and MCF-7 cell lines using **Rh-Azo-S** demonstrate the absence of the non-specific cell toxicity of the nanoparticle as no significant reduction in cell viability was observed (Figure 6B).

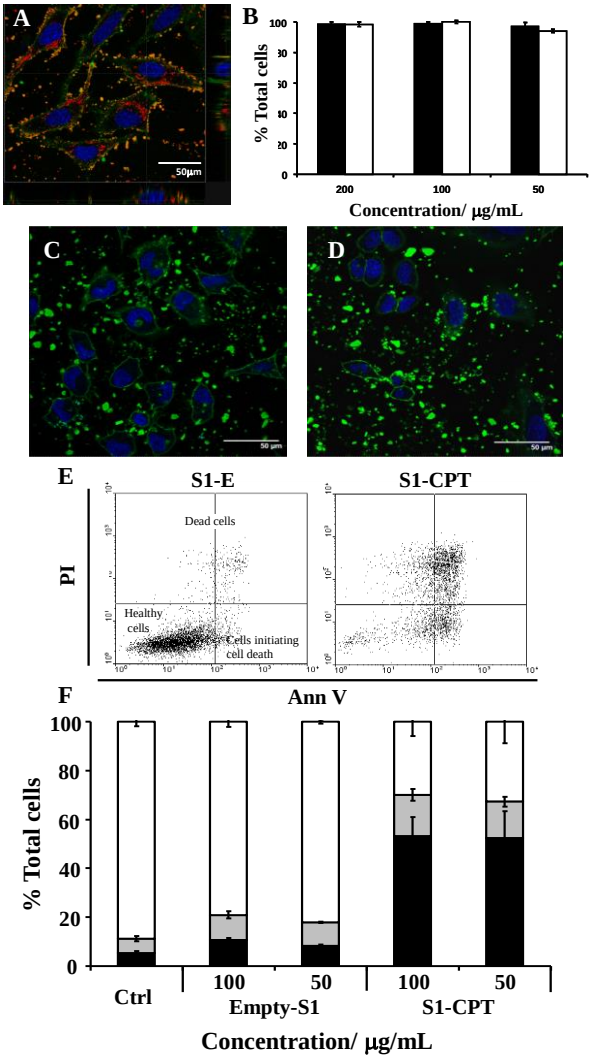

Figure 6. Cellular internalisation and cell viability studies. (A) Confocal microscopy image and cell stacking corresponding to the HeLa cells treated with solid **Rh-Azo-S** (100 µg/mL). The cellular uptake of **Rh-Azo-S** was followed by Rhodamine B-associated fluorescence (red) in the presence of DNA marker Hoechst 33342 (blue) and plasma membrane marker WGA Alexa Fluor 647 (green). Aggregates of non-internalised nanoparticles are shown in yellow. (B) Quantification of the WST-1 cell viability studies associated with **Rh-Azo-S** in the HeLa and MCF-7 cell lines. Cells were treated with the nanoparticle and after 24-hour incubation, the WST-1 reagent was added and cell viability was measured. (C-D) **CPT-Azo-S** cell death induction. HeLa cells were treated with 100 µg/mL of **CPT-Azo-S** (C) or **Azo-S** (D) for 48 h and then cell death was followed by confocal microscopy in the presence of nuclear marker Hoechst 33342 (blue) and plasma membrane marker WGA Alexa Fluor 647 (green). Then, flow cytometry studies were performed to quantify dead cells (black), cells undergoing cell death (grey) and viable cells. For the staining of dead cells and cells undergoing cell death, PI and Ann V were employed, respectively (E, F). Two independent experiments containing triplicates were developed. Statistically significant differences were observed ($P < 0.05$, Student's t-test).

We next analysed the use of these nanoparticles as drug delivery carriers. To this end, chemotherapeutic drug camptothecin (CPT) was selected as the cargo molecule. CPT is a cytotoxic quinoline alkaloid that inhibits DNA polymerase I by disrupting DNA replication and inducing apoptotic cell death. It has been broadly employed in the treatment of some cancer types, such as colon cancer or lymphoma.[36] It has been previously reported that CPT can be internalised by cells once inside MCM-41 nanoparticles.[37,38] Then, a new set of nanoparticles, **CPT-Azo-S**, capped with the **Azo** molecule and loaded with CPT, were synthesised. This solid was characterised by thermogravimetric analysis and TEM. Thermogravimetric studies allowed to calculate the amount of the **Azo** groups attached to the surface and CPT loaded on the mesopores (see Table 3), whereas TEM images showed that the mesoporous structure was conserved during the loading and functionalisation process (see Figure 7).

Table 3. Content (**α**) in millimol of anchored molecules and CPT in millimol per gram of SiO_2, for **CPT-Azo-S** material.

Solid	α **functionalised molecules** (mmol/g SiO_2)	α_{CPT} (mmol/g SiO_2)
CPT-Azo-S	0.249	0.568

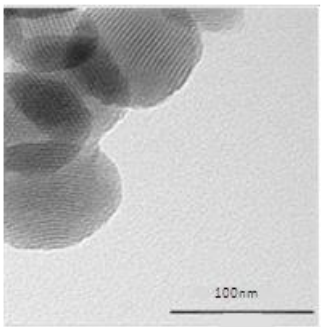

Figure 7.TEM image of solid **CPT-Azo-S** showing the typical porosity of the MCM-41 matrix.

The solid **CPT-Azo-S** was analysed in HeLa cells under the premise that if **CPT-Azo-S** could be endocytically internalised by the cells, lysosomal enzymes would cleave the **Azo** moiety by inducing an intracellular CPT release, which

would induce cell death. In fact, the HeLa cells treated at 100 and 50 μg/mL for 48 h showed apoptotic cell death, as determined by phosphatidylserine exposure (as determined by Annexin V (Ann V)) and the internalisation of propidium iodide (PI) dye in later stages of the process (Figure 6C and 6D). In contrast, the HeLa cells treated with the same concentrations of the empty **Azo-S** solid remained unaffected. In particular, at 48 h after the addition of 100 μg/mL of **CPT-Azo-S**, around 70% of the cells were dead (Figure 6E and 6F). These results were confirmed by flow cytometry experiments.

Conclusions

In summary, we report the use of a simple azo pyridine (**Azo**) derivative as a gatekeeper in the design of mesoporous materials capable of delivering the entrapped cargo in the presence of reductase or esterase. In particular, gated solid **Rh-Azo-S,** containing Rhodamine B as the cargo and the **Azo** compound as the capping group, was prepared and characterised. This material shows a "zero release" in an aqueous environment, whereas in the presence of reductase or esterase, a clear cargo delivery was observed due to the enzyme-induced rupture of the anchored **Azo** gatekeeper. This is one of the relatively few reported examples showing an enzyme-induced cargo delivery using gated silica mesoporous supports. A detailed characterisation of the specific enzyme action was carried out using ESI-TOF-MS and ^{13}C NMR measurements. These studies indicated the hydrolysis of the N=N bond in the presence of reductase enzyme, whereas esterase induced the rupture of the pyridinium salt. Moreover, it is shown that **Rh-Azo-S** nanoparticles are efficiently taken up by both the human cervix adenocarcinoma (HeLa) and breast cancer MCF-7 tumour cell lines. Confocal images corresponding to HeLa cells demonstrate the intracellular vesicular localisation of **Rh-Azo-S** nanoparticles in typical patterns associated with endocytosis and the subsequent localisation of nanoparticles in lysosomes. Cell viability studies demonstrate that **Rh-Azo-S** proves to be non-toxic for HeLa and MCF-7 cells at the tested concentrations. Finally, the possible application of capped nanoparticles as suitable delivery systems in the cells of

chemotherapeutic agents such as camptothecin (CPT) is proven, and cell viability substantially was reduced in the cancerous cells treated with solid **CPT-Azo-S**. The possibility of designing capped mesoporous supports showing a "zero release" which can be selectively opened in the presence of enzymes opens up a wide range of possibilities. For instance, capped solids showing selective cargo delivery when in contact with reductase or esterase might prove to be excellent candidates for their further use as a smart delivery system of drugs in colonic diseases. Further studies in this line are being carried out.

Experimental

General methods.

Nuclear magnetic resonance (NMR), HPLC and electrospray ionization time-of-flight mass spectroscopy (ESI-TOF-MS), powder X-ray (XRD), thermogravimetric analysis (TGA), transmission electronic microscopy (TEM), N_2 adsorption-desorption and fluorescence spectroscopy techniques were employed to characterise the synthesised materials. ^{1}H and ^{13}C nuclear magnetic resonance (NMR) spectra were acquired with a Varian 300 spectrometer (Sunnyvale, CA, USA). The ESI-TOF-MS measurements were carried out in a AB SCIEX TripleTOF™ 5600 LC/MS/MS System. The powder X-ray measurements were performed in a Brucker D8 Advance diffractometer using Cu Kα radiation. The thermo-gravimetric studies were carried out on a TGA/SDTA 851e Mettler Toledo balance using an oxidant atmosphere (air, 80 mL/min) with a heating programme consisting in a heating ramp of 10ºC per minute from 393 to 1273 K and an isothermal heating step at this temperature for 30 min. The TEM images were obtained with a 100 kV Philips CM10 microscope. The N_2 adsorption-desorption isotherms were recorded with a Micromeritics ASAP2010 automated sorption analyzer. Samples were degassed at 120ºC in vacuum overnight. Specific surface areas were calculated from the adsorption data in the low pressure range using the BET model. Pore size was determined following the BJH method. The fluorescence spectroscopy studies were carried out with a Felix 32 Analysis, version 1.2 (Build 56) PTI (Photon Technology International). The live cellular internalisation studies were performed

with a confocal Leica microscope handled with a TCS SP2 system equipped with an acoustic optical beam splitter (AOBS). Cell viability measurements were taken with a Wallac 1420 workstation. The flow cytometry studies were performed with a Cytomics FC 500 (Beckman Coulter Inc.).

Chemicals.

The chemicals tetraethylorthosilicate (TEOS), *n*-cetyltrimethylammonium bromide (CTAB), sodium hydroxide (NaOH), Rhodamine B, dichloromethane, 3-iodopropyltrimethoxysilane, esterase from porcine liver, anhydrous acetonitrile, concentrated nitric acid, concentrated phosphoric acid, 4-aminopyridine, *N*,*N*-dimethylaniline, sodium nitrite ($NaNO_2$), 2-methoxyethanol, triethylamine (TEA), hydrochloric acid, *N*,*N*-phenyldiethanolamine and sodium hydride (NaH) were provided by Aldrich. Sodium carbonate (Na_2CO_3), magnesium sulfate ($MgSO_4$), hexane and ethyl acetate were purchased from Scharlau. D-MEM with L-glutamine, foetal calf serum (FCS), trypan blue solution (0.4%) cell culture grade, trypsin, wheat germ agglutinin (WGA), Alexa Fluor 647 and Hoechst 33342 were provided by Gibco-Invitrogen. The cell proliferation reagent WST-1 was obtained from Roche Applied Science. Camptothecin was supplied by Sequoia Research Products, Ltd. Annexin V and propidiumiodide were acquired from BD Pharmingen. All the products were used as received.

Synthesis of mesoporous MCM-41 nanoparticles.

The MCM-41 mesoporous nanoparticles were synthesised by the following procedure: *n*-cetyltrimethylammonium bromide (CTAB, 1.00 g, 2.74 mmol) was first dissolved in 480 mL of deionised water. Then 3.5mL of NaOH 2.00 M in deionised water were added to the CTAB solution. Next the solution temperature was adjusted to 80°C. TEOS (5.00 mL, 2.57 x 10^{-2}mol) was then added dropwise to the surfactant solution. The mixture was stirred for 2 h to give a white precipitate. Finally, the solid product was centrifuged, washed with deionised water and ethanol, and was dried at 60°C (MCM-41 as-synthesised). To prepare the final porous material (MCM-41), the as-synthesised solid was calcined

at 550°C using an oxidant atmosphere for 5 h in order to remove the template phase.

*Synthesis of gatekeeping molecule **Azo**.*

Scheme 1 shows the synthetic sequence that leads to the preparation of compound **Azo,** which was used as a molecular gate. As observed, the synthetic sequence starts with a mesylation of 2-methoxyethanol (**1**), followed by a nucleophilic substitution reaction of the mesylated derivative (**2**) with the disodium salt of *N*,*N*-phenyldiethanolamine (**3**). These reactions yielded aniline derivative **4,** which was further coupled with 4-aminopyridine (**5**) by employing sodium nitrite.

*Synthesis of **2**.*

2-methoxyethanol (**1**) (2 mL, 0.025 mol) was dissolved in dichloromethane (34 mL) in a 100 mL round-bottomed flask. The solution was kept in an ice bath for 15 min, then triethylamine (6.9 mL, 0.05 mol) was added to the crude reaction. Mesyl chloride (3.1 mL, 0.025 mol), dissolved in dichloromethane (6 mL), was added drop-wise through a compensated addition funnel to the crude reaction for 30 min. After this addition, the crude reaction was stirred at room temperature for another 60 min period. Then, the crude reaction was poured onto a water-ice mixture containing concentrated hydrochloric acid (10 mL), and the organic layer was separated, washed three times with brine and dried with anhydrous $MgSO_4$. Dichloromethane was eliminated in a rotary evaporator to give the final product as yellow oil (3.6 g, 0.024mol, 96%). Spectroscopic data were coincident with those reported in the literature.

*Synthesis of **4**.*

N,*N*-phenyldiethanolamine (**3**) (1.80 g, 0.01 mol) was dissolved in dry acetonitrile (60 mL) and then the flask was purged several times with argon to remove oxygen and water from the atmosphere of the reaction. Sodium hydride (0.48 g, 0.02 mol) was gradually added at room temperature, after which a white precipitate appeared. Compound **2** (3.62 g, 0.024 mol) was dissolved in anhydrous

acetonitrile (10 mL) and then added drop-wise to the crude reaction using a compensated addition funnel. After this addition, the crude reaction was heated at reflux for 24 h. The crude reaction was filtered off and the organic solvent was eliminated using a rotary evaporator, yielding a yellow oil containing final product **4** together with other secondary compounds. Pure **4** (0.54 g, 1.80 mmol, 20%) was isolated as a yellow oil through column chromatography with aluminium oxide and hexane-ethyl acetate 5:1 v/v as the eluent. Spectroscopic data were coincident with those reported in the literature.

*Synthesis of **Azo**.*

4-aminopyridine (**5**) (36.7 mg, 0.4 mmol) was dissolved in a mixture of concentrated phosphoric acid (0.25 mL) and concentrated nitric acid (0.12 mL). This crude was slowly added to a solution containing sodium nitrite (33.4 mg, 0.48 mmol) and water (0.8 mL) at -5°C (using an ice bath). The generated diazonium salt of 4-aminopyridine was immediately added to a solution containing compound **4** (120 mg, 0.403 mmol) and 30% phosphoric acid (2 mL). The crude reaction was allowed to react for 30 min at -5°C and for 60 min at room temperature. The final dark red crude was neutralised with a saturated sodium carbonate solution and the organic product was extracted with dichloromethane. Organic layers were dried with $MgSO_4$, filtered off and the solvent was eliminated in a rotary evaporator. Product **Azo** (41 mg, 0.17 mmol, 24%) was isolated as a dark red solid through column chromatography with aluminium oxide and hexane-ethyl acetate 1:1 v/v as the eluent. ^{1}H-NMR (300 MHz, $CDCl_3$), δ (ppm): 8.7 (d, 2H), 7.9 (d, 2H), 7.7 (d, 2H), 6.8 (d, 2H), 3.8-3.5 (m, 16H), 3.2 (s, 6H). ^{13}C δ: 52.5, 59.8, 70.1, 73.2, 75.5, 114.6, 119.1, 126.2, 152.8.

*Synthesis of **Rh-S**.*

In a typical synthesis, 100 mg of template-free MCM-41 and rhodamine B dye (39 mg, 0.8 mmol rhodamine B/g MCM-41) were suspended in 25 mL of dry acetonitrile inside a round-bottomed amber flask in an inert atmosphere. The mixture was then stirred for 24 h at room temperature to achieve maximum

loading in the MCM-41 scaffolding pores. Finally, the solid (**Rh-S**) was filtered off, washed and dried at 37°C for 12 h.

*Synthesis of **Rh-I-S.***

Excess alkoxysilane derivative 3-iodopropyltrimethoxysilane (137μL, 0.7mmol) was added to the solution with the MCM-41 material loaded with Rhodamine B (**Rh-S**) and the final mixture was stirred for 24 h at room temperature. Finally, the solid (**Rh-I-S**) was filtered off, washed and dried at 37°C for 12 h.

*Synthesis of **Rh-Azo-S.***

The **Azo** (41 mg, 0.1 mmol) was dissolved in anhydrous acetonitrile (2 mL) and was added to 100 mg of MCM-41 loaded with Rhodamine B and externally functionalised with 3-iodopropyltrimethoxysilane (**Rh-I-S**) suspended in 20 mL of dry acetonitrile. Excess Rhodamine B was also added to the mixture in order to saturate the solution with dye, thus avoiding the dye leaving the inlets of the MCM-41 pores. The mixture was stirred and heated until reflux (110°C) for 72 h in a nitrogen atmosphere. The solid (**Rh-Azo-S**) was isolated as a dark violet solid by filtration, washed with 150 mL of acetonitrile, and dried at 40°C for 12 h.

*Synthesis of **Azo-S.***

In a typical synthesis, template-free MCM-41 (0.1 g) was suspended in 20 mL of dry acetonitrile. Then, excess alkoxysilane derivative 3-iodopropyltrimethoxysilane (130 μL, 0.66 mmol) was added to the solution with the MCM-41 material and the final mixture was stirred for 24 h at room temperature. **Azo** (33 mg, 0.082 mmol) was dissolved in anhydrous acetonitrile (2 mL) and was added to MCM-41 externally functionalised with 3-iodopropyltrimethoxysilane. The mixture was stirred and heated until reflux (110°C) fot 72 h in a nitrogen atmosphere. The solid (**Azo-S**) was isolated as a dark violet solid by filtration, washed with 50mL of acetonitrile, and dried at 40°C for 12 h.

*Synthesis of **CPT-Azo-S**.*

In a typical synthesis, template-free MCM-41 (100 mg) and chemotherapeutic agent camptothecin (56 mg, 0.16 mmol) were suspended in 25 mL of acetonitrile anhydrous:methanol 4:1 solution in a round-bottomed flask in an inert atmosphere. Excess alkoxysilane derivative 3-iodopropyltrimethoxysilane (130 μL, 0.66 mmol) was added to the solution with the MCM-41 material and the final mixture was stirred for 24 h at room temperature. **Azo** (33 mg, 0.082 mmol) was dissolved in anhydrous acetonitrile (2 mL) and was added to the MCM-41 externally functionalised with 3-iodopropyltrimethoxysilane. The mixture was stirred and heated until reflux (110°C) for 72 h in a nitrogen atmosphere. The solid (**CPT-Azo-S**) was isolated as a dark violet solid by filtration and washed with 200 mL of chloroform:methanol 3:1 mixture overnight. The final solid (**CPT-Azo-S**) was filtered and washed with 100 mL more of the chloroform:methanol 3:1 mixture. It was finally dried at 40°C for 12 h.

Dye release studies.

In a typical experiment, 6.8 mg of **Rh-Azo-S** were suspended in 17 mL of enzyme solution (17 mg of nitrate reductase in 17 mL of water at pH 7.5) and, at a certain time, an aliquot was separated and filtered. For the release studies with **Rh-Azo-S** without enzyme (blank), 6.8 mg of the solid were placed in 17 mL of water at pH 8 and, at a certain time, an aliquot was separated and filtered. The same quantities of **Rh-Azo-S** solid and enzyme were used in the esterase dye release studies, but at pH 8, which is the optimal for this enzyme. In both cases, the dye delivery from the pore voids to the aqueous solution was followed via dye fluorescence (Rhodamine B) at 580 nm emission (excitation at 554 nm).

Cell culture conditions.

The HeLa human cervix adenocarcinoma and the MCF-7 breast cancer cells were purchased from the German Resource Centre for Biological Materials (DSMZ) and were grown in D-MEM supplemented with 10% of FCS. Cells were maintained at 37°C in an atmosphere of 5% carbon dioxide and 95% air, and they underwent passage twice a week.

WST-1 cell viability assay.

HeLa and MCF-7 cells were cultured in sterile 96-well microtiter plates at a seeding density of 2500 and 3500 cells/well, respectively, and they were allowed to settle for 24 h. **Rh-Azo-S** in DMSO was added to cells at a final concentration of 200, 100 and 50 μg/mL. After 23 h, WST-1 (7 μL of a 5 mg/mL solution) was added to each well. Cells were further incubated for 1 h (a total of 24 h of incubation was therefore studied), and absorbance was measured at 450 nm and normalised versus absorbance at 690 nm.

*Live confocal microscopy **Rh-Azo-S**, **CPT-Azo-S** and **Azo-S** cellular internalisation assays.*

HeLa cells were seeded in 24 mm ϕ glass coverslips in 6-well plates at a seeding density of 50000 cells/well for 24 h. Then, cells were treated when indicated with **Rh-Azo-S**, **CPT-Azo-S** or **Azo-S** at concentrations of 100 and 50 μg/mL, Next, cells were incubated for 48 h prior to the confocal microscopy studies. For this purpose, cells were stained when indicated with 10 ng/mL of Hoechst 33342 and 5 mg/mL of WGA Alexa Fluor 647 for 30 min in PBS containing 10% FCS or by keeping the medium in case of **CPT-Azo-S** and **Azo-S** treatments. Slides were visualised under a confocal microscope.

*Cytofluorometry Studies Employing **CPT-Azo-S.***

To do the cytofluorometry studies, HeLa cells were seeded at 12500 cells/well in a 24-well in the case of HeLa. After 24 h, cells were treated with **CPT-Azo-S** or **Azo-S** at concentrations of 100 and 50 μg/mL. Then, cells were incubated for 48 h before staining them with PI and Ann V according to manufacturer's protocol (BD Pharmingen). Quantification of PI positive and Ann V positive staining was performed with the WinMDI programme, version 2.9.

Acknowledgements

We thank the Spanish Government (projects MAT2009-14564-C04, CTQ2007-64735-AR07 and SAF2010-15512) the Generalitat Valenciana (projects PROMETEO/2009/016 and /2010/005) for their support. We thank Eva Maria Lafuente and Alberto Hernández from the confocal microscopy service of CIPF for their technical support.

Keywords: Azopyridinium derivative • Enzymes • Intracellular controlled release • Gated materials.

References

1. a) R. Martínez-Máñez, F. Sancenón,*Coord. Chem. Rev.*, **2006**, *250*, 3081-3093; b) K. Ariga, J. P. Hill, M. V. Lee, A. Vinu, R. Charvet, S.Acharya, *Sci. Technol. Adv. Mater.*, **2008**, *9*, 014109-014204; c) P. Yang, S. Gai, J. Lin, *Chem. Soc. Rev.*, **2012**, *41*, 3679-3698; d) F. Tang, L. Li, D. Chen, *Adv. Mater.*, **2012**, *24*, 1504-1534.
2. a) Y. Zhu,M. Fujiwara, *Angew. Chem. Int. Ed*., **2007**, *46*, 2241-2244; b) M. Fujiwara, S.Terashima, Y. Endo, K.Shiokawa, H. Ohue, *Chem. Commun*., **2006**, 4635-4637.
3. B.G. Trewyn, I.I. Slowing, S. Giri, H.T. Chen, V.S.-Y.Lin, *Acc. Chem. Res*., **2007**, *40*, 846-853.
4. a) F. Torney, B. G. Trewyn, V.S.-Y. Lin, K. Wang, *Nat. Nanotechnol*. **2007**, *2*, 295-300; b) D.R. Radu, C.-Y.Lai, K. Jeftinija, E.W. Rowe, S. Jeftinija, V.S.-Y. Lin, *J. Am. Chem. Soc.*, **2004**, *126*, 13216-13217; c) S. Giri, B.G. Trewyn, M.P. Stellmaker, V.S.-Y. Lin, *Angew. Chem. Int. Ed.*, **2005**, *44*, 5038-5044; d) C.-Y. Lai, B.G. Trewyn,D.M. Jeftinija, K. Jeftinija, S. Xu, S.Jeftinija, V.S.-Y Lin, *J. Am. Chem. Soc*., **2003**, *125*, 4451-4459.
5. T.D. Nguyen, H.-R. Tseng, P. C. Celeste, A.H. Flood, Y. Liu, J.F.Stoddart, J.I. Zink, *Proc. Natl. Acad. Sci. USA*, **2005**, *102*, 10029-10034.
6. a) S. Angelos, M. Liong, E. Choi, J.I. Zink, *Chem. Eng. J.,* **2008**, *137*, 4-13; b) T.D. Nguyen, K.C.-F. Leung, M. Liong, C.D. Pentecost, J.F. Stoddart, J.I. Zink, *Org. Lett.***2006**, *8*, 3363-3366; c) K.C.-F. Leung, T.D. Nguyen, J.F. Stoddart, J.I. Zink, *Chem. Mater.*, **2006**, *18*, 5919-5928.
7. a) R. Casasús, E. Aznar, M.D. Marcos, R. Martínez-Mañez, F. Sancenón, J. Soto, P. Amorós, *Angew. Chem. Int. Ed*., **2006**, *45*, 6661–6664; b) R. Casasús, E. Climent, M.D. Marcos, R. Martínez-Mañez, F. Sancenón, J. Soto, P. Amorós, J. Cano, E. Ruiz, *J. Am. Chem. Soc*, **2008**, *130*, 1903-1917; c) A. Bernardos, E. Aznar, E.; C. Coll, R. Martínez-Máñez, J,M. Barat, M.D. Marcos, F. Sancenón, J. Soto, *J. Control. Release*, **2008**, *131*, 181-189.

8. a) E. Aznar, R. Martínez-Máñez, F.Sancenón, *Expert Opin. Drug. Deliv.*, **2009**, *6*, 643-655; b) E. Aznar, R. Casasús, B. García-Acosta, M. D. Marcos; R. Martínez-Máñez, F. Sancenón, J. Soto, P. Amorós, *Adv. Mater.*, **2007**, *19*, 2228-2231; c) E. Aznar, C.Coll, M.D. Marcos, R. Martínez-Máñez, F. Sancenón, J. Soto, P. Amorós, J. Cano, E. Ruíz, *Chem. Eur. J.*, **2009**, *15*, 6877-6888; d) E. Aznar, M.D. Marcos, R. Martínez-Máñez, F. Sancenón, J. Soto, P. Amorós, C. Guillem, *J. Am. Chem. Soc*., **2009***, 131*, 6833-6843.
9. a) N. Liu, Z. Chen, D.R. Dunphy, Y.B. Jiang, R.A. Assink, C. J. Brinker, *Angew. Chem.Int. Ed.*, **2003**, *42*, 1731-1734; b) Q. Lin, Q. Huang, C. Li,C.Bao, Z. Liu, F. Li, L. Zhu, *J. Am. Chem. Soc.*, **2010**, *132*, 10645-10647; c) S.-W. Song, K. Hidajat, S. Kawi, *Chem. Commun.*, **2007**, *42*, 4396-4398; d) Z. Wu, Y. Jiang, T. Kim, K. Lee, *J.Control. Release*, **2007**, *119*, 215-221.
10. N.K. Mal, M. Fujiwara, Y. Tanaka, *Nature*, **2003**, *421*, 350-353; b) N.K. Mal, M. Fujiwara, Y. Tanaka, T. Taguchi, M. Matsukata, *Chem. Mater.,* **2003**, *15*, 3385-3394.
11. R. Hernandez, H.-R. Tseng, J.W. Wong, J.F. Stoddart, J.I. Zink, *J. Am. Chem. Soc.*, **2004**, *126*, 3370-3371.
12. R. Casasús, M.D. Marcos, R. Martínez-Mañez, J.V. Ros-Lis, J. Soto, L.A. Villaescusa, P. Amorós, D. Beltrán, C. Guillem, J. Latorre, *J. Am. Chem. Soc.*, **2004**, *126*, 8612-8613.
13. C. Coll, R. Casasús, E. Aznar, M.D. Marcos, R. Martínez-Máñez, F. Sancenón, J. Soto, P. Amorós, *Chem. Commun.*, **2007**, 1957-1959.
14. Q. Fa, G.V.R. Rao, L.K. Ista, Y. Wu, B.P. Andrzejewski, L.A. Sklar, T.L. Ward, G.P. López, *Adv. Mater.*, **2003**, *15*, 1262-1266.
15. K. Patel, S. Angelos, W.R. Dichtel, A. Coskun, Y. –W. Yang, J. I. Zink, J. F. Stoddart, *J. Am. Chem. Soc.*, **2008**, 130, 2382-2383.
16. a) A. B. Descalzo, R. Martínez-Máñez, F. Sancenón, K. Hoffmann, K. Rurack, *Angew. Chem., Int. Ed.*, **2006**, *45*, 5924-5948; b) K. Ariga, A. Vinu, J.P. Hill, T. Mori, *Coord. Chem. Rev.*, **2007**, *251*, 2562-2591.
17. A. Schlossbauer, J.Kecht, T. Bein, *Angew.Chem. Int. Ed*., **2009**, *121*, 3138-3141.
18. C. Park, K. Lee, C. Kim, *Angew. Chem. Int. Ed*., **2009**, *48*, 1275-1278.
19. A. Bernardos, E. Aznar, M.D. Marcos, R. Martínez-Máñez, F. Sancenón, J. Soto, J.M. Barat, P. Amorós, *Angew. Chem. Int. Ed*., **2009**, *48*, 5884-5887..
20. R. Raffi, W. Franklin, C.E. Cerniglia, *Appl. Environ. Microbiol*., **1990**, *56*, 2146-2151.
21. M.K. Chourasia, S.K. Jain, *J Pharm. Sci.*, **2003**, *6*, 33-66.
22. R. Raffi, W. Franklin, C.E. Cerniglia, *Appl. Environ. Microbiol*., **1991**, *57*, 962-968.
23. R. Walker, A.J. Ryan, *Xenobiotica*, **1971**, *1*, 483-486.
24. V.R. Shina, R. Kumria, *Pharm. Res.*, **2001**, *18*, 557-564.
25. a) J.S. Beck, J.C. Vartuli, W. J. Roth, M. E. Leonowicz, C.T. Kresge, K. D. Schmitt, C.T. –W. Chu, D.H. Olson, E. W. Sheppard, S.B. McCullen, J. B. Hoggins, J.L. Schlenker, *J. Am. Chem. Soc.*, **1992**, *114*, 10834-10843; b) A.P. Wright, M.E. Davis, *Chem. Rev*., **2002**, *102*, 3589-3614; c) G. Kickelbick, *Angew. Chem. Int. Ed.*, **2004**, *43*, 3102-3104; d) K. Ariga, A. Vinu, Y. Yamauchi, Q. Ji, J. P. Hill, *Bull. Chem. Soc. Japan*, **2012**, *85*, 1-32.

26. S. K. Davidsen, J. B. Summers, D. H. Albert, J. H. Holms, H. R. Heyman, T. J. Magoc, R. G. Conway, D. A. Rhein, G. W. Carter, *J. Med. Chem.*, **1994**, *37*, 4423-4429.
27. J.V. Ros-Lis, B. García, D. Jiménez, R. Martínez-Máñez, F. Sancenón, J. Soto, F. Gonzalvo, M.C. Valldecabres, *J. Am. Chem. Soc.*, **2004**, *126*, 4064-4065.
28. a) J. El Haskouri, D. Ortiz de Zarate, C. C. Guillem, J. Latorre, M. Caldés, A. Beltrán, D. Beltrán, A.B. Descalzo, G. Rodríguez-López, R. Martínez-Máñez, M.D. Marcos, P. Amorós, *Chem. Commun.*, **2002**, 330-331; b) M. Comes, M. D. Marcos, R. Martínez-Máñez, F. Sancenón, J. Soto, L.A. Villaescusa, P. Amorós, D. Beltrán, *Adv. Mater.*, **2004**, *16*, 1783-1786; c) M. Comes, G. Rodríguez-López, M.D. Marcos, R. Martínez-Máñez, F. Sancenón, J. Soto, L.A. Villaescusa, P. Amorós, D. Beltrán, *Angew. Chem. Int. Ed.*, **2005**, *44*, 2919-2922.
29. C. T. Kresge, M.E. Leonowicz, W.J. Roth, J.C. Vartuli, J.S. Beck, *Nature*,**1992**, *359*, 710-712.
30. M. Vallet-Regí, *Chem. Eur. J.*, **2006**, *12*, 5934-5943.
31. E.P. Barret, L.G. Joyner, P.P. Halenda, *J. Am. Chem. Soc.*, **1951**,*73*, 373-380.
32. S. Brunauer, P.H. Emmett, E. Teller, *J. Am. Chem. Soc.*, **1938**, *60*, 309-319.
33. I. Goñi, A. Jiménez-Escrig, M. Gudiel, F.D. Saura-Calitxo, *Nutr. Res.*, **2005**, *25*, 60-615.
34. W.L Doyle, *J. Gen. Physiol.*, **1954**, *38*, 141–144.
35. A. Bernardos, L. Mondragón, E. Aznar, M. D. Marcos, R. Martínez-Máñez, F. Sancenón, J. Soto, J. M. Barat, E. Pérez-Payá, C. Guillem, P. Amorós, *ACS Nano*, **2010**, *4*, 6353-6368.
36. D. Abigerges, G.G. Chabot, J.P. Armand, P. Hérait, A. Gouyette, D. Gandia, *JCO*, **1995**, *13*, 210-221.
37. J. Lu, M. Liong, J.I. Zink, F.Tamanoi, *Small*, **2007**, *3*, 1341-1346.
38. A.Agostini, L. Mondragón, C. Coll, E. Aznar, E. Pérez-Payá, M.D. Marcos, R. Martínez-Máñez, F. Sancenón, J. Soto, P. Amorós, *Chem. Open,* **2012**, *1*, 17-20.

Chem. Eur. J. 2014, 20, 5271 – 5281.

2.3 *Enzyme-responsive intracellular-controlled release using silica mesoporous nanoparticles capped with ε–poly-L-lysine.*

*Laura Mondragón,[a,b,c,+] Núria Mas,[a,b,c,+] Vicente Ferragud,[a,b,c] Cristina de la Torre,[a,b,c] Alessandro Agostini,[a,b,c] Ramón Martínez-Máñez,[*a,b,c] Félix Sancenón,[a,b,c] Pedro Amorós,[d] Enrique Pérez-Payá,[†,e,f] and Mar Orzáez[e]*

[a]Centro de Reconocimiento Molecular y Desarrollo Tecnológico,
Unidad Mixta Universidad Politécnica de Valencia-Universidad de Valencia.
[b]Departamento de Química. Universidad Politécnica de Valencia
Camino de Vera s/n, E-46022 Valencia (Spain)
Fax: (+34) 96-387-93-49 E-mail:
[c]CIBER de Bioingeniería, Biomateriales y Nanomedicina (CIBER-BBN)
[d]Institut de Ciència del Materials (ICMUV)
Universitat de València. P.O. Box 2085, E-46071Valencia (Spain)
[e]Laboratorio Péptidos y Proteínas. Centro de Investigación Príncipe Felipe.
Avda. Autopista al Saler, 16, E-46012 Valencia, Spain.
[f]IBV-CSIC, Jaime Roig, 11, E-46010, Valencia.
[+]These authors contributed equally to this work.
[†]Deceased 28th May 2013.

We dedicate this work to the memory of Enrique Pérez-Payá. We will miss his enthusiasm for science and his brilliant remarks which made this, and previous works, possible.

Received: January 14, 2014
Published online: April 2, 2014

Abstract

The synthesis and characterization of two new capped silica mesoporous nanoparticles for controlled delivery purposes are described. Capped hybrid systems consist in MCM-41 nanoparticles functionalized on the outer surface with polymer ε–poly-L-lysine via two different anchoring strategies. In both cases, nanoparticles were loaded with model dye molecule $[Ru(bipy)_3]^{2+}$. An anchoring strategy involved the random formation of urea bonds by the reaction of propyl isocyanate-functionalized MCM-41 nanoparticles with the lysine amino groups located on the ε–poly-L-lysine backbone (solid **Ru-rLys-S1**). The second strategy involved a specific attachment through the carboxyl terminus of the polypeptide with azidopropyl-functionalized MCM-41 nanoparticles (solid **Ru-tLys-S1**). Once synthesized, both nanoparticles showed a nearly zero cargo release in water due to the coverage of the nanoparticle surface by polymer ε–poly-L-lysine. In contrast, a remarkable payload delivery was observed in the presence of proteases due to the hydrolysis of the polymer's amide bonds. Once chemically characterized, studies of the viability and the lysosomal enzyme-controlled release of the dye in intracellular media were carried out. Finally, the possibility of using these materials as drug-delivery systems was tested by preparing the corresponding ε–poly-L-lysine capped mesoporous silica nanoparticles loaded with cytotoxic drug camptothecin (CPT), **CPT-rLys-S1** and **CPT-tLys-S1**. Cellular uptake and cell death induction were studied. The efficiency of both nanoparticles as new potential platforms for cancer treatment was proved.

Introduction

Nanotechnology has brought about new innovative concepts to drug-delivery therapies.[1] In particular, drug delivery systems capable of releasing active molecules to certain cells in a controlled fashion have received much attention.[2] Among several potential drug delivery materials, silica mesoporous supports (SMPS) have been widely used in recent years as carriers for drug storage and delivery thanks to their unique properties, such as large loading capacity, low toxicity and easy functionalization.[3] Moreover, one highly appealing feature of SMPS as carriers is the possibility of functionalizing them with

molecular/supramolecular ensembles onto their external surface to develop gated-SMPS, which show "zero delivery" and can release their cargo on-command in response to specifically designed external stimuli.[4]

Different types of gated-SMPS have been reported and can be classified depending on the stimulus used to triggercargo delivery. Gated materials responding to light,[5] redox reactions,[6] pH,[7] change in polarity,[8] temperature[9] and certain bio-molecules[10] as stimuli have been reported. In the particular field where bio-molecules are employed as triggers, a recent demonstration showing that gated silica nanoparticles can be opened with high specificity via the selective enzyme-mediated hydrolysis of the cap[11] has extended the feasible use of SMPS to more biological and realistic contexts.[12] Moreover, the design of capped SMPS carriers that combine properties of polymers and mesoporous nanoparticles is an appealing approach, and may help develop new nanocarriers that combine the properties of both SMPS and polymer chemistries. One common stimulus used in the examples reported in the literature on polymer-functionalized SMPS to induce cargo delivery is temperature via the induction of polymer changes in conformation.[13] Together with temperature, conformation/volume modulations have also been employed in the design of gated mesoporous supports.[14] In addition, pH-associated changes have been used as a stimulus in the hydrogels covering the SMPS surface.[15] In the same context, redox-active organic polymers have also been attached to the surface of mesoporous matrices; in this case, the aperture of the pores is triggered by the rupture of S-S bonds with suitable reducing agents.[16] However, very few examples employing enzymes as external stimuli for the degradation and subsequent release of the cargo molecule have been described in polymer-containing SMPS.[17] In this context, the possibility of using enzymes for selective release applications opens up a wide range of new perspectives for the development of bio-compatible release systems.

In line with this, we selected polymer ε–poly-L-lysine as a suitable cap to be covalently anchored onto the external surface of SMPS. The ε–poly-L-lysine we selected consists of 25-35 repeated units of the L-lysine amino acid. Unlike normal

peptide bonds, which are linked by the alpha-carbon group, the lysine amino acids in ε–poly-L-lysine are linked molecularly by the epsilon amino group. ε–poly-L-lysine is obtained by natural fermentation in strains of bacteria in the genus *Streptomyces*.[18] Moreover, polymer ε–poly-L-lysine has been used as a drug-delivery and gene delivery carrier in the development of hydrogels, and also as an antimicrobial agent.[19] In addition, ε–poly-L-lysine has been reported to be non-toxic to humans, even at high doses, and as being biodegradable by amidases.[20] Another particular goal was to study the effect that using different anchoring procedures of capping polymer ε–poly-L-lysine on the SMPS surface has on the nanocarrier's performance. To achieve this objective, ε–poly-L-lysine was attached to the MCM-41 surface via two different strategies: through the amino groups in the lateral chains of the lysine amino acids (random); by means of the polymer's carboxy-terminal group (thread). The delivery performance in the absence and presence of amidases *in vitro* and in a cellular model was explored. This work aims to not only support previous observations made, which have proven that polymers are suitable caps in mesoporous systems for on-command cargo/drug delivery,[17] but to also demonstrate that the simple modulation of the release kinetics can be achieved based on the binding strategy used to anchor the polymer onto the surface of the mesoporous nanoparticles.

Results and Discussion

Gated materials.

The incorporation of gate-like ensembles into SMPS has proved a suitable approach to design nanoscopic solids for mass transport and controlled delivery applications.[4] As stated in the Introduction, among the reported gated materials, relatively very few use bio-molecules for capping or uncapping protocols. In particular, there are still very few examples that use enzymes as "biological keys" for opening gated SMPS.[11] Scheme 1 shows the proposed paradigm to prepare the gated material. In this approach, MCM-41 was used as an inorganic scaffold in the form of nanoparticles, functionalized in the pore outlets with ε-poly-L-lysine which is covalently attached to the SMPS in two different ways; randomly by the

nonspecific reaction of the amino groups of the polymer; specifically through the terminal C-side of the peptide (*vide infra*).

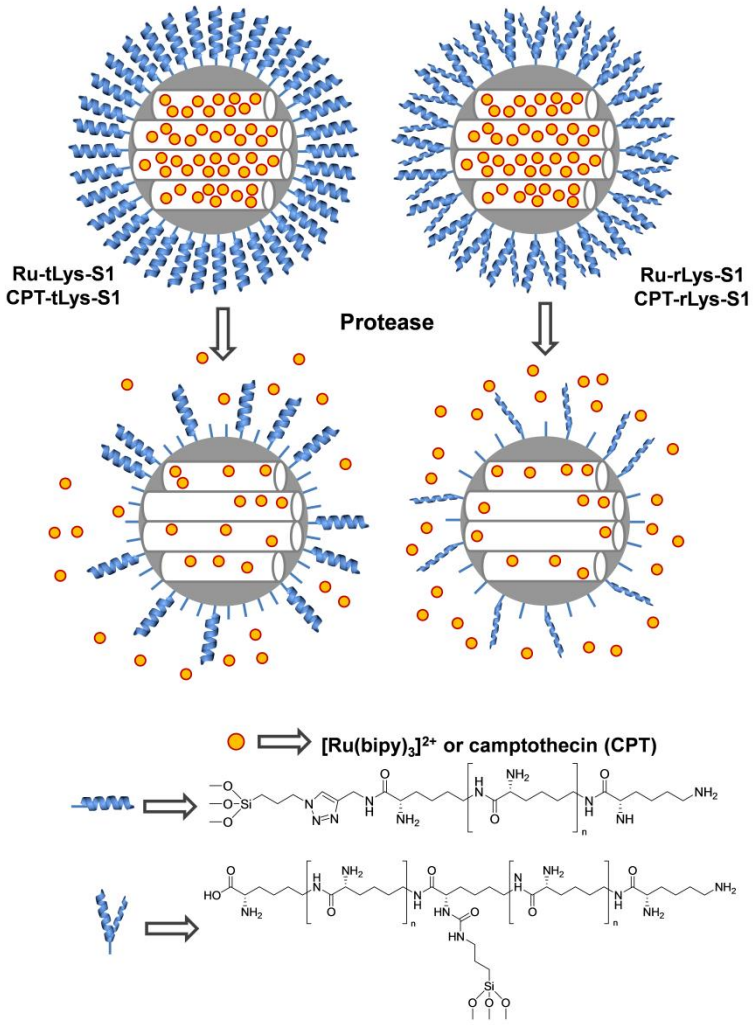

Scheme 1. Schematic representation of the prepared gated materials. **Ru-rLys-S1** and **CPT-rLys-S1** were capped with ε–poly-L-lysine randomly anchored onto MCM-41, whereas **Ru-tLys-S1** and **CPT-tLys-S1** were capped with ε-poly-L-lysine that was attached specifically through the C-terminal side of the peptide.

In a first step, the MCM-41 support was synthesized using tetraethyl orthosilicate (TEOS) as a hydrolytic inorganic precursor and surfactant

hexadecyltrimethylammonium bromide (CTAB) as the porogen species.[21] Calcination of the mesostructured phase resulted in the starting solid. Then $[Ru(bipy)_3]^{2+}$ was added to a methanol suspension containing the MCM-41 scaffolding.The mixture was stirred for 24 h in order to load the pores of the mesoporous support.

For the random attachment of polymer ε-poly-L-lysine, excess of 3-(triethoxysilyl)propyl isocyanate was added to the $[Ru(bipy)_3]^{2+}$-loaded nanoparticles and the final suspension was stirred for 2 h before adding ε-poly-L-lysine. This allowed the anchoring of the gate-like scaffolding by means of urea bond formation through the reaction of the isocyanate groups anchored onto the mesoporous nanoparticles with the amino groups in ε-poly-L-lysine (Scheme 1). The final solid was filtered, washed with methanol and dried. Following this procedure,the solid **Ru-rLys-S1** containing $[Ru(bipy)_3]^{2+}$ as a cargo and capped with ε-poly-L-lysine in a "random" configuration was obtained.

In a second strategy, we aimed to anchor polymer ε–poly-L-lysine in a "thread" conformation in which ε–poly-L-lysine is attached by one end of the polymeric chain in a thread-like arrangement around the SMPS nanoparticles. Among the different possible synthetic routes, a "click chemistry" azide alkyne Huisgen cycloaddition reaction was selected.[22] The aim was to first prepare an alkyne-ε–poly-L-lysine. This was carried out via the reaction of propargylamine with the carboxy terminus of the polymer to form an amide bond. In order to perform this reaction, the ε-poly-L-lysine-free amine groups were first protected by tBOC in order to avoid the nonspecific reactions of these primary amines with the activated carboxy-terminus of the polymer.

In a typical reaction, ε-poly-L-lysine was reacted with tBOC and the nonexistence of free primary amine groups was confirmed by Kaiser's test.[23] Then propargylamine was attached to the carboxyl group by means of an amide bond and by employing PyBOP and DIEA. After propargylamine had reacted, deprotection of the amine groups was done by 94% TFA in the presence of 5%

water and 1% TIS. Finally, the propargylamine-functionalized ε-poly-L-lysine was lyophilized and the modified polymer was characterized by mass spectrometry (MS). Figure 1 shows the MS spectra for ε-poly-L-lysine and the propargylamine-modified ε-poly-L-lysine polymers. The ε-poly-L-lysine spectrum shows a typical pattern for a polymer with a heterogenic size ranging from 3325.31 to 4477.25 g/mol (peaks from 1 to 10), which corresponds to 26 to 35 L-lysine units (128.09 g/mol once the amide bond is formed). In some cases, an increase in molecular weight of approximately 23 units g/molwas observed, which corresponded to the incorporation of Na^+. Addition of propargylamine (55.08 g/mol) should induce an increase of 37.06 g/mol in the former ε-poly-L-lysine polymer due to the formation of the amide bond and the release of a water molecule. When comparing both spectra, a clear correlation among the different peaks detected in the propargylamine-modified ε-poly-L-lysine (peaks a-h) and the original peaks (peaks 1-10) was noted, which indicates the proper attachment of the propargylamine molecule to the extreme of the ε-poly-L-lysine molecule (Figure 1B).

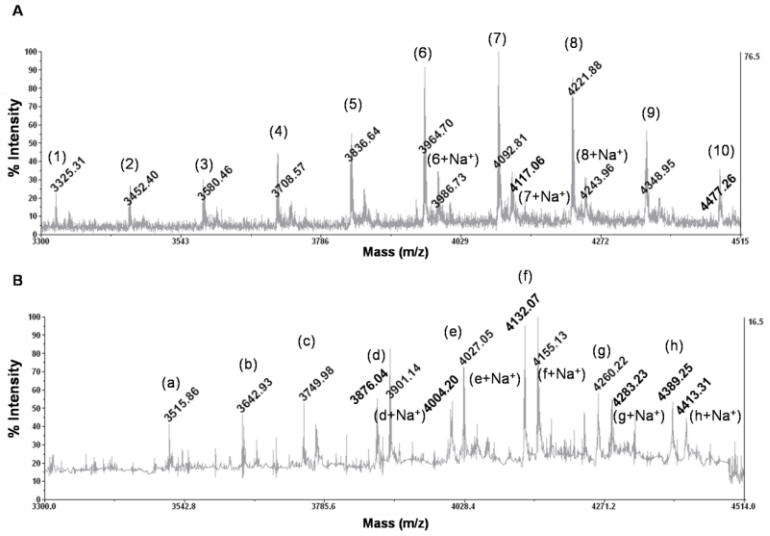

Figure 1. Mass spectroscopy spectra for ε-poly-L-lysine (A) and propargylamine-modified ε-poly-L-lysine (B). Correlation between peaks 1-10 and a-h: a, (2+Na^++P); b, (3+Na^++P); c, (4+P); d, (5+P); e, (6+P); f, (7+P); g, (2+P); h, (2+P). (P: Propargylamine incorporation, 37.08 g/mol; Na^+: Sodium incorporation, 23 g/mol). In all cases, differences of 2-3 g/mol were found, which are probably to the different protonation of the fragments under study.

For the polymer's "thread" attachment, $[Ru(bipy)_3]^{2+}$ loaded nanoparticles were first reacted with excess of 3-(azidopropil)triethoxysilane and the solid was isolated. Then the gated material was obtained by adding to the azide-functionalized nanoparticles propargylamine-functionalized polymer ε-poly-L-lysine, $CuSO_4 \bullet 5H_2O$ and sodium ascorbate 0.01 M. The final solid was filtered, washed with methanol to remove the unanchored excess of polymer ε-poly-L-lysine and dye outside the pores, and it was dried for at least 12 h. Following this procedure, the solid **Ru-tLys-S1** containing $[Ru(bipy)_3]^{2+}$ as a cargo and capped with ε-poly-L-lysine in a "thread" conformation was obtained (see Scheme 1).

Apart from the synthesis of **Ru-rLys-S1** and **Ru-tLys-S1,** two new solids (**CPT-rLys-S1** and **CPT-tLys-S1**, respectively) were synthesized by employing the same preparation strategies, but loaded with CPT (see the Experimental Section for further information).

Characterization of materials.

The prepared solids were characterized using standard techniques. Figure 2 shows the powder X-ray patterns of nanoparticles MCM-41 as-synthesized, MCM-41 calcined (**S1**), **Ru-rLys-S1**, **CPT-rLys-S1**, **Ru-tLys-S1** and **CPT-tLys-S1**. The X-ray pattern of the MCM-41 as-synthesized solid shows the four mesoporous characteristic low-angle reflections of a hexagonal-ordered array indexed as (100), (110), (200) and (210) Bragg peaks. Calcination of MCM-41 induced a significant shift of the (100) reflection. This displacement was accompanied by a slight broadening of the (110) and (200) reflections due to approximate cell contraction, which was induced for the condensation of silanols in the calcinations step and can be observed in all the synthesized solids. From the PXRD data, an a_0 (cell parameter) of 40.2 Å was calculated for the MCM-41 calcined starting material. Finally, the subsequent loading processes with $[Ru(bipy)_3]^{2+}$or CPT, and further functionalization with ε-poly-L-lysine with two different strategies to give solids **Ru-rLys-S1**, **CPT-rLys-S1**, **Ru-tLys-S1** and **CPT-tLys-S1,** resulted in the loss of the (110) and (200) reflections given the reduced contrast after the

loading/functionalization process. Notwithstanding, the permanence of the d_{100} peak still indicated that the mesoporous MCM-41 scaffolding was maintained in all these gated nanoparticles.

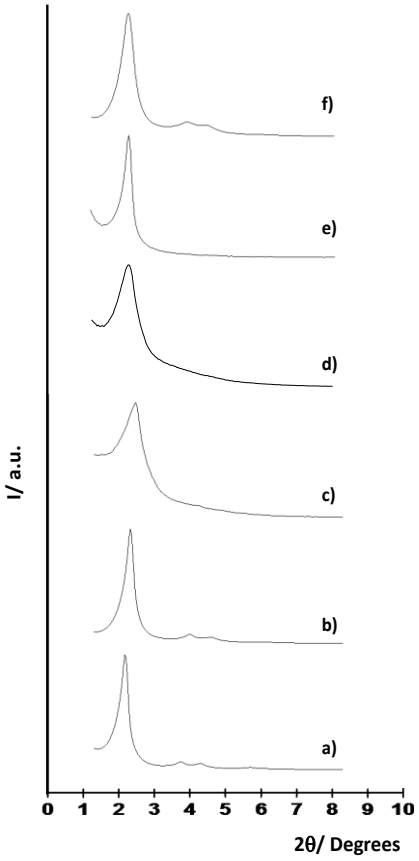

Figure 2. Powder X-ray patterns of the solids MCM-41 as synthesized (a), calcined MCM-41 (**S1**) (b) and final solids **Ru-rLys-S1** (c), **CPT-rLys-S1** (d), **Ru-tLys-S1** (e) and **CPT-tLys-S1** (f), respectively.

Together with the powder X-ray analysis, the preservation of the mesoporous structure in the final solids was also confirmed by Transmission Electron Microscopy (TEM). The TEM images of calcined MCM-41 **Ru-tLys-S1** and **CPT-tLys-S1** are shown in Figure 3. In all the solids, the characteristic channels of a mesoporous matrix were observed as alternate black and white lines. Moreover, the synthesized nanoparticles had diameters which fell within the 100-120 nm

range. The same features were observed for solids **Ru-rLys-S1** and **CPT-rLys-S1** (data not shown).

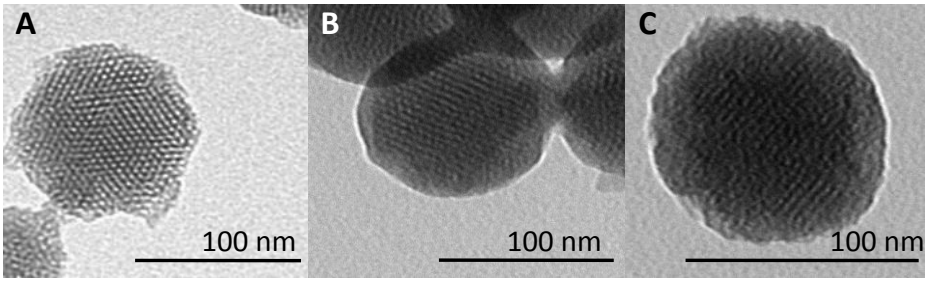

Figure 3. TEM images of calcined MCM-41 (A), **Ru-tLys-S1** (B) and **CPT-tLys-S1** (C). For all the materials, the typical porosity of the MCM-41 mesoporous matrix is shown.

Further, dynamic light scattering (DLS) studies showed particles with a mean diameter of 92.8 nm for calcined MCM-41, of 142.1 nm for **Ru-tLys-S1** and of 139.1 nm for **CPT-tLys-S1** (see Figure 4 and Table 1). The differences in the nanoparticle diameter could be ascribed to the surface functionalization with the bulky ε-poly-L-lysine polymer.

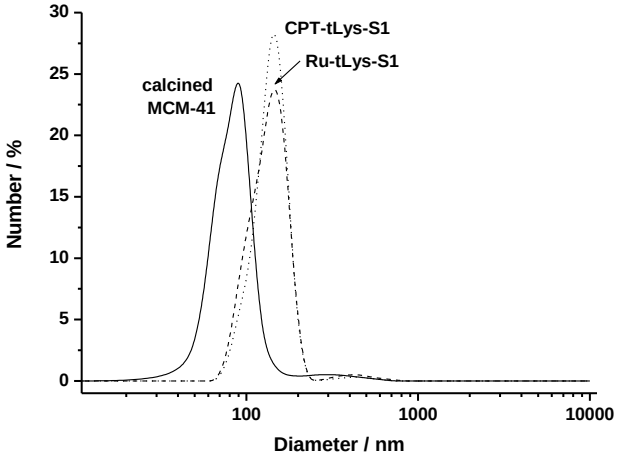

Figure 4. Size distribution by number of particles obtained by DLS studies for calcined MCM-41, **Ru-tLys-S1** and **CPT-tLys-S1**.

Also, Figure 4 showed that calcined MCM-41 nanoparticles and the final materials **Ru-tLys-S1** and **CPT-tLys-S1** formed aggregates of 390, 477.3 and 442.2 nm of diameter, respectively. However, only ca. 2-3% of the total nanoparticles are in the aggregated state (see also Table 1).

Table 1. Diameter of calcined MCM-41, **Ru-tLys-S1** and **CPT-tLys-S1** nanoparticles.

Solid	**Diameter** (nm)	**% of nanoparticles**
S1	92.8	96.6
	390	3.4
Ru-tLys-S1	142.1	97.9
	477.3	2.1
CPT-tLys-S1	139.1	98.6
	442.2	1.4

In Figure 5, the N_2 adsorption-desorption isotherms of the starting MCM-41 calcined nanoparticles (**S1**) are shown. The curve shows an adsorption step at P/P_0 values between 0.1 and 0.3, corresponding to a type IV isotherm, which is typical of mesoporous materials. This first step is attributed to nitrogen condensation in the mesopore inlets. With the Barret-Joyner-Halenda (BJH) model[24] on the adsorption curve of the isotherm, pore diameter and pore volume were calculated to be 3.8 nm and 1.03 cm^3g^{-1}, respectively. The absence of a hysteresis loop within this range and the low BJH pore distribution suggest a cylindrical uniformity of the mesopores. Using the BET model,[25] a total specific area of 1078 m^2g^{-1} was calculated. A second feature of the N_2 adsorption-desorption isotherms of the starting MCM-41 calcined nanoparticles is the characteristic H1 hysteresis loop that appeared on the curve at a high relative pressure (P/P_0> 0.8) and corresponded to the filling of the large pores between the nanoparticles due to textural porosity.

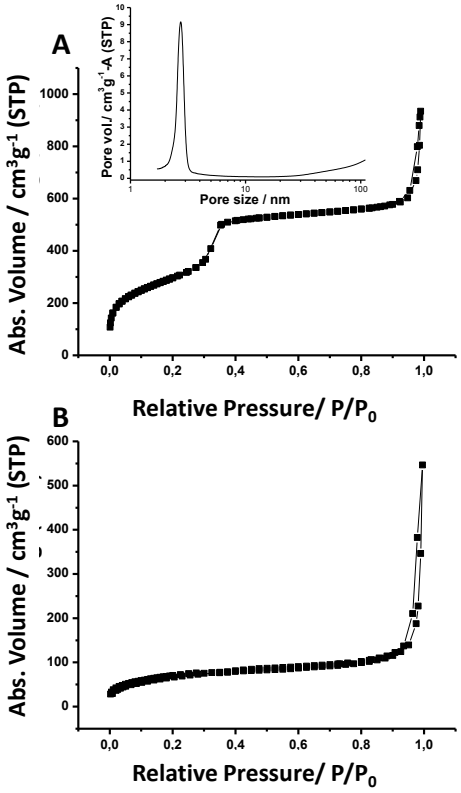

Figure 5. Nitrogen adsorption-desorption isotherms for A) MCM-41 calcined mesoporous material and B) **Ru-tLys-S1** material. The inset in A shows the pore size distribution of the MCM-41 mesoporous material.

For nanoparticles **Ru-rLys-S1**, **CPT-rLys-S1**, **Ru-tLys-S1** and **CPT-tLys-S1**, the N_2 adsorption-desorption isotherm is typical of mesoporous systems with partially filled mesopores. In this case, and as expected, a smaller N_2 adsorbed volume (BJH mesopore volumes within the 0.12-0.47 cm^3g^{-1} range) and surface area (within the 258-680 m^2g^{-1} range) were found when compared with the starting MCM-41 material. Moreover, Table 2 shows the BET-specific surface values, pore volumes and pore sizes, as calculated from the N_2 adsorption-desorption isotherms for MCM-41 calcinedand materials **Ru-rLys-S1**, **CPT-rLys-S1**, **Ru-tLys-S1** and **CPT-tLys-S1**.

Table 2. BET specific surface values, pore volumes and pore sizes calculated from the N_2 adsorption-desorption isotherms for selected materials.

Solid	S_{BET} ($m^2\ g^{-1}$)	Pore Volume [a] ($cm^3 g^{-1}$)	Pore size[b] (nm)
S1	1078	1.03	3.8
Ru-rLys-S1	495	0.44	3.6
CPT-rLys-S1	680	0.47	2.8
Ru-tLys-S1	258	0.12	2.4
CPT-tLys-S1	651	0.41	2.2

[a]Pore volumes and pore sizes were associated with only intraparticle mesopores.

[b]Pore size estimated by the BJH model applied to the adsorption branch of the isotherm.

Moreover, the contents of the grafted molecules and cargo in solids **Ru-rLys-S1**, **CPT-rLys-S1**, **Ru-tLys-S1** and **CPT-tLys-S1** were determined by elemental and thermogravimetric analyses, and are shown in Table 3. Similar amounts of the cargo and content of ε–poly-L-lysine were observed in all cases.

Table 3. Content of the molecular gate and guest molecule in the nanoparticles.

Solid	α_{Lys}	$\alpha_{guest\ molecule}$
Ru-rLys-S1	0.01	0.09
CPT-rLys-S1	0.02	0.11
Ru-tLys-S1	0.01	0.11
CPT-tLys-S1	0.01	0.09

[a]Grams of ε–poly-L-lysine ligand per gram of SiO_2 (α_{Lys}) and milimols of dye or CPT per gram of SiO_2 ($\alpha_{guest\ molecule}$) for **Ru-rLys-S1**, **CPT-rLys-S1**, **Ru-tLys-S1** and **CPT-tLys-S1**.

*Functional enzyme-driven-controlled release in solids **Ru-rLys-S1** and **Ru-tLys-S1.***

Solids **Ru-rLys-S1** and **Ru-tLys-S1** consist in mesoporous MCM-41-type nanoparticles containing $[Ru(bipy)_3]^{2+}$ in the pores, capped with polymer ε–poly-L-lysine attached to the MCM-41 surface by two different strategies; i.e., random (solid **Ru-rLys-S1**) and thread (solid **Ru-tLys-S1**). As part of the nanoparticles design, polymer ε–poly-L-lysine was expected to inhibit cargo delivery, yet the cargo was delivered in the presence of proteases via the protease-mediated

hydrolysis of the amide bonds contained in the polymer. In order to check this designed aperture mechanism of the gated nanoparticles, release kinetics studies were carried out using a mixture of proteases from *Streptomyces griseus*. In a typical experiment, 10 mg of the corresponding solid (**Ru-rLys-S1** and **Ru-tLys-S1**) were suspended in 25 mL of water at pH 7.5 in the presence or absence of the enzyme. Suspensions were stirred at room temperature for 24 h and aliquots of the samples were taken at a given time. The solid was then removed by centrifugation and dye delivery was monitored by measuring the emission of $[Ru(bipy)_3]^{2+}$ in the solution at 610 nm (λ_{ex} = 453 nm).[26]

The release kinetics obtained from solids **Ru-rLys-S1** and **Ru-tLys-S1** are depicted in Figure 6 as a percentage of total dye released at 24 h. As observed, solids **Ru-rLys-S1** and **Ru-tLys-S1** are tightly capped in the absence of the protease enzyme and no significant cargo release was observed. However in the presence of the protease enzyme, a clear delivery of the $[Ru(bipy)_3]^{2+}$ payload was noted for both solids.

When comparing the delivery profiles of the two different solids, it is important to remark that a faster release was observed for solid **Ru-rLys-S1** than for **Ru-tLys-S1**. At 6 h after protease addition, it was noteworthy that only 69% of the maximum dye release was achieved with nanoparticles **Ru-tLys-S1**, whereas it was 91% for **Ru-rLys-S1**. The greater release observed for solid **Ru-rLys-S1** may be ascribed to the random grafting of the attached peptide. This fact allowed the peptide to adopt an open conformation. Consequently, the peptidic bonds were more accessible to the enzyme, which could hydrolyze them more easily than in the case of solid **Ru-tLys-S1**.

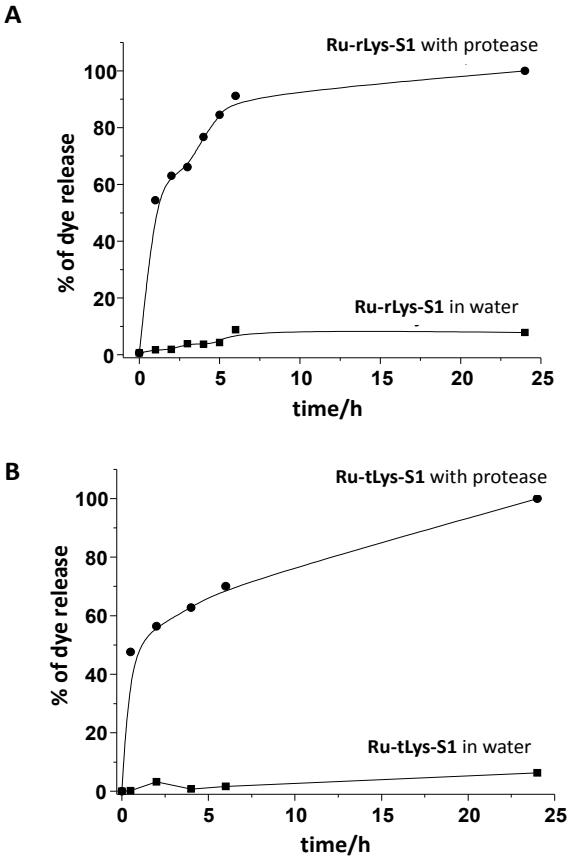

Figure 6. Release kinetics of $[Ru(bipy)_3]^{2+}$ from solids (A) **Ru-rLys-S1** and (B) **Ru-tLys-S1** at room temperature in the presence or absence of the proteases from *Streptomyces griseus.*

To further demonstrate that the protease enzyme was responsible for the release of the $[Ru(bipy)_3]^{2+}$ dye, other experiments were carried out. In a first test, the protease enzyme was denaturized by heating the solutions containing the enzyme (pH 7.5) at 60°C for at least 60 minutes before adding capped nanoparticles **Ru-rLys-S1** and **Ru-tLys-S1**. In a second experiment, solids **Ru-rLys-S1** and **Ru-tLys-S1** were incubated in the presence of other enzymes, such as amylases and β-D-galactosidase. In both experimental settings, no dye release was detected. This indicates the crucial role played by the protease enzyme in the opening mechanism.

Cellular uptake studies.

The cell internalization of the mesoporous silica nanoparticles bearing gated stimuli-responsive scaffoldings is a timely, appealing interdisciplinary research area in the nanosciencefield.[27] One goal of this study was to demonstrate that ε–poly-L-lysine-capped silica mesoporous nanoparticles can be used for in-cell delivery applications. Therefore, after the *in vitro* characterization of the different 'polylysine'-capped mesoporous scaffolds (*vide ante*), nanoparticles **Ru-rLys-S1** and **Ru-tLys-S1** were tested in further *ex vivo* assays.

It is well-known that cells display different mechanisms to internalize and obtain nutrients from the external medium. One such mechanism that is common is endocytosis. In this process, cells create an invagination in the plasma membrane to give a vesicle in which one portion of the external medium is "sequestered". Then this vesicle travels throughout the endosomal system until fusing to the so-called lysosomes. These are acidic vesicles containing different types of enzymes capable of degrading the molecules contained in the endocytosis vesicle (e.g., proteases, amylases, nucleases, lipases, etc.). Endocytosis is the typical way in which molecular entities, whose size is over 50 nm, are normally internalized.[28] Taking profit of this mechanism, it is conceivable to postulate that cargo-containing **Ru-rLys-S1** and **Ru-tLys-S1** can be transported to the lysosomes, where the activity of lysosomal enzymes, including proteases, will induce a polylysine hydrolysis-dependent release of the entrapped guest.

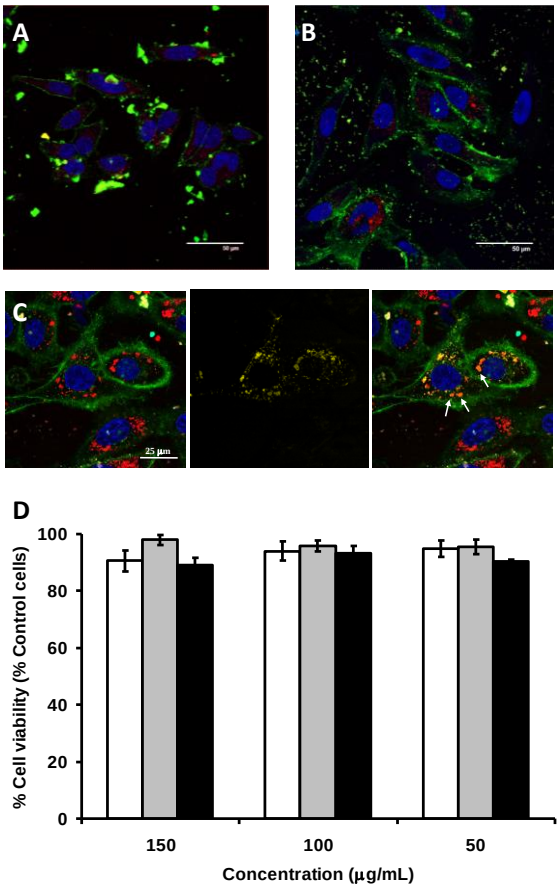

Figure 7. Cellular internalization and cell viability of the **Ru-rLys-S1** and **Ru-tLys-S1**. Confocal microscopy images corresponding to the HeLa cells treated with solid **Ru-rLys-S1** (A) and **Ru-tLys-S1** (B) at 150 μg/mL concentrations. The cellular uptake of the nanoparticles was followed by $[Ru(bipy)_3]^{2+}$-associated fluorescence (red) in the presence of DNA marker Hoechst 33342 (blue) and plasma membrane marker WGA-Alexa-Fluor 647 (green). C) To determine the lysosomal localization of the nanoparticles, HeLa cells were electroporated with LAMP1-GFP and treated with **Ru-tLys-S1** at 150 μg/mL concentrations. The colocalization of the LAMP1-GFP lysosoma-associated signal (yellow) and nanoparticle $[Ru(bipy)_3]^{2+}$-associated fluorescence (red) was observed in the presence of DNA marker Hoechst 33342 (blue) and plasma membrane marker WGA-Alexa-Fluor 647 (green), thus proving the lysosomal localization of the nanoparticles. White arrows indicate the colocalization of LAMP1-GFP with nanoparticles. D) For the cell viability studies, HeLa cells were treated with MCM-41, **Ru-rLys-S1** and **Ru-tLys-S1** and (white, gray and black bars, respectively) at concentrations of (150, 100 and 50 μg/mL), and after 48 h of incubation, WST-1 reagent was added and cell viability was measured. Two independent experiments containing triplicates were done. Data are expressed as (mean ± se).

Initially, the evaluation of cells' ability to internalize nanoparticles **Ru-rLys-S1** and **Ru-tLys-S1**, and nanoparticles' suitability in cellular toxicity terms, was made (see Figure 7). Confocal microscopy analyses were used to evaluate whether or not nanoparticles were internalized in the tumoral HeLa cell line (see the Experimental Section for detailed information) by tracking $[Ru(bipy)_3]^{2+}$-associated fluorescence. Moreover in these experiments, the cell nuclei and the cellular membrane were stained with Hoechst 33342 and fluorescent marker WGA Alexa Fluor 647, respectively. A dotted pattern of a $[Ru(bipy)_3]^{2+}$ fluorescent signal associated with intracellular vesicles was observed (see Figure 7), which suggests the internalization of nanoparticles. Additionally, a WST-1 cell viability assay was used to determine any nonspecific toxicity of **Ru-rLys-S1** and **Ru-tLys-S1**. The output of this assay indicated that both the nanoparticles were well-tolerated by HeLa cells under the experimental conditions.

The presence of **Ru-rLys-S1** or **Ru-tLys-S1**-containing intracellular vesicles suggested endosomal- (or endosomic)-mediated cellular internalization. In order to complete the characterization of the way that the prepared nanoparticles were internalized, HeLa cells were transfected with lysosomal-associated membrane protein 1 (LAMP1) fused to the green fluorescent protein (GFP, LAMP1-GFP). LAMP1 is a glycoprotein embedded in the lysosomal membrane, which presents a dotted pattern distribution when fused to the GFP that is related to its lysosomal membrane association. Once transfected, HeLa cells were incubated in the presence of **Ru-tLys-S1** and the fluorescence relating to the $[Ru(bipy)_3]^{2+}$ dye was determined. After this experimental procedure, a certain number of cells showed a dotted $[Ru(bipy)_3]^{2+}$ pattern that colocalized well with the LAMP1-GFP-associated vesicles, suggesting that the actual location of cell internalized **Ru-tLys-S1** is mainly in the lysosomes (see Figure 7C).

In another step, HeLa cells were treated with **CPT-rLys-S1** and **CPT-tLys-S1** to not only prove the lysosomal protease-mediated degradation of the capping ε–poly-L-lysine in the prepared nanoparticles, but to also test the potential use of

these capped nanoparticles in therapeutic applications. CPT is a hydrophobic drug that exerts its cytotoxic activity by inhibiting DNA polymerase I, thus disrupting DNA replication.[29] One of the main drawbacks of CPT is its low solubility in aqueous media, which makes its administration to patients difficult. However certain analogs of CPT, such as irinotecan, have been widely employed in the treatment of some cancer types, such as colon cancer or lymphoma.[30]

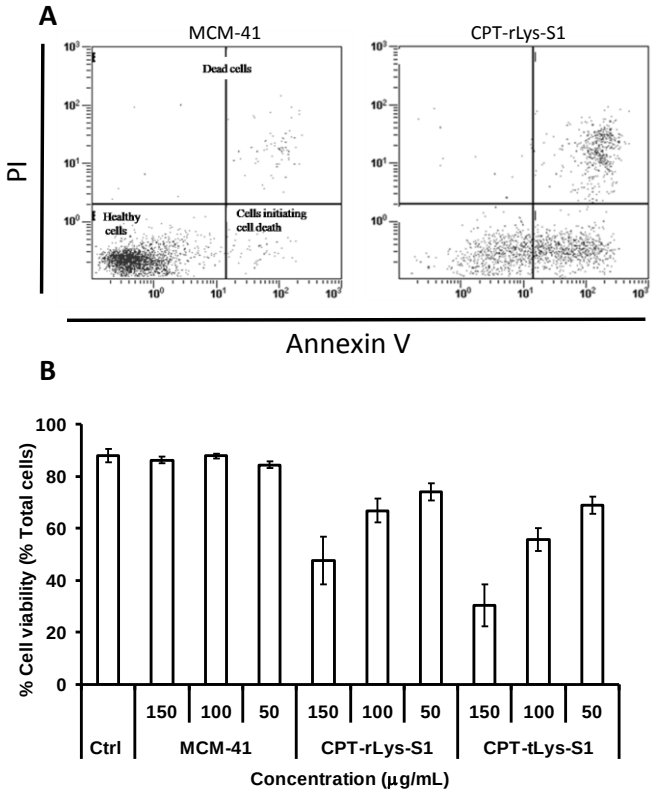

Figure 8. Cell death induction by solids **CPT-rLys-S1** and **CPT-tLys-S1**. HeLa cells were treated with concentrations of 150, 100 and 50 μg/mL of MCM-41, **CPT-rLys-S1** or **CPT-tLys-S1** for 48 h.Then flow cytometry studies were performed. PI and Ann V were employed to stain dead cells and those cells undergoing cell death, respectively. A) An example of PI and Ann V staining obtained after treatment with MCM-41 and **CPT-rLys-S1** is depicted. B) Quantification of viable cells (PI^-AnnV^-) is shown.Two independent experiments containing triplicates were performed. Statistically significant differences were observed ($P<0.05$, Student's t-test) among the cells treated with 150 μg/mL of **CPT-rLys-S1** or **CPT-tLys-S1** when compared to the control and MCM-41 treated cells. The results are expressed as (mean ± se).

In previous works, it has been demonstrated that CPT can be easily internalized by cells once inside the mesoporous nanoparticles.[31] HeLa cells were treated with concentrations of 150, 100 and 50 μg/mL of **CPT-rLys-S1** and **CPT-tLys-S1**, and cell death was examined. As controls, the MCM-41 nanoparticles were also added under the same conditions.

In order to obtain a more detailed analysis of the cell death processes related to the in-cell release of CPT from the nanoparticles, cell viability dye propidium iodide (PI) and early-stages cell death marker Annexin V (Ann V) were employed. Figure 8 shows the results obtained. Cell viability was seen to significantly reduce 48 h after the addition of **CPT-tLys-S1**. In particular, only 30% of the cells treated were completely viable (PI-AnnV-), the rest were dead or had started cell death processes when cells were treated with 150 μg/mL concentrations of this solid. **CPT-rLys-S1** also induced cell death; after 48 h of treatment, in this case, 50% of the cells were completely viable and the rest had died or had initiated cell death processes. In both cases, a dose-dependent induction of cell death was noted. If cells were treated with the same amounts of the MCM-41 nanoparticles, no significant cell death was induced and the cell viability values were similar to those observed in the control cells. These results prove that ε–poly-L-lysine functionalized nanoparticles are suitable supports for the delivery of entrapped molecules into cells for biological applications.

Conclusions

It has been demonstrated that the attachment of ε–poly-L-lysine as a gatekeeper onto the SMPS surface is a suitable method for designing carriers showing a zero release, but are still able to deliver the entrapped guest in the presence of suitable enzymes. Specifically, mesoporous silica nanoparticles **Ru-rLys-S1** and **Ru-tLys-S1** were prepared. These consist in SMPS loaded with the $[Ru(bipy)_3]^{2+}$ dye and capped with ε–poly-L-lysine via two different chemical reactions. In **Ru-rLys-S1**, the anchoring strategy involved the random formation of urea bonds via the reaction of propyl isocyanate-functionalized MCM-41

nanoparticles with the lysine amino groups located on the ε–poly-L-lysine backbone. For solid **Ru-tLys-S1**, the strategy consisted in a specific attachment through the carboxyl terminus of the polypeptide with azidopropyl-functionalized MCM-41 nanoparticles. *In vitro* release kinetics studies were done. Both functionalized nanoparticles (i.e.,**Ru-rLys-S1** and **Ru-tLys-S1**) showed no cargo release in the absence of proteases, which proves to be a suitable enzyme-dependent control of delivery. Moreover, a different delivery profile was also found depending on the method used to anchor the ε–poly-L-lysine backbone onto the mesoporous surface. Both nanoparticles **Ru-rLys-S1** and **Ru-tLys-S1** are efficiently taken up by tumoral (HeLa) cells. The cellular uptake of the nanoparticles occurs via endocytosis by targeting them to lysosomes, where the capping ε–poly-L-lysine is hydrolyzed by lysosomal enzymes and the cargo is delivered. Moreover, the possible use of ε–poly-L-lysine-capped nanoparticles as suitable delivery systems in cells of the chemotherapeutic agent camptothecin (CPT) is demonstrated, and reduced cell viability has been observed in those cells treated with solids **CPT-rLys-S1** and **CPT-tLys-S1**. These results indicate that it is possible to use relatively simple polymer-based derivatives to prepare biocompatible capped delivery nanodevices based on silica mesoporous supports. We believe that the possibility of using a wide range of capping systems, which can be selectively opened by bio-molecules (such as enzymes), opens up a wide range of opportunities in the design of nanodevices for controlled delivery applications.

Experimental Section

General Methods.

PXRD, TGA, N_2 adsorption-desorption, elemental analysis, mass spectroscopy and fluorescence spectroscopy techniques were employed to characterize the synthesized materials. Powder X-ray measurements were performed in a Seifert 3000TT diffractometer using Cu K_α radiation. Thermo-gravimetric analyses were carried out on a TGA/SDTA 851e Mettler Toledo balance using an oxidant atmosphere (air, 80 mL/min) with a heating program

consisting in a heating ramp of 10°C per minute from 393 to 1273 K and an isothermal heating step at this temperature for 30 minutes. The N_2 adsorption-desorption isotherms were recorded by a Micromeritics ASAP2010 automated sorption analyser. Samples were degassed at 120°C in vacuum overnight. The specific surface areas were calculated from the adsorption data within the low pressures range using the BET model. Pore size was determined following the BJH method. Dynamic Light Scattering (DLS) studies were conducted at 25 °C using a Malvern ZetasizerNano ZS instrument. All measurements were performed in triplicate on previously sonnicated highly dilute water dispersions. Fluorescence spectroscopy was carried out with a Felix 32 Analysis Version 1.2 (Build 56) PTI (Photon Technology International). The elemental analysis was performed in a CE Instrument EA-1110 CHN Elemental Analyzer. The mass spectrometry analysis was performed by employing a MALDI TOF/TOF 4700 Proteomics Analyzer (Applied Biosystems). Live cellular internalization studies were carried out with a Cytomics FC 500 (Beckman Coulter Inc.) and a confocal Leica microscope managed by a TCS SP2 system equipped with an acoustic optical beam splitter (AOBS). The cell viability and fluorescence spectroscopy measurements were carried out with a Wallac 1420 workstation.

Chemicals.

Chemicals tetraethylorthosilicate (TEOS), *n*-cetyltrimethylammonium bromide (CTAB), sodium hydroxide, tris(2,2'-bipyridyl)ruthenium (II) chloride hexahydrate ($[Ru(bipy)_3]Cl_2 \cdot 6H_2O$), 3-(triethoxysilyl)propyl isocyanate, triethylamine, di-tert-butyl dicarbonate (tBOC), propargylamine, ethyl 2-cyano-2-(hydroxyimino)aceate (OXYMA), diisopropylethylamine (DIEA), anhydrous dimethylformamide (DMF), trifluoroacetic acid (TFA), triisobutylsilane (TIS) and the protease enzyme from *Streptomyces griseus* were purchased from Sigma-Aldrich Química S.A. (Madrid, Spain) and were used without further purification. 3-(azidopropyl)triethoxysilane was provided by SelectLab Chemicals. Sodium ascorbate and copper (II) sulfate pentahydrate ($CuSO_4 \cdot 5H_2O$) were obtained from Scharlab (Barcelona, Spain). The HPLC-grade solvents and benzotriazol-1-yl-oxytripyrrolidinophosphonium hexafluorophosphate (PyBOP) were acquired from

Merck (Barcelona, Spain). ε–Poly-L-lysine was purchased from Chengdu Jinkai Biology Engineering Co., Ltd. All the other reagents were of a general laboratory grade and were purchased from Merck, unless otherwise stated. For the cell biology studies, D-MEM with L-glutamine, fetal calf serum (FCS), trypan blue solution (0.4%) cell culture grade, trypsin, wheat germ agglutinin Alexa Fluor 647 and Hoechst 33342 were provided by Gibco-Invitrogen. Cell proliferation reagent WST-1 was obtained from Roche Applied Science. Camptothecin was provided by Sequoia Research Products, Ltd. Annexin V and propidiumiodide were supplied by BD Pharmingen.

Synthesis of the mesoporous support (MCM41-type material).

MCM-41-like mesoporous nanoparticles were synthesized by the following procedure: *n*-cetyltrimethylammonium bromide (CTAB, 2.00 g, 5.4mmol) was first dissolved in 960 mL of deionized water. NaOH (aq) (2.00 M, 7 mL) was added to the CTAB solution, and the solution temperature was adjusted to 95°C. TEOS (10 mL, $5 \cdot 10^{-2}$ mol) was then added drop-wise to the surfactant solution. The mixture was left to stir for 3 h to give a white precipitate. The solid product was centrifuged and washed with deionized water until a neutral pH. Finally, the solid was dried at 60°C (MCM-41 as-synthesized). To prepare the final porous material (MCM-41), the as-synthesized solid was calcined at 550°C using an oxidant atmosphere for 5 h to remove the template phase.

Synthesis of propargyl-amide-ε-poly-L-lysine.

In order to specifically attach ε-poly-L-lysine through its carboxyl group to the silica mesoporous material, 0.5 g of polymer (0.1 mmol of polymer, 3.7 mmol of amine groups) was suspended in 40 mL of methanol and trietilamine (0.3 mL, 0.3 mmol). Once the polymer was dissolved, di-tert-butyl dicarbonate (tBOC, 0.8 g, 4 mmol) was added and the mixture was stirred for 2 h. Then methanol was removed by employing a rotary evaporator. The total protection of the amine groups was assessed by Kaiser's test. Afterward, 0.65 g of BOC-ε-poly-L-lysine (approx. 0.1 mmol of polymer) was suspended in dichloromethane, and propargylamine (23 μL, 0.4 mmol) was attached to the carboxyl group by an

amide bond employing PyBOP (0.52 g, 1 mmol), OXYMA (0.142 g, 1 mmol) and DIEA (0.348 mL, 2 mmol). Then the solvent was removed using a rotary evaporator, the crude was dissolved in 40 mL of TFA: H_2O:TIS (94:5:1) and stirred at room temperature for 4 h to deprotect the amine moieties. The final product was precipitated as a white solid by the addition of *t*-butylmethyl ether (30 mL) to the crude reaction at -20°C. This precipitate was isolated by centrifugation, dissolved in water and lyophilized prior to use. The final product was characterizedby mass spectroscopy.

*Synthesis of **Ru-rLys-S1** and **CPT-rLys-S1**.*

In a typical synthesis, 0.5 g of MCM-41 and 0.3 g (0.4 mmol) of $[Ru(bipy)_3]Cl_2{\cdot}6H_2O$ or 0.14 g (0.4 mmol) of camptothecin (CPT) were suspended in 50 mL of methanol or chloroform:methanol (4:1 v/v), respectively, inside a round-bottom flask in an inert atmosphere. The mixture was stirred for 24 h at room temperature in order to achieve maximum loading in the pores of the MCM-41 scaffolding. Excess of 3-(triethoxysilyl)propylisocyanate (0.5 mL, 2 mmol) was added and the final mixture was stirred for 5.5 h at room temperature. Then, 0.5 g of ε–poly-L-lysine (0.1 mmol of polymer, 3.7 mmol of the amine groups), dissolved in 20 mL of methanol, was added and stirred for 2 h. Finally, the solids (**Ru-rLys-S1** and **CPT-rLys-S1**) were filtered off. Once dried, the solid was resuspended in 80 mL of methanol or chloroform:methanol (4:1) in the case of **Ru-rLys-S1** or **CPT-rLys-S1**, respectively, and was stirred to remove the dye remaining outside the pores. After 12 h, the solids were filtered and dried at 37°C for 24 h.

*Synthesis of **Ru-tLys-S1** and **CPT-tLys-S1**.*

In a typical synthesis, 0.5 g of MCM-41 and 0.3 g (0.4 mmol) of $[Ru(bipy)_3]Cl_2{\cdot}6H_2O$ or 0.14g (0.4 mmol) of camptothecin (CPT) were suspended in 50 mL of methanol or chloroform:methanol (4:1 v/v), respectively, inside a round-bottom flask in an inert atmosphere. The mixture was stirred for 24 h at room temperature to achieve maximum loading in the pores of the MCM-41 scaffolding. Then excess of 3-(azidopropil)triethoxysilane (0.5 mL, 2 mmol) was added and the final mixture was stirred for 5.5 h at room temperature. Once the

3-(azidopropil)triethoxysilane was anchored onto the surface of the material, the nanoparticles were filtered off and dried at 37°C for 12 h. Finally for the preparation of the **Ru-tLys-S1** and **CPT-tLys-S1** nanoparticles, a mixture of azide-functionalized nanoparticles (0.2 g) and propargylamine-ε-poly-L-lysine (0.2 g, 0.04 mmol) was suspended in a 50:50 mixture of DMF and H_2O (30 mL), followed by the addition of ruthenium (II) dye $Ru(bipy)_3^{2+}$ (0.15 g, 0.2 mmol) to avoid the delivery of the dye from the pores to the bulk solution during the synthesis of the solids (for solid **CPT-tLys-S1** synthesis, CPT was not added to the bulk solution given its low DMF solubility). Then 150 µL of a solution of $CuSO_4 \cdot 5H_2O$ 10^{-3} M and sodium ascorbate 0.01 M were added. The final mixture was stirred at 90°C for 3 day. The nanoparticles were centrifuged and washed thoroughly with water to remove unreacted and adsorbed molecules. The resulting nanoparticles (**Ru-tLys-S1** and **CPT-tLys-S1**) were finally dried under vacuum conditions.

Cargo release studies.

In a typical experiment, the evaluation of the gate-like effect was made by studying the release of $[Ru(bipy)_3]^{2+}$ from the pore voids of the capped materials. In a typical experiment, 10 mg of solids **Ru-rLys-S1** and **Ru-tLys-S1** were placed in water (25 mL) at pH 7.5 in the presence of the protease enzyme (0.12 mg mL^{-1}) from *S. griseus*. At a certain time, the aliquots were separated and filtered. The delivery of the $[Ru(bipy)_3]^{2+}$ dye was monitored by the fluorescence emission band of $[Ru(bipy)_3]^{2+}$ at 610 nm (λ_{ex} = 453 nm).

Cell Culture Conditions.

HeLa human cervix adenocarcinoma cells were purchased from the German Resource Centre for Biological Materials (DSMZ) and were grown in D-MEM supplemented with 10% of FCS. Cells were maintained at 37°C in an atmosphere of 5% carbon dioxide and 95% air, and underwent passage twice a week.

WST-1 Cell Viability Assays.

Cells were cultured in sterile 96-well microtiter plates at a seeding density of 2500 cells/well for HeLa and were allowed to settle for 24 h. MCM-41, **Ru-rLys-S1** and **Ru-tLys-S1** were added to the cells at a final concentration of 150, 100 and 50 μg/mL. After 47 h, WST-1 (7 μL of a 5 mg/mL solution) was added to each well. Cells were further incubated for 1 h (a total of 24 hours of incubation was therefore studied), and absorbance was measured at 450 nm and normalized versus 690 nm with a Wallac 1420 workstation.

*Live confocal microscopy with **MCM-41**, **Ru-rLys-S1**, **CPT-rLys-S1**, **Ru-tLys-S1** and **CPT-tLys-S1**.*

Cellular Internalization: HeLa and MCF-7 cells were seeded on 24 mm ϕ glass coverslips in 6-well plates at a seeding density of $50 \cdot 10^3$ cells/well for 24 h. After 24 h, cells were treated, whenever indicated, with MCM-41, **Ru-rLys-S1**, **CPT-rLys-S1**, **Ru-tLys-S1** or **CPT-tLys-S1** at concentrations of 150 μg/mL. Next cells were incubated for 48 h prior to the confocal microscopy studies. For this purpose, cells were stained whenever indicated with 10 ng/mL of Hoechst 33342 and 5 mg/mL of wheat germ agglutinin (WGA) Alexa Fluor 647. Slides were visualized under a confocal microscope. Two independent experiments were done and gave similar results.

*Cytofluorometry studies employing **Ru-rLys-S1**, **CPT-rLys-S1**, **Ru-tLys-S1** and **CPT-tLys-S1**.*

HeLa cells were seeded at $12.5 \bullet 10^3$ cells/well in a 24-well plate. After 24 h, cells were treated with MCM-41, **Ru-rLys-S1**, **CPT-rLys-S1**, **Ru-tLys-S1** or **CPT-tLys-S1** at concentrations of 150, 100 and 50 μg/mL. Cells were incubated for 48 h prior to staining them with PI and Ann V according to the manufacturer's protocol (BD Pharmingen). Quantification of PI-positive and Ann V-positive staining was performed with theWinMDI program, version 2.9. Two independent experiments containing triplicates were performed with similar results.

Acknowledgements

We thank the Spanish Government (Project MAT2012-38429-C04, CTQ2007-64735-AR07 and SAF2010-15512) and the Generalitat Valenciana (Project PROMETEO/2009/016) for support. LM and AA thank the Generalitat Valenciana for their post-doctoral contract VALI+D and Santiago Grisolía PhD fellowship, respectively. NM thanks The Spanish Ministry of Science and Innovation for her FPI fellowship. CT thanks the Universitat Politècnica de València for her PhD fellowship. MO thanks the CIPF for her post-doctoral fellowship. We thank the confocal microscopy service, Alberto Hernández and Eva María La Fuente from CIPF for their technical support.

Keywords: anchoring strategy•capped silica mesoporous nanoparticles•enzyme-responsive•intracellular release•ε-poly-L-lysine

References

1. a) Z. Ge, S. Liu, *Chem. Soc. Rew*., **2013**, *42*, 7289-7325; b) O. C. Farokhzad, R. Langer,*ACS Nano*, **2009**,*3*, 16-20; c) S. Wang,*Micropor.Mesopor.Mater.***, 2009**,*117*, 1–9; d) X.-X. Zhang, H. S. Eden, X. Chen, *J.Control. Release,***2012**, *159*, 2–13; e) Q. He, J. Shi, *Adv. Mater.*, **2014**, *26*, 391-411.
2. K. M. L. Taylor-Pashow, J. Della Rocca, R. C. Huxford, W. Lin, *Chem. Commun*. **2010**, *46*, 5832–5849; b) P. Yang, S. Gai, J. Lin, *Chem. Soc. Rew*., **2012**, *41*, 3679-3698; c) Z. Li, J. Barnes, A. Bosoy, J.F.Stoddart, J.I. Zink, *Chem. Soc. Rew*., **2012**, *41*, 2590-2605; d) M. Colilla, B. González, M. Vallet-Regí, *Biomat. Sci*., **2013**, *1*, 114-134; e) Q. He, J. Shi, *J. Mater. Chem.*, **2011**, *21*, 5845-5855.
3. a) N. Vadia, S. Rajput, *Asian J. Pharmac. Clin. Res.* **2011**, *4*, 44 –53; b) J. S. Beck, J. C. Vartuli, W. J. Roth, M. E. Leonowicz, C. T. Kresge, K. D. Schmitt, C. T. W. Chu, D. H. Olson, E. W. Sheppard, S. B. McCullen, J. B. Hoggins, J. L. Schlenker*, J. Am. Chem. Soc.***1992***, 114*, 10834 – 10843;c) A. P. Wright, M. E. Davis*, Chem. Rev.***2002**, *102*, 3589 –3614; d) G. Kickelbick, *Angew. Chem.***2004**, *116*, 3164 – 3166; *Angew.Chem.Int. Ed*. ***2004***, *43*, 3102 – 3104; e) K. Ariga, A. Vinu, Y. Yamauchi, Q. Ji, J.P. Hill, *Bull. Chem. Soc. Japan*, **2012**, *85*, 1-32; f) D. Tarn, C. E. Ashley, M. Xue, E. C. Carnes, J. I. Zink, C. J. Brinker, *Acc. Chem. Res.*, **2013**, *46*, 792-801.
4. a) C. Coll, A. Bernardos, R. Martıínez-Máñez, F. Sancenón*, Acc.Chem. Res*., **2013**, *46*, 339-349; b) E. Aznar, R. Martıínez-Máñez, F. Sancenón, *ExpertOpin*. *Drug Delivery*, **2009**, *6*, 643-

655; c) K. Cotí, M. E. Belowich, M. Liong, M. W. Ambrogio, Y. A. Lau, H. A. Khatib, J. I. Zink, N. M. Khashab. J. F. Stoddart, *Nanoscale*, **2009**, *1*, 16-39.

5. a) E. Johansson, E. Choi, S. Angelos, M. Liong, J. I. Zink, *Sol-Gel Sci. Technol*., **2008**, *46*, 313-322; b) Q. Lin, Q. Huang, C. Li, C. Bao, Z. Liu, F. Li, L. Zhu, L. *J. Am. Chem. Soc.*, **2010**, *132*, 10645-10647; c) J. Lai, X. Mu, Y. Xu, X. Wu, C. Wu, C. Li, J. Chen, Y. Zhao*, Chem. Commun*., **2010**, *46*, 7370-7372; d) A. Agostini, F. Sancenón, R. Martínez-Máñez, M.D. Marcos, J. Soto, P. Amorós, *Chem. Eur. J*.,**2012**, *18*, 12218-12221.
6. a) R. Hernandez, H. –R. Tseng, J. W. Wong, J. F. Stoddart, J. I. Zink, *J. Am. Chem. Soc*., **2004**, *126*, 3370-3371; b) R. Mortera, J. Vivero-Escoto, I. I. Slowing, E. Garrone, B. Onida, V. S.-Y. Lin, *Chem. Commun*., **2009**, 3219-3221.
7. a) R. Casasus, M. D. Marcos, R.Martínez-Máñez, J. V. Ros-Lis, J. Soto, L. A. Villaescusa, P. Amorós, D. Beltrán, C. Guillem, J. Latorre, *J. Am. Chem. Soc*., **2004**, *126*, 8612-8613; b)V. Cauda, C. Argyo, A. Schlossbauer, T. J. Bein, *J. Mater. Chem.*, **2010**, 20, 4305-4311; c) S. Angelos, Y. –W. Yang, K. Patel, J. F. Stoddart, J. I. Zink, Angew. Chem. Int. Ed., **2008**, 47, 2222-2226; d) H. Meng, M. Xue, T. Xia, Y. –L. Zhao, F. Tamanoi, J. F. Stoddart, J. I. Zink, E. A. Nel, *J. Am. Chem. Soc*., **2010**, *132*, 12690-12697;e) J. Liu, X. Du, *J. Mat. Chem*., **2010**, *20*, 3642-3649; f) W. Guo, J. Wang, S. -J. Lee, F. Dong, S. S. Park, C. –S. Ha, *Chem. Eur. J*., **2010**, *16*, 8641-8646; g) A. Popat, J. Liu, G. Q. Lu, S. Z. Qiao, J. Mater. Chem., **2012**, *22*, 11173-11178; h) Y. Zhu, J. Shi, W. Shen, X. Dong, J. Feng, M. Ruan, Y. Li, *Angew. Chem. Int. Ed.*, **2005**, *44*, 5083-5087; i) Q. He, Y. Gao, L. Zhang, Z. Zhang, F. Gao, X. Ji, Y. Li, J. Shi, *Biomaterials*, **2011**, *32*, 7711-7720.
8. C. Coll, R. Casasús, E. Aznar, M. D. Marcos, R. Martínez-Máñez, F. Sancenón, J. Soto, P. Amorós. *Chem. Commun*, **2007**, *19*, 1957 – 1959.
9. a) C. Liu, J. Guo, W. Yang, J. Hu, C. Wang, S. Fu, J. Mat. Chem., **2009**, *19*, 4764-4770; b) C. R. Thomas, D. P. Ferris, J. –H. Lee, E. Choi, M. H. Cho, E. S. Kim, J. F. Stoddart, J. –S. Shin, J. Cheon, J. I. Zink, *J. Am. Chem. Soc.*, **2010**, *132*, 10623-1025; c) E. Aznar, L. Mondragón, J.V. Ros-Lis, F. Sancenón, M.D. Marcos, R. Martínez-Máñez, J. Soto, E. Pérez-Payá, P. Amorós, *Angew. Chem. Int. Ed*., **2011**, *50*, 11172-11175.
10. E.Climent, R. Martínez-Máñez, F. Sancenón, M.D. Marcos, J. Soto, A. Maquieira, P. Amorós, *Angew. Chem. Int. Ed*., **2010**, *49*, 7281-7283; b) M. Oroval, E. Climent, C. Coll, R. Eritja, A. Aviñó, M.D. Marcos, F. Sancenón, R. Martínez-Máñez, P. Amorós, *Chem. Commun.,* **2013**, *49*, 5480-5482; c) N. Mas, I. Galiana, L. Mondragón, E. Aznar, E. Climent, N. Cabedo, F. Sancenõn, J.R. Murguía, R. Martínez-Máñez, M.D. Marcos, P. Amorós, *Chem. Eur. J*., **2013**, *19*, 11167-11171; d) E. Climent, L. Mondragõn, R. Martínez-Máñez, F. Sancenón, M-D. Marcos, J.R. Murguía, P. Amorós, K. Rurack, *Angew. Chem. Int. Ed*., **2013**, *52*, 8938-8942.
11. See for example: a) K. Patel, S. Angelos, W. R. Dichtel, A. Coskun, Y.-W. Yang, J. I. Zink, J. F. Stoddart, *J. Am. Chem. Soc*., **2008**, 130, 2382-2383; b) A. Schlossbauer, J. Kecht, J. Bein, *Angew. Chem., Int. Ed.*, **2009**, 48, 3092-3095; c) C. Park, H. Kim, S. Kim, C. Kim*, J. Am. Chem. Soc*., **2009**, *131*, 16614-16615; d) A. Bernardos, E. Aznar, M. D. Marcos, R. Martínez-Máñez, F. Sancenón, J. Soto, J. M. Barat, P. Amorós, *Angew. Chem. Int. Ed*., **2009**, *48*, 5884-

5887; e) A. Bernardos, L. Mondragon, E. Aznar, M. D. Marcos, R. Martínez-Máñez, F. Sancenón, J. Soto, J. M. Barat, E. Pérez-Payá, C. Guillem, P. Amorós, *ACS Nano*, **2010**, *4*, 6353-6368;f) P. D. Thornton, A. Heise, *J. Am. Chem. Soc*., **2010**, *132*, 2024-2028;g) C. Coll, L. Mondragón, R. Martínez-Máñez, F. Sancenón, M. D. Marcos, J. Soto, P. Amorós, E. Pérez-Payá, *Angew. Chem. Int. Ed*., **2011***, 50*, 2138-2140.

12. a) K. Ariga, Q. Ji, T. Mori, M. Naito, Y. Yamauchi, H. Abe, J. P. Hill, *Chem. Soc. Rev.*, **2013**, *42*, 6322-6345; b) S. H. Lee, J. H. Kim, C. B. Park, *Chem. Eur. J.*, **2013**, *19*, 4392-4406; c) A. Agostini, L. Mondragón, A. Bernardos, R. Martínez-Máñez, MD Marcos, F. Sancenón, J. Soto, A. Costero, C. Manguan-García, R. Perona, M. Moreno-Torres, R. Aparicio-Sanchis, J.R. Murguía, *AngewChemInt Ed Engl*, **2012**, *42*,10556-10560.
13. a) B. Yan, Q. Kai, X. Wang, *Inorg. Chim.Acta*, **2011**, 376, 302 –309; b)K. Zhang, W. Wu, K. Guo, J. Chen, P. Zhang, *Langmuir*, **2010**, *26*, 7971 – 7980.
14. a) Q. Fu, G.V.R. Rao, L.K. Ista, Y. Wu, B.P. Andrzejewski, B. A. Sklar, T.L.Ward, G.P. López, *Adv. Mater.* **2003**, *15*, 1262 – 1266; b) Q. Fu, G.V.R. Rao, T.L. War, Y. Lu, G.P. López, *Langmuir,* **2007**, *23*, 170 – 174; c) Y.Z. You, K.K. Kalebail, S.L. Brock, Oupicky D, *Chem. Mater.* **2008**, *20*, 3354 –3359; d) Z.Y. Zhou, S.M. Zhu, D. Zhang, *J. Mater. Chem.,* **2007**, *17*, 2428 – 2433; e) S. Zhu, Z. Zhou, D. Zhang, C. Jin, Z. Li, *Micropor. Mesopor. Mater.,* **2007**, *106*, 56 –61; f) Y. Zhu, S. Kaskel, T. Ikoma, N. Haganata, *Micropor. Mesopor. Mater.* **2009**, *123*, 107 –112.
15. G.J. Copello, A.M. Mebert, M. Raineri, M.P. Pesenti, L.E. Diaz, *J. Hazard Mater.***2011**, *186*, 932 – 939.
16. R. Liu, X. Zhao, T. Wu, P. Feng, *J. Am. Chem. Soc.***2008**, *130*, 14418 – 14419.
17. A. Bernardos,L. Mondragón,I. Javakhishvili,N. Mas,C. de la Torre, R. Martínez-Máñez,F. Sancenón, J. M. Barat, S. Hvilsted, M. Orzáez, E. Pérez-Payá, P. Amorós*, Chem. Eur. J*., **2012**,*18*, 13068–13078.
18. S. Shima, H. Sakai, *Agric. Biol. Chem*.,**1977**,*41*, 1807–1809.
19. C. Zhou,P. Li,X. Qi,A. R. M. Sharif,Y. F. Poon,Y. Cao,M. W. Chang, S. Su Jan Leong, M. B. Chan-Park, *Biomaterials*,**2011**, *32*, 2704–2712.
20. a) S. Shima, H. Matsuoka, T. Iwamoto, H. Sakai, *J Antibiot*, **1984**, *37*, 1449–1455 b) J. Hiraki, *Fine Chem.*, **2000**, *29*, 25–28 c) I.L. Shih, M.H. Shen, Y.T. Van, *Bioresour Technol.*, **2006**, *97*, 1148–1159.
21. S. Cabrera, J. El Haskouri, C. Guillem, J. Latorre, A. Beltrán, D. Beltrán, M.D- Marcos, P. Amorós, *Solid State Sci*., **2000**, *2*, 405-420.
22. a) V. V. Rostovtsev, L. G. Green, V. V. Fokin, K. B. Sharpless,*Angew. Chem. Int. Ed*. **2002**,*41*, 2596 – 2599; b) C. W. Tornoe, C. Christensen, M. Meldal,*J. Org. Chem.***2002**, *67*, 3057 – 3064; c) H. C. Kolb, M. G. Finn,K. B. Sharpless, *Angew. Chem. Int. Ed.***2001**, *40*, 2004 – 2021; d) R. Huisgen, *Angew. Chem. Int. Ed. Eng*. **1963**, *2*,565 – 598.
23. E.Kaiser, R. L. Colescott, C. D. Bossinger, P. Cook, *Anal. Biochem*., **1970**, *34*,595–598.
24. E. P. Barrett, L. G. Joyner, P. P. Halenda,*J. Am. Chem. Soc.,***1951**,*73*, 373–380.
25. S. Brunauer, P. H. Emmett, E. Teller,*J. Am. Chem. Soc.,***1938**,*60*,309–319.

26. a) F. Felix, J. Ferguson, H.U Gudel, A. Ludi, *J. Am. Chem. Soc*, **1980**, *102*, 4096-4102; b) F. E. Lytle, D. M. Hercules, *J. Am. Chem. Soc,* **1969***,91,*253-257.
27. J.M. Rosenholm, A. Meinander, E. Peuhu, R. Niemi, J.E. Eriksson C. Sahlgren, M. Linden, *ACS Nano*, **2009**, *3*, 197-206.
28. a) T.-G. Iversena, T. Skotlanda, K. Sandviga, *Nano Today*, **2011**, *6*,176-185; b) H. Kettiger,A. Schipanski,P. Wick, J. Huwyler,*J. Int J Nanomedicine*, **2013**, *8*, 3255-3269.
29. F. Farabegoli, M. Govoni, F. Novello,*Biol Cell*, **1992**, *74*, 281-286.
30. D. Abigerges, G. G. Chabot, J. P. Armand, P. Hrait, A. Gouyette,D. Gandia, *J Clin. Oncol,***1995**, *13*, 210 – 221.
31. a) N. Mas, A. Agostini, L. Mondragón, A. Bernardos, F. Sancenón, M.D. Marcos, R. Martínez-Máñez, A.M. Costero, S. Gil, M. Merino-Sanjuán, P. Amorós, M. Orzáez, E. Pérez-Payá;*Chem. Eur. J.*,**2013**,*19*,1346-1356; b)A. Agostini, L. Mondragón, L. Pascual, E. Aznar, C. Coll, R. Martínez-Máñez, F. Sancenón, J. Soto, M.D. Marcos, P. Amorós, A.M. Costero, M. Parra, S. Gil, *Langmuir*, **2012**, *28*, 14766-14776;c) I. Candel, E. Aznar, L. Mondragón, C. de la Torre, R. Martínez-Máñez, F. Sancenón, M.D.Marcos, P. Amorós, C. Guillem, E. Pérez-Payá, A. Costero, S. Gil, M. Parra, *Nanoscale*, **2012**, *4*,7237-7245.

2.4 *Towards the development of smart 3D "gated scaffolds" for on-command delivery.*

Núria Mas,[a] Daniel Arcos,[b] Lorena Polo,[a] Elena Aznar,[a] Sandra Sánchez-Salcedo,[b] Félix Sancenón,[a] Ana García,[b] M. Dolores Marcos,[a] Alejandro Baeza,[b] María Vallet-Regí,[,b] and Ramón Martínez-Máñez*[,a]*

[a] Centro de Reconocimiento Molecular y Desarrollo Tecnológico (IDM). Unidad Mixta Universitat de València – Universitat Politècnica de València and Departamento de Química. Camino de Vera s/n, 46022, Valencia, Spain and CIBER de Bioingeniería, Biomateriales y Nanomedicina (CIBER-BBN), Spain.
E-mail: rmaez@qim.upv.es

[d] Departamento de Química Inorgánica y Bioinorgánica. Facultad de Farmacia, Universidad Complutense de Madrid. Instituto de Investigación Sanitaria Hospital 12 de Octubre i+12. Plaza Ramón y Cajal s/n, 28040 Madrid, Spain, and CIBER de Bioingeniería, Biomateriales y Nanomedicina (CIBER-BBN), Spain.
E-mail: vallet@farm.ucm.es

Article first published online: 30th July 2014

Porous biomaterials using polymers, ceramics, metals, or glasses, have been extensively studied, and are widely used as scaffolds for tissue and bone regeneration in a multi-millionaire market context.[1,2] Porous scaffolds provide a three-dimensional environment that preserves tissue volume, supports cell interactions and, in some cases, delivers biological agents for repairing, maintaining, restoring or improving the function of organs and tissues.[3] In all these cases, it is highly desirable to have scaffolds that can regulate the delivery of biological agents (for instance, drugs, cells, etc.) because control over release can improve the safety and efficiency of agents, and allows the design of advanced scaffolds and new therapies. However, most of the porous scaffolds currently used in tissue engineering are mainly non-active; that is, they deliver biological agents through passive mechanisms which typically involve material degradation coupled with molecular diffusion.[4-11] Moreover, the drug release kinetics of these systems is usually uncontrolled and supports are unable to retain the drug payload for a long time.[12]

From a different point of view, progress in bio-molecular chemistry and nanotechnology have recently resulted in the design of biologically inspired systems with innovative bio-related functions and fuelling areas, such as bio-engineering, bio-sensing, bio-nanotechnology and drug delivery in new directions. Drug-delivery systems capable of releasing active molecules in a controlled manner have recently gained much attention. In this field, mesoporous silica nanoparticles (MSN) have been widely used as reservoirs for drug storage given their unique mesoporous structure, large specific volume and easy functionalisation.[13] Additionally, MSN can be functionalised with molecular/supramolecular ensembles on their external surface to develop gated MSN which show “zero delivery” (i.e., the hybrid material is unable to release the payload), but are capable of releasing their cargo in response to external stimuli.[14-18] The great potential of designing a hybrid material with nanometric controlled delivery features has motivated scientists to develop a wide variety of stimuli-responsive MSN-capped systems capable of being opened by chemical[19-25]

(i.e., redox molecules, selected anions, pH changes and biomolecules), physical[26-31] (i.e., light, temperature or magnetic fields) or biochemical[32-37] triggers.

Given the need to develop scaffolds for advanced therapies which can improve features of conventional systems, in this communication, we show for the first time (as far as we are aware) a new approach to design tailor-made scaffolds capable of displaying selective and controlled cargo delivery based on the combination of suitable 3D supports and gated mesoporous materials.

As a proof of concept, our strategy involves the preparation of a biomaterial of potential application in bone tissue engineering. It consists of a macroporous scaffold, prepared by rapid prototyping (RP) techniques, that incorporates capped MSN designed to deliver the cargo under specific events. In particular, the designed MSN can be opened on command in the presence of acid phosphatase (APase), an enzyme whose concentration is used to assess osteoclast activity in bone remodelling processes[38,39] and as a biochemical marker for the presence of bone metastases.[40,41] Accordingly, this stimuli-responsive "gated scaffold" opens up new alternatives to treat osteoporotic fractures and bone cancer.

For this study, MCM-41-based MSN (ca. 100 nm) were selected as the inorganic scaffold. Calcined MSNs were loaded with tris(2,2'-bipyridyl)ruthenium(II) chloride and the external surface of the silica mesoporous nanospheres was functionalised with 3-[2-(2-aminoethylamino)ethylamino]propyl-trimethoxy silane to yield solid **S1**. The final material (solid **S2**) was obtained by treating the neutral aqueous solutions of **S1** with adenosine triphosphate (ATP). This is expected to cap the pores by the formation of a dense network in pore outlets through supramolecular hydrogen-bonding interactions, and electrostatic forces between the large negatively charged ATP anions and the positively charged ammonium groups on MSN. The presence of ATP in **S2** would inhibit cargo release, whereas the hydrolysis of the ATP cap by APase is anticipated to induce it, as depicted in Scheme 1.

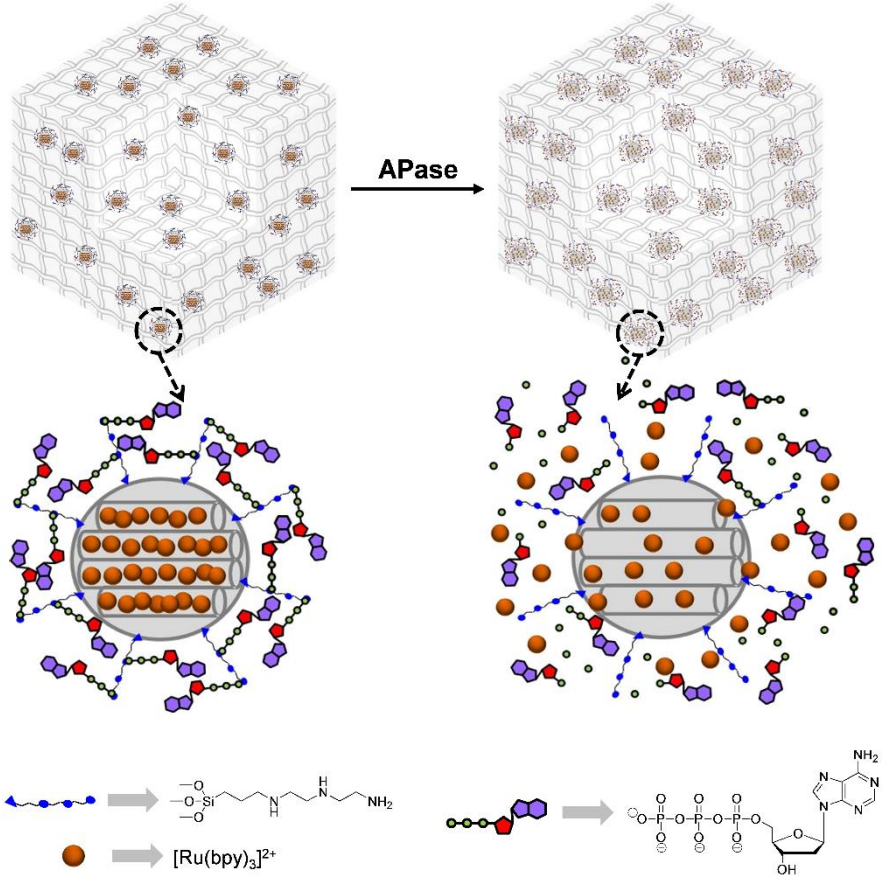

Scheme 1. Schematic representation of the APase-driven MSN system.

The calcined starting MSN and solids **S1** and **S2** were characterised by standard techniques. Figure 1A shows the diffraction pattern of the prepared solids, which display typical features of the MCM-41 phase, indicating that the mesopores in the nanoparticles were preserved throughout the filling process, external amines anchoring and capping with ATP. Figure 1B depicts a representative TEM image of solid **S2**, in which the black and white strips, typical of the porosity of the MCM-41 phase, can be clearly seen.

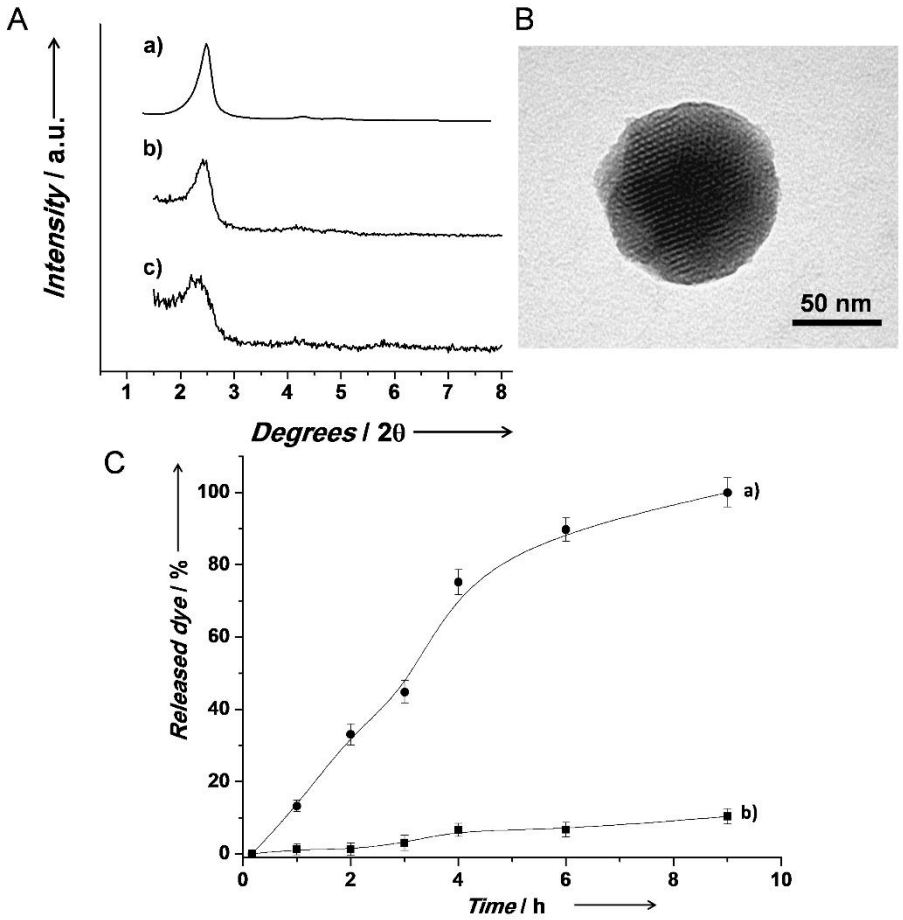

Figure 1. (A) Powder X-Ray diffraction pattern of a) starting calcined MCM-41, b) nanoparticulated **S2**, c) **S3** scaffold (vide infra). (B) Representative TEM image of the **S2** gated nanoparticles. (C) Kinetic dye release studies done at 37°C in water of ATP-capped solid **S2** a) in the presence and b) absence of APase.

The N_2 adsorption-desorption isotherm of the starting calcined MSN showed a typical type-IV curve from which a specific surface area of 931.5 m^2g^{-1}, a narrow pore size distribution and an average pore diameter of 2.39 nm were calculated. In contrast, the N_2 adsorption-desorption isotherm of final gated materials **S2** was typical of the capped and filled mesoporous systems. In this case, a lower N_2 adsorbed volume and a smaller surface area (24.6 m^2g^{-1}) were found when compared with the starting material (see Supporting Information for

further details). Moreover, the organic content of solids **S1** and **S2** calculated from thermogravimetry and elemental analysis are shown in Table 1.

Table 1. Organic content (α, mmol/g of solid) in solids **S1** and **S2**

Solid	α_{dye}	$\alpha_{polyamine}$	α_{ATP}
S1	0.16	1.70	----
S2	0.04	1.35	0.14

After characterisation, cargo release studies were carried out with **S2**. In a typical experiment, 4 mg of **S2** were suspended in water in both the presence and absence of APase. Suspensions were kept at 37°C, and at certain time intervals, fractions of both suspensions were taken and centrifuged to remove the solid. Dye delivery into the solution was then measured by the fluorescence of $[Ru(bpy)_3]^{2+}$ at 593 nm (λ_{ex} 454 nm). The delivery profiles of $[Ru(bpy)_3]^{2+}$ in both the presence and absence of APase enzyme are shown in Figure 1C. As seen, nanoparticles **S2** are tightly capped in the absence of APase and show a negligible release of $[Ru(bpy)_3]^{2+}$ (Figure 1C, curve b); in contrast, the presence of APase induces the opening of the pores and the subsequent cargo release.

The observed performance confirms the proposed paradigm. When APase enzyme is absent, ATP molecules interact strongly with the polyamines anchored in **S2** and are able to block the release of the entrapped dye. However in the presence of APase, the enzyme hydrolyses the phosphate-phosphate ATP bonds by disassembling the polyamine-phosphate interactions, and by inducing the pore aperture and the subsequent dye release. The APase-mediated hydrolysis of ATP in **S2** was confirmed by STEM-EDX studies which, in turn, confirmed that the P/Si ratio in **S2** was 3-fold lower when the solid was treated with APase. Moreover ^{31}P-NMR studies done in the aliquots collected in the release studies clearly showed the presence of increasing amounts of phosphate (at δ +2.1 ppm), which correlated well with the amount of released cargo. Finally, in order to further confirm that the uncapping mechanism was driven by APase, dye release studies

on **S2** in the presence of other enzymes, such as esterase and pepsin, and in the presence of denatured APase, were performed. Under these conditions, no significant cargo release was observed (see Supporting Information).

Bearing in mind the promising results obtained with capped solid **S2**, we take a step forward towards the possibility of designing gated 3D macroporous scaffolds for potential applications for filling bone defects. In these designed supports, the scaffold macropore system must be highly interconnected and large enough to support bone ingrowth and angiogenesis. Depending on the kind of the host bone, i.e. cortical or cancellous bone, these parameters can vary, but the pore size must be large enough to allow the formation of mature bone within the macropore arrangement, being considered an appropriate pore size a range between 300-2000 micrometers for the bone ingrowth after implantation.[42,43] In this context many processes have been developed to prepare macroporous supports, such as replicas of porous sponges and coral exoskeletons, production of gas bubbles via gas evaporation, chemical reactions, and introduction of porogens (such as organic volatile particles) in a ceramic slip and gel-casting, either alone or in combination with a multiple tape-casting method.[44-46] However, pore size, shape and its interconnectivity, cannot be fully controlled in these approaches. In contrast, rapid prototyping (RP) is a good alternative to fulfil requirements for manufacturing suitable scaffolds for different clinical applications and individuals. Following these concepts, the **S2** nanoparticles were incorporated into a 3D gelatin framework produced using rapid prototyping 3D printing[40,41] to obtain the final gated 3D scaffold **S3**.

In a typical experiment to prepare **S3**, an aqueous solution of gelatin at 37°C was mixed with **S2** nanoparticles under vigorous stirring. Then a solution containing glutaraldehyde as a cross-linker was added. The mixture was stirred at room temperature until it formed a paste of appropriate consistency for injection. The scaffold was fabricated by direct ink deposition over a pre-cooled plate to build 3D-pieces with tetragonal symmetry. After frizzing samples, they were cut into smaller ca. 6 × 6 × 4 mm new dimensions, and were once again placed in a

glutaraldehyde solution. Finally after a new freeze and drying process, **S3** was obtained.

The **S3** gated scaffolds were characterised by X-ray diffraction (XRD), thermogravimetry and SEM. The presence of the (100) reflection in the **S3** XRD pattern (Figure 1Ac) confirmed mesostructure preservation during the scaffold manufacturing process. From the thermogravimetric analysis, a content of 25±3% in weight of SiO_2 was calculated. It is estimated that around 35% in weight of **S3** is composed of **S2** nanoparticles. The SEM analysis of the **S3** scaffolds showed several porosity levels, resulting in a hierarchical porous system. At the macroscopic level, **S3** presented orderly distributed pores from 900 to 1200 µm, which are the product of the porosity architecture designed by the rapid prototyping of the scaffold surface and the scaffold fracture, respectively (Figure 2A and B). A second porosity level is also observed (Figure 2C and D) in the sinus of the scaffold walls. This second level is formed by pores from 40-100 µm, whose size and presence are determined by the degree of cross-linking of the gelatin. This macroporosity makes the permeability of the surrounding medium possible (in which the APase can be included) in the inner scaffold walls. Finally, the images taken at higher magnifications (Figure 2D and E) show a sponge-like structure formed by gelatin covers that surrounds the **S2** nanoparticles. The observed scaffold features were also studied by EDX analysis, which was performed at several **S3** sites (Figure 2F). The presence of Si and P in the magnified images of **S3** confirmed the incorporation of the **S2** nanoparticles into the scaffold. Moreover, in vitro degradability of **S3** in water was studied. In a typical experiment, a piece of 8 mg of **S3** was placed in 1 mL of distilled water under orbital stirring at 37 ºC. The weight of the hydrated scaffolds was measured after ten months and only a 10 % of weight lost was observed.

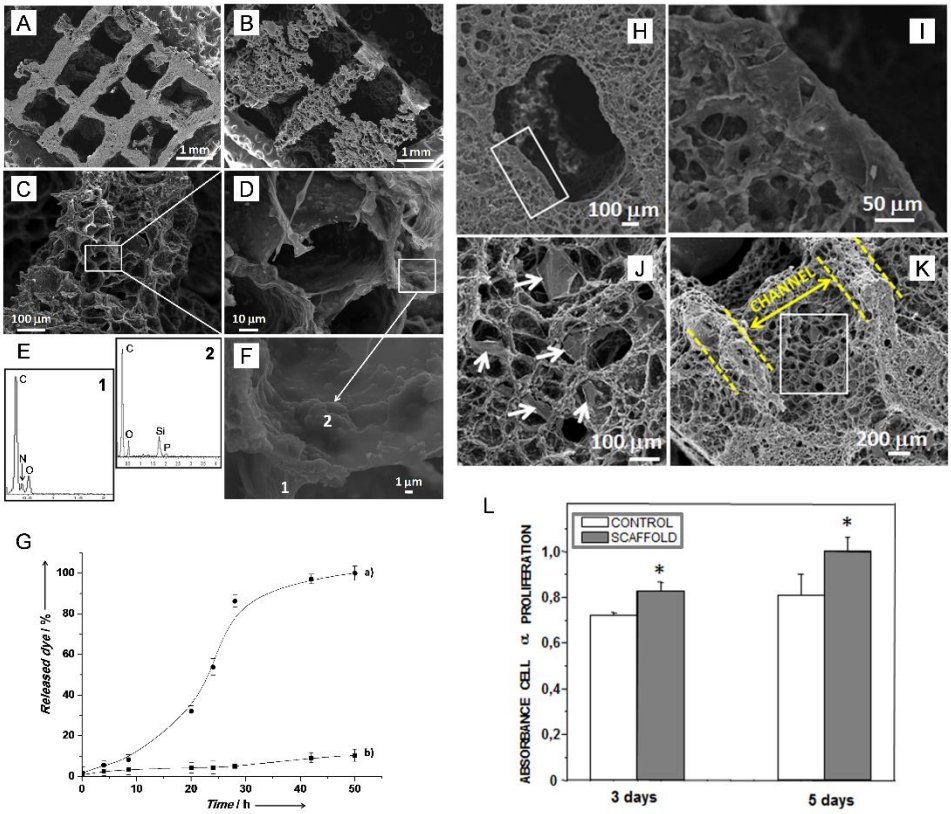

Figure 2. (A) SEM Image at low magnifications of the **S3** surface and (B) the **S3** fracture, showing giant macroporosity. (C) Image of **S3** at high magnifications in which a second porosity level can be observed due to the gelatin cross-linking, (D) second macroporosity level showing the incorporated **S2** nanoparticles. (E) Higher magnification shows a wall scaffold with embedded **S2** nanoparticles. (F) EDX microanalysis of image E at sites 1 (wall) and 2 (**S2** nanoparticles). (G) Dye release kinetics in PBS at 37°C from **S3** (a) in the presence and (b) absence of APase. SEM micrographs of the scaffolds after 48 hours of HOS culture. (H) Detail of c.a. 900 µm macropore prepared by 3D printing. The selected area indicates a fully coated border site by HOS cells; higher magnification of this area (I). (J) Transversal section of the scaffolds; double arrow points the channel width and dotted lines mark the struts. The selected area is magnified in (K), where spread HOS cells can be observed (arrows). (L) Cell proliferation assay after 3 and 5 days of culture. Significant differences were observed between the control and scaffolds results for cell proliferation tests. *($p<0.05$).

Then release studies were performed. In a typical experiment, "gated scaffold" **S3** was immersed in a PBS solution in the presence and absence of APase. Both solutions were stirred for 50 h at 37°C and, at a set time, an aliquot of each experiment was taken to monitor cargo release. The obtained results are

shown in Figure 2G. As observed, delivery was found only when the enzyme was present, thus confirming that the APase-driven release mechanism found for **S2** was maintained in the **S3** scaffold. Slower release kinetics was also found for **S3** when compared with **S2**, most probably due to the enzyme's different accessibility to the hierarchical hybrid structure in the gated scaffold when compared with free nanoparticles. The permeability of these 3D scaffolds to large macromolecules was confirmed after placing them in a solution with fluorescein-labelled avidin macromolecules as an enzyme model. After 1 day, scaffolds were sliced into thin films and intense fluorescence was observed in all the pieces (see Supporting Information). As far as we know, this is the first example of gated scaffolds obtained by combining biomaterials and gated stimuli-controlled nanoparticles.

Finally, in order to assess the biocompatibility of the scaffold, *in vitro* cell culture tests were carried out on 3D gelatin framework containing silica nanoparticles. For that pourpose, a human osteoblast-like cell line denoted HOS was used. Cell proliferation, cytotoxicity and spreading assays were performed (see Supporting Information for further details). In these experiments (see Figure 2L) it was found that HOS cells proliferate even better than in the control (plastic culture plate), and the LDH levels do not show significant differences in the presence of the scaffolds compared with the control ones, indicating that the scaffolds do not elicit any cytotoxic effect. Finally, SEM micrographs (see Figures 2H-K) confirmed that HOS cells adhere, proliferate and spread well within the scaffold, confirming that the macroporous architecture and the strut thickness is appropriated for the scaffold colonization by HOS cells.

In summary, we report herein a new approach for the design of "gated scaffolds" which consists in combining capped silica mesoporous nanoparticles and classical porous biomaterials. In particular, we have prepared MSN functionalised with amines and capped with ATP, which can be selectively opened with an APase enzyme. We have also integrated capped nanoparticles into a 3D gelatin support prepared by rapid prototyping 3D printing techniques. The

obtained “gated scaffold” remains tightly capped in competitive aqueous buffered solutions yet is able to deliver the cargo in the presence of APase. The present study has focused on the capability of active gelatin-based 3D macroporous scaffolds for on-command cargo delivery in the presence of APase, an enzyme whose concentration is used to assess osteoclast activity in bone remodelling processes and as a marker for bone metastases. We also expect this general gated scaffolds preparation approach, will find broader applications. In particular, the combination of gated nanoparticles, which can be opened at will using chemical, physical or biochemical stimuli with different supports based on polymers, ceramics or metals, opens up the possibility of preparing a number of advanced gated scaffolds, which we envision can help find applications in regenerative medicine and bone cancer therapy.

Keywords: biomaterial, controlled release, enzyme-driven, mesoporous silica nanoparticles, 3D scaffolds.

Supporting Information

Supporting Information is available from the Wiley Online Library or from the author.

Acknowledgements

The authors thank the Spanish Government (projects MAT2012-38429-C04-01, AGL2012-39597-C02-02, MAT2012-35556 and CSO2010-11384-E) the Generalitat Valenciana (Project PROMETEO/2009/016) and the CIBER-BBN (the BIO-GATES Project) for their support. N.M. also thanks the Spanish Ministry of Science and Innovation for her FPI grant.

References

1. V. Karageorgiou, D. Kaplan, *Biomaterials*, **2005**, *26*, 5474–5491.
2. Q.L. Loh, C. Choong, *Tissue Eng Part B* **2013**, *19*, 485–502.
3. M. Vallet-Regí, E. Ruíz-Hernández, *Adv. Mater.* **2011**, *23*, 5177–5218.
4. K. Whang, T.K. Goldstick, K.E. Healy, *Biomaterials* , **2000**, *21*, 2545-255.

5. J.W. Lee, K. Shin Kang, S. Ho Lee, J.-Y. Kim, B.-K. Lee, D.-W. Cho, *Biomaterials*, **2011**, *32*, 744-752.
6. C.-X. He, N. Li, Y-L. Hu, X.-M. Zhu, H.-J. Li, M.-H., P.-H. Miao, Z.-J. Hu, G. Wang, W.-Q. Liang, Y. Tabata, J.-Q. Gao*, Pharm Res*, **2011**, *28*,1577–1590.
7. S. Kedong, L. Yingchao, H. M. Macedo, J. Lili, L.Chao, M. Guanyu, L. Tianqing, *Mater.Sci.Eng. C*, **2013**, *33*, 1506–1513.
8. J. Hu, P. X. Ma, *Pharm Res,* **2011**, *28*, 1273–1281.
9. G. Poologasundarampillai, B. Yu, O. Tsigkou, E. Valliant, S. Yue, P. D. Lee, R. W. Hamilton, M. M. Stevens, T. Kasugad and J. R. Jones, *Soft Matter*, **2012**, *8*, 4822–4832.
10. L. S. Sefcik, C. E. Petrie Aronin, K. A. Wieghau, E. A. Botchwey, *Biomaterials*, **2008**, *29*, 2869–2877.
11. Q. Peng, Y.-J.Yang, T. Zhang, C.-Y. Wu, Q. Yang, X. Sun, T. Gong, L. Zhang, Z.-R. Zhang, *Pharm Res,* **2013**, *30,* 1077–1085.
12. W. Habraken, J.G.C. Wolke, J.A. Jansen JA., *Adv. Drug Deliv. Rev.*, **2007**, *59*, 234–248.
13. M. Vallet-Regí, F. Balas, D. Arcos, *Angew. Chem.* **2007**, *119*, 7692 – 7703; *Angew. Chem. Int. Ed.* **2007**, *46*, 7548 – 7558.
14. J. L. Vivero-Escoto, I. I. Slowing, B. G. Trewyn, V. S.-Y. Lin, *Small* **2010**, *6*, 1952 – 1967.
15. P. Yang, S. Gai, J. Lin, *Chem. Soc. Rev,* **2012**, *41*, 3679-3698.
16. Z. Li, J.C. Barnes, A. Bosoy, J. F. Stoddart, Zink. *Chem. Soc. Rev*, **2012**, *41*, 2590-2605.
17. B. G. Trewyn, I. I. Slowing, S. Giri, H. –T. Chen, V. S. –Y. Lin, *Acc. Chem. Res.*, **2007**, *40*, 846-853.
18. C. Coll, A. Bernardos, R. Martínez-Máñez, F. Sancenón, *Acc. Chem. Res.* **2013**, *46*, 339 – 349.
19. C.-Y Lai, B.G. Trewyn, D.M. Jeftinija, K. Jeftinija, S. Xu, S. Jeftinija, V. S. –Y. Lin, *J. Am. Chem. Soc.* **2003**, *125*, 4451
20. C. Park, K. Oh, S.C. Lee, C. Kim, *Angew. Chem. Int. Ed.* **2007**, *46*, 1455.
21. R. Liu, X. Zhao, T. Wu, P. Feng, *J. Am. Chem. Soc.*, **2008**, *130*, 14418-14419.
22. Z. Luo, K. Cai, Y. -Hu, L. Zhao, P. Liu, L. Duan, W. Yang, *Angew. Chem.* **2011**, *123*, 666 – 669; *Angew. Chem. Int. Ed.* **2011**, *50*, 640 – 643.
23. C. Wang, Z. Li, D. Cao, Y.-L. Zhao, J. W. Gaines, O. A. Bozdemir, M.W. Ambrogio,M. Frasconi, Y. Y. Botros, J. I. Zink,J. F. Stoddart, *Angew. Chem*. **2012**, *124*, 5556 – 5561; Angew. Chem. Int. Ed. **2012**, *51*, 5460 – 5465.
24. a) Y. Zhang, Q. Yuan, T. Chen, X. Zhang, Y. Chen, W. Tan, *Anal. Chem.* **2012**, *84*, 1956 – 1962; b) D. Tarn, M. Xue, J. I. Zink, *Inorg. Chem.* **2013**, *52*, 2044 – 2049.
25. a) E. Climent, R. Martínez-Máñez, A. Maquieira, F. Sancenón, M.D. Marcos, E.M. Brun, J. Soto, P. Amorós, *ChemistryOpen* **2012**, *1*, 251 – 259; b) E. Aznar, R. Villalonga, C. Giménez, F. Sancenón, M.D. Marcos, R. Martínez-Máñez, P. Díez, J.M. Pingarrón, P. Amorós, *Chem. Commun.* **2013**, *49*, 6391 – 6393.
26. N. K. Mal, M. Fujiwara, Y. Tanaka, *Nature*, **2003**, *421*, 350-353.

27. A. Schlossbauer, S. Warncke, P. M. E. Gramlich, J. Kecht, A. Manetto, T. Carell, T. Bein, *Angew. Chem*. **2010**, *122*, 4842 – 4845; *Angew. Chem. Int. Ed.* **2010**, *49*, 4734 – 4737.
28. E. Ruiz-Hernández, A. Baeza, M. Vallet-Regi, *ACS Nano* **2011**, *5*, 1259 – 1266.
29. D. He, X. He, K.Wang, J. Cao, Y. Zhao, *Adv. Funct. Mater.* **2012**, *22*, 4704 – 4710.
30. E. Aznar, L. Mondragón, J.V. Ros-Lis, F. Sancenón, M.D. Marcos, R. Martínez-Máñez, J. Soto, E. Pérez-Payá, P. Amorós, *Angew. Chem. Int. Ed.* **2011**, *50*, 11172.
31. A. Baeza, E. Guisasola, E. Ruiz-Hernández, M. Vallet-Regi, *Chem. Mater.* **2012**, *24*, 517 – 524.
32. A. Schlossbauer, J. Kecht, T. Bein, *Angew. Chem*. **2009**, *121*, 3138 – 3141; *Angew. Chem. Int. Ed.* **2009**, *48*, 3092 – 3095
33. C. Park, H. Kim, S. Kim, C. Kim, *J. Am. Chem. Soc***. 2009**, *131*, 16614 – 16615.
34. A. Bernardos, L. Mondragón, E. Aznar, M.D. Marcos, R. Martínez-Máñez, F. Sancenón, J. Soto, J. M. Barat, E. Pérez-Payá, C. Guillem, P. Amorós, *ACS Nano* **2010**, *4*, 6353 –6368.
35. P. D. Thornton, A. Heise, *J. Am. Chem. Soc.*, **2010**, *132*, 2024-2028.
36. A. Popat, B. P. Ross, J. Liu, S. Jambhrunkar, F. Kleitz, S. Z. Qiao, *Angew. Chem.* **2012**, *124*, 12654 – 12657; *Angew. Chem. Int. Ed*. **2012**, *51*, 12486 – 12489.
37. a) Z. Chen, Z. Li, Y. Lin, M. Yin, J. Ren, X. Qu, *Chem. Eur. J.* **2013**, *19*, 1778 – 1783; b) L. Mondragón, N. Mas, V. Ferragud, C. de la Torre, A. Agostini, R. Martínez-Máñez, F. Sancenón, P. Amorós, E. Pérez-Payá, M. Orzáez, *Chem. Eur. J.* **2014**, *20*, 5271 – 5281.
38. C. Minkin, *Calcified Tissue Int.,* **1982**, *34*, 285–290.
39. J.S. Hanker, A.D. Dixon, G.R. Smiley, *Histochemie*, **1973**, *35*, 39-50.
40. M. Tavassoli, M. Rizo, L.T.Yam. *Cancer*, **1980**, *45*, 2400-2403.
41. N. Wadu, S. Ishii, T. Ikeda, K. Enomoto, M. Kitajima. *Anticancer Res* **1999**, 19, 4515-4521.
42. V. Karageorgiou, D. Kaplan, *Biomaterials*, **2005**, *26*, 5474–5491.
43. L. Guan, J.E. Davies, *J. Biomed. Mater. Res.*, **2004**, *71A*, 480–487.
44. R.P. del Real, J.G.C. Wolke, M. Vallet-Regí, J.A. Jansen, *Biomaterials*, **2002**, *23*, 3673–3680.
45. S. Padilla, S. Sánchez-Salcedo, M. Vallet-Regí, *J. Biomed. Mater. Res.*, **2007**, *81A*, 224–232.
46. S. Sánchez-Salcedo, J. Werner, M. Vallet-Regí, *Acta Biomater.,* **2008**, *4*, 913–922.

Small, 2014, DOI: 10.1002/smll.201401227.

Towards the development of 3D "gated scaffolds" for on-command delivery

Supporting Information

Núria Mas, Daniel Arcos, Lorena Polo, Elena Aznar, Sandra Sánchez-Salcedo, Félix Sancenón, Ana García, M. Dolores Marcos, Alejandro Baeza, María Vallet-Regí, and Ramón Martínez-Máñez**

Chemicals

The chemicals tetraethylorthosilicate (TEOS) (98%), *n*-cetyltrimethylammonium bromide (CTAB) (≥99 %), sodium hydroxide (≥98%), tris(2,2'-bipyridyl)ruthenium(II) chloride hexahydrate, 3-[2-(2-aminoethylamino)ethylamino]propyl-trimethoxysilane, adenosine 5'-triphosphate disodium salt hydrate (ATP), acid phosphatase from potato (APase), gelatin Ph Eur and glutaraldehyde 50 wt.% solution in water where purchased from Aldrich. $Na_2HPO_4 \cdot 7H_2O$, KH_2PO_4, NaCl and KCl where purchased from Scharlab. All reagents were used as received.

General Techniques

Powder XRD, TG analysis, elemental analysis, TEM, SEM, zeta potential measurements, and N_2 adsorption-desorption techniques were employed to characterize the prepared materials. Powder X-ray diffraction measurements were performed on a Philips D8 Advance diffractometer using Cu K_α radiation. Thermogravimetric analysis were carried out on a TGA/SDTA 851e Mettler Toledo

balance, using an oxidant atmosphere (air, 80 mL/min) with a heating program consisting on a heating ramp of 10°C per minute from 393 to 1273 K and an isothermal heating step at this temperature during 30 minutes. Elemental analysis was performed in a CE Instrument EA-1110 CHN Elemental Analyzer. TEM images were obtained with a 100 kV Jeol JEM-1010 microscope. Z potential measurements were performed in a Zetasizer Nano instrument from Malvern. N_2 adsorption-desorption isotherms were recorded on a Micromeritics ASAP2010 automated sorption analyser. The samples were degassed at 120°C in vacuum overnight. The specific surface areas were calculated from the adsorption data in the low pressures range using the BET model. Pore size was determined following the BJH method. STEM analysis was performed with a 200 kV Jeol JEM 2100F. ^{31}P nuclear magnetic resonance (NMR) was acquired with a Brucker Avance III. Surface and cross-sectional scanning electron microscopy (SEM) micrographs of **S3** and EDX analysis of the scaffolds were recorded with a field emission scanning electron microscope (JEOL model JSM-6335, Tokyo, Japan) at an acceleration voltage of 15 kV. For scaffolds manufacture, an EnvisionTEC GmbH 3-D Bioplotter™ was used. In release experiments, fluorescence spectroscopy was carried out with a Jasco Spectrofluorometer FP-8500.

Synthesis of the mesoporous silica support

The MCM-41 mesoporous nanoparticles were synthesised by the following procedure: *n*-cetyltrimethylammonium bromide (CTAB, 1.00 g, 2.74 mmol) was first dissolved in 480 mL of deionised water. Then 3.5 mL of NaOH 2.00 M in deionised water were added to the CTAB solution. Next, the solution temperature was adjusted to 80°C. TEOS (5.00 mL, 2.57×10^{-2} mol) was then added dropwise to the surfactant solution. The mixture was stirred for 2 h to give a white precipitate. Finally, the solid product was centrifuged, washed with deionised water and ethanol, and was dried at 60°C (MCM-41 as-synthesised). To prepare the final porous material (MCM-41), the as-synthesised solid was calcined at 550°C using an oxidant atmosphere for 5 h in order to remove the template phase, obtaining the porous material.

Synthesis of S1.

In a typical synthesis, 2.5 g of template-free MCM-41 were suspended in a solution of 1.5 g (2 mmol) of tris(2,2'-bipyridyl)ruthenium(II) chloride hexahydrate ($[Ru(bpy)_3]^{2+}$) dye in 80 mL of anhydrous acetonitrile in a round-bottomed flask. Then 10 ml of acetonitrile were distilled with a dean-stark, in order to remove the possible water present in the pores of the solid. Afterwards the mixture was stirred at room temperature during 24 hours. Subsequently, 10 mL (15 mmol/g of MCM-41) of 3-[2-(2-aminoethylamino)ethylamino]propyl-trimethoxysilane were added and the mixture was stirred for 5.5 h. Then the solid was filtered, washed with 10 mL of acetonitrile and dried at 37°C overnight to obtain the functionalised and filled solid **S1**.

Synthesis of S2

2.5 g of the loaded and prefunctionalised solid **S1** were suspended in a solution 0.01 M of ATP at pH 6 adjusted with H_2SO_4. This suspension was stirred for 5.5 hours at room temperature and then filtered under vacuum and washed with water at pH 6. This final solid **S2** was dried under vacuum and stored at 37°C for 12 h.

Synthesis of S3

Gated MSN-scaffolds were prepared using **S2** nanoparticles. In particular, 0.5 g of gelatin were dissolved in 3.75 mL of milli-Q water at 37°C. Thereafter, 0.3 g of **S2** were slowly added under vigorous stirring. Once all the NPs were added, the mixture was stirred for 40 min at 37°C. Finally, 2.50 mL of a glutaraldehyde as cross-linking solution 0.4% v/v was added. This mixture was stirred at room temperature until it formed a paste with appropriated consistency for injection. The paste was placed in polyethylene cartridge fixed with a dispensing tip of 0.51 mm (EFD-Nordson) internal diameter and the spacing between struts was set to 1.8 mm. The scaffolds were fabricated by direct ink deposition over a pre-cooled plate (10-15°C) by robocasting using an EnvisionTEC GmbH 3-D Bioplotter™. Each layer was 90° rotate to the next one, building 3D-pieces with tetragonal

symmetry. The dimension of scaffolds was ca. 18 × 18 × 4 mm and consisted of 15 layers. They were frozen at -80°C for 2 h and they were cut on smaller ca. 6 × 6 × 4 mm new dimensions. The small scaffolds produced were then cross-linked by exposure to 10 mL of a 2.5% v/v glutaral-dehyde aqueous solution for 10 s. Finally, the scaffolds were freeze-dried at -80°C for 4 h. The final series ob-tained were called **S3**.

Calcined MCM-41, S1 and S2 characterization.

All the mesoporous nanoparticles were characterized following standard techniques. The powder X-ray diffraction (XRD) pattern of the different synthesized solids is shown in Figure SI-1. In relation to the siliceous MCM-41 nanoparticles as synthesized the four low-angle reflections typical of a hexagonal array, indexed as (100), (110), (200), and (210) Bragg peaks are shown (curve a). A significant displacement of 4 Å of the (100) peak in the XRD pattern of the MCM-41 calcined nanoparticles is evident in the X-ray pattern of MCM-41 calcined, due to further condensation of silanol groups during the calcination step (curve b). Finally, the X-ray diffraction pattern of both functionalized solids **S1** and **S2** can be observed in curves c) and d), respectively. An intensity decrease and a broadening of the (110) and (200) reflections can be appreciated, related to a loss of contrast due to the filling of the pore voids with the $[Ru(bpy)_3]Cl_2 \cdot 6H_2O$ dye and the external surface functionalization. Even so, the intensity of the (100) peak in this pattern strongly indicates that the mesoporous structure of the MCM-41 scaffold has not been modified after the loading and functionalization processes in the final **S2** material.

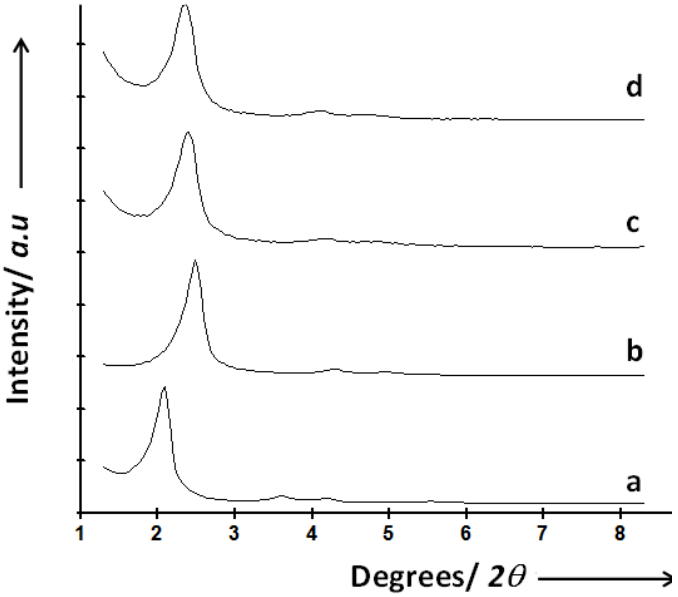

Figure SI-1. Powder X-Ray pattern of (a) MCM-41 as made, (b) MCM-41 calcined and (c) **S1** solid and (d) **S2** solid.

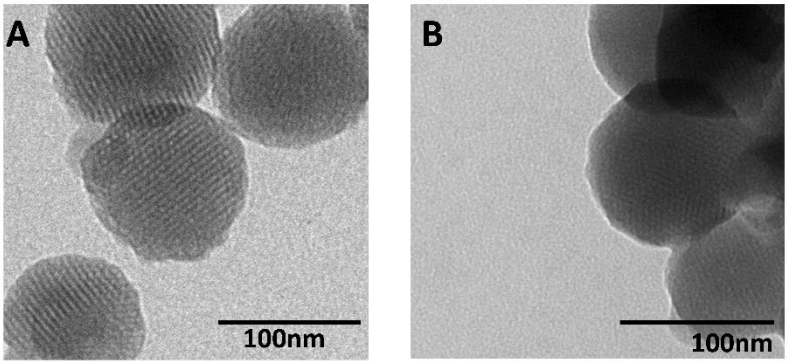

Figure SI-2. Representative TEM image of A) the inorganic MCM-41 calcined matrix. B) **S2** gated solid.

Moreover, the presence of the mesoporous structure was confirmed by TEM analysis of the prepared solids. As it can be observed in Figure SI-2, the typical channels of the MCM-41 matrix can be visualised as alternate black and white stripes in which the typical hexagonal porosity of the MCM-41 calcined material can also be observed. TEM images also show that the prepared MCM-41-based support is obtained as spherical nanoparticles with diameters ranging from

80 to 100 nm. TEM image of the final solid **S2** (Figure SI-2b) also confirmed the ordered mesostructure of the final material. In that image, although the contrast between the black and white strips has decreased due to the loading of the pores with the dye, it can be confirmed that the spherical shape of the nanoparticles and their typical mesoporous structure remains.

N_2 adsorption-desorption isotherms for calcined MCM-41 nanoparticles and the gated solid **S2** were registered and are shown in Figure SI-3. Curve a) corresponds to the calcined matrix showing a sharp adsorption step with a P/P_0 value between 0.2 and 0.35, corresponding to a type IV isotherm, typical of these mesoporous materials. This first step is due to nitrogen condensation in the mesopore inlets. With the BJH model on the adsorption curve of the isotherm, the pore diameter and pore volume were calculated to be 2.39 nm and 0.69 cm^3g^{-1}, respectively. The absence of a hysteresis loop in this pressure range and the low BJH pore distribution (see inset in Figure SI-3) is due to the cylindrical uniformity of mesopores. The total specific area was 931.5 m^2g^{-1}, calculated with the BET model. Also using the a_0 cell parameter (4.06 nm) calculated form XRD measurements and the pore diameter (2.39 nm), a wall thickness value of 1.67 nm, was calculated. Other important feature of the curve is the characteristic H1 hysteresis loop that appears in the isotherm at a high relative pressure (P/P_0> 0.8) which can be closely associated with a wide pore size distribution which corresponds to the filling of the large pores among the nanoparticles (0.69 cm^3g^{-1} calculated by the BJH model) due to textural porosity. In the case of the final **S2** material, the N_2 adsorption-desorption isotherm is typical of mesoporous systems with filled mesopores (see Figure SI-3, curve b). In this way, and as it was expected, a lower N_2 adsorbed volume (BJH mesopore volume = 0.11 cm^3g^{-1}) and surface area (24.6 m^2g^{-1}) were determined, when compared with the initial MCM-41 material. As it can be observed in curve b, this solid presents a function with no gaps at low relative pressure values if compared to the mother MCM-41 array (curve a). A remarkable data is that **S2** did not show a maximum in the pore size distribution curve, which can be explained by the presence of closed pores because of the entrapped dye and the functionalization moieties in the external

surface. Table SI-1 shows a summary of the BET-specific surface values, pore volumes and pore sizes calculated from the N_2 adsorption-desorption isotherms for MCM-41 calcined and **S2**.

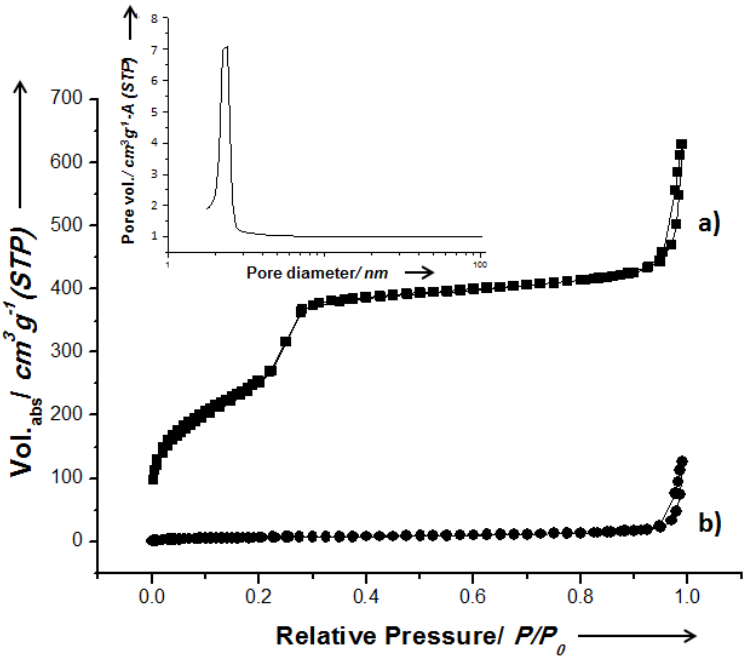

Figure SI-3. Nitrogen adsorption-desorption isotherms for (a) calcined MCM-41 mesoporous material (b) **S2**. Inset: Pore size distribution of calcined MCM-41 mesoporous material.

Table SI-1. BET specific surface values, pore volumes and pore sizes calculated from the N_2 adsorption-desorption isotherms for selected materials.

Solid	S_{BET} ($m^2\ g^{-1}$)	**Pore Volume** ($cm^3 g^{-1}$)	**Pore size** (nm)
Calcined MCM-41	931.5	0.69	2.39
S2	24.6	0.11	----

Thermogravimetric studies of the final **S2** solid were also carried out. The thermogravimetric curve showed four weight losses steps which could be associated to the following processes: 7.00 % (T < 150°C, corresponding to solvent removal), 14.9 % (150 < T < 400 °C, assigned to the decomposition of the organic

moieties functionalizing the silica support), 12.8 % (400 < T < 550^{o}C, also due to combustion of organics) and 0.364 % (T > 550^{o}C, attributed to condensation of silanols in the siliceous surface).

The surface charge of the synthesized nanoparticles was characterized using a Malvern Zetasizer Nano ZS instrumentation. After appropriate dilution of the different suspensions of the nanoparticles, the parameters of electrophoretic mobility (EM), zeta potential (ζ) and conductivity (σ) were determined. Samples from the prepared suspensions were diluted in ultra-purified water and placed in the measurement cell. At least three different measurements were made for each sample. The final results obtained are shown in Table SI-2. MCM-41 calcined nanoparticles, showed a negative ζ value, due to the silanol groups present in the material's surface. In relation to the prefunctionalized solid **S1**, a strong change in the sign of potential was induced, making it clearly positive because of the positive charges of the polyamine moieties. And finally, as it was expected, **S2** showed a low positive ζ value due to the presence of the ATP anions used as caps.

Table SI-2. Physicochemical properties of the prepared solids.

Solid	**EM** (μm·cm/V·S)	**ζ** (mV)	**σ** (mS/cm)
MCM-41 calcined	-2.719 ± 0.004	-34.7 ± 0.6	0.0171
S1	2.695 ± 0.007	34.4 ± 1.1	0.0544
S2	1.409 ± 0.002	17.9 ± 0.2	0.0207

S3 characterization

Scaffold series were characterized by standard techniques such as X-ray diffraction (XRD), thermogravimetry and SEM. In relation to the XRD pattern at low angle, diffraction peak was registered which can be attributed to the (100) reflexion typical of the hexagonal lattice p6m of the MCM-41 materials (see Figure SI-4). This fact indicated that the incorporation of the MSN nanoparticles in the scaffolds did not affect at the mesoporous structure of **S2**. Despite, when MSN were incorporated in the gelatin scaffold, a significant decrease in (100) reflexion peak was observed. This can be explained by a resolution loss in the maximum

diffraction peaks of the mesoporous nanoparticles because of high gelatin content in the scaffold or because of a small degree of structural defects created in the lyophilization process.

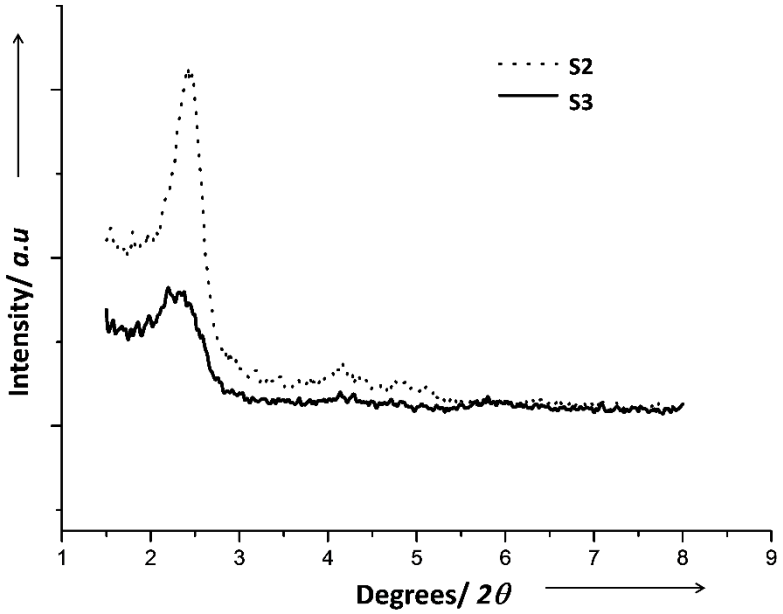

Figure SI-4. XRD pattern of **S2** nanoparticles and **S3** scaffold.

The performed thermogravimetric analysis (TGA) in the temperature range from 30°C to 950°C determined the percentage contents of nanoparticles and gelatin incorporated in the ink for the scaffold printing. Several samples were analyzed by TG, in order to confirm the homogeneity of the method. From this technique, a 25 ± 3.2% weight content of SiO_2 from **S2** nanoparticles was calculated. Then, from these data and **S2** organic content quantification, it can be estimated that around a 35% in weight of the **S3** scaffold is composed by **S2** nanoparticles

Kinetic studies with S2

In order to investigate the gating properties of **S2** material, two samples of 4 mg of **S2** were suspended in 10 mL of water at 37 °C in the presence and in

the absence of APase. The two samples were stirred at 200 rpm and then several 150 µL aliquots were taken of each sample at different times. These aliquots were centrifuged at 9500 rpm and 110 µL of the supernatant was taken in order to monitor the $[Ru(bpy)_3]^{2+}$ release (λ_{ex} 454 nm, λ_{em} 593 nm) by fluorescence spectroscopy.

S3 permeability assays

An experimental assay with fluorescent avidin was carried out in order to demonstrate that the scaffold walls were permeable to macromolecules, and consequently APase could access to the MSN nanoparticles. For this assay a gelatin scaffold containing calcined MCM-41 nanoparticles (the synthesis procedure was the same than the one described for **S3** material, but containing non gated nanoparticles instead of **S2**) was immersed in a 4 mg/mL solution of fluorescent avidin in phosphate buffer solution (PBS) for 24 hours. Then, the scaffolds were intensely washed with fresh PBS in order to remove the externally adsorbed protein and cut in different levels in order to observe the fluorescence in the inner walls by fluorescence microscopy. The registered images showed fluorescence in all levels, which indicated that the scaffold walls were impregnated of avidin.

Kinetic studies with S3

In order to investigate the gating properties of **S3** material, two **S3** scaffolds were immersed in PBS solution (0.32 mL per gram of **S3**) at 37°C in the presence and in the absence of APase. The two samples were stirred at 200 rpm for 50 h and several 150 µL aliquots were taken of each sample at different times. The fluorescence of the aliquots were registered (λ_{ex} 454 nm, λ_{em} 593 nm) in order to monitor the $[Ru(bpy)_3]^{2+}$ release.

Effect of the pH, the presence of other enzymes and denatured APase.

Moreover, in order to determine the selectivity of the enzymatic action of phosphatase, several studies were carried out in presence of other enzymes, such as esterase (at pH 8) or pepsin (at pH 4), with **S2** nanoparticles. Likewise, APase

was denatured by heating at 70°C for 1h, to prove that the dye delivery was produced due to the enzyme activity. It was used the same experimental procedure described above (see kinetic studies with **S2**). In Figure SI-5 it can be observed that satisfactorily a strong dye delivery was produced in presence of APase at pH 4.8 (curve a) compared to the low release of dye in absence of enzyme in water at pH 4.8 and at pH 8 (curves b and c) or with esterase, pepsin or denatured APase (curves d, e, f).

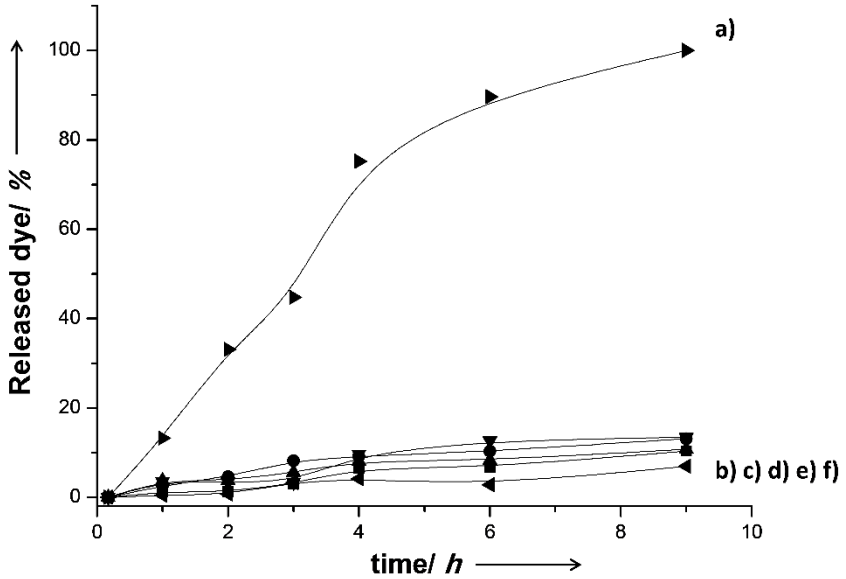

Figure SI-5. Kinetic of the dye release from **S2** in the presence of APase at pH 4.8 (a) in the absence of enzyme at pH 4.8 (b) in the absence of enzyme at pH 8 (c) in the presence of esterase at pH 8 (d) in the presence of pepsin at pH 4 (e) in the presence of denatured Apase (f). All in water at 37°C.

Biocompatibility studies

In order to assess the biocompatibility, *in vitro* cell culture tests were carried out on 3D gelatin framework containing silica nanoparticles. A human osteoblast-like cell line denoted HOS was used. This cell line, obtained through the European Collection of Cell Cultures (ECACC, no. 87070202), was derived from an osteosarcoma of an old Caucasian female. The cells were cultured in Dulbecco's modified Eagle medium (DMEM) containing 2 mM glutamine, 100 U/mL penicillin, 100 μg/mL streptomycin, and 10% fetal calf serum (FCS) at 37°C in a humidified

atmosphere of 95% air and 5% CO_2. Osteoblast-like cells were routinely subcultured by trypsinization. Before seeding, the scaffolds were conditioned by soaking in complete medium for 24 hours at 37°C.

Cell proliferation assay.

For this particular assay, the cells were seeded onto the scaffolds surface in 24-well plates at a seeding density $4 \cdot 10^4$ cells·mL^{-1} in supplemented complete medium and incubated under standard conditions. Cell proliferation determinations were performed by using the MTT (3-[4,5-dimethylthiazol-2-yl]-2,5-diphenyltetrazolium bromide) assay at 3 and 5 days after seeding.

Cytotoxicity assay: Lactate deshidrogenase (LDH) activity.

LDH activity released from the osteoblast-like cells was considered for cell injury measurement. The measurements were made at 3 and 5 days of seeding by using a commercially available kit (Spinreact).

Cell-spreading assay.

The spreading degree and morphology of the osteoblast-like cells were visualized by SEM after 48 h. The attached cells were rinsed four times in PBS and fixed with 2.5% (v/v) glutaraldehyde in 0.1 M phosphate buffer. Dehydration was performed with slow water replacement by a series of graded ethanol solutions with final dehydration in absolute ethanol before critical-point drying. The materials were mounted on stubs, gold plated in vacuum using a sputter coater (Balzers SCD 004 (Wiesbaden-Nordenstadt, Germany), and analyzed by SEM in a JEOL 6400 microscope (Tokyo, Japan).

Statistics

Data obtained from biocompatibility are expressed as means ± standard deviations of the independent experiments indicated in each case. Statistical analysis was performed using the Statistical Package for the Social Sciences (SPSS) version 19 software. Statistical comparisons were made by analysis of variance (ANOVA). Scheffé test was used for post hoc evaluation of difference among

groups. In all statistical evaluations, $p < 0.05$ was considered as statistically significant.

The results obtained from the mitochondrial activity at 3 and 5 days (Figure SI-6) indicate that, in the presence of the scaffolds, HOS cells proliferate even better than in the control (plastic culture plate). For the same periods, the LDH levels do not show significant differences in the presence of the scaffolds compared with the control ones, indicating that the scaffolds do not elicit any cytotoxic effect (Figure SI-7).

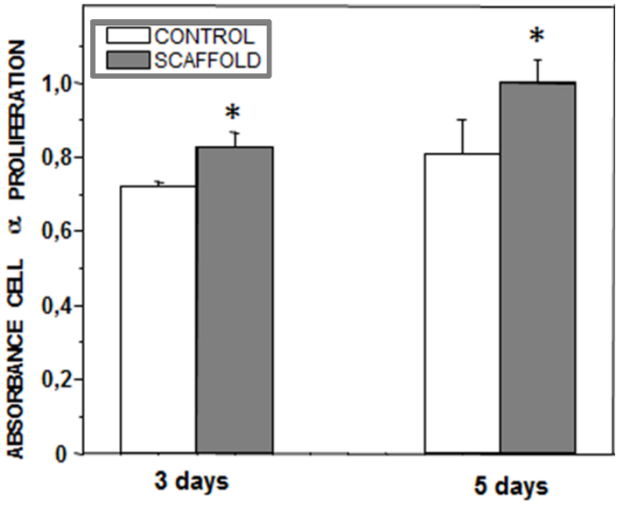

Figure SI-6. Cell proliferation assay after 3 and 5 days of culture. Significant differences were observed between the control and scaffolds results for cell proliferation tests. *($p<0.05$).

HOS cells adhere, proliferate and spread well within the scaffold, as it is evidenced in SEM micrographs (Figure SI-8). The macroporous architecture and the strut thickness seem to be appropriated for the scaffold colonization by HOS cells. In fact, after 48 hours, the osteoblasts exhibit spread morphologies with numerous anchoring elements in both the most external and accessible surface, as well as within the macroporous channels tailored by means of the rapid prototyping method used in this work.

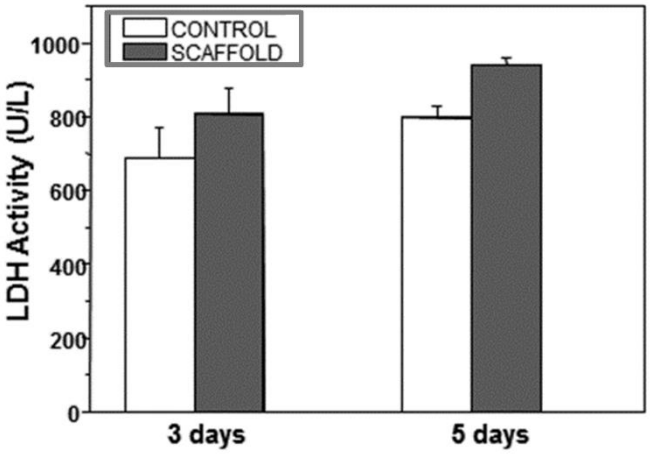

Figure SI-7. LDH activity after 3 and 5 days of culture.

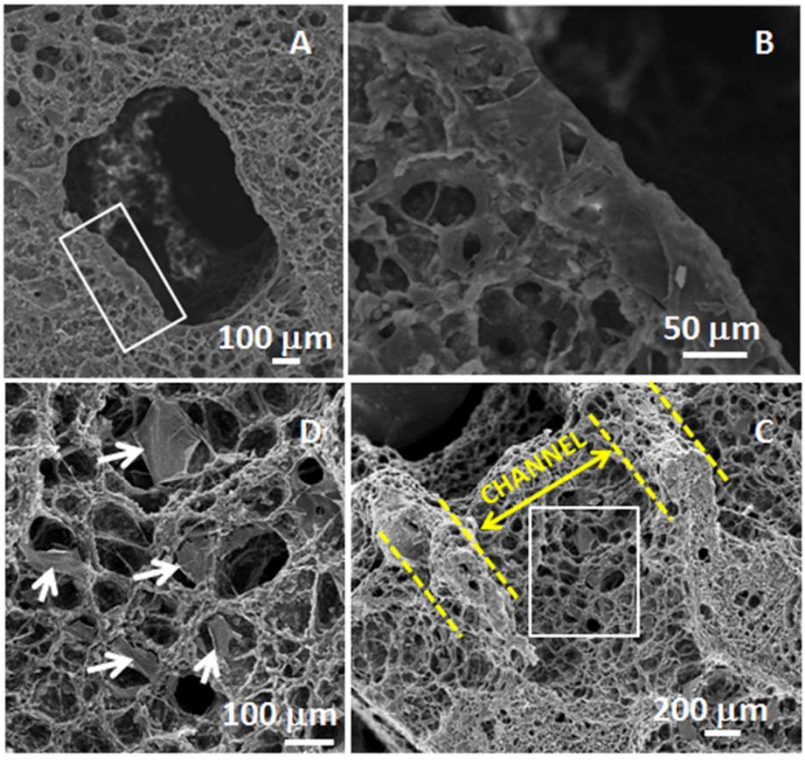

Figure SI-8. SEM micrographs of the scaffolds after 48 hours of HOS culture. (A) Detail of *c.a.* 900 µm macropore prepared by 3D printing. The selected area indicates a fully coated border site by HOS cells; higher magnification of this area (B). (C) Transversal section of the scaffolds; double arrow points the channel width and dotted lines mark the struts. The selected area is magnified in (D), where spread HOS cells can be observed (arrows).

3. New gated nanodevices to enhance antifungal and antibacterial activity.

3.1 **Objectives**

Following with the wide range of applications of biogated nanodevices we considered to design new hybrid materials which could respond to the presence of some pathogenic microorganisms, such as bacteria or fungi.

Thus, the main objective of this chapter is the design and development of new organic-inorganic hybrid materials able to deliver antifungal or antibacterial drugs in a controlled manner. To develop these new nanodevices, MCM-41 mesoporous silica nanoparticles were used as inorganic matrix. Moroever the inorganic support was loaded with the corresponding drug and capped with suitable gates which are opened in the presence of certain fungi or bacteria. An additiona aim was to demonstrate the possibility to enhance and broaden the spectrum of action of some antifungal and antibacterial drugs when the nanoformulation setup was used.

Specifically, our objectives are:

- ✓ Design, development and antifungal applications of a tebuconazole loaded support capped with pH-driven gatekeeping moieties tested in presence of *Saccharomyces cerevisiae*.
- ✓ Design, preparation and antibacterial applications against Gram-negative bacteria of a vancomicyn loaded nanodevice capped with ε-poly-L-lysine.

3.2 *Enhanced antifungal efficacy of tebuconazole using gated pH-driven mesoporous nanoparticles.*

Núria Mas,[1,2,3] Irene Galiana,[3] Silvia Hurtado,† Laura Mondragón,[1,2,3] Andrea Bernardos,[1,2,3] Félix Sancenón,[1,2,3] María D. Marcos,[1,2,3] Pedro Amorós,[4] Nuria Abril-Utrillas,[5] Ramón Martínez-Máñez[1,2,3] and José Ramón Murguía*[1,3]*

[1] Centro de reconocimiento Molecular y Desarrollo Tecnológico (IDM). Centro mixto Universidad Politécnica de Valencia- Universidad de Valencia. Tel. +34 96 3877343 Fax: (+) 96-387-9349

[2] Departamento de Química. Universidad Politécnica de Valencia. Camino de Vera s/n, 46022, Valencia, Spain.

[3] CIBER de Bioingeniería, Biomateriales y Nanomedicina (CIBER-BBN, Spain).

[4] Institut de Ciència del Materials (ICMUV). Universitat de València P.O. Box 2085, 46071, Burjassot, Valencia, Spain.

[5]Servicio Ginecología y Obstetricia. Hospital de la Plana • Ctra. de Vila-real a Burriana km. 0,5 • 12540 Vila-real. Spain

† Silvia Hurtado passed away in September 2013

We dedicate this article to the loving memory of Silvia Hurtado who passed away in September 2013.

Received: 24 December 2013. Accepted: 07 February 2014
Published: 23 May 2014

Abstract

pH-sensitive gated mesoporous silica nanoparticles have been synthesized. Increased extracellular pH and internalization into living yeast cells, triggered molecular gate aperture and cargo release. Proper performance of the system was demonstrated with nanodevices loaded with fluorescein (**S1-FL**), or with the antifungal agent tebuconazole (**S1-Teb**). Interestingly, **S1-Teb** significantly enhanced tebuconazole cytotoxicity. As alterations of acidic external pH are a key parameter in the onset of fungal vaginitis, this nanodevice could improve the treatment for vaginal mycoses.

Introduction

Vaginitis is an inflammation of the vagina often associated with irritiation or infection of the vulva. Vulvo vaginitis is very common and affects women of all ages. Indeed, 75% of all women will suffer from this condition at least once throughout their lives.[1] If left untreated, it can lead to further complications especially for pregnant women. Infectious vaginitis can account for more than 90% of all vulvovaginitis cases. It is caused by, either bacterial or, most frequently, *Candida* infections.[2]

Candida is among the normal organisms that are part of the commensal flora of the gut, mouth and genital tract.[3] These yeasts will multiply when their habitat becomes altered under particular conditions, such as immunosuppression, administration of antibiotics, pregnancy, luteal phase of menstrual cycle, diabetes mellitus or oral contraceptive intake.[3,4] As a consequence, *Candida* infection causes the elimination of beneficial microorganisms from the endogenous vaginal flora (especially Döderlein bacillus), one of the natural mechanisms of defense. Metabolism of lactobacillus present in the genital tract generates acid lactic, which is the principal responsible for maintaining a normal vaginal pH around 3.8-4.4. This acid environment hinders the growth of other pathogenic microorganisms, acting as a protecting barrier. If there is an increase in the pH to

values around 5.5-6.8, an overgrowth of *Candida* occurs, thus causing the most common vulvo-vaginal infections.[4]

Management of vaginal candidiasis includes oral or topical antibiotics and/or antifungal creams, or similar medications.[4] Most of the available effective antifungal agents are based on polyenes (amphotericin B), triazoles (fluconazole, itraconazole) or echinocandins.[1,5] Although both oral and topical treatments are equally effective, oral therapies are strongly associated with systemic side effects. Topical therapies are less frequently associated with adverse effects and these include irritation, itching, burning, and development of yeast resistance to antifungal agents.[5] The better therapeutic profile together with its cost effectiveness makes topical therapies the option of choice for management of vaginal candidiasis.

Although silver[5,6] and silica nanoparticles[7] have been used as antifungals against *Candida spp*., we believe that the use of gated mesoporous materials could be an interesting alternative as drug carriers in order to avoid the mentioned adverse effects.

The development of nanoscopic hybrid materials able to deliver cargo under a certain external trigger action has been considered a high interesting area of research and it has been extensively explored in the last years.[8,9] These nanodevices have been demonstrated to be an excellent approach for advanced controlled release research.[9-17] Gated mesoporous supports are composed basically by two subunits, a suitable scaffolding and certain entities anchored on the support surface.[18] The support is employed as container in which certain chemical species could be stored; whereas the grafted molecules in the outer surface of the scaffold act as molecular gate, controlling the cargo release at will. The selection of both scaffold and anchored entities of the nanodevice has to be carefully done, given the required functionalities of the final system.

In this context, silica mesoporous supports are widely used as inorganic scaffolds thanks to several favorable features including homogeneous porosity, high chemical inertness, robustness, thermal stability, high loading capacity, biocompatibility and ease of functionalization through the well-known chemistry of alkoxysilanes.[19-28] Although mesoporous silica supports have been used for the simple diffusion-controlled release of certain antibiotics[29-31] and antifungals[4,32] similar studies using capped materials showing zero release and able to only deliver cargo in the presence of fungi have not been described.

We aimed to design and test a new nanodevice for the intracellular controlled release of an antifungal in opportunistic fungi, such as *Candida spp*. reproducing the biological conditions of the vagina ecosystem. When growing in the yeast form, *Candida albicans* is morphologically similar to *Saccharomyces cerevisiae*,[33] validating budding yeast as a model for fungal infections.[34] Furthermore*, S. cerevisiae* itself can also cause vaginal yeast infections.[35] We hypothesize that, apart from the increase of the vaginal pH under certain conditions, nanoparticle internalization in budding yeast would trigger the opening of the nanodevice and the release of the entrapped antifungal molecule. This would be so because at pH<5 the amine groups are protonated and the electrostatic repulsions between the organic moieties and the interaction with anions in the medium maintains the gate closed. At pH>5 the amine groups are less protonated, weakening the electrostatic interactions and causing opening of the gate, which is followed by a massive outflow of the entrapped moieties .[36,37]

Material and methods

Chemicals

The chemicals tetraethylorthosilicate (TEOS) (98 %), *n*-cetyltrimethylammonium bromide (CTAB) (≥99 %), sodium hydroxide (≥98%), fluorescein (FL), tebuconazole and 3-[2-(2-aminoethylamino)ethylamino]propyltrimethoxysilane (N3) were provided by

Aldrich. The culture yeast was also provided by Aldrich. Solvents were purchased from Scharlab. All reagents were used as received.

General Techniques

Powder XRD, TG analysis, elemental analysis, TEM and N_2 adsorption-desorption techniques were employed to characterize the prepared materials. Powder X-ray diffraction measurements were performed on a Philips D8 Advance diffractometer using Cu Kα radiation. Thermo-gravimetric analysis were carried out on a TGA/SDTA 851e Mettler Toledo balance, using an oxidant atmosphere (air, 80 mL/min) with a heating program consisting on a heating ramp of 10°C per minute from 393 to 1273 K and an isothermal heating step at this temperature during 30 minutes. Elemental analysis was performed in a CE Instrument EA-1110 CHN Elemental Analyzer. TEM images were obtained with a 100 kV Jeol JEM-1010 microscope. N_2 adsorption-desorption isotherms were recorded on a Micromeritics ASAP2010 automated sorption analyser. The samples were degassed at 120°C in vacuum overnight. The specific surface areas were calculated from the adsorption data in the low pressures range using the BET model.[38] Pore size was determined following the BJH method.[39] Fluorescence spectroscopy was carried out on a Felix 32 Analysis Version 1.2 (Build 56) PTI (Photon Technology International). Yeast cultures were inoculated in a Telstar AH100 cell culture hood, grown at 30°C using a microbiology culture shaker (Kühner 25 mm) and were monitored under microscopy with a Nikon Eclipse E500.

Synthesis of the nanoparticles

Synthesis of the silica support

The MCM-41 mesoporous nanoparticles were synthesised by the following procedure: *n*-cetyltrimethylammonium bromide (CTAB, 1.00 g, 2.74 mmol) was first dissolved in deionised water (480 mL). After that, NaOH (3.5 mL, 2.00 M) in deionised water was added to the CTAB solution. Next the solution temperature was adjusted to 80°C. TEOS (5.00 mL, $2.57 \cdot 10^{-2}$ mol) was then added dropwise to the surfactant solution. The mixture was stirred for 2 h to give a white precipitate. Finally, the solid product was centrifuged, washed with

deionised water and ethanol, and was dried at 60°C (MCM-41 as-synthesised). To prepare the final porous material (MCM-41), the as-synthesised solid was calcined at 550°C using an oxidant atmosphere for 5 h in order to remove the template phase, (CTAB) thus eliminating any residual CTAB that might negatively affect cell viability.

*Synthesis of **S1-Teb***

In a typical synthesis, template-free MCM-41 (150 mg) was suspended in a solution of tebuconazole (16 mg in 7 mL of CH_2Cl_2 for a ratio of 0.35 mmol of tebuconazole/g MCM-41) and the subsequent suspension stirred for 24 h at room temperature.[40] Then, an excess of 3-[2-(2-aminoethylamino)-ethylamino]propyltrimethoxysilane (N3, 0.4 mL, 1.4mmol) was added and the mixture was stirred for 5.5 h at room temperature. The obtained solid was filtered, washed with CH_2Cl_2 (4 mL) and dried under vacuum. Then, this solid was suspended in water at pH 2 (25 mL) in presence of sulphate during 10 minutes, in order to maintain the gate "closed" due to amine protonation. The final solid **S1-Teb** was dried under vacuum and stored at 37°C for 24 h.

Yeast preparation for S1-Teb uptake and cell viability assay

Following a similar yeast treatment than for solid **S1-FL** assays, BY4741 cells were cultured in YPD medium overnight at 28°C with continuous agitation at a density of 10^8 cells/mL. 9 mL of this suspension were centrifuged 1 minute at 3000 rpm and the precipitate was re-suspended with 900 μL of simulated vaginal fluid (SVF). Two more washes were done by adding 900 μL of SVF to the previous pellet, and 100 μL of the final cell suspension were introduced in different eppendorfs. The SVF was prepared as described by Marques et al.[41] SVF composition in g/L: sodium chloride 3.51, potassium hydroxide 1.40, calcium hydroxide 0.222, bovine serum albumin (BSA) 0.018, lactic acid 2.00, acetic acid 1.00, glycerol 0.16, urea 0.40, glucose 5.00. Then, SVF was adjusted at pH 4.2 with HCl and saved by using a sterilized vacuum filtration system.

Results and discussion

Firstly, a material (**S1-FL**) consisting of MSN support (MCM-41) loaded with a dye and capped with an organic molecular entity was designed. The starting nanoparticulated MCM-41 mesoporous solid was synthesized following well-known procedures using *n*-cetyltrimethylammonium bromide (CTAB) as template and tetraethylorthosilicate (TEOS) as hydrolytic inorganic precursor.[19-24] Then, MCM-41 solid was obtained after calcinations and loaded with the fluorescein dye (FL). As molecular gate the organic entity 3-[2-(2-aminoethylamino)ethylamino]propyl-trimethoxysilane (N3), that contains three amine groups per molecule, was selected.

This solid was synthesized, characterized and tested in vitro (See Supplementary material for synthesis, characterization and in vitro results of **S1-FL**). For the in vitro assays, *S. cerevisiae* cells were incubated in a medium at pH 3.7 with **S1-FL** at different concentrations (0.65, 1.25, 2.5 and 5 mg/mL) at 40°C for 6 hours. After the heat shock treatment, cells were seeded in plates and incubated for 72 hours. It was previously studied that under these incubation conditions (40°C for 6 hours) the optimum nanoparticles' internalization was achieved and did not affect to the cells viability. Moreover, 72h is the average required time for yeast colonies to growth up to a size of 1-2 mm, where they can be visually quantitated Cellular uptake was monitored by fluorescence microscopy (See Supplementary materials).

The cellular uptake of nanoparticles was followed by fluorescein-associated fluorescence (green). The cells incubated at pH 3.7 and treated with **S1-FL** showed a normal phenotype when compared to control cells. Besides, a fluorescein-associated fluorescence signal was observed, thus proving the internalization and aperture of nanoparticles. In order to rule out any possible toxic effect of nanoparticles under the test conditions, cell viability was monitored throughout the experiments by clonogenic assays. No cell toxicity associated with **S1-FL** was observed (See Supplementary materials).

After these satisfactory results with **S1-FL** nanoparticles, we next designed, prepared, characterized and test a new material, **S1-Teb**, as a possible therapeutic antifungal carrier. This nanoparticle design and action mechanism is shown in Scheme 1.

Under normal vaginal conditions (Figure 1A), pH remains between 3.8-4.4. As a consequence, the molecular gate in **S1-Teb** material is closed, and no tebuconazole release is produced. Only, few nanoparticles could cross the vaginal epithelium, with virtually no toxicity because tebuconazole's molecular target, encoded by the ERG 11 gene,[42] is not present in human cells. When a *Candida albicans* infection occurs in the vaginal environment (Figure 1B), pH is increased (pH>5.5), thus opening the gate and releasing tebuconazole.

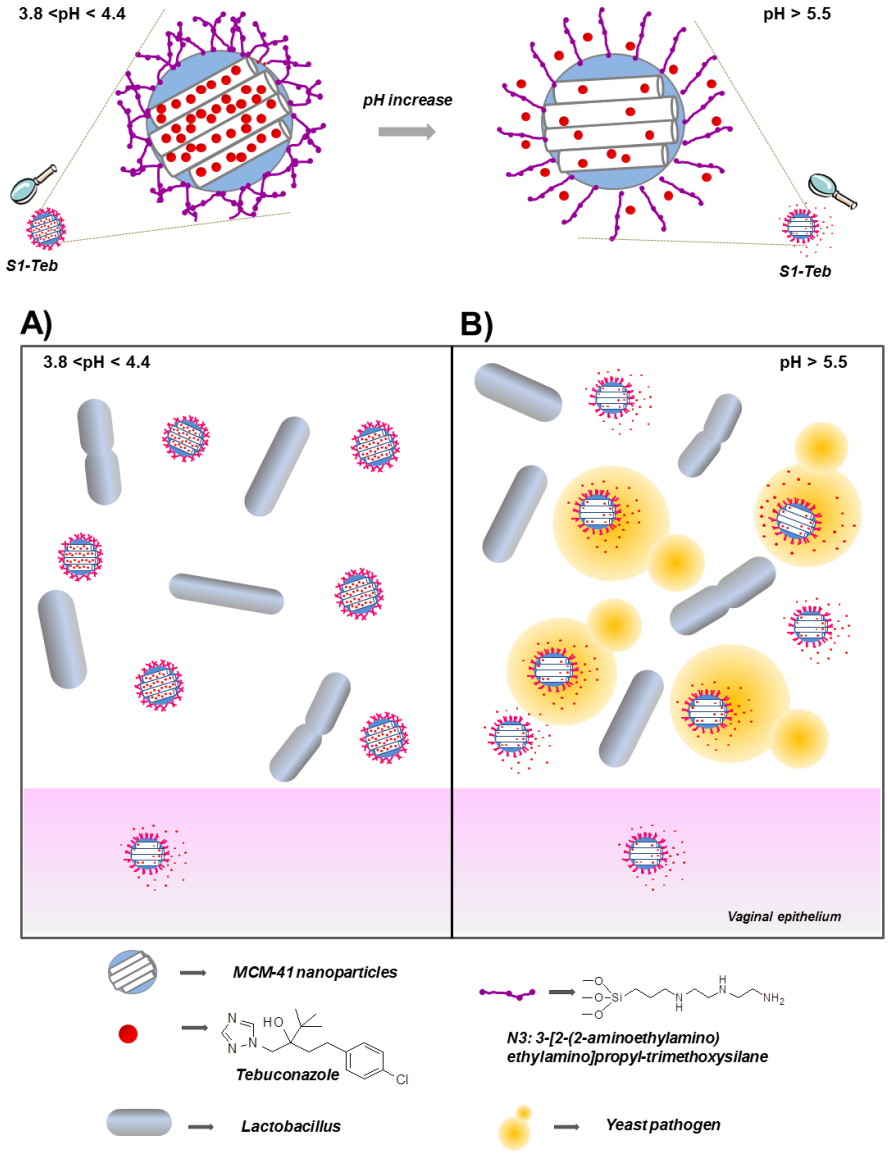

Figure 1. Schematic representation of the design and action mechanism of **S1-Teb** solid under usual vaginal conditions (A) and in presence of *Candida albicans* (B) (*Saccharomyces cerevisiae* has been used in experimental assays as model organism).

Moreover, some of the **S1-Teb** nanoparticles would be internalized in *Candida albicans* (*S. cerevisiae* in our case), where tebuconazole delivery should also occur. Increased lethality of *C. albicans* cells should be expected in this case.

Nanometric mesoporous MCM-41 phase (ca. 100 nm) was selected as inorganic support. MCM-41 nanoparticles were synthesized following the same procedures than **S1-FL**[19-24] and obtained after calcination. Then, this calcined material was loaded in this case with tebuconazole (Teb), an antifungal drug from the triazoles' family whose solubility and size properties resemble those of econazole nitrate.[4] Then the external surface of the nanoparticles was also functionalized with N3 (See Materials and methods for experimental details).

The MCM-41 structure was confirmed by powder X-ray diffraction and transmission electron microscopy TEM techniques (See Figure 2A and 2B), which presented the expected features of this type of mesoporous materials.

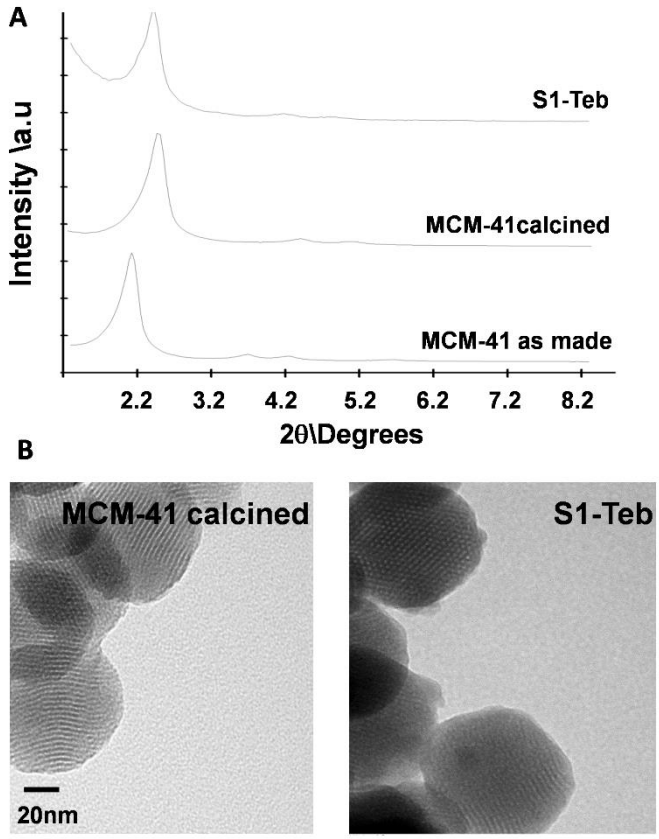

Figure 2. **S1-Teb** characterization results. A) Powder X-Ray pattern of MCM-41 as-made, MCM-41 calcined and **S1-Teb**. B) TEM image of MCM-41 calcined and **S1-Teb.**

The N_2 adsorption-desorption isotherms of the prepared phase (See Figure 3A) shows a typical type IV-curve with a specific surface area of 998.4 m^2g^{-1}, calculated with the BET[38] model. The absence of a hysteresis loop in this interval and the narrow BJH[39] pore size distribution, with an average pore diameter of 2.45 nm, indicate the existence of uniform cylindrical mesopores with a pore volume of 0.76 cm^3g^{-1}.

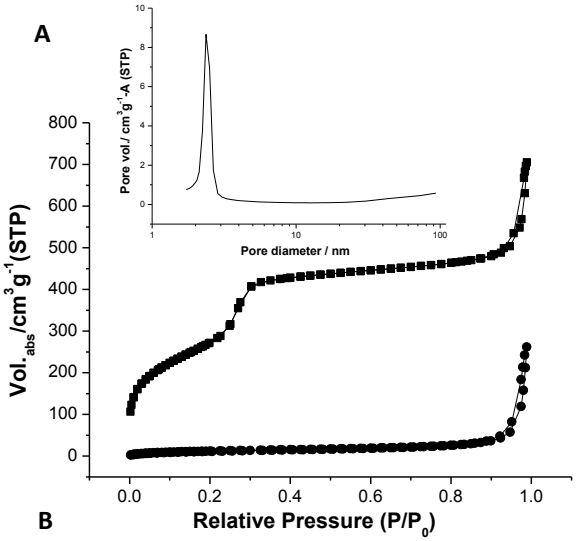

	α_{Teb} (mmol/g SiO_2)	α_{N3} (mmol/g SiO_2)
S1-Teb	0.064	2.43

Figure 3. S1-Teb characterization results. A) N_2 adsorption-desorption isotherms of MCM-41 calcined and **S1-Teb**, B) Contents in mmol/g SiO_2 for **S1-Teb**.

The prepared solid **S1-Teb** was also characterized using standard techniques**. S1-Teb** displays expected characteristics of the MCM-41 phase as it can be observed in the X-Ray pattern (Figure 2A) and TEM image in Figure 2B. This suggests that loading and functionalization procedures did not modify the mesoporous structure of the starting material. Additionally, the N_2 adsorption-desorption isotherm of **S1-Teb** was the typical of gated and filled mesoporous

systems and a significant decrease in the N_2 volume adsorbed was observed (0.04 cm^3g^{-1}) and in surface area (46.3 m^2g^{-1}) when compared with the starting MCM-41 material (See Figure 3A). Finally, the organic content of the final **S1-Teb** solid was determined by thermogravimetric and elemental analysis. The amounts of tebuconazole and capping molecule, N3 obtained in the final material were 0.064 and 2.43 mmol / g SiO_2, respectively (See Figure 3B).

Yeast uptake and cell viability assay with S1-Teb

Different solutions of free tebuconazole and suspensions of solid **S1-Teb** with several concentrations (from 0 to 200 μg tebuconazole/mL) were prepared by adding DMSO 2x and simulated vaginal fluid (SVF), at a final volume of 200 μL and 2% DMSO concentration. The amount of free drug used in the study was the same to that contained in the capped solid **S1-Teb**, calculated by elemental analysis and thermogravimetry studies (See Supplementary material). Then, 100 μL of the above solutions or solid suspensions were added to the different eppendorf containing 100 μL of the yeast suspension (for yeast preparation treatment see Supplementary materials). These final yeast suspensions containing different amounts of free tebuconazole or **S1-Teb** (from 0 to 100 μg tebuconazole/mL) were incubated for 6h at 37°C with no stirring. After the incubation period, approximately 300 cells were seeded in an YPD plate and incubated at 28°C for 72h. Finally, colony formation units (CFU) were quantified. The results of the experiments containing duplicates were repeated twice (See Figure 4).

Satisfactorily, as it can be observed, when a 100 μg/mL of antifungal is used for both formulations (free and **S1-Teb**) a very low cell growth value was obtained with the nanoparticles (around a 10%CFU were quantified), whereas most of cells were growth (around a 90%CFU) with the free antifungal. Practically no death was achieved by the use of free drug when a closed to 90% death with **S1-Teb**.

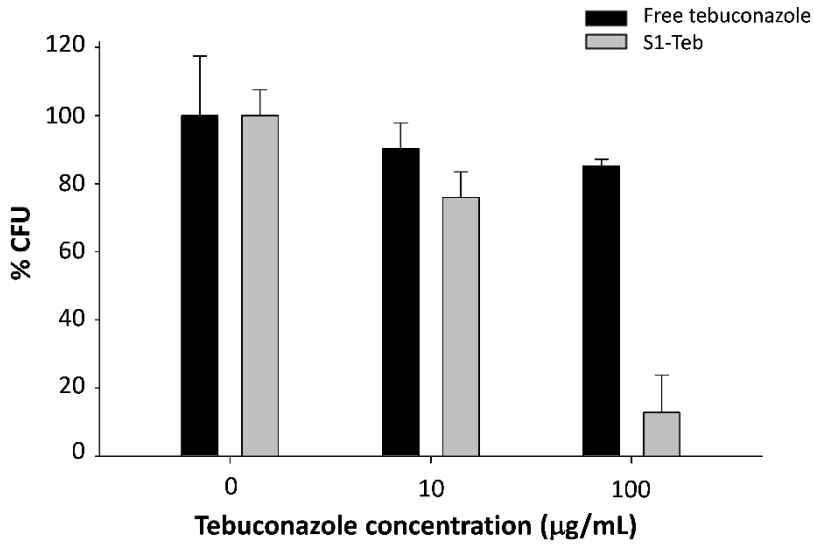

Figure 4. Cell viability assay results of free tebuconazole and **S1-Teb** in presence of *Saccharomyces cerevisiae*. %CFU (Colony Formation Units) growth versus tebuconazole concentration in μg/mL is represented.

Conclusion

In summary, a study of controlled release of different cargo molecules from a mesoporous silica-based material gated with a polyamine, able to remain closed at an acidic pH, is described. For the capped solid loaded with fluorescein (**S1-FL**), in vitro studies showed a selective delivery over 5.5 pH, while the molecular gate remains closed at an acidic pH 3.7. Intracellular cargo release and cell viability studies were carried out to analyze the behaviour of the solid by employing *S. Cerevisiae*, which is a microorganism that survives in acidic environments, and perfectly suits the aperture mechanism of synthesized nanoparticles. Satisfactorily, **S1-FL** cell viability studies demonstrated the non-toxicity of the material. Moreover, this solid perfectly internalized in yeast cells, producing the subsequent fluorescein delivery due to the 5.5 pH, as the fluorescence microscopy images demonstrated (See Supplementary material). In order to demonstrate the potential of this capped material in a therapeutical field, as a possible antifungal carrier, other material (**S1-Teb**) consisting of silica mesoporous support containing an antifungal, tebuconazole, was prepared.

Accordingly, a 9-fold increase in tebuconazole cytotoxicity was obtained by using **S1-Teb** nanoparticles, when compared to that of free antifungal. Therefore, the designed nanoformulation considerably improves tebuconazole efficacy. The enhancement of tebuconazole action could potentially i) overcome the adverse side effects associated with topical therapies for vulvo-vaginal infection, and ii) significantly improve its cost effectiveness.

Keywords: capped mesoporous nanoparticles, intracellular release, pH-responsive nanoparticles, *Saccharomyces cerevisiae*, tebuconazole loading.

Acknowledgments

Authors thank the Spanish Government (project MAT2012-38429-C04-01) the Generalitat Valenciana (project PROMETEO/2009/016) and the CIBER-BBN for their support. N.M. also thanks the Ministerio de Ciencia e Innovación for her FPI grant.

Disclosure

The author reports no conflicts of interest in this work.

References

1. P. Makela, D. Leaman, J.D. Sobel. Vulvovaginal trichosporonosis. *Infect Dis Obstet Gynecol*. 2003; 11: 131–133.
2. L. Edwards. The diagnosis and treatment of infectious vaginitis. *Dermatol. Ther*. 2004; 17: 102–110.
3. T. Hainsworth. Diagnosis and management of candidiasis vaginitis. *Nurs.Times.net.* 2002; 98: 30.
4. V. Ambrogi, L. Perioli, C. Pagano, et al. Econazole Nitrate-loaded MCM-41 for an antifungal topical powder formulation. *J. Pharm. Sci*. 2010; 99: 4738-4745.
5. A. Panácek, M. Kolár, R. Vecerová, et al. Antifungal activity of silver nanoparticles against Candida spp. *Biomaterials*. 2009; 30: 6333-6340.
6. C. Georgea, S. Kuriakosea, S. Georgea, T. Mathewb. Antifungal activity of silver nanoparticle-encapsulated β-cyclodextrin against human opportunistic pathogens. *Supramolecular Chem*. 2011; 23: 593-597.

7. C.S.O. Paulo, M. Vidal, L.S. Ferreira. Antifungal nanoparticles and surfaces. *Biomacromolecules*. 2010; 11: 2810-2817.
8. S. Saha, K.C.F. Leung, T.D. Nguyen, J. F. Stoddart, J.I. Zink. Nanovalves. *Adv. Func. Mater*. 2007; 17: 685-693.
9. B.G. Trewyn, I.I. Slowing, S. Giri, H.T. Chen, V.S.Y. Lin. Synthesis and functionalization of a mesoporous silica nanoparticle based on the sol-gel process and applications in controlled release. *Acc. Chem. Res*. 2007; 40: 846-853.
10. C. Coll, A. Bernardos, R. Martínez-Máñez, F. Sancenón. Gated silica mesoporous supports for controlled release and signaling applications. *Acc. Chem. Res*. 2013; 46: 339-349.
11. P. Yang, S. Gai, J. Lin. Functionalized mesoporous silica materials for controlled drug delivery. *Chem. Soc. Rev*. 2012; 41: 3679-3698.
12. Z. Li, J.C. Barnes, A. Bosoy, J.F. Stoddart, J.I. Zink. Mesoporous silica nanoparticles in biomedical applications. *Chem. Soc. Rev*. 2012; 41: 2590-2605.
13. N.K. Mal, M. Fujiwara, Y. Tanaka. Photocontrolled reversible realease of guest molecules from coumarin- modified mesoporous silica. *Nature*. 2003; 421: 350-353.
14. A. Schlossbauer, J. Kecht, T. Bein. Biotin-avidin as a protease-responsive cap system for controlled guest release from colloidal mesoporous silica. *Angew. Chem. Int. Ed*. 2009; 48: 3092-3095.
15. P.D. Thornton, A. Heise. Highly Specific Dual Enzyme-Mediated Payload Release from Peptide-Coated Silica Particles. *J. Am. Chem. Soc*. 2010; 132: 2024-2028.
16. C. Park, H. Kim, S. Kim, C. Kim. Enzyme Responsive Nanocontainers with Cyclodextrin Gatekeepers and Synergistic Effects in Release of Guests. *J. Am. Chem. Soc*. 2009; 131: 16614-16615.
17. R. Liu, X. Zhao, T. Wu, P. Feng. Tunable Redox-Responsive Hybrid Nanogated Ensembles. *J. Am. Chem. Soc.* 2008; 130: 14418-14419.
18. E. Aznar, R. Martínez-Máñez, F. Sancenón. Controled release using mesoporous materials containing gate -like scaffoldings. *Expert Opin. Drug Deliv*. 2009; 6: 643-655.
19. J. El Haskouri, D. Ortiz de Zarate, C. Guillem, et al. Silica-based powders and monoliths with bimodal pore systems. *Chem. Commun*. 2002; 330 – 331.
20. M. Comes, M.D. Marcos, R. Martínez-Máñez, et al. Chromogenic Discrimination of Primary Aliphatic Amines in Water with Functionalized Mesoporous Silica. *Adv. Mater*. 2004; 16: 1783 –1786.
21. M. Comes, G. Rodríguez-López, M.D. Marcos, et al. Host Solids Containing Nanoscale Anion-Binding Pockets and Their Use in Selective Sensing Displacement Assays. *Angew. Chem. Int. Ed*. 2005; 44: 2918 – 2922.
22. C.T. Kresge, M.E. Leonowicz, W.J. Roth, J.C. Vartuli, J.S. Beck. Ordered mesoporous molecular sieves synthesized by a liquid-crystal template mechanism. *Nature*. 1992; 359: 710 – 712.
23. A. Rámila, B. Muñoz, J. Pérez-Pariente, M. Vallet-Regí. Mesoporous MCM-41 as Drug Host System. *J. Sol-Gel Sci. Technol*. 2003; 26: 1199 – 1202.

24. M. Vallet-Regí. Ordered Mesoporous Materials in the Context of Drug Delivery Systems and Bone Tissue Engineering. *Chem. Eur. J*. 2006; 12: 5934 –5943.
25. N. Vadia, S. Rajput. Mesoporous material, MCM41: a new drug carrier. *Asian J. Pharm. Clin. Res*. 2011; 4: 44-53.
26. J.S. Beck, J.C. Vartuli, W.J. Roth, et al. A new family of mesoporous molecular sieves prepared with liquid crystal templates. *J. Am. Chem. Soc*. 1992; 114: 10834-10843.
27. A.P. Wright, M.E. Davis. Design and Preparation of Organic–Inorganic Hybrid Catalysts. *Chem. Rev*. 2002; 102: 3589-3614.
28. G. Kickelbick. Hybrid Inorganic–Organic Mesoporous Materials. *Angew. Chem. Int. Ed*. 2004; 43: 3102-3104.
29. C.-Y. Lai, B.G. Trewyn, D.M. Jeftinija, et al. A Mesoporous Silica Nanosphere-Based Carrier System 373 with Chemically Removable CdS Nanoparticle Caps for Stimuli-Responsive 374 Controlled Release of Neurotransmitters and Drug Molecules. *J. Am. Chem. Soc*.2003; 125: 4451-4459.
30. A.L. Doadrio, J.C. Doadrio, J.M. Sánchez-Montero, J.A. Salinas, M. Vallet-Regí. A rational explanation of the vancomycin release from SBA-15 and its derivative by molecular modeling. *Micropor. Mesopor. Mater*. 2010; 132: 559-566.
31. D. Molina-Manso, M. Manzano, J.C. Doadrio, et al. Usefulness of SBA-15 mesoporous ceramics as a delivery system for vancomycin, rifampicin and linezolid: a preliminary report. *Int. J. Antimicrob. Agents*. 2012; 40: 252-256.
32. R. Mellaerts, C.A. Aerts, J.V. Humbeeck, P. Augustijns, G.V.d. Mooter, J.A. Martens. Enhanced release of itraconazole from ordered mesoporous SBA-15 silica materials. *ChemComm*. 2007; 13: 1375-1377.
33. M. Premanathan, F.A. Amaar Shakurfow, A.A. Ismail, M.A. Berfad, A.T. Ebrahim, M.M. Awaj. Treatment of oral candidiasis (thrush) by Saccharomyces cerevisiae. *Int. J. Med.Med. Sci*. 2011; 3: 83-86.
34. O.R. Homann, J. Dea, S.M. Noble, A.D. Johnson. A phenotypic profile of the Candida albicans regulatory network. *PLOS Genetics*. 2009; 5: 1-12.
35. W. Shaw. Yeast and fungi. How to control them. *Biological Treatments for Autism and PDD*. 3rd Edition. 2008: Chapter 4: Part I.
36. R. Casasús, M.D. Marcos, R. Martínez-Máñez, et al. Toward the Development of Ionically Controlled Nanoscopic Molecular Gates. *J. Am. Chem. Soc*. 2004; 126: 8612-8613.
37. R. Casasús, E. Climent, M.D. Marcos, et al. Dual Aperture Control on pH- and Anion-Driven Supramolecular Nanoscopic Hybrid Gate-like Ensembles. *J. Am. Chem. Soc*. 2008; 130: 1903-1917.
38. S. Brunauer, P.H. Emmett, E. Teller. Adsorption of Gases in Multimolecular Layers. Adsorption of gases in multimolecular layers.*J. Am. Chem. Soc.* 1938; 60: 309-319.

39. E.P.Barret, L.-G. Joyner, P.P. Halenda. The determination of pore volume and area distributions in porous substance I. Computations from Nitrogen isotherm. *J. Am. Chem. Soc*. 1951; 73: 373-380.
40. R. Mellaerts, C. A. Aerts, J. Van Humbeeck, P. Augustijns, G. Van den Mooterc, J. A. Martens, Enhanced release of itraconazole from ordered mesoporous SBA-15 silica materials. *Chem Comm.* 2007, 1375-1377.
41. M. R. C. Marques, R. Loebenberg and M. Almukainzi. Simulated biological fluids with possible application in dissolution testing. *Dissolut. Technol.* 2011, 18: 15-28.
42. J.L. Song, J.B. Harry, R.T. Eastman, B.G. Oliver, T.C. White. The Candida albicans lanosterol 14-alpha-demethylase (ERG11) gene promoter is maximally induced after prolonged growth with antifungal drugs. *Antimicrob Agents Chemother*. 2004; 48: 1136-1144.

Enhanced antifungal efficacy of Tebuconazole using gated pH-driven mesoporous nanoparticles.

Supplementary materials

Núria Mas, Irene Galiana, Silvia Hurtado, Laura Mondragón, Andrea Bernardos, Félix Sancenón, María D. Marcos, Pedro Amorós, Nuria Abril-Utrillas, Ramón Martínez-Máñez and José Ramón Murguía**

Synthesis of S1-FL

In a typical synthesis, template-free MCM-41 (100 mg) and fluorescein (16.8 mg, 0.007 mmol) were suspended in methanol (40 mL) inside a round-bottomed flask in an inert atmosphere. The mixture was stirred for 24 h at room temperature in order to achieve maximum loading in the pores of the MCM-41 scaffolding. Then, an excess of 3-[2-(2-aminoethylamino)-ethylamino]propyltrimethoxysilane (N3, 0.2 mL, 0.7 mmol) was added and the final mixture was stirred for 5.5 h at room temperature. Finally, the solid (**S1-FL**) was filtered and washed with methanol (40 mL). Once it was dried, the solid was suspended in water at pH 2 in the presence of sulphate (at this pH, the molecular gate is “closed”) in order to remove the dye remaining outside the pores. After 12 h, the solid was filtered and dried at 37°C for 24 h.

S1-FL Characterization

Synthesised material **S1-FL** was characterised by standard techniques. Figure S1A shows the powder X-ray diffraction (PXRD) patterns of solids MCM-41 as-synthesised, MCM-41 calcined and **S1-FL**. The PXRD of the mesoporous MCM-41 as-synthesised material (curve a) showed four peaks, which are typical of a hexagonal ordered array, indexed as (100), (110), (200), and (210) Bragg reflexions. From the PXRD data, an a_0 cell parameter of 2.27 Å was calculated. In curve b (the MCM-41 calcined sample), an important shift of the (100) to lager angles in PXRD and a broadening of the (110) and (200) reflections were clearly found and attributed to the condensation of the silanol groups in the calcination step. Figure 1 also depicts the PXRD pattern for solid **S1-FL**. For this material, reflections (110) and (200) were almost lost, probably due to diminished contrast as a result of the loading and functionalisation process. Nevertheless, the clear presence in **S1-FL** of the d100 peak in the XRD patterns supports that pore loading, and the additional functionalisation with the amine derivative, did not modify the mesoporous structure of the starting MCM-41 scaffolding.

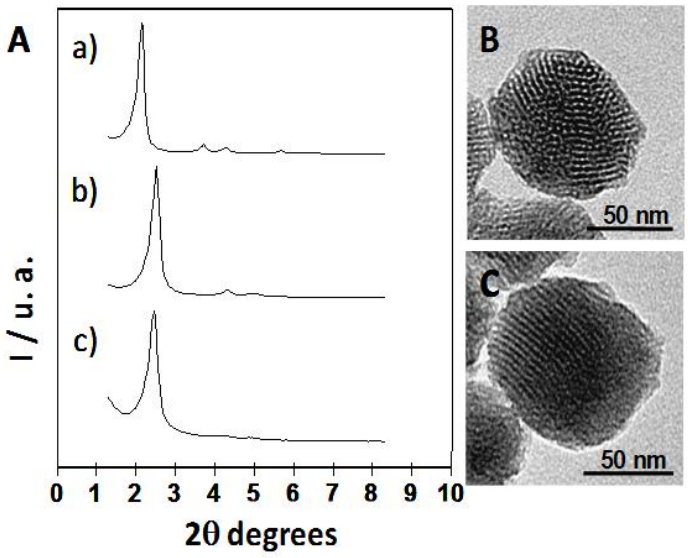

Figure S1. A) The powder X-ray patterns of the solids (a) MCM-41 as synthesised (b) calcined MCM-41 (c) solid **S1-FL** containing the FL dye and N3. The TEM images of B) the calcined MCM-41 sample and C) **S1-FL** showing the typical porosity of the MCM-41 mesoporous matrix.

Preservation of the mesoporous structure in both the calcined MCM-41 material and the final functionalised solid **S1-FL** was also confirmed by means of the transmission electron microscopy (TEM) images. In both solids, the characteristic channels of a mesoporous matrix were observed as alternate black and white lines. Figure S1B shows the morphology of the prepared mesoporous MCM-41 and **S1-FL** materials as spherical nanoparticles with a mean diameter of ca. 100 nm.

In order to complement the information provided by the X-ray and TEM analyses, porosimetry studies for the MCM-41 calcined and the final **S1-FL** materials were carried out (Table S1). The N_2 adsorption-desorption isotherms of the nanoparticulated MCM-41 calcined material are shown in Figure S2A. A typical curve for these mesoporous solids, consisting of an adsorption step at an intermediate P/P_0 value (0.1-0.3), is observed. The absence of a hysteresis loop in this interval and the narrow BJH pore distribution suggest the existence of uniform cylindrical mesopores (pore diameter of 3.09 nm and pore volume of 0.935 $cm^3\ g^{-1}$ calculated by the BJH model on the adsorption branch of the isotherm). The application of the BET model resulted in a value of 1096 m^2/g for the total specific surface. For **S1-FL**, the N_2 adsorption-desorption isotherm (Figure S2) presented the typical characteristics of a mesoporous system with partially filled mesopores. Therefore, lower N_2 adsorbed volume (BJH mesopore volume = 0.482 $cm^3\ g^{-1}$) and surface area (424 m^2/g) values were calculated. Despite the significant drop in pore volume, some features were still observed in the BJH mesopore size distribution, such as a maximum at ca. 1.8 nm (on the border between meso- and micropores).

Table S1. BET Specific Surface Values, Pore Volumes and Pore Sizes Calculated from the N_2 Adsorption-Desorption Isotherms for Selected Materials.

Solid	S_{BET} ($m^2\ g^{-1}$)	Pore Volume ($cm^3 g^{-1}$)	Pore size (nm)
MCM-41	1097	0.94	3.09
S1-FL	424	0.48	3.49

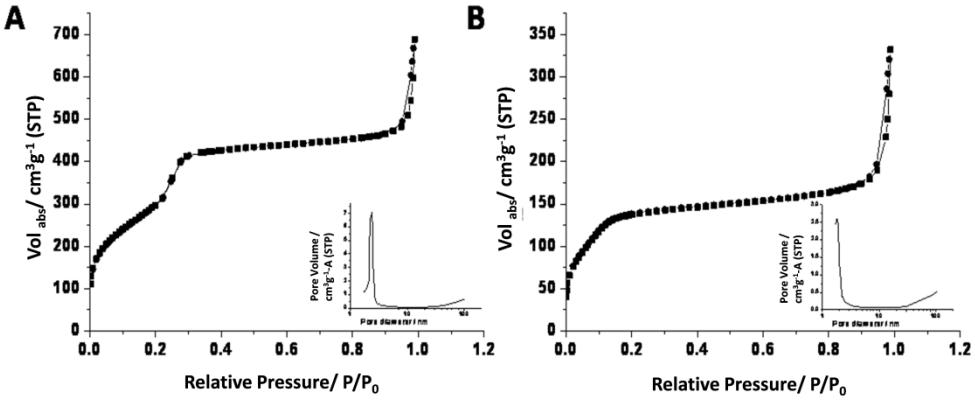

Figure S2. Nitrogen adsorption-desorption isotherms for A) MCM-41 mesoporous material, B) **S1-FL** material. Inset: Pore size distribution of the MCM-41 mesoporous material and of **S1-FL** solid.

Having determined the structure of the nanoparticles synthesised, the amount of guest molecule and N3 on solid **S1-FL** was determined by a thermogravimetric analysis. Table S2 offers the results obtained.

Table S2. Content (α) in mmol of N3 and dye per gram of SiO_2 for **S1-FL**.

Solid	α_{N3}	α_{FL}
S1-FL	0.549	0.376

Release kinetics of S1-FL.

In order to check the proper aperture mechanism of solid **S1-FL**, 10 mg were suspended in 25 mL of water containing sulphate anions at a final concentration of 0.01 M at different pH (3.7 and 5.5). Suspensions were stirred at room temperature, and at a given time, aliquots were separated and filtered. The delivery of FL from the pore voids to the aqueous solution was monitored via its fluorescence emission band at 517 nm (λ_{ex} = 494 nm). Due to the influence of pH on the fluorescence of FL, all the taken aliquots were treated with the amount of NaOH required to increase their pH to 8.

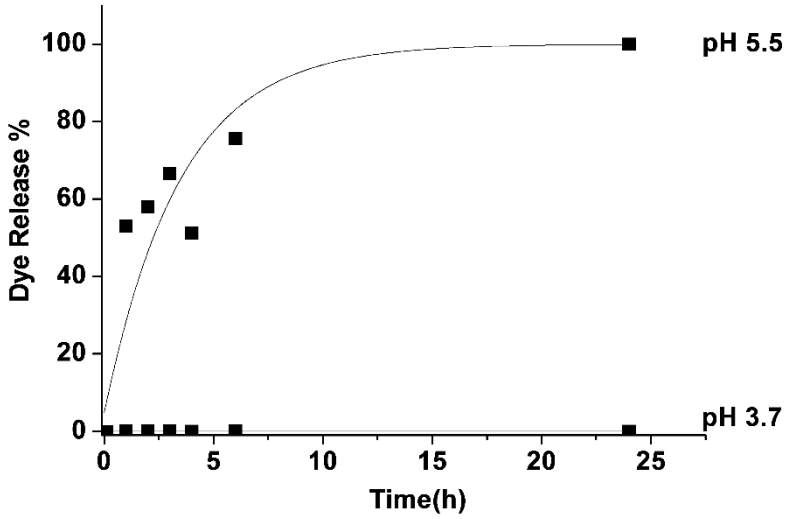

Figure S3. Kinetic release of FL from solid **S1-FL** at pH 3.7 and pH 5.5.

The dye delivery at different pH is depicted in Figure S3. At the more acidic pH of 3.7, **S1-FL** was tightly capped and displayed no significant FL release. In contrast at pH 5.5, the cargo molecule was released. The interpretation of such behaviour lies in the different degrees of protonation of amines at different pH values and in the interaction of protonated amines with certain anions. Despite the fact that these pK_a values can be modified when a number of polyamines is anchored onto the silica surface, it is clear that at pH 3.7, amines become more protonated than at pH 5.5. It has been reported that when protonated, tethered open-chain polyamines tend to adopt a rigid-like conformation that pushes them towards to the pore openings. This results in a pore blockage that partially inhibits the dye release. A second effect is related to the interaction of protonated amines with anions (in our case, sulphate). This is based on the capacity that polyamines have to coordinate anionic species. Polyamines have, thus, been extensively explored as suitable groups for designing abiotic ligands for inorganic and biologically important anionic guests. Amine-containing receptors are polycations (polyammonium ligands), especially at an acidic pH, and they bind anionic species via hydrogen bonding and Coulombic forces. At pH 5.5 and pH 3.7, a combination

of both ammonium and amine groups anchored onto the **S1-FL** surface is expected to occur, where the percentage of ammonium groups grows as pH lowers. For the correct interpretation of the interaction of sulphate with the anchored polyamines, it is important to note that sulphate shows a logarithm for its first protonation of 1.9, indicating that at pH 3.7 and pH 5.5, sulphate acts like SO_4^{2-} species. The observed behaviour (i.e., sulphate is able to close the "gate" at pH 3.7, but is unable to inhibit dye release at pH 5.5) can be explained bearing in mind the larger proportion of positively charged ammonium groups at pH 3.7, which results in a larger electrostatic interaction with sulphate anions. Nevertheless, hydrogen-bonding interactions between the amine/ammonium groups and sulphate cannot be ruled out since SO_4^{2-} can act as a hydrogen bond acceptor, whereas amines/ammonium groups can behave as hydrogen bond donors.[1]

Yeast uptake of S1-FL

We next tested the applicability of SMPS based on MCM-41 as nanocarriers for intracellular release in *S. cerevisiae*. Our hypothesis was based on the fact that the designed nanoparticle presents a "zero release" of the cargo molecule in acidic environments (at a pH of around 3-4) in the presence of sulphate in which yeasts are able to grow. Having internalised the solid, the lower acidity inside *S. Cerevisiae* (pH 5.5), where the nanoparticles will be located, allows the entrapped molecule to be released (See Figure S4).

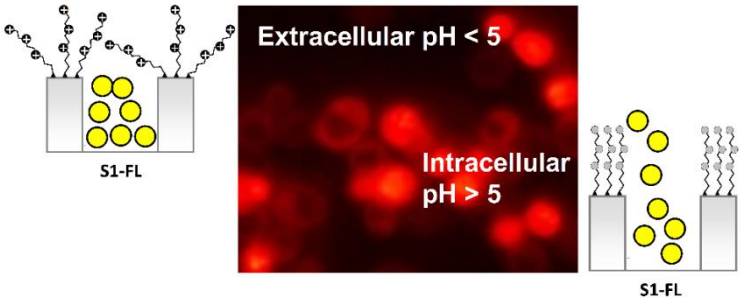

Figure S4. Schematic representation of the hybrid system **S1-FL** performance.

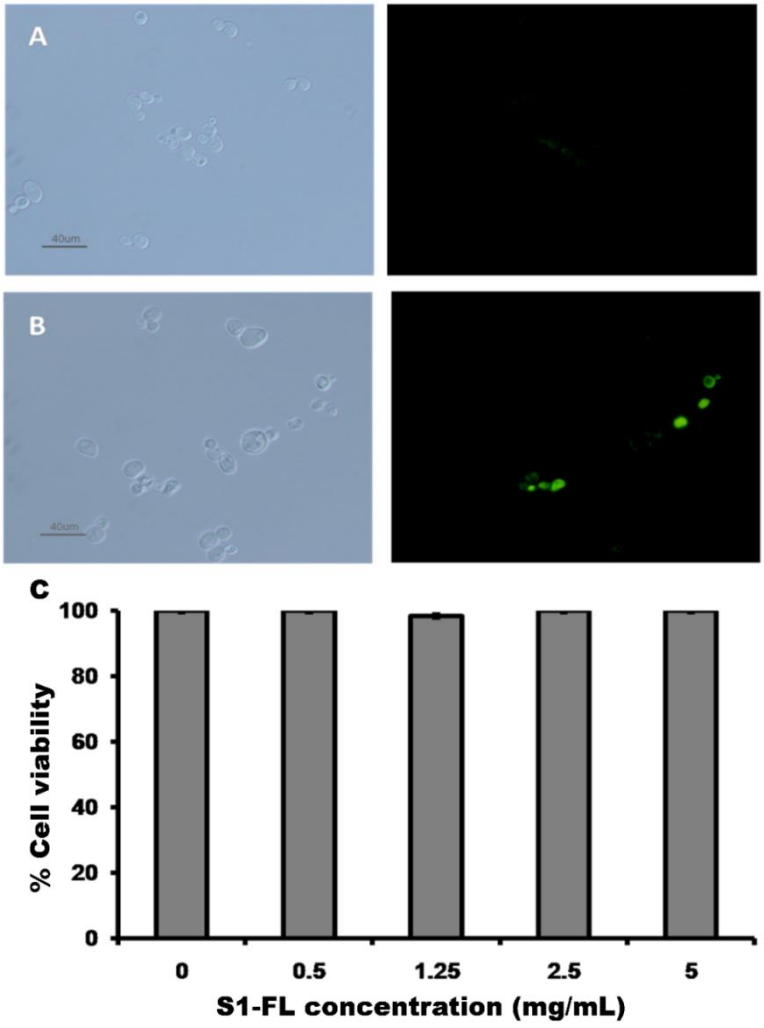

Figure S5. **S1-FL** internalization and cell viability assays. Fluorescence microscopy images corresponding to the *S. cerevisiae* cells treated with 5 mg/mL of solids (A) MCM-41 and (B) **S1-FL** and incubated at 40°C for 6 h. The cellular internalization of solid **S1-FL** was followed by fluorescein-associated fluorescence (green). For the clonogenic cell survival assays (C), *S. cerevisiae* cells were treated with 5, 2.5, 1.25, 0.5 mg/mL of **S1-FL**.Two independent experiments were performed and data are reported as (mean ± SE).

The conditions for nanoparticles internalisation in yeast cells were then optimized. We first focused on determining the optimal incubation temperature

of *S. cerevisiae* cells with nanoparticles and the different agitation rates of cultures. Three different temperatures were tested: 30°C, 37°C and 40°C. Consequently, 40 ºC proved the most efficient temperature for nanoparticles uptake, probably due to the increased plasmatic membrane permeability at higher temperatures. Then, internalization and cell viability assays were carried out with **S1-FL** at 40 ºC (See Figure S5). When different agitation rates were chosen, no agitation proved optimal for the cellular uptake of solids.

References

1. S.W. Song, K. Hidajat, S. Kawi, pH-controllable drug release using hydrogel encapsulated mesoporous silica.*Chem Comm*. 2007; 42:4396–4398.

3.3 *Enhanced efficacy and broadening of antibacterial action of drugs via the use of capped mesoporous nanoparticles.*

Núria Mas,[a,b] Irene Galiana,[b] Laura Mondragón,[a,b] Elena Aznar,[b,a] Estela Climent,[a,b] Nuria Cabedo,[c] Félix Sancenón,[a,b] José Ramón Murguía,[d,b] Ramón Martínez-Máñez,*[a,b] María D. Marcos[a,b] and Pedro Amorós[e]*

[a]Centro de Reconocimiento Molecular y Desarrollo Tecnológico (IDM). Departamento de Química. Universidad Politécnica de Valencia. Universidad Politécnica de Valencia. Camino de Vera s/n, 46022, Valencia, Spain. Fax: (+)96-387-9349 E-mail: rmaez@qim.upv

[b]CIBER de Bioingeniería, Biomateriales y Nanomedicina (CIBER-BBN, Spain).

[c]Centro Ecología Química Agrícola-Instituto Agroforestal Mediterráneo. Universidad Politécnica de Valencia. Avenida de los Naranjos s/n, Edificio 6C, 46022 Valencia, Spain.

[d]Instituto Universitario Mixto de Biología Molecular y Celular de Plantas. Universidad Politécnica de Valencia. Camino de Vera s/n, 46022, Valencia, Spain E-mail: muribajo@ibmcp.upv.es

[e]Institut de Ciència del Materials (ICMUV).
Universitat de Valencia. P.O. Box 2085, 46071, Burjassot, Valencia , Spain.

Received: June 7 2013
Published online: July 9 2013

Because of antibacterial agents abuse, the escalation of bacterial resistance to many common antibiotics is a serious concern for modern medicine.[1] As a consequence, this resistance is decreasing the effectiveness of current infections' treatments, causing high number of hospitalizations and deaths.[1,2,3] Therefore, the improvement of the efficacy and the broadening of antibiotics spectrum of action is of outmost importance in pharmaceutical and biomedical research.[4,5]

One of the most drug resistant pathogens are Gram-negative bacteria.[6] The distinction between Gram-positive and Gram-negative bacteria is based on their different membrane structures and composition. The cell wall of Gram-positive bacteria contains a 30 nm thick peptidoglycan layer[4] whereas Gram-negative bacteria present a complex envelope that comprises a thin peptidoglycan layer and an outer membrane which contains as unique component lipopolysaccharides, which increases the negative charge of the membrane.[3] This constitutes a sophisticated barrier which protects the cell against external toxic compounds[6] and makes them highly resistant to a wide range of antibiotics.[3] Different chemical and technological approaches have been described for antibacterial agents to cross the outer membrane of Gram-negative bacteria.[7] Some involve alterations in the composition/stability of the membrane, whilst others affect the influx/efflux of molecules into the cell.[6] In this regard, the design of non-traditional antibiotic agents have become of interest in overcoming resistance (*vide infra*).

The design of gated mesoporous supports able to deliver their cargo under certain environmental conditions is a captivating area of research that has attracted the attention of scientists in the latest years. This technology has demonstrated to be an excellent approach for the development of smart nanodevices for advanced delivery applications.[8-16] In this context, silica mesoporous supports are widely used as inorganic scaffolds thanks to their unique characteristics such as high homogeneous porosity, inertness, robustness,

thermal stability and high loading capacity.[17-20] The main advantage of such approach is that it is possible to design nanoparticles loaded with a suitable cargo and capped in such a way that zero delivery is observed until the presence of target stimuli.

In this context, although mesoporous silica supports have been used for the simple diffusion-controlled release of certain antibiotics,[21-23] similar studies using capped materials showing zero release and able to deliver the cargo in the presence of bacteria have not been described. Accordingly, there are not reports dealing with the potential use of mesoporous supports to enhance or widen the spectrum of antimicrobial drugs.

Under this background, the nanoparticles shown in Scheme 1 were designed. As inorganic scaffolding a nanometric mesoporous MCM-41 phase (ca. 100 nm) was selected. The MCM-41 nanoparticles were loaded with rhodamine B or vancomycin. Then the external surface of both materials was functionalized with *n*-[(3-trimethoxysilyl) propyl] ethylendiaminetriacetic acid trisodium salt (compound **1** in Scheme 1). Finally, the pores were capped by the addition of ε-poly-L-lysine (ε-PL) cationic polymer (through electrostatic interactions with the negatively charged nanoparticles surface) to finally obtain **S1-Rho** (loaded with rhodamine) and **S1-Van** (loaded with vancomycin) solids (see Supporting Information for details).

Although ε-PL has been reported to display antibiotic features for Gram-negative bacteria, vancomycin is a glycopeptide antibiotic which selectively targets Gram-positive bacteria,[24,25] since it binds with the terminal D-Ala-D-Ala moieties of the peptide units to the surface of their cell wall.[3,26] Once reacted, vancomycin blocks the intrachain bond formation thus inhibiting the steps in murien (peptidoglycan) bio-synthesis.[25,27] Due to its high molecular weight and size, vancomycin is unable to pass through porins in the additional outer membrane of Gram-negative bacteria to reach the D-Ala-D-Ala target. Therefore, Gram-negative bacteria are intrinsically resistant to this class of antibiotics.[7]

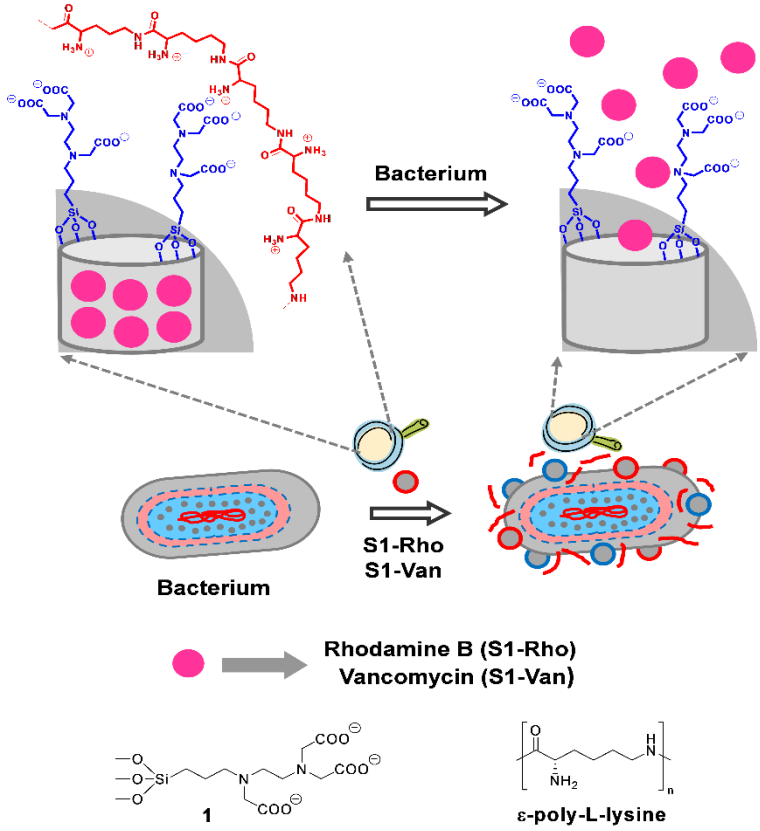

Scheme 1. Schematic representation of the action mechanism of **S1-Rho** and **S1-Van** solids in the presence of *Escherichia coli*.

As mentioned above, the design of non-traditional antibiotic agents based in nanoformulations have become of interest in overcoming resistance of certain bacteria to antibiotics.[5] In fact some attempts have been described for the enhancement of vancomycin toxicity to resistant Gram-positive bacteria[28-30] and to overcome intrinsic resistance of Gram-negative bacteria to vancomycin. In this context, for instance, the combination of silver nanoparticles and vancomycin has been reported to enhance vancomycin toxicity to Gram-positive strains, whereas only a low improvement was observed for Gram-negative bacteria.[31] Other approaches to enhance vancomycin toxicity to Gram-negative bacteria included

the surface functionalization of gold[32] or Fe_3O_4[33] nanoparticles with vancomycin and the use of some carriers loaded with vancomycin based in pH-dependent polymeric nanoparticles,[24] chitosan nanoparticles[27] and fusogenic liposomes.[7] However, in most cases, toxicity of these nanoformulations to Gram-negative bacteria is partial and most of these systems still show relatively high minimum inhibitory concentrations (MIC).

Following our approach (see Scheme 1) we synthesised the starting nanoparticulated MCM-41 mesoporous solid following well-known procedures using *n*-cetyltrimethylammonium bromide (CTAB) as template and tetraethylorthosilicate (TEOS) as hydrolytic inorganic precursor.[34-38] The starting MCM-41 solid was obtained after calcination. The MCM-41 structure was confirmed by powder X-ray diffraction and transmission electron microscopy TEM. The N_2 adsorption-desorption isotherms of the prepared phase shows a typical type IV-curve with a specific surface area of 981.2 m^2g^{-1}, a narrow pore size distribution and an average pore diameter of 2.3 nm (see Supporting Information).

In Figure 1A the powder X-ray pattern of the final **S1-Rho** and **S1-Van** materials is shown. Both solids display the expected features of the MCM-41 phase, indicating that the mesopores in the inorganic scaffolding are preserved throughout the filling process, external anchoring of **1** and capping process with ε-PL. Moreover Figure 1B shows TEM images of both solids displaying the typical porosity of the MCM-41 phase. The N_2 adsorption-desorption isotherms of **S1-Rho** and **S1-Van** (see Supporting Information) are typical of gated and filled mesoporous systems and a significant decrease in the N_2 volume adsorbed was observed when compared with the starting MCM-41 material. The organic content for both capped nanoparticles is shown in Table 1 (see Supporting Information for details). The contents of **1** and ε-PL for both solids are very similar but the content of the loaded cargo (in mmol/g solid) is lower for **S1-Van** most likely due to the larger size of vancomycin when compared with rhodamine dye.

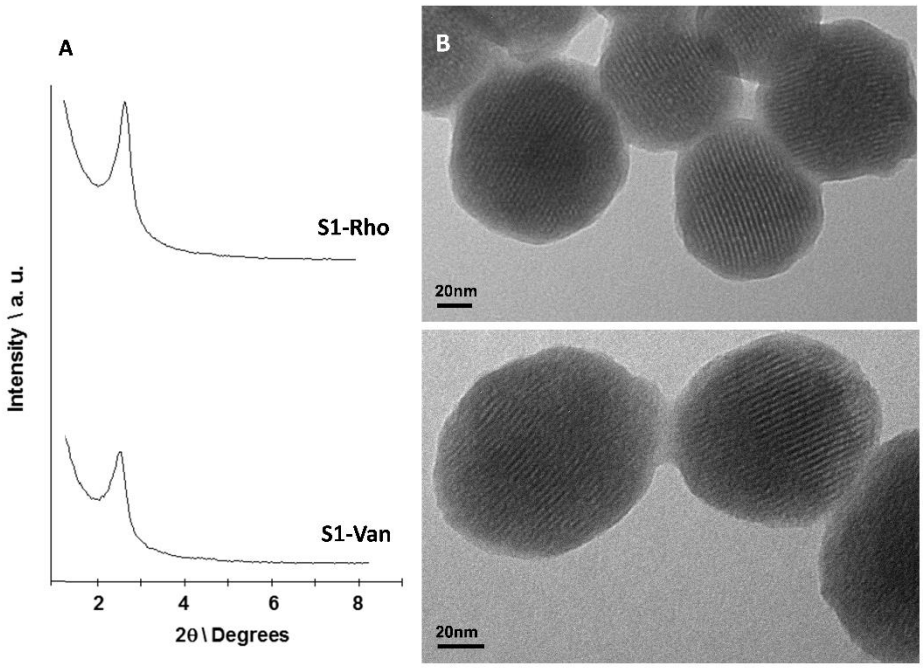

Figure 1. (A) Powder X-Ray pattern of **S1-Rho** and **S1-Van** solids. (B) TEM image of **S1-Rho** and **S1-Van**.

Table 1. Contents (α) in mmol/g solid for **S1-Rho** and **S1-Van**.

Solid	α_{Rho} (mmol/g solid)	α_{Van} (mmol/g solid)	α_1 (mmol/g solid)	$\alpha_{\varepsilon-PL}$ (mmol/g solid)
S1-Rho	0.021	----	0.388	0.025
S1-Van	----	0.010	0.390	0.021

In vitro dye release studies were carried out with **S1-Rho** solid to test the correct working of the gating mechanism and optimize bacteria (*E. coli*, DH5α strain) concentration. In a typical experiment solid **S1-Rho** was suspended in water at pH 7 and divided in two aliquots. Moreover, *E. coli*. was added to one of these aliquots. Both suspensions were kept at room temperature and at given times fractions of both suspensions were taken and centrifuged in order to

remove the solid. Dye delivery from **S1-Rho** was then measured via the monitorisation of the absorbance of rhodamine B (λ_{abs} = 555nm) (see Figure 2). In the absence of *E. coli* a negligible dye release was observed indicating that the nanoparticles were tightly capped. In contrast in the presence of bacteria the uncapping of the pores was clearly found. This cargo delivery triggered by the presence of *E. coli*, is attributed to the adhesion of the ε-PL-capped positively-charged **S1-Rho** support with the negatively charged bacteria wall[39,40] and the weakening of the interaction between ε-PL and the carboxylate-functionalised surface of the nanoparticles which results in cargo delivery. Different bacteria concentrations (from 10^6 to 10^3cells/mL) were tested in presence of **S1-Rho**. From these studies an optimum bacteria concentration of 10^5cells/mL was determined.

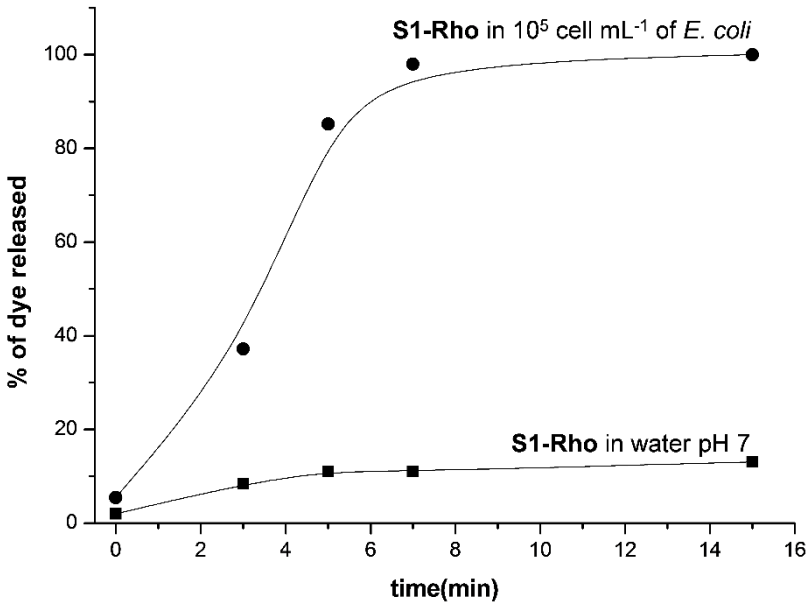

Figure 2. Kinetic release profiles of rhodamine B from a water suspension in the absence and in the presence of *E.coli.*

To test the *in vivo* effect of the prepared solids on bacterial cell integrity, clonogenic cell viability assays were carried out with MCM-41calcined, **S1-Rho** and **S1-Van**. The solid concentrations studied for both materials ranged from 1 mg solid/mL to 0.5 μg solid/mL in water at pH 7. Also a negative control (0 μg of solid/mL) was prepared in order to quantitate cell growth. Cell viability assays

were also done with free vancomycin, free ε-PL and free ε-PL/vancomycin mixtures. The amounts of free drugs (ε-PL and vancomycin) used in these studies were the same contained in the capped **S1-Rho** and **S1-Van** solids (see Table 1). Seeded plates were incubated at 37°C for 15-18 h. Then, colony formation units (CFU) were quantified. As not all the ε-PL in solids surface was going to be totally effective against bacteria, because of the existence of an equilibrium between ε-PL interacting with the nanoparticles and with the bacteria cell wall, a pharmacological adjustment was done between free ε-PL and **S1-Rho** viability curves to evaluate equitoxic concentrations. Remarkably, the antibiotic nanoformulation of ε-PL (solid **S1-Rho**) exacerbated ε-PL cytotoxicity 4-fold, being the EC_{50} for **S1-Rho** 0.14 μg/mL and for free ε-PL 0.47 μg/mL, with $P < 0.0001$ in both cases (see Figure 3).

As expected, neither MCM-41 nor free vancomycin showed detectable toxicity against *E. coli* bacteria (Figure 4). Furthermore no synergism was detected when the toxicity of free ε-PL and a mixture containing free ε-PL and vancomycin against *E. coli* was compared; i.e., both systems show the same minimum inhibitory concentration (MIC) (see Figure 4B). In contrast a remarkable synergistic effect was observed when we used ε-PL and vancomycin in the nanoformulation (see Figure 4A). Accordingly **S1-Van** exhibited a noteworthy 6-fold decrease in MIC (2.89 μg ε-PL/mL) when compared to that of **S1-Rho** (16.7 μg ε-PL /mL), with $P<0.0001$ in all cases.

Enhancement of vancomycin toxicity to Gram-negative bacteria, is tentatively attributed to interaction of the positively charged **S1-Van** nanoparticles with the bacteria and displacement of the capping ε-PL which binds to the cell wall. Moreover ε-PL induces bacterial wall damage which allowed the entrapped vancomycin to gain access into the cell (see Scheme 1).

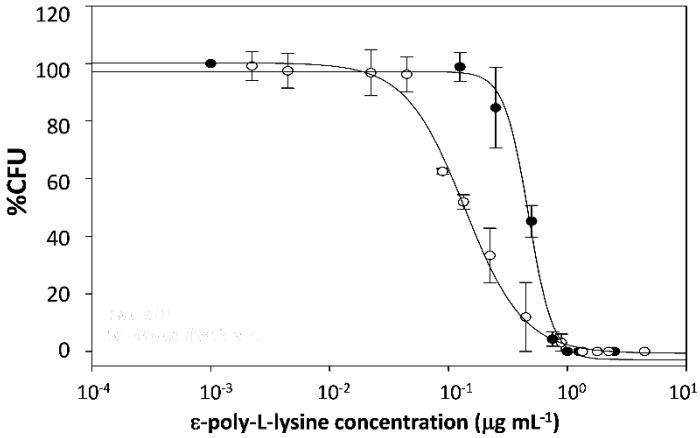

Figure 3. Free ε-poly-L-lysine (•) and **S1-Rho** equitoxic ε-poly-L-lysine (o) concentration vs. % CFU.

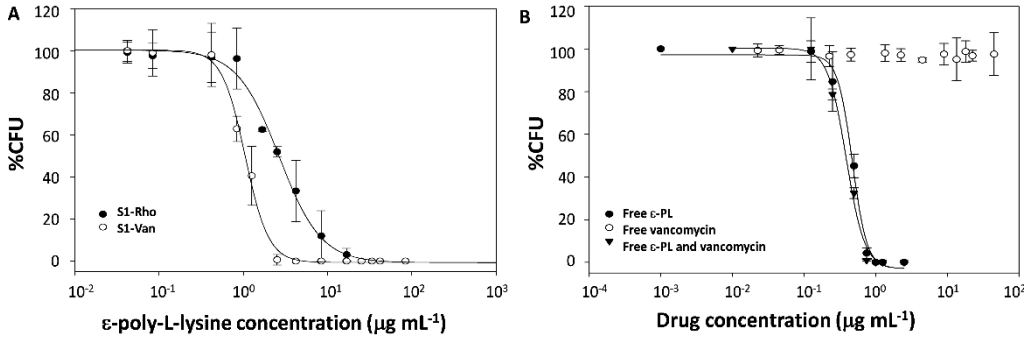

Figure 4. (A) Different solids concentration vs. % CFU. (B) Free different drugs concentration vs. % CFU.

Given the promising results obtained with *E. coli* DH5α, we explored whether the **S1-Van** solid behaved similarly with other Gram-negative bacteria strains such as *E.coli* 100, *E.coli* 405, *S. typhi* and *E. Carotovora*. To address this, we performed a cytotoxicity analysis by the standard broth microdilution method in 96-well plate format (see Supporting Information for details).[41] This assay, although less sensitive than viability studies, allows to quickly quantitate cytotoxicity in a high number of microorganisms simultaneously. Bacterial growth was determined turbidimetrically (OD_{620}) using a Thermo Scientific Multiskan FC multimode plate reader. Each experiment was performed twice and the measured

antibacterial activity was expressed as MIC range. Percentage growth inhibition was determined using plate-based microliter dilution assay. EC_{50} values with their standard error were obtained using nonlinear regression analysis for all bacterial strains (see Table 2), $P < 0.01$ in all cases.

As cell growth and not cell viability is quantitated in the cytotoxicity assays, discrepancies in the effective dose observed for each solid could occur with the clonogenic viability assays. To avoid this, we included in the cytotoxicity experiments the reference strain E. coli DH5α. This internal control allowed us to fully compare both experimental approaches. In order to evaluate the effectiveness of the **S1-Van** nanoparticles, free vancomycin, free ε-PL and free ε-PL/vancomycin mixtures were also tested at the same concentrations than those present in **S1-Van** for the different solid suspensions (see Table 2). Vancomycin, was not toxic for the tested Gram-negative bacteria at concentration as large as 15 μg/mL, whereas ε-PL did not reached MIC even at concentrations larger than 83 μg/mL. As in the above studies with *E. coli* DH5α, no synergism was found when free ε-PL and mixtures containing free ε-PL and vancomycin were tested against *E.coli* 100, *E.coli* 405, *S. typhi* and *E. carotovora* (data not shown). In contrast remarkable MIC values measured with **S1-Van** indicated a strong inhibition of bacterial growth and a large synergistic effect when this nanoformulation was used. Taken together, these results indicated that **S1-Van** dramatically enhanced vancomycin antibiotic effect, not only in *E. coli* laboratory experimental strains but also in other Gram-negative bacteria, in terms of growth inhibition and cell viability.

Table 2. Minimum inhibitory concentration (MIC) ranges (μg vancomycin /mL) and EC50 (μg vancomycin /mL) for **S1-Van**, free vancomycin (Van, μg Van/mL) and free ε-PL (μg ε-PL/mL) against different Gram-negative bacterial.

	***Escherichia coli* 100**		***Eschrichia coli* 405**		***Salmonella typhi***		***Erwinia carotovora***		***Escherichia coli DH5α***	
	MIC	***EC_{50}***	***MIC***	***EC_{50}***	***MIC***	***EC_{50}***	***MIC***	***EC_{50}***	***MIC***	***EC_{50}***
S1-Van	0.75	0.333(3) [a]	0.75	0.494(8) [a]	0.75	0.356(2) [a]	1.5	0.413(5) [a]	1.5	0.75(3) [a]
Van	>15 [b]	>15 [b]	>15 [b]	>15 [b]	>15 [b]	>15 [b]	>15 [b]	>15 [b]	>15 [b]	>15 [b]
ε-PL	>83 [c]	41.5(4) [a]	>83 [c]	16.6(2) [a]	>83 [c]	41.5(5) [a]	>83 [c]	16.6(3) [a]	5	16.6(2) [a]

[a]Values in parentheses are standard error on the last significant digit.

[b]Highest free vancomycin concentrations tested which was equal to the corresponding highest vancomycin concentration employed when using **S1-Van**.

[c]Highest free ε-PL concentrations tested which was equal to the corresponding highest ε-PL concentration employed when using **S1-Van**.

In summary, a novel nanodevice consisting of mesoporous nanoparticles loaded with vancomycin and capped with ε-PL has been prepared, and its interaction with different Gram-negative bacteria (*E.coli* DH5α, *E.coli* 100, *E.coli* 405, *S. typhi* and *E. carotovora*) studied. An interesting and remarkable enhancement of the toxicity of ε-PL (in **S1-Rho** solid) was found when compared with free ε-PL in solution. Most important when ε-PL and vancomycin were used in **S1-Van** a potent synergistic effect was observed which does not occur in the free formulation. As far as we are aware, this is the first time that the potential use of gated mesoporous nanoparticles to improve the efficacy of antimicrobial drugs (in our case ε-PL) and to increase the antimicrobial spectrum of certain drugs (such as vancomycin) is described. These results suggest that capped mesoporous nanoparticles may be suitable platforms for the design of smart antimicrobial nanodevices for a wide range of applications.

Keywords: mesoporous nanoparticles • gated materials • synergistic effects • broadening antimicrobial spectrum • vancomycin • ε-poly-L-lysine

Acknowledgements

Authors thank the Spanish Government (project MAT2012-38429-C04-01) the Generalitat Valenciana (project PROMETEO/2009/016) and the CIBER-BBN for their support. N.M. also thanks the Ministerio de Ciencia e Innovación for her FPI grant.

References

1. A. M. Allahverdiyev, K. V. Kon, E. S. Abamor, M. Bagirova, M. Rafailovich. *Expert Review of Anti-Infective Therapy* **2011**, *9*, 1035-1052.
2. L. Matthews, R. K. Kanwar, S. Zhou, V. Punj, J. R. Kanwar. *Open Tropical Medicine Journal*, **2010**, *3*, 1-9.
3. M. J. Hajipour, K. M. Fromm, A. A. Ashkarran, D. Jimenez de Aberasturi, I. Ruiz de Larramendi, T. Rojo, V. Serpooshan, W. J. Parak, M. Mahmoudi. *Trends in Biotechnology,* **2012**, *30*, 499-511.
4. M. K. Rai, S. D. Deshmukh, A. P. Ingle, A. K. Gade. *Journal of Applied Microbiology*, **2012**, 112, 841-852.
5. A. J. Huh, Y. J. Kwon. *Journal of Controlled Release*, **2011**, *156*, 128-145.
6. J. M. Bolla, S. Alibert-Franco, J. Handzlik, J. Chevalier, A. Mahamoud, G. Boyer, K. Kiec-Kononowicz, J. M. Pagès. *FEBS Letters*, **2011**, *585*, 1682-1690.
7. D. Nicolosi, M. Scali, V. M. Nicolosi, R. Pignatello. *International Journal of Antimicrobial Agents,* **2010**, *35*, 553-558.
8. C. Coll, A. Bernardos, R. Martínez-Máñez, F. Sancenón. *Acc. Chem. Res*, **2013**, *46*, 339-349.
9. P. Yang, S. Gai, J. Lin, *Chem. Soc. Rev,* **2012**, *41*, 3679-3698.
10. Z. Li, J.C. Barnes, A. Bosoy, J. F. Stoddart, Zink. *Chem. Soc. Rev*, **2012**, *41*, 2590-2605.
11. B. G. Trewyn, I. I. Slowing, S. Giri, H. –T. Chen, V. S. –Y. Lin, *Acc. Chem. Res.*, **2007**, *40*, 846-853.
12. N. K. Mal, M. Fujiwara, Y. Tanaka, *Nature*, **2003**, *421*, 350-353.
13. A.Schlossbauer, J. Kecht, T. Bein, *Angew. Chem. Int. Ed.*, **2009**, *48*, 3092-3095.
14. P. D. Thornton, A. Heise, *J. Am. Chem. Soc.*, **2010**, *132*, 2024-2028.
15. C. Park, H. Kim, S. Kim, C. Kim, *J. Am. Chem. Soc.*, **2009**, *131*, 16614-16615.
16. R. Liu, X. Zhao, T. Wu, P. Feng, *J. Am. Chem. Soc.*, **2008**, *130*, 14418-14419.
17. N. Vadia, S. Rajput, *Asian Journal of Pharmaceutical and Clinical Research*., **2011**, *4*, 44-53.
18. J. S. Beck, J. C. Vartuli, W. J. Roth, M. E. Leonowicz, C. T. Kresge, K. D. Schmitt, C. T. –W. Chu, D. H. Olson, E. W. Sheppard, S. B. McCullen, J. B. Hoggins, J. L. Schlenker, *J. Am. Chem. Soc.*, **1992**, *114*, 10834-10843.
19. A. P. Wright, M. E. Davis, *Chem. Rev.*, **2002**, *102*, 3589-3614.
20. G. Kickelbick, *Angew. Chem. Int. Ed.*, **2004**, *43*, 3102-3104.
21. C. –Y. Lai, B. G. Trewyn, D. M. Jeftinija, K. Jeftinija, S. Xu, S. Jeftinija, V. S. –Y. Lin, *J. Am. Chem. Soc.*, **2003**, *125*, 4451-4459.
22. A. L. Doadrio, J. C. Doadrio, J. M. Sánchez-Montero, J. A. Salinas, M. Vallet-Regí, *Micropor. Mesopor. Mater.*, **2010**, *132*, 559-566.
23. D. Molina-Manso, M. Manzano, J. C. Doadrio, G. Del Prado, A. Ortíz-Pérez, M. Vallet-Regí, E. Gómez-Barrena, J. Esteban, *Int. J. Antimicrob. Agents*, **2012**, *40*, 252-256.

24. A. F. Radovic-Moreno, T. K. Lu, V. A. Puscasu, C. J. Yoon, R. Langer, O. C. Farokhzad, *ACSNano,* **2012**, *6*, 4279-4287.
25. J. E. Bandow, N. Metzler-Nolte. *ChemBioChem*, **2009**, *10*, 2847-2850.
26. W. C. Huang, P. J. Tsai, Y. C. Chen. *Nanomedicine*, **2007**, *2*, 777-787.
27. S. P. Chakraborty, S. K. Sahu, P. Pramanik, S. Roy, *Int. J. Pharm.,* **2012**, *436*, 659-676.
28. G. Fontana, D. Schillaci*. Gazz. Med. Ital.* **2009**, *168*, 89-93.
29. D. Pornpattananangkul, L. Zhang, S. Olson, S. Aryal, M. Obonyo, K. Vecchio, C.-M. Huang, L. Zhang. *J. Am. Chem. Soc.,* **2011***,133,*4132-4139.
30. Y. Wan, D. Zhamg, Y. Wang, P. Qi, J. Wu, B. Hou, *J. Hazard. Mater.,* **2011***,186,*306-312.
31. A. R. Shahverdi, A.Fakhimi, H. R. Shahverdi, S. Minaian. *Nanomedicine: NBM*, **2007**, 5, 168-171.
32. H. Gu, P.L. Ho, E. Tong, L. Wang, B. Xu. *Nano Lett*., **2003***, 3*, 1261-1263.
33. K.-H. Choi, H.-J. Lee, B.J. park, K.-K. Wang, E. P. Shin, J.-C. Park, Y. K. Kim, M.-K. Oh, Y.-R. Kim. *Chem. Commun*., **2012**, *48*, 4591-4593.
34. M. Vallet-Regí, *Chem. Eur. J,* **2006**, *12*, 5934-5943.
35. J. S.M. Smith, A.J. Beyhan, M. R. Gillings, M.P. Holley, A.J. Stow, C.L. Turnbull, P.D. Wilson, D. A. Briscoe, *Microbiol. Methods*, **2008**, *72*, 103-106.
36. J. El Haskouri, D. Ortiz de Zarate, C. C. Guillem, J. Latorre, M. Caldés, A. Beltrán, D. Beltrán, A.B. Descalzo, G. Rodríguez-López, R. Martínez-Máñez, M.D. Marcos, P. Amorós. *Chem. Commun*, **2002**, 330-331.
37. M. Comes, M. D. Marcos, R. Martínez-Máñez, F. Sancenón, J. Soto, L.A. Villaescusa, P. Amorós, D. Beltrán. *Adv. Mater*, **2004**, *16*, 1783-1786.
38. M. Comes, G. Rodríguez-López, M.D. Marcos, R. Martínez-Máñez, F. Sancenón, J. Soto, L.A. Villaescusa, P. Amorós, D. Beltrán. *Angew. Chem. Int. Ed,* **2005**, *44*, 2919-2922.
39. C. A. Strassert, N. Otter, R. Q. Albuquerque, A. Höne, Y. Vida, B. Maier, L. De Cola, *Angew. Chem. Int. Ed.,* **2009**, *48*, 7928-7931.
40. Z. Popovic, M. Otter, G. Calzaferri, L. De Cola. *Angew. Chem. Int. Ed.,* **2007**, *46*, 6188-6191.
41. C. T. Kresge, M.E. Leonowicz, W.J. Roth, J.C. Vartuli, J.S. Beck. *Nature,* **1992**, *359*, 710-712.

Enhanced efficacy and broadening of antibacterial action of drugs via the use of capped mesoporous nanoparticles

Supporting Information

Núria Mas, Irene Galiana, Laura Mondragón, Elena Aznar, Estela Climent, Nuria Cabedo, Félix Sancenón, José Ramón Murguía, Ramón Martínez-Máñez*, María D. Marcos and Pedro Amorós*

Chemicals

The chemicals tetraethylorthosilicate (TEOS) (98 %), *n*-cetyltrimethylammonium bromide (CTAB) (≥99 %), sodium hydroxide (≥98 %), rhodamide B and vancomycin were provided by Aldrich. ε-poly-L-lysine (ε-PL) was purchased from Chengdu Jinkai Biology Engineering Co. Ltd. *N*-[(3-trimethoxysilyl)propyl]ethylendiamine triacetic acid trisodium salt was purchased from FluoroChem. $Na_2HPO_4{\cdot}7H_2O$, KH_2PO_4 , NaCl, NH_4Cl, $MgSO_4$, glucose and $CaCl_2$ where purchased from Scharlab (used for the preparation of M9 minimal medium). All reagents were used as received.

General Techniques

Powder XRD, TG analysis, elemental analysis, TEM and N_2 adsorption-desorption techniques were employed to characterize the prepared materials. UV-visible was used for the quantification of rhodamine B and vancomycin

contents of the synthesized materials. Powder X-ray diffraction measurements were performed on a Philips D8 Advance diffractometer using Cu K_α radiation. Thermo-gravimetric analysis were carried out on a TGA/SDTA 851e Mettler Toledo balance, using an oxidant atmosphere (air, 80 mL/min) with a heating program consisting on a heating ramp of 10°C per minute from 393 to 1273 K and an isothermal heating step at this temperature during 30 minutes. Elemental analysis was performed in a CE Instrument EA-1110 CHN Elemental Analyzer. TEM images were obtained with a 100 kV Jeol JEM-1010 microscope. N_2 adsorption-desorption isotherms were recorded on a Micromeritics ASAP2010 automated sorption analyser. The samples were degassed at 120°C in vacuum overnight. The specific surface areas were calculated from the adsorption data in the low pressures range using the BET model. Pore size was determined following the BJH method. Zetasizer Nano from Malvern was used for the characterization of the surface charge of the nanoparticles. UV-visible spectroscopy was carried out with a Lambda 35 UV/visible spectrometer (Perkin-Elmer Instruments). Thermo Scientific Multiskan FC multimode plate reader was used to evaluate the turbidimetry at OD_{620}.

Synthesis of the mesoporous silica support

The MCM-41 mesoporous nanoparticles were synthesised by the following procedure: *n*-cetyltrimethylammonium bromide (CTAB, 1.00 g, 2.74 mmol) was first dissolved in 480 mL of deionised water. Then 3.5 mL of NaOH 2.00 M in deionised water were added to the CTAB solution. Next the solution temperature was adjusted to 80°C. TEOS (5.00 mL, 2.57 x 10^{-2} mol) was then added dropwise to the surfactant solution. The mixture was stirred for 2 h to give a white precipitate. Finally, the solid product was centrifuged, washed with deionised water and ethanol, and was dried at 60°C (MCM-41 as-synthesised). To prepare the final porous material (MCM-41), the as-synthesised solid was calcined at 550°C using an oxidant atmosphere for 5 h in order to remove the template phase.

Synthesis of S1-Rho

In a typical synthesis, 750 mg of template-free MCM-41 were suspended in a solution of 340 mg of rhodamine B dye in 23 mL of mili Q water in a round-bottomed flask, which corresponds to 0.8 mmol of dye/g MCM-41. After 24 h stirring at room temperature, 15 mmol/g MCM-41 of *N*-[(3-trimethoxysilyl)propyl]ethylendiamine triacetic acid trisodium salt (**1**, 6.55 mL) were added and the mixture was stirred for 5.5 h at room temperature. The obtained solid (850 mg, **S1**) was filtered, and dried under vacuum. Then, this pre-functionalized solid was suspended in a solution containing 3.4 g of ε-poly-L-lysine in 45 mL of M9 (minimal medium) in order to cover the external surface of the loaded and functionalized nanoparticles. This suspension was stirred for 1h at room temperature. Finally, this solid was filtered and washed with 200 mL of M9 and 800 mL of mili Q water in order to remove the unreacted alkoxysilane and the dye remaining outside the pores. The final solid **S1-Rho** was dried under vacuum and at 37 °C for 12 h.

Synthesis of S1-Van

In a typical synthesis, 200 mg of template-free MCM-41 were suspended in a solution of 30 mg of vancomycin (0.1 mmol of vancomycin/g MCM-41) in 2 mL of 10 mM pH 7.4 PBS (Phosphate Buffer Solution). After stirring at room temperature for 24 h, 15 mmol/g MCM-41 of *N*-[(3-trimethoxysilyl)propyl]ethylendiamine triacetic acid trisodium salt (**1**, 1.75 mL) diluted in 1 mL of PBS were added and the mixture was stirred for 12 h at room temperature. The obtained solid was filtered, and dried under vacuum. Then, this pre-functionalized solid was suspended in a solution containing 1.025 g of ε-poly-L-lysine in 3 mL of PBS in order to cover the external surface of the loaded and functionalized nanoparticles with an excess of 20 mg of vancomycin (in order to minimize the leaching of the loaded vancomycion from the inside of the pores). This suspension was stirred during 1 h at room temperature. Finally, this solid was filtered and washed twice by centrifugation with 8 mL of PBS in order to remove

the unreacted alkoxysilane and the dye remaining outside the pores. The final solid **S1-Van** was dried under vacuum and at 37 °C for 12 h.

Materials Characterization

MCM-41 as-synthesized, MCM-41 and the final **S1-Rho** and **S1-Van** synthesized materials were characterized through standard techniques. Figure SI-1 (A) shows the X-ray diffraction (XRD) patterns of the nanoparticulated MCM-41 matrix as-synthesised, the MCM-41 calcined and the final **S1-Rho** solid. The MCM-41 as-synthesised (curve a) displayed the four typical low-angle reflections of a hexagonal-ordered matrix indexed at (100), (110), (200) and (210) Bragg peaks. In curve b (MCM-41 calcined), a significant shift of the (100) peak in the XRD and a broadening of the (100) and (200) peaks are observed. These changes are due to the condensation of silanols in the calcination step, which caused an approximate cell contraction of 4 Å. Finally, curve c shows the **S1-Rho** solid XRD pattern. For this material, reflections (110) and (200) were mostly lost due to a reduction in contrast related to the functionalisation process and to the filling of mesopores with rhodamine B. Even so, the intensity of the (100) peak in this pattern strongly indicates that the loading process with the dye and the additional functionalisation with *N*-[(3-trimethoxysilyl)propyl]ethylendiamine triacetic acid trisodium salt and the coating with ε-poly-L-lysine did not modify the mesoporous MCM-41 scaffold. In the same way, in Figure SI-1 X-ray diffraction (XRD) patterns of the nanoparticulated MCM-41 matrix as-synthesised, the MCM-41 calcined and the final **S1-Van** solid can be observed. It can be also confirmed by the intensity of the (100) peak that in the final functionalized and loaded (with vancomycin in this case) hybrid material the MCM-41 porous scaffold remains unchanged.

Moreover, in the TEM analysis of the prepared solids the typical channels of the MCM-41 matrix can be visualised as alternate black and white stripes in which the typical hexagonal porosity of the MCM-41 calcined material can also be observed (see Figure SI-2). TEM images for the final solids **S1-Rho** and **S1-Van** are shown in Figure 1 in the manuscript. TEM images also show that the prepared MCM-41-based supports is obtained as spherical nanoparticles with diameters

between 80 and 100 nm. This spherical shape remains after the loading and functionalization processes, as can be seen in the **S1-Rho** and **S1-Van** images.

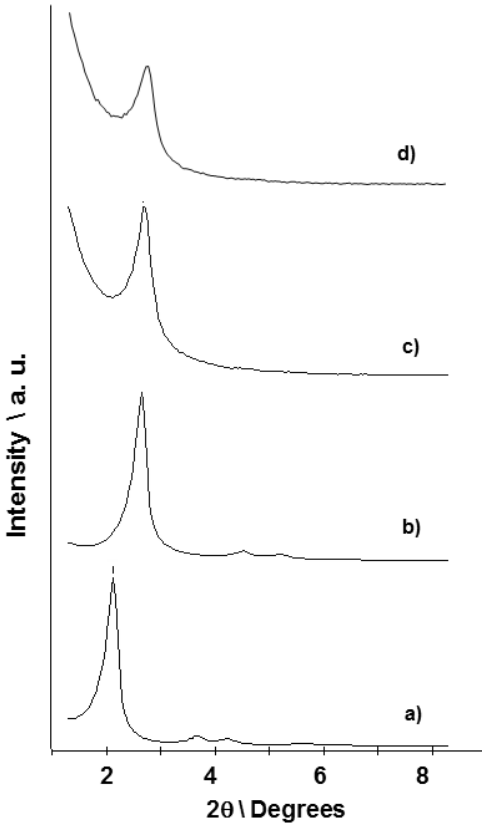

Figure SI-1. Powder X-Ray diffractograms showing X-Ray patterns of MCM-41 scaffolding as synthesized (a), MCM-41 after the calcination process (b), final solid **S1-Rho** (c) and final solid **S1-Van** (d).

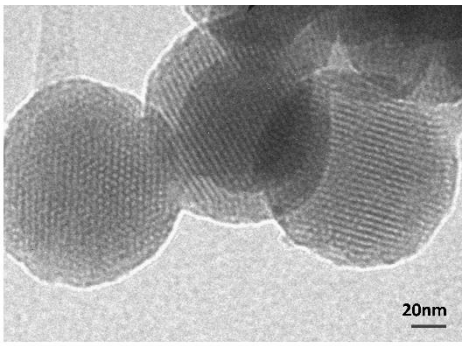

Figure SI-2. TEM image of the inorganic MCM-41 calcined matrix.

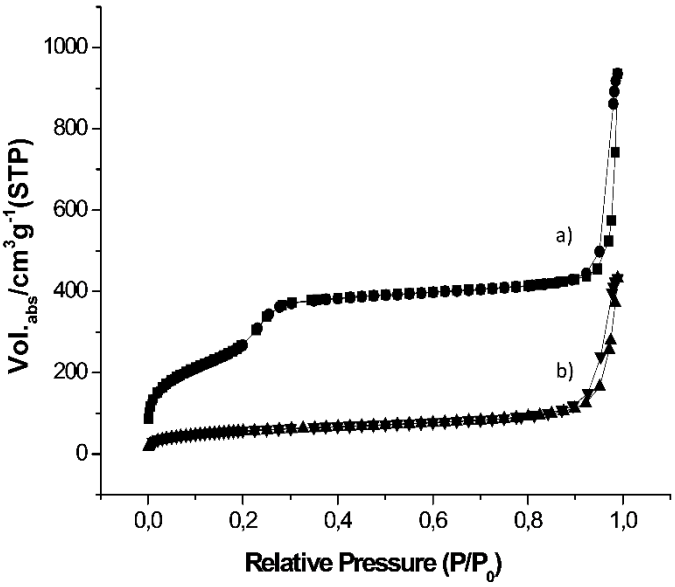

Figure SI-3. Nitrogen adsorption-desorption isotherms for (a) MCM-41 mesoporous material (b) **S1-Rho**.

Figure SI-3 (curve a) showed the N_2 adsorption-desorption isotherms of the MCM-41 calcined nanoparticles. This curve displays an adsorption step with a P/P_0 value between 0.2 and 0.35, corresponding to a type IV isotherm, which is typical of mesoporous materials. This first step is due to nitrogen condensation in the mesopore inlets. With the BJH[1] model on the adsorption curve of the isotherm, the pore diameter and pore volume were calculated to be 2.32 nm and 0.69 cm^3g^{-1}, respectively. The absence of a hysteresis loop in this pressure range

and the low BJH pore distribution is due to the cylindrical uniformity of mesopores. The total specific area was 981.2 m^2g^{-1}, calculated with the BET model.[2] The a_0 cell parameter 38.083 Å (d_{100}= 32.981 Å), the pore diameter (2.32 nm) and the wall thickness value, 14.88 Å, were calculated by the XRD, porosimetry and TEM measurements. Other important feature of the curve is the characteristic H1 hysteresis loop that appears in the isotherm at a high relative pressure (P/P_0> 0.8) which can be closely associated with a wide pore size distribution. This corresponds to the filling of the large pores among the nanoparticles (0.56 cm^3g^{-1} calculated by the BJH model) due to textural porosity.

On the other hand, for the **S1-Rho** material, the N_2 adsorption-desorption isotherm is typical of mesoporous systems with filled mesopores (see Figure SI-3, curve b). In this way, and as it can be expected, a lower N_2 adsorbed volume (BJH mesopore volume = 0.15 cm^3g^{-1}) and surface area (204.9.9 m^2g^{-1}) were found, when compared with the initial MCM-41 material. As observed, this solid presents a curve with no gaps at low relative pressure values if compared to the mother MCM-41 matrix (curve a). Another important feature of **S1-Rho** is that no maximum was observed in the pore size distribution curve, which can be explained by the presence of closed pores (see Figure SI-4 for pore size distributions). Table SI-1 shows a summary of the BET-specific surface values, pore volumes and pore sizes calculated from the N_2 adsorption-desorption isotherms for MCM-41 calcined and **S1-Rho.**

Table SI-1. BET specific surface values, pore volumes and pore sizes calculated from the N_2 adsorption-desorption isotherms for selected materials.

Solid	S_{BET} ($m^2\ g^{-1}$)	**Pore Volume** (cm^3g^{-1})	**Pore size** (nm)
MCM-41	981.2	0.69	2.32
S1-Rho	204.9	0.15	----

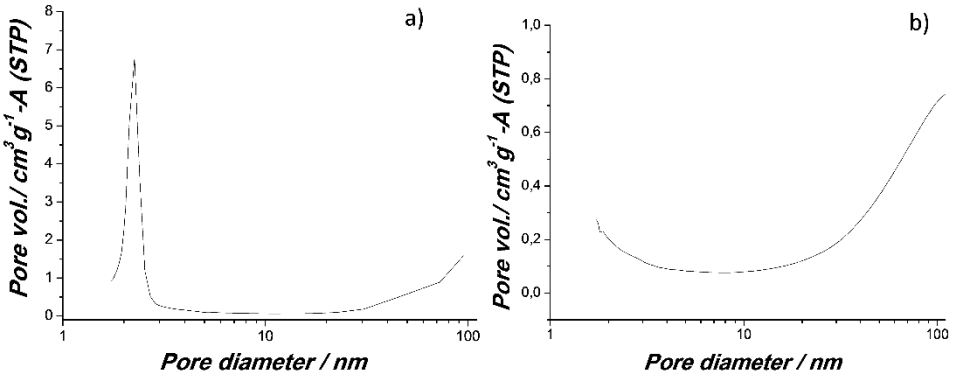

Figure SI-4. Pore size distributions for (a) MCM-41 mesoporous material (b) **S1-Rho**.

Moreover, the contents of grafted molecules (*N*-[(3-trimethoxysilyl)propyl]ethylendiamine triacetic acid trisodium salt and ε-poly-L-Lysine) and dye (rhodamine B) or drug (vancomycin) in solids **S1-Rho** and **S1-Van**, respectively, were determined by a combination of UV-vis, thermogravimetric and elemental analyses. In the UV-vis studies two calibration curves were obtained, one for rhodamine B (λ_{abs} = 555 nm) and other for vancomycin (λ_{abs} = 280 nm). The molar extinction coefficients obtained were: $\varepsilon_{\text{rhodamineB,555}}$ = 86679 L mol^{-1} cm^{-1} and $\varepsilon_{\text{vancomycin,280}}$ = 9091 L mol^{-1} cm^{-1}. The content of rhodamine B (**S1-Rho**) and vancomycin (**S1-Van**) present in the washing solutions of both solids were quantified and subtracted to the quantities used in the loading process of the solids (see synthesis of **S1-Rho** and **S1-Van**). This method allowed us to quantify the rhodamine B and vancomycin presents in the final **S1-Rho** and **S1-Van** materials.

Thermogravimetric studies of both **S1-Rho** and **S1-Van** solids were also carried out. The thermogravimetric curves of both solids showed four weights loss steps (see Figure SI-5A and SI-5B). For **S1-Rho** solid (Figure SI-5A) weight losses of 8.19 % (T < 150 ^{o}C, corresponding to solvent elimination), 6.80 % (150 < T < 300 ^{o}C, assigned to the decomposition of the organic groups anchored onto the siliceous support), 13.57 % (300 < T < 520 ^{o}C, also due to combustion of organics) and 2.49 % (T > 520 ^{o}C, attributed to condensation of silanols in the siliceous

surface) were observed. For the **S1-Van** solid, these weight losses were: 7.64 % (T < 150 ^{o}C), 25.04 %, 9.13 % (150 < T < 600 ^{o}C) and 0.63 % (T > 600 ^{o}C).

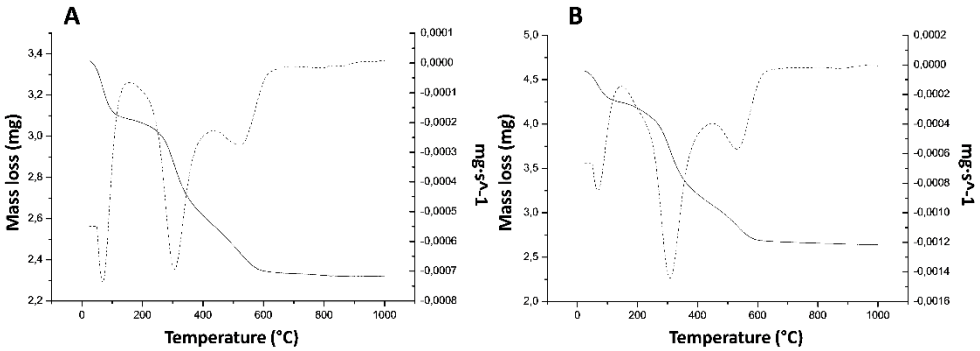

Figure SI-5. Thermogravimetric curve (solid line) and its first derivative (dashed line) obtained from the thermogravimetric analysis of **S1-Rho** (A) and **S1-Van** (B).

Thermogravimetric studies of both **S1-Rho** and **S1-Van** solids were also carried out. The thermogravimetric curves of both solids showed four weights loss steps (see Figure SI-5A and SI-5B). For **S1-Rho** solid (Figure SI-5A) weight losses of 8.19 % (T < 150 ^{o}C, corresponding to solvent elimination), 6.80 % (150 < T < 300 ^{o}C, assigned to the decomposition of the organic groups anchored onto the siliceous support), 13.57 % (300 < T < 520 ^{o}C, also due to combustion of organics) and 2.49 % (T > 520 ^{o}C, attributed to condensation of silanols in the siliceous surface) were observed. For the **S1-Van** solid, these weight losses were: 7.64 % (T < 150 ^{o}C), 25.04 %, 9.13 % (150 < T < 600 ^{o}C) and 0.63 % (T > 600 ^{o}C).

Finally, elemental analyses for **S1-Rho** and **S1-Van** materials were performed and the content of rhodamine B (in **S1-Rho**), vancomycin (in **S1-Van**), functionalized product **1** and ε-PL were calculated. Rhodamine B and vancomycin contents calculated by this procedure compared well with those obtained from UV-vis studies. The final content values are shown in Table SI-2.

Table SI-2. Content (α, mmol/g of solid) of the different loading and functionalization moieties of the materials.

Solid	$\alpha_{rhodamine\ B}$	$\alpha_{Vancomycin}$	α_1	$\alpha_{\varepsilon-PL}$
S1-Rho	0.021	----	0.388	0.025
S1-Van	----	0.010	0.390	0.021

The surface charge of the synthesized nanoparticles was determined using a Malvern Zetasizer Nano instrumentation. After appropriate dilution of the different suspensions of the nanoparticles, electrophoretic mobility (EM), zeta potential (ζ) and conductivity (σ) were determined. Samples from the prepared suspensions were diluted in ultra-purified water and placed in the measurement cell, with its position adjusted, being a folded capillary cell. At least two different measurements were made for each sample. The final results obtained are shown in Table-SI-3. As it can be observed, **S1** has, as expected, a negative ζ valuedue to the negative charge present in **1** (grafted in the outer surface) at neutral pH. Addition of ε-PL (for capping the pores through electrostatic interactions with the negatively charged **1**) induced a change in the sign of ζ in the final solids **S1-Rho** and **S1-Van**.

Table SI-3. Physicochemical properties of different prepared nanoparticles.

Solid	EM (μm·cm/V·S)	ζ (mV)	σ (mS/cm)
S1	-1.777 ± 0.3997	-22.7 ± 5.1	0.0172
S1-Rho	1.505 ± 0.3607	19.2 ± 4.6	0.0155
S1-Van	1.85 ± 0.3951	23.6 ± 5.04	0.0255

Cell viability studies with E. coli DH5α

For viability studies, bacteria (*Escherichia coli*) cell culture DH5α was used. (Bacto)-Tryptone, (Bacto)-Yeast Extract and American Bacteriological Agar

were provided from Laboratorios Conda. All reagents were used following manufacturer's conditions.

E. coli DH5α culture conditions

Bacteria cells were grown and maintained (4°C) in Luria Bertani medium (LB) supplemented with 2% of bacto-agar when the solid medium was prepared. For the assays, cells were grown for 24 h at 37°C and constant stirring with 5 mL of liquid LB medium. LB medium was prepared by mixing (bacto)-tryptone 1% (10 g/L), (bacto)-yeast extract 0.5% (5 g/L), NaCl 1% (10 g/L, 0.17 M) at pH 7.

DH5α cells were cultured in LB medium at 37°C overnight with continuous stirring, as explained above Cells from 1 ml culture were collected by centrifugation for 30 seconds at 13000 rpm and resuspended in 1 mL milliQ water at pH 7. Then a dilution of 10^5 cells/mL was prepared. The working bacteria concentration was determined with experiments carried out with **S1-Rho** in vitro. This bacteria concentration is able to displace the ε-PL that covers the external surface of **S1-Rho** solid with the subsequent release of the entrapped rhodamine B. The same procedure was carried out for all viability assays.

Optimizing the assay conditions

In this section, different assays for the evaluation of the optimal working conditions for the viability tests of the prepared materials are described.

Clonogenic viability assays to determine **S1-Rho** and MCM-41 cytotoxicity

3 mL aliquots of the diluted bacterial cultures were prepared, corresponding to negative control (1) (without any kind of nanoparticles), MCM-41 (2) and **S1-Rho** (3) respectively. 3 mg of the corresponding solid were added in the vials 2 and 3 and the three samples were stirred at 200 rpm. 200 μL aliquots were taken after 30 minutes and 60 minutes from each vial and introduced in the multiwell plate. At least two replicates were prepared for each sample. After that,

the samples were 10-fold serially diluted and plated onto LB Petri plates. Colonies were quantitated after 2-5 days in all cases. Data represented are the mean +/- S.E. of at least two independent experiments each one done in duplicate. MCM-41 nanoparticles seemed to be mostly innocuous for cell bacteria, as no differences in cell growth were observed between MCM-41 samples and the negative control. However, a significant decrease in cell growth was shown in the presence of **S1-Rho** material, probably due to the ε-PL adsorbed in the nanoparticle surface.

Clonogenic cell viability assay with MCM-41, **S1-Rho** and **S1-Van**.

The same procedure was carried out for the three synthesized solids MCM-41, **S1-Rho** and **S1-Van**. At this respect, different suspensions of the three solids with several concentrations (1000, 500, 400, 300, 200, 100, 50, 30, 20, 15, 10, 5, 1, 0.5 and 0 μg solid/mL) were prepared and then a solution of bacteria (10^5 cell/mL) was added. After the addition of bacteria, the samples were stirred at 200 rpm for 5 minutes. Then, a 100 μL aliquot was taken twice from each vial (duplicate for each studied concentration) and introduced in an eppendorf. In order to obtain a cell growth of approximately 300 cells per plate, which is easy to quantify, 30 μL of the aliquot were diluted in 1 mL milliQ water at pH 7, and finally 100 μL of the new dilutions were seeded in LB plates and incubated at 37°C for 18 h. Then Colony Formation Units (CFU) were quantified. To quantitate the cytotoxicity of free ε-poly-L-lysine, free vancomycin and free ε-poly-L-lysine/vancomycin, similar assays were performed at the indicated doses.

Statistical analysis

A further statistical analysis of the data was carried out using Sigma Plot software. The samples were inoculated in technical duplication for each case. Each experiment was at least four times reproduced for *E. coli DH5α* and two times for the rest of bacterial strains. A pharmacological fitting was studied in order to obtain the Minimum Inhibitory Concentration (MIC) and the EC_{50} values with their corresponding standard errors. This pharmacology fitting corresponds to the following standard equation analysis:

$$y = \frac{min + (max - \min)}{\left(1 + \left(\frac{x}{EC_{50}}\right)^{Hillslope}\right)}$$

where *max* and *min* are the maximum and minimum value respectively, *Hillslope*: Hill coefficient and EC_{50} values. Minimum inhibitory concentrations (MICs) in this case were determined by the standard broth microdilution method in 96-well plate format. The experiment procedure consisted of eight microplates. Four of them were filled with 100 μL of the corresponding bacterial suspension which were serially diluted with medium to achieve a final bacterial concentration of 10^5 colony-forming units/mL in each well (corresponding to a turbidimetry of 0.005 OD_{620}),. Other microplate wells were filled only with 200 μL of Difco Nutrient broth. One of these four microplates was filled with 100 μL of a **S1-Van** suspension (corresponding to 15 μg vancomycin/mL and 83 μg ε-PL/mL), whereas the other three microplates were filled with free ε-PL, free vancomycin and a mixture of ε-PL and vancomycin, respectively. The concentrations used for free vancomycin or ε-PL corresponded to the vancomycin or ε-PL present in the **S1-Van** suspension. Four more microplates were also prepared as control by mixing the different compounds (**S1-Van**, free ε–PL, free vancomycin or a mixture of ε-PL and vancomycin, respectively in each microplate) with Difco nutrient broth medium and without any bacteria. The concentrations tested were the same than those used in microplates with bacteria. By following serial dilutions with the same medium in all the microplates, consecutive concentrations of each compound were thus obtained. Control well consisted of 200 μL of Difco nutrient broth alone. Microplates were then incubated without shaking at 37°C or 28°C, depending on each strain growth conditions overnight (16 h). Bacterial growth was determined turbidimetrically (OD_{620}) using a Thermo Scientific Multiskan FC multimode plate reader. Each experiment was performed twice; the measured antibacterial activity was expressed as the MIC range. Percentage growth inhibition was determined using plate-based microliter dilution assay, and EC_{50}

values with their standard error were also obtained using nonlinear regression analysis for all bacterial strains, $P < 0.01$ in all cases. The EC_{50} and MIC for the DH5α reference bacterial strain were one order of magnitude higher than those obtained in the viability studies, discrepancy that is expected when cell growth and cell viability experiments are compared.

References

1. E.P. Barret, L.G. Joyner, P.P. Halenda, *J. Am. Chem. Soc.*, **1951**,73, 373-380.
2. S. Brunauer, P.H. Emmett, E. Teller, *J. Am. Chem. Soc.*, **1938**, 60, 309-319.

4. Conclusions and perspectives

Design of stimuli-responsive gated nanodevices has recently attracted significant attention in areas such as controlled delivery, offering a wide range of future applications. The present thesis has attempted to contribute to this field. In fact, all hybrid materials here presented have been designed in order to respond to several biomedical needs and have been developed as proof of concept for possible future therapeutic applications.

First of all, a general introduction has been included in the first chapter of this thesis, showing the principles, perspectives, and recent developments in the field of supramolecular chemistry. The main properties of mesoporous materials have been then described. Moreover a brief summary describing some significant examples of molecular gated systems based on mesoporous silica supports for controlled delivery applications has been presented.

In the next two chapters different molecular gated nanodevices, developed during this thesis, for controlled delivery applications, have been described. Some of them were based on enzyme-triggered systems whereas other were focused on the recognition and killing of some pathogen microorganisms.

More specifically, in the second chapter of this work, biocompatible systems for the controlled release of bioactive molecules into cells based on enzyme-driven molecular gates have been developed. Three different organic-inorganic hybrid materials have been presented. In all cases the same inorganic nanoscopic silica matrix (MCM-41) was employed to store the cargo to be released yet different capping moieties were anchored onto the outer surface. The first example was a dual enzyme-driven (esterase and reductase) nanodevice composed by silica nanoparticles capped with azopyridinium salts for potential controlled delivery applications in the colon. The material was designed to show “zero delivery” and to display a cargo release in the presence of reductases and esterases, which are usually present in the colon microflora. HeLa cells were employed for testing the 'non'-toxicity of nanoparticles and the intracellular

controlled delivery. Furthermore, similar nanoparticles loaded with the cytotoxic camptothecin were also prepared and used as delivery nanodevices in HeLa cells. When this solid was employed, cell viability decreased significantly due to the nanoparticles internalisation and delivery of the cytotoxic agent. On the other hand, a second example involving the design, synthesis, characterization and application of a new protease-responsive nanodevice for intracellular-controlled release using silica mesoporous nanoparticles capped with ε–poly-L-lysine has been described. Two different anchoring procedures of the polymer were studied, both of them yielding good results in controlled delivery applications. Moreover, the possible use of ε–poly-L-lysine-capped nanoparticles as suitable intracellular delivery devices of the chemotherapeutic agent camptothecin (CPT) was demonstrated. Finally, the third example included in this second chapter, was focused on the design and application of a smart 3D "gated scaffold" which consisted in the combination of capped silica mesoporous nanoparticles and classical porous biomaterials for on-command delivery induced by acid phosphatase. Acid phsophatase is an enzyme whose activity is used to assess osteoclast activity in bone remodelling processes, as well as a biomarker for bone metastases. This combination in the design of functional materials opens up the possibility of preparing a number of advanced gated scaffolds, which could help in regenerative medicine and bone cancer therapy applications.

In relation to the thrid chapter, other possible applications of mesoporous silica nanoparticles capped with molecular gates for controlled delivery of drugs were presented. In this case, the design and development of new organic-inorganic hybrid materials was based on the use of MCM-41 mesoporous silica nanoparticles as inorganic matrix, capped with organic moieties that could respond to the presence of target pathogen microorganisms. Along this line, the first example in this chapter showed the antifungal applications of a tebuconazole loaded support capped with pH-driven gatekeeping moieties. In a second example, the development and antibacterial applications against Gram-negative bacteria of a vancomycin-loaded nanodevice capped with ε-poly-L-lysine was reported. In both cases, it was demonstrated that the use of a nanoformulation

setup can achieve an enhancement and broadening of the spectrum of some drugs, what opens a wide range of possible applications of these gated nanodevices.

In summary, it can be concluded that new hybrid organic-inorganic solids have been developed and their application as controlled delivery systems have been described in this thesis. I hope that the obtained results in this thesis will inspire the future design of advanced hybrid materials for biotechnological and biomedical applications.